frontiers

RESEARCH TOPICS

DIGITAL BRAIN ATLASES

Hosted by
Randolf Menzel

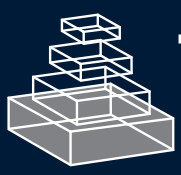

frontiers in
SYSTEMS NEUROSCIENCE

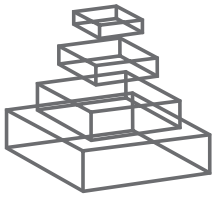

frontiers

Cover image provided by Ibbl sarl, Lausanne CH

ISSN 1664-8714
ISBN 978-2-88919-031-7
DOI 10.3389/978-2-88919-031-7

ABOUT FRONTIERS

Frontiers is more than just an open-access publisher of scholarly articles: it is a pioneering approach to the world of academia, radically improving the way scholarly research is managed. The grand vision of Frontiers is a world where all people have an equal opportunity to seek, share and generate knowledge. Frontiers provides immediate and permanent online open access to all its publications, but this alone is not enough to realize our grand goals.

FRONTIERS JOURNAL SERIES

The Frontiers Journal Series is a multi-tier and interdisciplinary set of open-access, online journals, promising a paradigm shift from the current review, selection and dissemination processes in academic publishing.
All Frontiers journals are driven by researchers for researchers; therefore, they constitute a service to the scholarly community. At the same time, the Frontiers Journal Series operates on a revolutionary invention, the tiered publishing system, initially addressing specific communities of scholars, and gradually climbing up to broader public understanding, thus serving the interests of the lay society, too.

DEDICATION TO QUALITY

Each Frontiers article is a landmark of the highest quality, thanks to genuinely collaborative interactions between authors and review editors, who include some of the world's best academicians. Research must be certified by peers before entering a stream of knowledge that may eventually reach the public - and shape society; therefore, Frontiers only applies the most rigorous and unbiased reviews.
Frontiers revolutionizes research publishing by freely delivering the most outstanding research, evaluated with no bias from both the academic and social point of view.
By applying the most advanced information technologies, Frontiers is catapulting scholarly publishing into a new generation.

WHAT ARE FRONTIERS RESEARCH TOPICS?

Frontiers Research Topics are very popular trademarks of the Frontiers Journals Series: they are collections of at least ten articles, all centered on a particular subject. With their unique mix of varied contributions from Original Research to Review Articles, Frontiers Research Topics unify the most influential researchers, the latest key findings and historical advances in a hot research area!
Find out more on how to host your own Frontiers Research Topic or contribute to one as an author by contacting the Frontiers Editorial Office: researchtopics@frontiersin.org

DIGITAL BRAIN ATLASES

Hosted By
Randolf Menzel, Freie Universiät Berlin, Germany

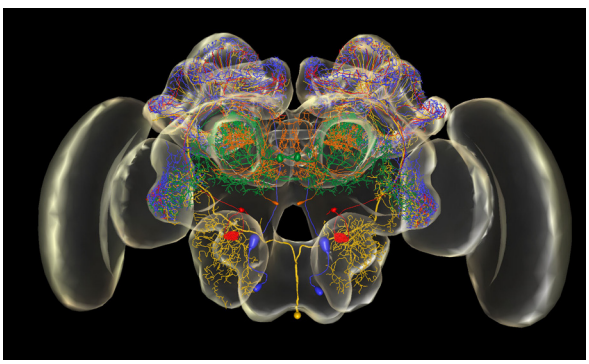

Digital microscopy (confocal microscopy, multiphoton microscopy, electron microscopy) has revolutionized neuroanatomy. Atlases of whole brains, of parts of the brain and of neural circuits are becoming more and more important to accumulate neuroanatomical data in 3D, construct reference atlases ("standard brains"), provide an interactive graphical surface for databanks on brain and neuron related data, and to quantify morphological data. These diverse options require highly sophisticated software and close interaction between neuroanatomists, physiologists and science computing experts. The various attempts and developments include not only research institutions but also software companies. How can the multiple and diverse work going on in many research groups and companies coordinated and integrated for improving the experimental and computational workμ Which problems should be solved with first priority and which can be postponed for laterμ Which developments on the side of the instruments (light and electron microscopes) should be fostered.

Image: It shows 4 neurons (on each side) registered into the standard brain atlas of the honeybee brain. These neurons are: in red and yellow two olfactory projection neurons of the lateral antenno-glomerularis tract, blue: one olfactory projection neuron of the median antenno-glomerularis tract, and in green an identified mushroom body extrinsic neuron, the neuron PE1.

Image Courtesy: Dr. Jürgen Rybak

Table of Contents

frontiers in
SYSTEMS NEUROSCIENCE

EDITORIAL
published: 17 April 2012
doi: 10.3389/fnsys.2012.00024

Introduction to the research topic on standard brain atlases

Randolf Menzel*

Neurobiology Unit, Freie Universiät Berlin, Berlin, Germany
**Correspondence: menzel@neurobiologie.fu-berlin.de*

Understanding neural function is based on knowledge about the wiring of the brain (Ramon y Cajal, 1897). Neuroanatomy has made an enormous leap in recent years with the advent of confocal and multi-photon microscopy, powerful graphic computers, cheap digital storage material, and the internet. Several initiatives have been successfully created aiming to convert neuroanatomy into a quantitative science. Whole brains or parts of them are documented in digital data sets that are accessible via the internet and allow for an ever-increasing collection of well-organized and carefully documented anatomical data.

Challenged by the need to integrate the rapidly growing data in neuroscience, digital brain atlases have become an important tool serving as databases for neural substrates with full 3D spatial information. The intension is to provide common frameworks into which neuroanatomical and physiological data can be registered and spatially related. Registration of neuroanatomical data in an atlas allows accumulating structural data from different brains of the same animal species into structural neural networks as well as identifying locations and distributions of synaptic interactions in the network.

Due to large differences in brain size, atlases differ in resolution and completeness. Invertebrate ganglia and brains are small enough to be analyzed by light microscopy as a whole on the level of single neurons and clusters of synaptic connections. The concept of the identified neuron is a powerful guide in the understanding of neural function in invertebrates requiring the identification, localization, and characterization of each neuron in the respective ganglion and brain. A neuron can be classified as identified on the single cell level when its Gestalt, functional properties and cellular components as compared to other neurons is found to be unique. Although we are far from this goal for most invertebrates (not even mentioning vertebrates) the tools are available as one can learn from the data on the nervous system of the nematode worm *Caenorhabditis elegans* (Hall and Russell, 1991), and the insect *Drosophila* (Chiang et al., 2011). In a long run the working of nervous systems will be understood only if the networks of such neurons are anatomically and functionally characterized, a goal that has been reached already for a small invertebrate ganglion, the stomatogastric ganglion of Decapoda crustaceans (Nusbaum and Beenhakker, 2002). Functional imaging at high resolution speeds up the process of network characterization, an experimental approach that will be productive only if the structure of the network is known and accessible in form of a 3D atlas.

The contributions to this special issue focus on optical methods (confocal, multiple photon, and ultra microscopy) for the analysis of neural structures aiming to construct a virtual 3D environment, the brain atlas. This atlas compiles the anatomical structures, and allows for the registration of neurons and their networks down to the level tight appositions between neighboring neurons and synaptic complexes. Electron microscopical analyses will be the next step, a step that requires an atlas as a 3D guide.

The first section (Digital Brain Atlases, Creation, Composition, Use, and Maintenance) addresses a range of questions related to the processes of constructing standardized brain atlases, how they are used and what kind of problems we face when maintaining them. As pointed out in the article by Kei Ito the maintenance of the large data sets of a brain atlas is a challenging task for which the structure of our laborites and research agencies are not well prepared. He argues in favor of a new form of researcher, the biocurator, who receives recognitions by the science community to provide access to well-organized and world wide usable data of a brain atlas. Indeed this is an enormously important move as everybody knows who has failed in getting research grants approved that aim to establish and maintain a brain atlas for the international science community. Kei Ito points also to another problem which we need to take seriously. "It is ironical that, whereas we can read and cite anatomical books and papers written even more than 150 years ago to access the knowledge and thoughts of our predecessors, most of the effort we are putting into computer-based database will (probably) not be seen by the people who live 150 years later." This problem is faced for all digital data, and needs to be solved for the whole humankind but is particularly pressing for the science community.

The second section (Digital Atlases of Insect brains) gives first five examples for standard brain atlases (for the locust, the honeybee, two moth species *Heliothis* and *Manduca*, and the beetle *Tribolium)*. The last two chapters are concerned about the use of existing brain atlases for specific problems. The first five chapters address the questions of creating and using standard atlases from multiple view points. Should one construct an average atlas from multiple specimens or select a typical individual example? Is the atlas predominantly used for registering single marked neurons or for estimating ontogenetic and evolutionary developments of brain areas? How shall one deal with structural variability at the level of identified neurons or brain areas? These and many more questions are dealt with on the basis of large data sets with respect of the number of brains analyzed, the brain areas studied, and the neurons registered into the respective atlas. Furthermore, recent developments of volume rendering and automatic registration are discussed and evaluated on the basis of experiences with these particular brains. Finally the chapter on the honeybee discusses the use of the standard atlas as a graphical surface and an organizing principle for an ontology of data beyond the structural components. These chapters should be read in connection to recent publications on

the *Drosophila* brain (Peng et al., 2010; Shinomiya et al., 2011; Milyaev et al., 2012, see also http://penglab.janelia.org/proj/v3d) since the genetic tools available for *Drosophila* allowing to mark types of neurons or even single neurons enhance the power of insect brains as models for the development, use, and maintain standard brain atlases.

REFERENCES

Chiang, A. S., Lin, C. Y., Chuang, C. C., Chang, H. M., Hsieh, C. H., Yeh, C. W., Shih, C. T., Wu, J. J., Wang, G. T., Chen, Y. C., Wu, C. C., Chen, G. Y., Ching, Y. T., Lee, P. C., Lin, C. Y., Lin, H. H., Wu, C. C., Hsu, H. W., Huang, Y. A., Chen, J. Y., Chiang, H. J., Lu, C. F., Ni, R. F., Yeh, C. Y., and Hwang, J. K. (2011). Three-dimensional reconstruction of brain-wide wiring networks in *Drosophila* at single-cell resolution. *Curr. Biol.* 21, 1–11.

Hall, D. H., and Russell, R. L. (1991). The posterior nervous system of the nematode *Caenorhabditis elegans*: serial reconstruction of identified neurons and complete pattern of synaptic interactions. *J. Neurosci.* 11, 1–22.

Milyaev, N., Osumi-Sutherland, D., Reeve, S., Burton, N., Baldock, R. A., and Armstrong, J. D. (2012). The virtual fly brain browser and query interface. *Bioinformatics* 28, 411–415.

Nusbaum, M. P., and Beenhakker, M. P. (2002). A small-systems approach to motor pattern generation. *Nature* 417, 343–350.

Peng, H., Ruan, Z., Long, F., Simpson, J. H., and Myers, E. W. (2010). V3D enables real-time 3D visualization and quantitative analysis of large-scale biological image data sets. *Nat. Biotechnol.* 28, 348–353.

Ramon y Cajal, S. (1897). Las leyes de la morfologia y dinamismo de lascelulas-nerviosas. *Rev. Trim Microgr.*

Shinomiya, K., Matsuda, K., Oishi, T., Otsuna, H., and Ito, K. (2011). Fly brain neuron database: a comprehensive database system of the *Drosophila* brain neurons. *J. Comp. Neurol.* 519, 807–833.

Received: 08 March 2012; accepted: 26 March 2012; published online: 17 April 2012.

Citation: Menzel R (2012) Introduction to the research topic on standard brain atlases. Front. Syst. Neurosci. ***6****:24. doi: 10.3389/fnsys.2012.00024*

frontiers in
SYSTEMS NEUROSCIENCE

ORIGINAL RESEARCH ARTICLE
published: 18 June 2010
doi: 10.3389/fnsys.2010.00026

Technical and organizational considerations for the long-term maintenance and development of digital brain atlases and web-based databases

Kei Ito*

Institute of Molecular and Cellular Biosciences, The University of Tokyo, Tokyo, Japan

Edited by:
Randolf Menzel, Freie Universiät Berlin, Germany

Reviewed by:
Jürgen Rybak, Max Planck Institute for Chemical Ecology, Germany
Hanchuan Peng, Howard Hughes Medical Institute, USA

****Correspondence:***
Kei Ito, Institute of Molecular and Cellular Biosciences, The University of Tokyo, 1-1-1 Yayoi, Bunkyo-ku, Tokyo, 113-0032, Japan.
e-mail: itokei@iam.u-tokyo.ac.jp

Digital brain atlas is a kind of image database that specifically provide information about neurons and glial cells in the brain. It has various advantages that are unmatched by conventional paper-based atlases. Such advantages, however, may become disadvantages if appropriate cares are not taken. Because digital atlases can provide unlimited amount of data, they should be designed to minimize redundancy and keep consistency of the records that may be added incrementally by different staffs. The fact that digital atlases can easily be revised necessitates a system to assure that users can access previous versions that might have been cited in papers at a particular period. To inherit our knowledge to our descendants, such databases should be maintained for a very long period, well over 100 years, like printed books and papers. Technical and organizational measures to enable long-term archive should be considered seriously. Compared to the initial development of the database, subsequent efforts to increase the quality and quantity of its contents are not regarded highly, because such tasks do not materialize in the form of publications. This fact strongly discourages continuous expansion of, and external contributions to, the digital atlases after its initial launch. To solve these problems, the role of the biocurators is vital. Appreciation of the scientific achievements of the people who do not write papers, and establishment of the secure academic career path for them, are indispensable for recruiting talents for this very important job.

Keywords: brain, atlas, image database, molecular marker, neuron, curator

INTRODUCTION

Atlases of the brain provide images and information about neurons and glial cells, brain regions, fascicles, and arborizations, transmitters and other brain-related chemicals, antibodies, and strains for labeling specific cell types, known functions, and developmental origins of the neurons and brain regions, etc. The term "digital brain atlas" has been used for referring to several kinds of neuroanatomical projects. In the simplest meaning, it refers to the electronic version of the conventional atlases that have been published in the form of books. More sophisticated digital atlases feature computer-based three-dimensional visualization systems to generate maps of the brain, which are used as tools and platforms for analyzing neurons and brain structures (Toga and Thompson, 2001; Rein et al., 2002; Van Essen, 2002; Brandt et al., 2005; Kurylas et al., 2008; El Jundi et al., 2009a,b; Kvello et al., 2009; Dreyer et al., 2010; Huetteroth et al., 2010; Jahrling et al., 2010; Lofaldli et al., 2010; Peng et al., 2010).

Digital atlases are not only useful for conducting researches to be published in the form of research articles. Many digital atlases serve as publicly accessible information resources, in which data are stored in host server computers and provided over the Internet upon users' request. Such atlases can be regarded as a specific kind of image databases, and the number of such online atlases is increasing (**Table 1**). They will become useful platforms for providing comprehensive information about the entire projection patterns of all the neurons – called the projectome (Kasthuri and Lichtman, 2007), and connectivity data of all the neurons – called the connectome (Sporns et al., 2005; Seung, 2009).

Atlases of the brain have traditionally been provided as printed books (Strausfeld, 1976; Wullimann et al., 1996; Valverde, 1998; Woolsey et al., 2003; Mai et al., 2004; Paxinos and Watson, 2005; Puelles et al., 2007; Franklin and Paxinos, 2008; Schambra, 2008). Compared to web-based digital atlases, conventional paper-based atlases still have several advantages. First, it is easier to browse high-resolution images. Whereas even the best computer monitor can display images at only less than 110 dots per inch (DPI), typical commercial printing offer the resolution of 350 DPI for photographs and 2,540 DPI for text and line drawings. A page of a printed atlas can present several high-resolution images and detailed text explanation at the same time. On the other hand, even a large computer monitor can display only a single high-resolution image. To view more than one full-resolution image or to display an image and its complete text explanation, users have to scroll the screen or switch between different windows, which significantly decreases readability.

And second, a paper-based atlas has a much more reliable value as an archive. Because the hard copies of the atlas are stored in public libraries, they will be accessible for a long time in the future even if the authors would die, the books would become out of press, or the publishers may go out of business. Web-based atlases, on the other hand, are highly unstable. Useful web sites may disappear

Table 1 | Examples of web-based digital atlases.

Vertebrates		
Humans	The Human Brain Atlas	https://www.msu.edu/~brains/brains/human/
	The Whole Brain Atlas	http://www.med.harvard.edu/AANLIB/home.html
	The HumanBrain.Info	http://www.thehumanbrain.info/
Monkeys	Marmoset Brain Atlas	http://marmoset-brain.org:2008/ (Tokuno et al., 2009)
Mice	The Allen Brain Atlas	http://www.brain-map.org/ (Ma et al., 2005; Lein et al., 2007)
	Blue Brain Project	http://bluebrain.epfl.ch/ (Markram, 2006)
Birds	AvianBrain.org	http://avianbrain.org/atlases.html
	Avian Brain Circuitry Database	http://www.behav.org/abcd/
	Zebra Finch MRI Atlas	http://webh01.ua.ac.be/biomag/zebrafinch_mri_atlas.htm (Poirier et al., 2008)
Fish	Zebrafish Atlas	http://zfatlas.psu.edu/index.php
VARIOUS ORGANISMS INCLUDING THE ABOVE		
	The Brainmaps	http://brainmaps.org/ (Mikula et al., 2008)
	Comparative Mammalian Brain Collections	http://www.brainmuseum.org/
INVERTEBRATES		
Flies	Flybrain	http://www.flybrain.org/ (Armstrong et al., 1995)
	Flytrap	http://www.fly-trap.org/ (Armstrong and van Hemert, 2009)
	Virtual Insect Brain Lab for *Drosophila* Standard Brain	http://132.187.25.13/ (Rein et al., 2002)
	Flybrain at Stanford	http://flybrain.stanford.edu/ (Jefferis et al., 2007)
Bees	The Virtual Atlas of the Honeybee Brain	http://www.neurobiologie.fu-berlin.de/beebrain/ (Brandt et al., 2005)
Moths	Moth Standard Brain	http://www.ntnu.no/biolog/english/neuroscience/brain/ (Kvello et al., 2009)
	Manduca Standard brain	http://online-media.uni-marburg.de/biologie/3d_brain/manduca/standardbrain/ (El Jundi et al., 2009b)
Locusts	Schistocerca Standard Brain	http://online-media.uni-marburg.de/biologie/3d_brain/schistocerca/ (Kurylas et al., 2008)
Nematodes	Wormatlas	http://www.wormatlas.org/
	Database of Synaptic Connectivity of *C. elegans* for Computation	http://ims.dse.ibaraki.ac.jp/ccep/
INDIVIDUAL IDENTIFIED NEURONS IN THE BRAIN		
	The NeuroMorpho.org	http://neuromorpho.org/ (Ascoli et al., 2007; Halavi et al., 2008)
	Neuron Bank	http://neuronbank.org/ (Katz et al., 2010)
	Flybrain Neuron Database	http://ndb.flybrain.org/ (Shinomiya et al., in preparation)

when the person who established the server moves or retires, or the financial support that covers its operational cost is cut out. Even during the period when the database is maintained actively, some of the contents may be revised or even deleted in the future so that original version becomes inaccessible.

In spite of these shortcomings, computer-based digital atlases gain increasingly popular support, because they have also various advantages that are unmatched by conventional printed atlases. First, digital atlases can in principle provide much more data. Whereas the amount of information that can be put in a printed atlas is limited by the practical size and page number of a book, the volume of a digital atlas is limited only by the size of the hard disk storage, which is practically infinite (Howe et al., 2008; Van Horn and Toga, 2009).

Second, computer-based approach offers more flexible ways of navigation. Though paper-based atlases are easier to read through, locating pages that mention a particular item is difficult, especially if it is not listed in the index. Digital atlases equipped with adequate search engines enable users to locate whatever terms they are interested in. In addition, hyperlinks provide a convenient way to jump to other parts of the atlas that offer relevant information.

Third, digital atlases can present images in more versatile ways. Unlike printed atlases, they can provide not only still images but also movies and interactive images, with which users may view particular parts of the brain sections of different samples at various depths, or watch three-dimensional structure of neurons from different viewing angles with various visualization parameters. Combined with hyperlinks embedded in the graphics, interactive images offer easy-to-use navigation that is useful especially for the users who are not familiar with brain anatomy.

And fourth, contents of the digital atlases can be updated dynamically. Paper-based atlases remain stable once they are published. Though this ensures their value as archives, some of the information may become obsolete as the time goes by. Because

of the relatively limited readership and the high cost of printing, it is financially not feasible to publish revised editions at regular intervals except for the atlases of human and a few clinical model animals. On the contrary, revision is very easy with computer-based atlases. The first version of an atlas could be started with a minimum amount of contents just to present the outline of the brain structure of that organism, and new data will be added incrementally thereafter. This is especially suited for modern molecular-oriented neuroanatomy, where new techniques for visualizing neurons are being developed rapidly.

These advantages, however, mean that people working for a digital atlas have to be engaged in the project for a much longer period than those who write a printed atlas. Though it may take several years to prepare for the figures and manuscripts of a paper-based atlas, authors are freed from the tasks for its distribution and archival once it is published. Publishers and libraries will take care of these issues. On the other hand, people who develop a digital atlas are responsible for its maintenance, archival, and regular updates for tens of years after it is first established. There are various technical and organizational issues that are keys to the steady long-term maintenance and development of the web-based databases. Compared to the technical issues for developing novel visualization and navigation tools, however, such organizational issues are not discussed very often.

The Flybrain[1] is one of the first digital brain atlases operating on the Internet. It was established in 1995 by a consortium of a few laboratories working on the *Drosophila* brain (Armstrong et al., 1995). My laboratory joined soon after its establishment as one of the organizers and is contributing to its maintenance since then. Based on this 15-year experience, in this semi-review paper I will discuss various problems that may affect the development of digital atlases and web-based databases after it is first established.

DOCUMENTING THE POSITIONS IN THE BRAIN

In the first seven sections I will discuss issues concerning the design of the digital atlas that is easy to maintain and expand. A digital atlas is in a manner similar to the databases of genes and proteins, because they all provide comprehensive information about important aspects of an organism. Describing the structure of a gene or a protein is easy, because it is essentially a one-dimensional chain of clearly defined units (four nucleotides or 20 amino-acid residues, respectively). Three-dimensional morphology of a protein can also be documented unambiguously using the coordinates of each atom. Documenting the structure of a neuron is much more demanding, because it has a complex three-dimensional architecture spanning various parts of the brain. The location of the cell body, trajectories, and branching points of the neural fibers, and areas of dendritic and terminal arborizations could in principle be documented using the coordinates of the labeled areas (pixels/voxels) of the image of the neuron. However, because of the inter-individual variability in the overall size, shape, and relative positions of brain regions, coordinates of a corresponding part of the brain may not be identical from sample to sample, making simple coordinates useless for describing the positions in the brain.

There have been two approaches to address this issue. One approach is to divide the brain into morphologically and functionally meaningful regions, such as cortical areas and nuclei in the mammalian brain and neuropils of the insect brain. Each region can further be subdivided into smaller parts, such as glomeruli in the insect antennal lobe (Laissue et al., 1999), layers in the optic lobe neuropils (Fischbach and Dittrich, 1989; Otsuna and Ito, 2006), and strata and segments in the central complex and mushroom body lobes (Hanesch et al., 1989; Tanaka et al., 2008). The names of these subregions can be used as unambiguous descriptors of the neural position, because such subregions should exist in all the brain samples even if their respective locations may slightly vary (**Figures 1A,B**).

Another approach is to standardize the shape of each dataset of the brain into a standard framework using a computer program. In the simplest form, the width, height, thickness, and axes of the brain samples are transformed using linear expansion and rotation. Coordinates of all the parts of the brain cannot usually be matched with such simple affine transformation, however, because some parts of a brain sample may be twisted or disproportionally larger or smaller than the corresponding structure in other samples (**Figure 1C**). Non-linear registration, so-called morphing or warping, is necessary to attain a better match (Tanaka et al., 2004; Guetat et al., 2006; Jenett et al., 2006; Jefferis et al., 2007; Kurylas et al., 2008; Yap et al., 2009). Because all the brain samples can be fit into a standard shape, positions in the brain can be described using the coordinates in the standardized brain (**Figure 1D**).

These two approaches are comparable to the two ways we use for specifying the location on the earth, using either address (name of the country, state, city, and street) or latitude/longitude coordinates. The former address-like specification system is more intuitive and convenient for text-based search: Users can easily recognize the position of the brain from the region name, and all the neurons that project to a particular area can be looked up by simply using the region name as the search key. The latter coordinate-based specification is less intuitive for humans but advantageous for quantitative analyses: The length of the neural fibers, distance, and potential contact between two neurons, etc., can be calculated using the standardized coordinates. The resolution of the positional specification is higher, because fine differences within a defined brain subregion can be distinguished by the coordinate values. The two specification systems are therefore complementary. Ideally, documentation in both ways should better be provided in a digital atlas.

A potential problem of the address-like approach is that there has been some inconsistency in the names of the brain regions: Apparently comparable brain regions are given different names depending on the researchers and species. In addition, the areas of the brain that have not been attracted extensive research were not given clearly defined names and boundaries. Discrepancy in the nomenclature of the brains of various avian species has been resolved by a proposal of a coordinated naming scheme (Reiner et al., 2004a,b)[2]. A similar attempt is going way for the insect brain; a working group of neuroanatomists of various insect species is discussing the issue, and the controlled

[1]http://www.flybrain.org/

[2]http://avianbrain.org/

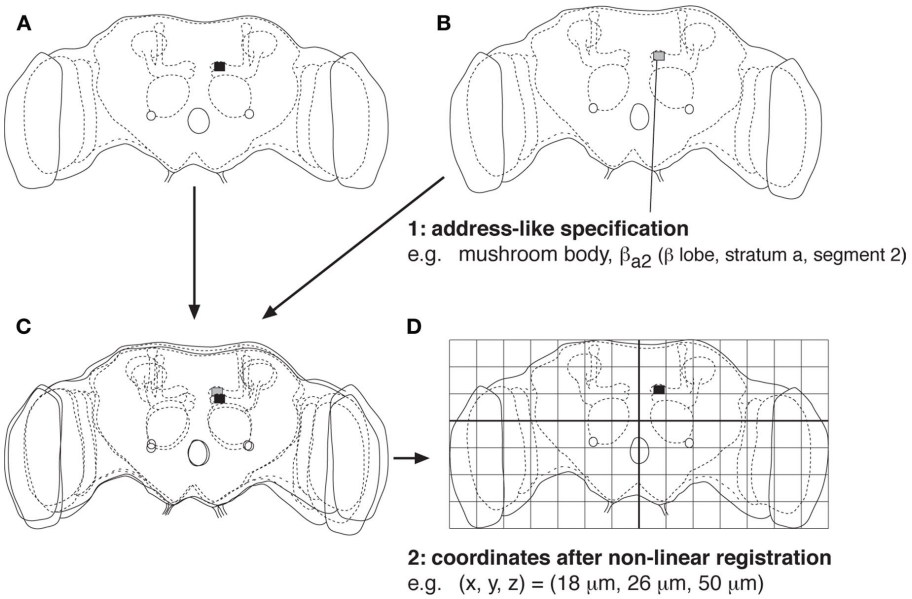

FIGURE 1 | Specification of the position in the brain. (A,B) Illustrations of two brain samples, whose shape are slightly different because of individual variability. Position in the brain can nevertheless be specified by the area of the brain region and distinct subregions within it. An example is shown for a particular subregion of the mushroom body lobe of the *Drosophila* brain (Tanaka et al., 2008). **(C)** Comparison of the two brain samples after linear affine transformation. Best match cannot be attained, because individual brain region may have slightly different size, shape, and orientation. **(D)** Comparison of the two brain samples after non-linear registration (so-called morphing or warping). All the brain samples can be fit into a standardized framework, in which the position in the brain can be specified using coordinates.

nomenclature system and the definition of neuropil boundaries using the *Drosophila* brain as a model will be proposed in the near future, which is going to be adopted by various databases of the fly brain. Such a system will enable the description of the locations of the cell bodies, branching points of neural fibers, and synaptic arborizations in a consistent manner, making it easier to compile information reported in various papers by various researchers.

KEEPING CONSISTENCY OF THE INFORMATION ABOUT NEURONS, IMAGES, AND MOLECULAR MARKERS

An atlas usually provides two types of images. The overall architecture of the brain will be presented with the serial sections of the entire brain, visualized with histological labeling methods such as Bodian, Ethylgallate, Nissl, and hematoxylin–eosin stain or with antibodies against ubiquitous molecules associated with synapses, membranes, cytoskeletons, etc. The structure of specific types of neurons and glial cells will be shown with the images visualized with various techniques including Golgi impregnation, dye filling, cell-specific antibodies, and transgenic expression driver strains. It is important to note that multiple types of neurons tend to be labeled in a single image, and that a single neuron type may be visualized in several images (**Figure 2A**). Thus, the relationship between neurons and the images in which they are presented is not one-to-one but many-to-many. The texts that describe the structure of a particular neuron would therefore appear in multiple parts of the atlas.

In addition, a molecular marker like an antibody or an expression driver often labels more than one type of neuron in the brain. Thus, a particular marker is likely to be mentioned in multiple parts of the atlas. Each part of the atlas describes a distinct subset of the neurons labeled by the marker, without mentioning the labeling patterns in other neurons (**Figure 2A**). A comprehensive list of all the neurons that are labeled by that marker is not directly available in many cases. Likewise, a particular brain region receives projections from many neurons and is visualized by various molecular markers. Thus, many parts of the atlas mention a particular brain region, while none of them provides comprehensive information about all the neurons that project to the area.

In case of paper-based atlases, only a few images are usually presented to describe each neuron type, molecular marker, and brain region because of the space limitation of a book. This has effectively reduced the problem of redundancy. Because there is no limiting factor to restrict the overall amount of database records, on the contrary, digital atlases may contain much more data that describe a particular neuron, marker, and brain region than paper-based atlases do. The number of such records, and the number of the texts that describe various aspects of the same neurons, markers, and brain regions is likely to increase over time as new data are added.

It may seem easy to keep track of such distributed and redundant information in digital atlases, because electronic text search systems will provide the list of all the records that mention a particular item. However, this approach runs into difficulty as the number of records increases. Because (1) different images reveal different aspects of the same neuron, (2) a molecular marker is utilized in a particular record to describe only a small subset of the neurons it labels, and (3) a brain region is mentioned in the context of diverse neurons and molecular markers, each record is likely to lack certain

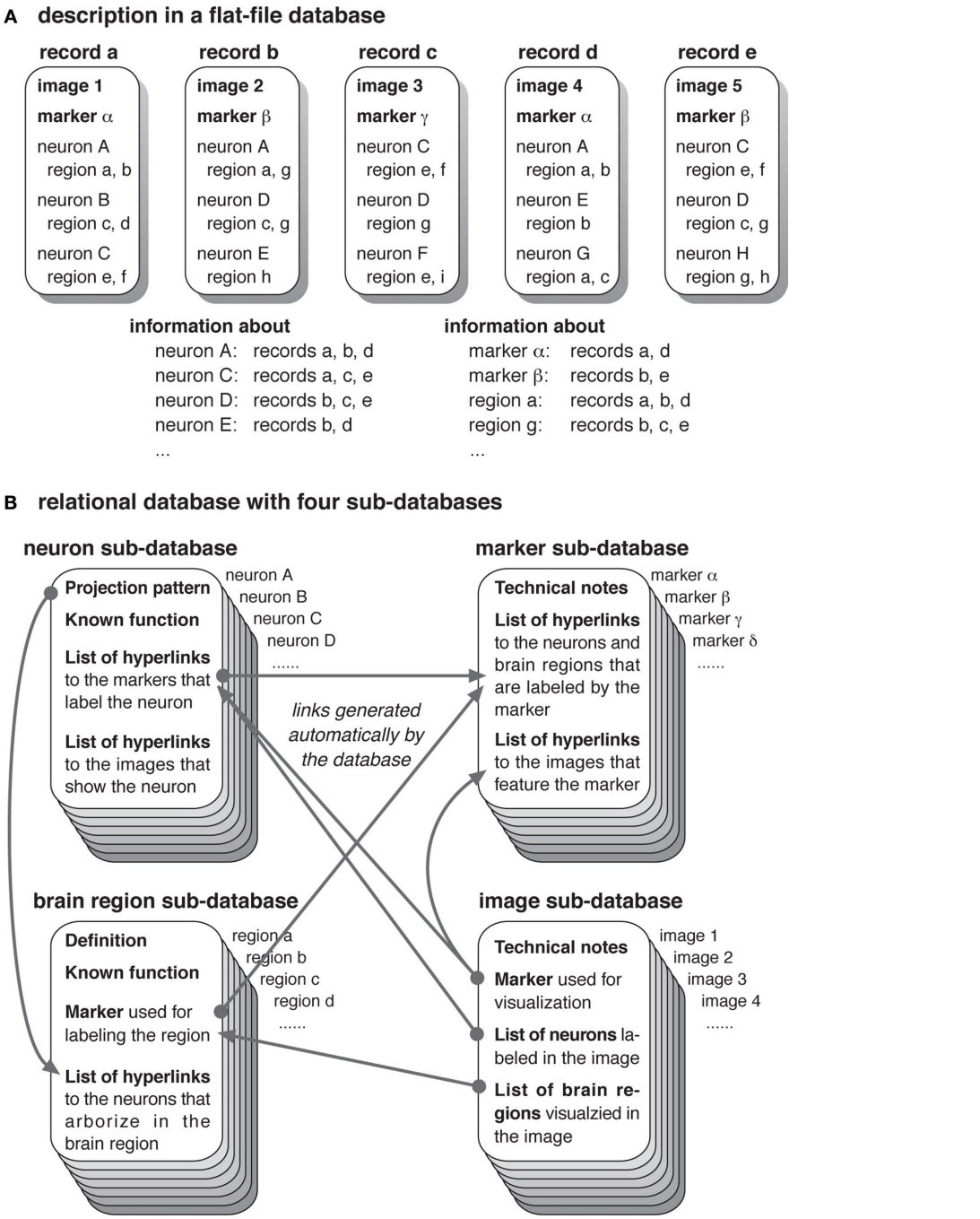

FIGURE 2 | Composition of the records for ensuring consistency. (A) A schematic example of a typical image database. Each record presents an image, or a set of images, visualizing particular groups of neurons with a particular molecular marker, showing particular regions of the brain. Different images may visualize the same neuron type with different combinations, and the same molecular marker is used for visualizing multiple types of neurons. As each record describes particular area of the brain, only a subset of the arborization targets of a neuron may be mentioned. Thus, description of a specific neuron type, marker, or brain region is scattered in the database, causing redundancy and possible inconsistency. **(B)** An example of a relational database with the sub-databases dedicated for the records of neurons, markers, brain regions, and images. Information about the complete projection patterns of the neurons, definition, and known functions of the brain regions, and technical details of the molecular markers and image preparation, are documented in respective records. When a new record is added, respective information in other records will automatically be updated.

information that is described in various other records of the database. Though users may be able to search all the records that mention particular neuron, marker, and brain region, comprehensive information can only be obtained by reading through all these documents scattered in the database, many of which may partially be redundant. This is not very efficient.

Moreover, having such redundancy increases the likelihood of inconsistent documentation between records. Images of a single neuron, marker, or brain region may appear slightly differently in different samples, either by technical differences or by inter-individual variations. Developmental and experience-dependent plasticity would also affect the appearance of the same neuron in different data (Livneh and Mizrahi, 2010). Because explanatory texts of different records may be written at different times and possibly by different staffs of the database organization, documentation in some records might become inconsistent with those in other records. Users are faced to resolve such contradicting information.

To avoid such situation, a database should feature a system to help keeping the consistency of neuron, marker, and brain region data. This is best achieved by making a relational database that keeps description of each neuron type, molecular marker, brain region, and image separately (**Figure 2B**). A relational database consists of a set of sub-databases each of which keeps records of particular items like neurons, markers, brain regions, and images. Relevant data field in one sub-database is linked (or related) with the corresponding field in another sub-database, providing hyperlinks between the information provided in each sub-database.

In this approach, each record of the image sub-database will provide information about its technical feature, the marker used for visualization, and a list of all the neuron types that are shown in the image. Relevant images, such as those of the same brain sample before and after registration described in the previous section (**Figure 1**), and still images and movies generated from the same three-dimensional dataset, will be kept in separate records of the sub-database and mutually linked.

Description of each neuron type, such as the location of the cell bodies, projection targets, brain regions in which pre- and postsynaptic sites are distributed, physiological properties such as transmitters and electrophysiological responses to stimuli, and known functions in behavioral experiments, will be provided in a single record of the neuron sub-database (**Figure 2B**). A record in the marker sub-database will provide its technical specification such as antigens of the antibody or genetic characteristics of the expression driver strain. A record in the brain region sub-database will explain the definition of the region boundary, methods to visualize the area, general architecture of its neural circuits, and known functions. Hyperlinks generated by the relational database engine will provide the list of all the neurons and images that feature a particular marker, the list of all the images and markers that visualize a particular neuron type and brain region, as well as the list of all the neurons that arborize in a particular brain region. These lists will be updated automatically whenever new records are added.

Such separation of neuron, marker, brain region, and image data enables keeping all the information of a particular neuron type, marker, and brain region in a single place of the database, avoiding redundancy, and possible inconsistency. When writing descriptive documentation of a new image data, novel information about the neurons visualized in the newly added image should be appended to the documentation of the neuron record rather than noted sporadically in the image records. By doing so, it becomes easy for the database organizers to check whether there is any inconsistency between the description in the neuron record and the structure visualized in the new image data. This approach also enables users and database organizers to keep consistency of the information provided. Because of the automatic hyperlinks between relational sub-databases, documentation of the neurons labeled with a particular molecular marker will automatically be reflected in the list of the labeled cells in the marker sub-database, and addition of new data about the arborization areas of a particular neuron will automatically update the list of contributing neurons in the respective record of the brain region sub-database.

KEEPING TRACK OF REVISIONS

As mentioned earlier, the fact that it is easy to revise contents of digital atlases can be regarded as both advantage and disadvantage. There are two occasions when a digital atlas is cited in literature. First, the existence of the digital atlas itself may be cited, just like citing a paper-based atlas in its entirety. Second, information provided in a particular part of the database may be cited, just like citing a page or a chapter of a book atlas. In the latter case, it is important that the readers of the literature can access the same information as the author had obtained when she/he wrote it. Though revisions of the digital atlases enable incorporation of latest observations and correction of inadequate descriptions, they would modify, or erase, certain contents that users of the database may have cited in their literature. In case of books, older editions remain available in the library and are therefore citable, even if some of the contents are revised in the following editions. In the digital database, however, previous versions of the documents usually become inaccessible from the database server.

This causes a serious problem as the reliability of digital atlases as reference sources. If a user of the database cites a document in the database in her/his paper, and if the document is revised after the paper is published, readers of the paper can no longer access the document in the form it was cited (**Figure 3A**). It would especially cause a trouble, if the revision involves correction or deletion of a particular aspect of the documentation that the user wanted to cite. For example, a neuron may be documented as excitatory in a digital atlas, and later it turned out to be wrong and the digital atlas organizer revised the relevant documentation to be inhibitory. If a user of the atlas cites the document before this revision, and a reader of the literature accesses the atlas after the revision, confusion should occur. Because scientific papers rely on the references that readers can examine by themselves, digital atlases should consider that the previous versions of the documents should remain accessible after they are revised.

Presenting latest and older versions of the same record in the database, on the other hand, may cause problems because users might accidentally access older versions even though they are interested only in the latest information. Thus, it is important to design the database so that the latest version of the record is presented usually, while providing a way to access older versions if users want. The simplest way to achieve this is to attach a list of hyperlinks to older versions of the document at the bottom of each revised record (**Figure 3B**). The revisions should be designated by the date of modification rather than version numbers, so that users can easily identify the version that was cited in a paper published at a particular time. To avoid human-related error and inconsistency, such a revision tracking links should better be generated automatically by the database.

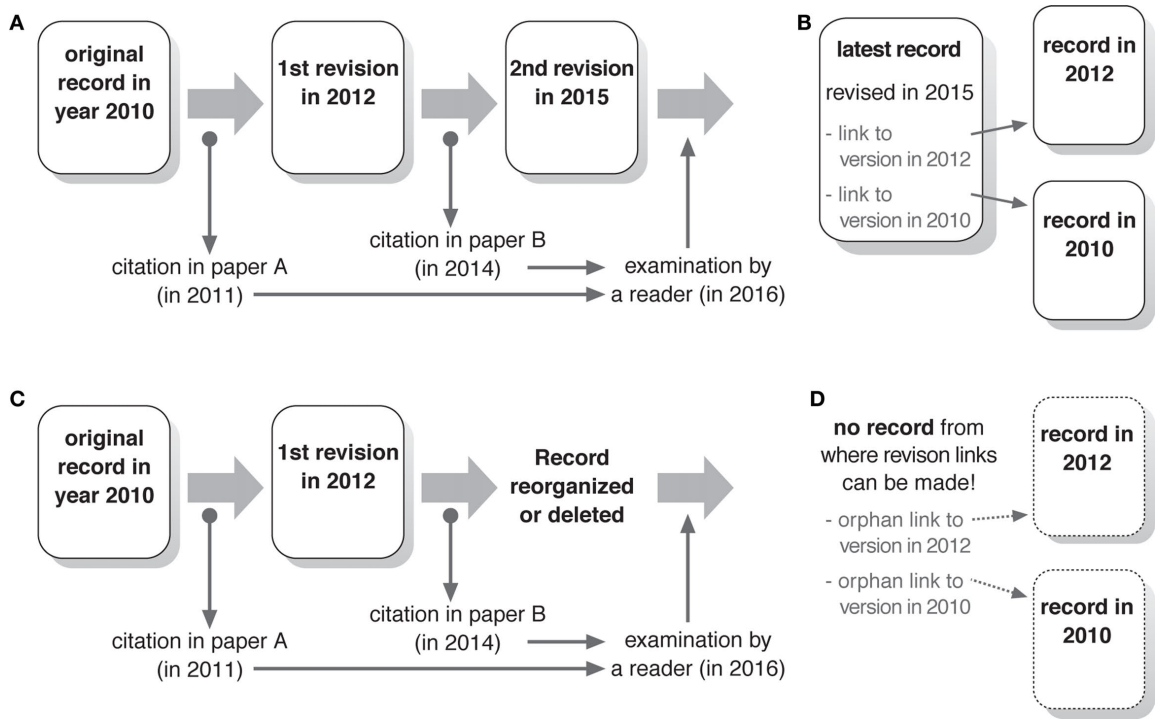

FIGURE 3 | Importance of the revision tracking system. (A) A schematic example of the citation of the database at different periods. Two papers refer to the same database record at different periods before and after revision. This may cause inconsistency between what are cited. If a reader of these papers examines the database at a later period, the person may not be able to get the same information cited in these papers. **(B)** Record with a revision tracking system. Links to the previous versions ensure examination of the data cited in previous papers. Indication of the date of revision enables the identification of the versions cited at a particular period. This is not possible if only version numbers are provided. **(C)** Situation when the entire database is reorganized, causing the deletion of the record that has been cited in literature. **(D)** Because there is no record from which previous versions can be traced, previous cited data become inaccessible.

Access to the older version of records is even more difficult, when the entire architecture of the digital atlas is modified to accommodate latest database technologies or when the atlas database is integrated into another database. Because contents of all the database records might be reorganized, each record of the old database may not have corresponding record in the new database (**Figure 3C**). This makes revision tracking between old and new databases practically impossible (**Figure 3D**). In such cases, the old database should better be kept accessible for the archival purpose, so that users who specifically want to read the contents of the old version can reach the information in its original form.

PROVIDING A RELIABLE WAY TO CITE RECORDS

It is not straightforward to cite particular contents of a digital atlas. Information source in the Internet is in general referred to with the uniform resource locator (URL; the string that starts with "http://"), which consists of the location of the host server (indicated by the characters before the first slash in the string) and the location of the file within it (characters after the first slash). The documents indicated in this way, however, tend to become inaccessible over time. There are two problems concerning this issue: the "file not found" problem and "host not found" problem.

The former problem occurs if the server cannot find the file requested by the user. A record of the digital atlas is typically constructed as a computer file. Writing the directory path of the file in the URL is the easiest way to make it accessible via the Internet. The directory path, however, is a highly vulnerable way to describe the location of information. A file becomes inaccessible even if just a single character of a file or directory name is changed. Connections may also be lost easily, if the directory that contains certain data files is moved within the host computer. Thus, using directory paths is not recommended for citing documents.

Many databases therefore assign numbers to each record, which is often called the accession number. Because this logical identifier is independent from the actual name and location of the file, it is robust against reorganization of the database. The records of all the sub-databases (e.g., neurons, images, brain regions, and markers) should be given different accession numbers. In addition, each identified neuron may also be given unique identification number, like the digital object identifier (DOI) of journal publication and ID numbers in genomic databases. To make use of these accession numbers, a digital atlas has to provide an easy way to search its contents with the accession number.

It would also be necessary to distinguish different versions of the data, especially when the original data were modified when putting into the digital atlas. For example, the dataset of the original microscopy data may be modified by non-linear registration for standardization, or signals and noises of the images may be enhanced or cleaned. In such cases, the original and modified data should be given different accession numbers.

KEEPING THE DATABASE ACCESSIBLE FOR A VERY LONG PERIOD

The latter "host not found" problem occurs in two cases. The first case is that the database exists but the URL has become invalid. This may occur because (1) the name of the host computer has been changed, (2) the institution that hosts the database was reorganized or renamed so that it acquired a new URL, or (3) the laboratory or organization that maintains the digital atlas has moved to a different institution. In these cases, users have to look for the atlas database that is operational with a new URL. This problem is relatively easy to address, because it is rather likely that the new URL can be spotted using popular Internet search services.

The second case is much more difficult to address: the digital atlas has stopped its operation because of the personnel, financial, or technical problems. Many web-based database sites have disappeared because the people who made the database have moved or retired. Only very large, public databases are run by organizations that can sustain their activity over a long period. Many scientific databases are maintained by a single laboratory or a group of only a few laboratories. Few if any institutions have a system to take over the maintenance of such databases after the people who established them have left the institute.

A database web site may also cease to exist, if the grant that has supported its operation is cut out. Many databases are funded by competitive money source. Such grants are unlikely to be awarded to the efforts that simply keep operation of old databases tens of years after they were established.

Even if the people responsible for the digital atlas remain active with enough financial support, maintenance of atlases may become difficult, when the computer system that runs the database becomes obsolete. Unlike printed atlases or their online versions provided as simple electronic files like the portable document format (PDF), a digital atlas is often a complex database with specialized software running on a computer. During the last decades, many computer platforms have disappeared from the market, making it impossible to use the software and even data that are made for older systems. Companies developing commercial database software continuously make updates and stop support for older versions. Old software often does not run on new computers, and new versions of the software that do run on the latest computers often fail to read data of their older versions properly. Considering that computer hardware must break sooner or later, it is a serious problem that long-term backward compatibility is hardly respected by computer and software companies.

In all, most digital atlases are destined to disappear within less than a couple of decades after they are established. I am confident that people in the twenty-second century will be able to read the article I am writing now, because it will be archived in many libraries, and because its electronic version in a popular industry-standard PDF format will remain accessible for a long period. On the other hand, it is not likely that someone would maintain the digital atlas I have been making to keep it accessible through the next century, long after I die. It is ironical that, whereas we can read and cite anatomical books and papers written even more than 150 years ago to access the knowledge and thoughts of our predecessors, most of the effort we are putting into computer-based database will not be seen by the people who live 150 years later; we cannot inherit our knowledge to our descendants. All the scientists who work with computer-based knowledge accumulation system should seriously think about this problem.

There would be several ways to avoid, or at least improve, this scenario. The best, but the most demanding, solution would be to establish a public organization that archive databases, just like libraries archive books and journals. Some university libraries and computer centers provide services for hosting databases in their servers, but the scope is usually limited to help the people who are currently working in the institute, not to keep these databases functional for the next 100 years.

Long-term maintenance will not be a problem for popular databases that are used widely by the research community, because there will be strong incentive to keep them functional. On the other hand, more specialized databases that are accessed only occasionally but yet provide important information are destined to disappear, because there would not be enough incentive to update them once they become obsolete. Libraries keep old books and journals even if they are accessed rarely. Only a very few scientific literature written before the nineteenth century are cited rather often. But information provided in other, less popular articles remain available: They just sit idle in the bookshelves of the libraries until someone want to read them. Likewise, old databases should be maintained even if they would attract few accesses per year.

Considerable financial support and political decision would be necessary to make such venture possible. For example, besides providing a portal site for cross-searching various life science databases, the Integrated Database Project by the Ministry of Education, Culture, Sports, Science and Technology of Japan[3] is attempting to take over the operation of useful existing databases that suffer from bad maintenance. Such a project could in principle serve as a library-like archive of old databases, but the Japanese government recently decided to restructure this project to be merged with another bioinformatics-associated agency. Whether this archival activity can be sustained through the next century is not yet clear.

Another approach would be to establish a business model for maintaining databases by commercial companies such as journal publishers. Because publishers already have the systems to store and distribute electronic text, image, and supplementary data of their journals, publishing databases is technically feasible in a similar framework. The operating cost of the database could be passed on to users, but ideally such scientific databases should be available free of charge like open access journals. Though the help by the publishers will significantly reduce the workload of the scientists who organize the databases, however, private companies may not be as stable as public library-like archive in the long term.

A more decent solution would be to establish a system that fellow scientists of the relevant field should take over the maintenance of the database. Though this may be done on a private basis for some databases, a more systematic approach is required to ensure that all the databases in the field should be maintained, even if no people is interested in the further development of the database.

[3]http://lifesciencedb.mext.go.jp/en/

This, however, is not easy under current circumstances, because it is very difficult to get financial support for the people who inherit the database just to keep it operational.

Archiving image databases is much more difficult than archiving electronic documents and web pages. If a digital atlas consists of only static data files, such as html and PDF documents and industry-standard graphic and movie files, it is easy to copy the atlas to other computers while keeping it accessible (**Figure 4A**). However, more sophisticated atlases that feature complex relational databases, search engines and interactive navigation systems are more vulnerable, because the associated software that enables such functions may not run on different computer platforms and may conflict with the programs of other databases that are archived in the same computer (**Figures 4B,C**). Even if the software successfully runs in the new server, it may become incompatible when the current computer hardware would get broken and replaced in the future.

When the data transfer rate of the Internet was still rather slow, we set up mirror sites of the original Flybrain digital atlas[4] in the United States, Germany, and Japan to ensure speedy access from respective local community. Because the Flybrain atlas is essentially a set of static html, jpeg, and movie files, it was easy to port most of its contents to mirror servers. The dedicated search engine and graphic navigation system, however, did not run properly in the mirror sites. The platform on which the original Flybrain was established, the Silicon Graphics workstation with the Irix operating system, has long been out of production.

Recently we are building a new atlas, the Flybrain Neuron Database[5] (Shinomiya et al., in preparation), which provides information about the projection patterns and known functions of all the *Drosophila* brain neurons reported so far in a unified format. It is a true relational database but requires two servers to run, one for the database engine and the other for the interactive visualization tool. All the contents are stored as database records rather than static html files. Though this makes the new atlas much more versatile, maintenance of the servers and porting of its contents to other institutes are much more demanding than in the case of the classic Flybrain. It is a dilemma for digital atlas designers: The more sophisticated the atlas database is, the more difficult to maintain it for a long period, especially after the people who made the database leave or retire.

One approach to address this problem is to establish a common sophisticated digital atlas platform architecture, i.e., the same set of relational sub-databases, data fields, methods to specify the locations in the brain, revision tracking system, accession number system, etc. If digital brain atlases of diverse organisms provided by various organizations can share such a platform, long-term maintenance and integration of databases will be easier. Unfortunately, industry standard does not yet exist in this field of electronic databases; researchers are exploring the best solutions. Imposing common database architecture at this stage may be too preliminary, because it may disturb further development of better alternatives. Establishment of a compatible database architecture and eventual integration to it, nevertheless, should be considered as one of the long-term goals of the digital atlas projects.

Coordination of diverse digital brain atlas projects is going on under the initiative of the International Neuroinformatics Coordinating Facility (INCF[6]; Bjaalie and Grillner, 2007; De Schutter, 2009). Besides organizing workshops and promoting communication between the people working in the field, INCF provides useful research tools and aims at developing standard techniques for neural data archival and presentation. Such activity would serve as a basis for establishing a common digital atlas platform in the future.

[4]http://www.flybrain.org/

[5]http://ndb.flybrain.org/

[6]http://www.incf.org/

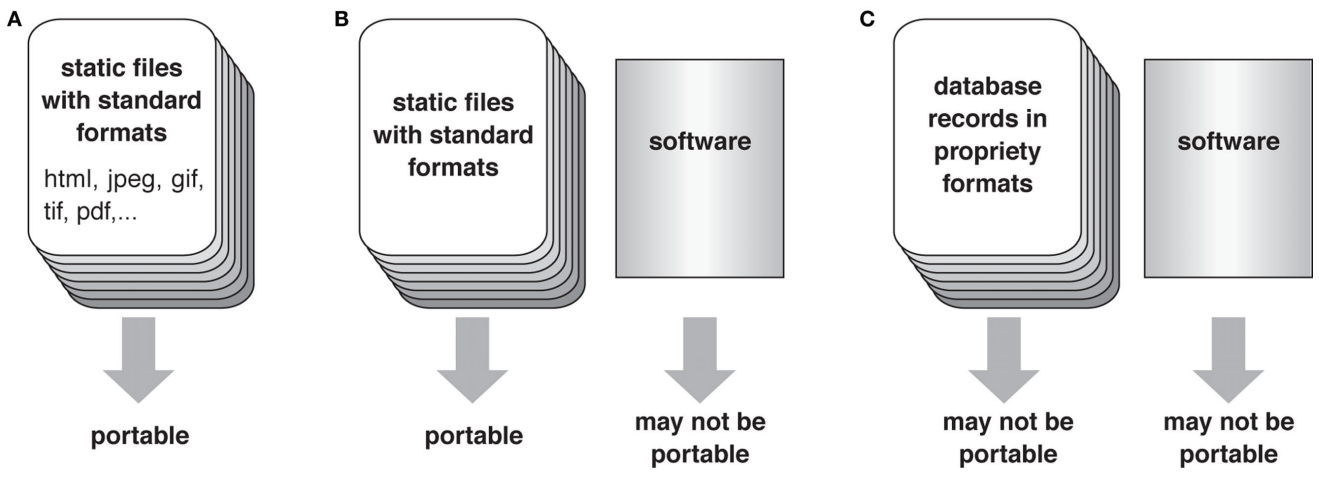

FIGURE 4 | Portability of the database. (A) A database with only files of standard formats is easy to port to other computers. **(B)** If a database consists of standard format files and software for navigation, visualization, and search system, the software part may not function properly when copied to different computers. **(C)** If the documents are composed as relational records of a database program, even the data may not be accessible when copied to a platform that is not compatible with the database software used in the original system.

SELECTION OF DATA FORMATS

A digital brain atlas transfers various types of files to users, which should be displayed properly on their computers. Selection of the data formats is therefore an important issue to ensure accessibility. Whereas formats of the text and two-dimensional image files have been standardized and can be decoded by most of the computers and web browsers provided by diverse venders, formats of the movies and three-dimensional image datasets are not yet standardized. Many of these data formats require so-called decoders, helper applications, or plug-in files to be installed in the users' computer. Such plug-ins are not always provided for all kinds of computer platforms; they often require specific combinations of the operation system and web browsing software. To make things worse, not all of such propriety data formats survive the competition. Development of the plug-in software for the formats that do not gain enough support may be stopped, and the existing plug-ins may not run in the newer versions of operation systems and web browsers.

This causes a severe problem for the digital atlas. For example, the classic Flybrain features a section that provides description of the three-dimensional brain structure using the virtual reality modeling language (VRML). The VRML was established in 1997 as ISO/IEC 14772-1:1997 standard and enables interactive visualization and manipulation of three-dimensional data, a seemingly ideal format at that time. Because most web browsers did not handle VRML files, users had to download and install the VRML plug-in files. However, such plug-in files ran smoothly only on just a few computer platforms. In other computers they were either very slow or tended to crash. Because of the low usability, the VRML format never got strong support, and few plug-in files are provided for the latest computers and browsers. Thus, the section of the Flybrain that features VRML has effectively become inaccessible to most users. The efforts that were paid for generating this part of the atlas essentially came to naught.

To avoid such unfortunate consequences, it is important to stick to the file formats that have already become industry standards. This sometimes contradicts with the intention of the digital atlas designers, who want to resort to cutting-edge computer technology for offering so far unprecedented functions. However, a digital atlas is not a test bench of computer science but a venue for conveying anatomical information to as many users as possible for a very long period in the future. Careful consideration is therefore required when using latest data formats. In recent years, Adobe Acrobat 3D[7] and Cortona3D Viewer[8] have evolved as possible alternatives to VRML. Whether they would survive as industry standards or not, however, remains to be seen.

PROBLEMS IN ATTRACTING THE DEPOSITORY OF EXTERNAL DATA: DIFFERENCES BETWEEN JOURNALS AND DIGITAL ATLASES

In the following sections, I will discuss less technical issues that might hamper steady accumulation of data once a digital atlas is first established. The first problem concerns the recruitment of data from the people who are not directly working on the database.

The laboratories that run digital brain atlases may not have all sorts of data that are suitable for the atlas, and other laboratories that have useful image data may not publish their own digital atlases. Users will feel it more convenient, if one or just a few digital atlases provide a comprehensive set of image data rather than many independent digital atlases each describes fragmental sets of information. Thus, it seems effective to ask a broad group of scientists for contributing their data to the atlas. This, however, is actually not so easy, or, practically unrealistic to be honest.

To recruit data from other laboratories, the classic Flybrain database set up a submission and review system similar to those of scientific journals in year 1995. People were in principle willing to provide data, but in reality few contributions were materialized. There were two problems underlying this consequence.

Scientists are generally very busy, and we have to allocate our resource (money, time, and personnel) to achieve the best outcome per effort. Preparing data for contributing to an atlas requires certain effort by the contributors. It is not just sending image files away by email; it requires detailed explanation of the technical procedure for the preparation of images, precise description of the neurons visualized in them, and conversion of the original propriety microscope data to standard web formats. Contributing to an image database is essentially similar to writing a mini paper. As it demands time and labor of the contributor, a strong incentive is needed to justify the effort. Because publishing papers in journals is considered mandatory for scientists, people are willing to spend time and energy to this aim. Giving data away to a database run by other scientists, on the contrary, is not regarded as an equally important job of scientists. To make the situation worse, the data that are put into a database are regarded as already published and are no longer suitable for publication as an original research article. This effectively gives a negative incentive not to contribute original data to digital atlases.

A more delicate issue is that a digital atlas like Flybrain is run by fellow scientists, whereas journals are run by public organizations. Advancement of the Flybrain is more often regarded as the achievements of its organizers rather than the achievements of the people who contribute their data. Considering this, it is understandable that people other than the database organizers would not want to spend time for the task that would not receive due appreciation from the research community.

To solve these problems, we once considered putting Flybrain under the aegis of certain public organization that issues scientific journals. This, however, could result in the restriction of the control by the original organizers, because the journal publisher gets rights on the management of the database. Also, there is a significant difference between journals and digital atlases. A journal is a venue for publishing various documents that are essentially independent from each other. It can, for example, publish papers that report contradicting observation in the same issue, or papers that describe similar contents using different terminology. Documents in a digital atlas should be more integrated with each other. It is not considered adequate that an atlas provides contradicting reports of a single neuron in different pages. Terminology should be consistent throughout the database. Organizers of a digital atlas therefore have more power of influence on its contents. This, however, may not always match the interests of the potential contributors who want to report their findings in the form they prefer.

[7]http://www.adobe.com/

[8]http://www.cortona3d.com/

To expect extensive contribution of data by the people other than the database organizers, a database should (1) be regarded mandatory by the scientific community to submit data to it in order to publish papers, and (2) collect simple information that does not require modification by the organizers. Databases that collect DNA and protein sequences, such as GenBank, fall in this category. It is difficult for anatomical databases to fulfill such conditions at this moment.

LACK OF THE SYSTEM FOR EVALUATING THE ACHIEVEMENTS OF THE PEOPLE WORKING WITH DATABASE

Because it is difficult to attract external contributions, contents of a digital atlas should be prepared mostly by the people who run the database. This seemingly simple task, however, is actually not easy to achieve.

When the Flybrain database was first established in 1995, its development was reported in a rather popular journal (Armstrong et al., 1995), even though the provided data were still in an initial, rather preliminary state. New data and better navigation tools were implemented extensively during the following years. Such subsequent efforts, however, could not be published as papers. As described earlier, new contents added in the database are regarded as already published and are no longer suitable for publication in a journal. However, whereas publication of a paper is commonly accepted as a scientific achievement of the person, addition of data to an existing database is almost always not evaluated as scientific achievements. This causes serious problems when students and postdoctoral fellows who are engaged in the digital atlas project write their curriculum vitae. If we consider that the efforts of our laboratory members should result in maximum rewards to them, reporting precious data in the database instead of in papers is suicidal.

Acknowledging this problem, the classic Flybrain shifted the strategy to provide contents that are already published elsewhere. But preparation of data for the database is by itself a laborious task, which requires a comparable amount of time and effort as those required for writing a paper. Considering that such effort would not be regarded as distinct scientific achievements once the original paper has been published, it is difficult to ask students and postdoctoral fellows for spending time for such unappreciated task. It is better for their carrier, if they instead use their precious time for doing new experiments for writing another paper. Indeed, even though we have identified many neurons in the fly brain and reported them in papers during the past decade, I did not ask my laboratory members for putting the obtained information in the Flybrain database.

The same evaluation holds true for the potential external contributors of the digital atlas. Scientists generate a lot of data when writing a paper, but many of them are eventually not presented in the final publication. It is often proposed that such data, e.g., the screening data of the materials that are not used in the study and the experimental data that are not put in the final manuscript because they do not fit in the context of the paper, should be donated to databases so that other people can access them to avoid the duplication of work. This, however, is essentially unrealistic as a matter of practice. To publish papers in the competitive field of neuroscience, research should be performed as efficiently as possible, concentrating only to the things that are publishable. Screening is practiced to select promising materials and discard others as quickly as possible, not to document observations of all the materials examined. Spending any effort to prepare such unused data to make them accessible to other people is a waste of time and decreases the competitiveness of the research group. Preparation of data for papers and preparation of data for databases require different approaches and, in reality, often pose a conflict of interest.

It is an ironical situation that development of a new a database system and development of novel visualizing or data mining tools are regarded as scientific achievements, whereas adding concrete contents to the existing database is not. Though the latter is in principle considered as an important contribution, we have to accept the hard fact that such effort does not materialize in the form of a journal paper and that the activity of a person or a laboratory is measured primarily by the number of published papers, not the amount of the data put into databases.

Given this trend, the most effective way to help the carrier development of the laboratory members and to raise the chance of getting grants for the laboratory leaders is as follows: First, write a paper that reports the establishment of a new database or the development of a technical tool, with a minimum amount of raw data to show its functionality. Once the paper is published, it is not wise to spend time to add new contents to the database. Instead, it is much more rewarding to develop yet another database or tools to write a new paper, leaving the initial database untouched to let it become incomplete and obsolete. Though this may sound bizarre, it is the only strategy to generate the maximum number of papers per the effort of the laboratory members.

IMPORTANCE OF THE BIOCURATORS

In the previous section I explained the inherent problem that discourages paying due effort to add new contents to the databases once they are established and a paper announcing its development is published. Our new Flybrain Neuron Database[9] is trying to address a popular demand: providing information about all the known neurons of the *Drosophila* brain. A tremendous amount of work was necessary for extracting information from previous publications to make the core contents of the database. Because it is made as an entirely new database, a paper describing its system and possible application is publishable (Shinomiya et al., in preparation). If the contents had been put into the records of the existing classic Flybrain database instead of the new database, however, the effort could not be considered worthy of journal publication. Likewise, the effort for adding further information to the new Flybrain Neuron Database would hardly lead to another publication. It would be convenient, if such information could be sampled and imported to the atlas automatically by knowledge database software. However, as computers cannot read papers and write review articles by themselves, database records cannot be prepared automatically by computers. Human brain is required for the job.

If researchers cannot spend enough time for this very important task of adding new contents to the existing database, someone else have to do this. Contribution of the people called biocurators is vital in this respect (Howe et al., 2008; St Pierre and McQuilton, 2009). The curators originally mean the people who work in the

[9]http://ndb.flybrain.org/

museums to maintain the collections, prepare annotations to them, and collect new items to be exhibited. These are exactly what are needed for the online database.

Unlike technicians, biocurators are academic staffs, because they require specialized scientific knowledge about the collection they maintain. In case of the digital brain atlas, biocurators should have detailed knowledge about brain anatomy and computer technology. They will perform experiments to generate data that will be presented in the atlas database, and ask laboratory members to provide data that can be published in the database. They will then convert these data to the formats that can be distributed on the Internet. They will also read latest papers in the field and update relevant parts of the digital atlas to keep the documentation up to date. They will ask people of other laboratories to provide relevant data. If digital data are provided, biocurators will perform all the tasks for converting them to the form that can be put into the atlas, thereby minimizing the burden of the contributors. If raw samples or original drawings are provided, they will photograph or scan them. They may also scan the figures of old publications that have not been digitized. They will then put all these materials into database records with sufficient annotations. They will also design the database and develop navigation and visualization tools to optimize its function and usability. Such diverse tasks may not be performed by a single person. A team of biocurators with different types of expertise would often be required.

Large databases are employing such biocurators. For example, the FlyBase[10], a central database of *Drosophila* biology that collects all the data about genome sequences, known genes and molecules, and natural, mutant and transgenic strains, hires around 13 biocurators as of now (D. Sutherland, personal communication). Most of them are postdoctoral fellows with *Drosophila* background. These people not only gather and compile data to be incorporated into the database but also actively ask individual scientists of the community for providing information that is missing in their published materials. Without their contribution, the FlyBase cannot sustain its activity. The primary reason why FlyBase can successfully accumulate extensive data, in my view, is that it does not rely on the good intentions of external contributors but instead relies on the exhaustive efforts of its team of biocurators to actively collect information by itself.

Unfortunately, biocurators are often confused with competent technical staffs. Even laboratory leaders who conduct large-scale neuroscience projects often think that well-trained technicians will be sufficient for the job. Problem of such misappreciation will be clear, if we compare the people who are required for writing papers and for making digital atlases. In many cases, a scientific research to be published in papers cannot be conducted with only a laboratory head and technicians (**Figure 5A**). Active scientists such as postdoctoral fellows and senior PhD students make detailed research plans, gather information that is vital for the project from publications and fellow scientists, organize the work that should be performed by the technical staff and train them, perform key experiments to generate data for the paper, and write the draft of the manuscripts. Likewise, a digital atlas cannot be materialized if there are only a laboratory head and technical staff. Someone has to make detailed plans of the atlas, gather information that is vital for the database, organize the work that should be performed by the technical staff and train them, perform key experiments to generate data for the database, and write the documents of the database records (**Figure 5B**). The role of the biocurators is indeed comparable to that of scientists.

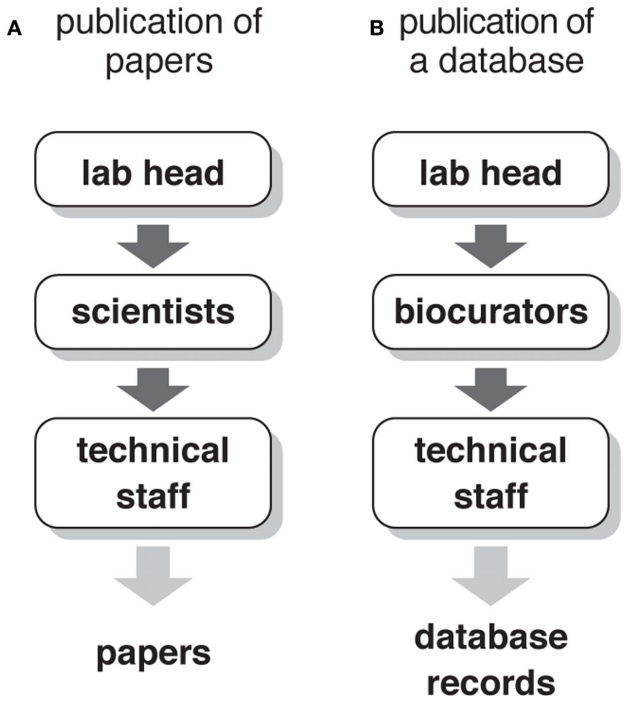

FIGURE 5 | Role of scientists and biocurators. (A) People who are involved in a publication of journal papers. Scientists (e.g., postdoctoral fellows and senior PhD students) play decisive roles in materializing the overall project envisaged by the laboratory head. Technical staff helps scientists but cannot by themselves complete the study for writing up the papers. **(B)** People who are involved in a publication of databases such as digital brain atlases. Biocurators perform the roles that are equivalent to that of scientists for writing papers. Without them, technical staff cannot complete the database.

Many brain databases including our Flybrain have not yet reached the state to finance such employee. However, contribution of the biocurators is indispensable for ensuring substantial and continuous addition of contents after the database is first launched. The role of the biocurators is especially decisive for the so-called "omics" projects. In case of the genome analysis, for example, the initial release of the *Drosophila* genome sequence was published in year 2000 (Adams et al., 2000) and attracted a broad interest, despite the fact that the data contained numerous gaps where sequencing was incomplete. These gaps are subsequently filled, and extensive annotation and association with other data have been continuously performed during the last entire decade. Though successive releases of improved genome data (now release 5.27) have been vital for the promotion of the fly genome science, few of these efforts were reported in the form of journal publications; refining previous data is not considered qualified as independent research papers. It is likely that the anatomical omics projects (e.g., projectome and connectome for documenting the entire neural projections

[10]http://flybase.org/

and connectivity, respectively; Sporns et al., 2005; Kasthuri and Lichtman, 2007; Seung, 2009) will also require extensive refining efforts after the announcement of their initial versions is published in journals. Hiring and training of expert biocurators are therefore keys to the success of such large-scale digital atlas projects.

A demanding problem in this respect is the difficulty of recruiting able person for the job. As explained above, the tasks of biocurators generally requires the scientific capability that is equivalent to that of the experienced postdoctoral fellows. Keeping track of newly published papers and incorporating relevant information to the database with adequate explanatory text requires the same level of academic capability as those for writing review articles or textbooks. In spite of this, they can hardly write papers by themselves, because the vast amount of their activity should be published in the form of database records. If they spend their time writing papers instead of database records, it conflicts with their expected duty. Therefore, the performance of the biocurators should never be measured by the number of their paper publications, but instead by the quality and quantity of the database they prepared. However, as discussed earlier such activity has not been receiving appreciation as scientists.

There will be two ways to address this apparent contradiction. A practical but passive approach is to look for the people who are trained as scientists but for some reason chose not to pursue the carrier. Because the number of people who obtain PhD degree largely exceeds the number of academic positions available each year, many people end up working as non-scientists. In addition, some researchers perform better compiling the data obtained by other people rather than doing experiments by themselves. The job of biocurators will become an attractive choice for such people, if it is possible to provide appropriate salary and future carrier path. The latter is especially important, because people would not want to jump into a job that does not offer the prospect until the age of retirement. A job market of the biocurators should be established, so that they can move from one database project to another depending on varying requirement of work force. Experienced biocurators should be awarded with higher salary and authority, so that there is enough incentive for personal development.

A more proactive approach is to change the way we evaluate scientific performance. It is in principle possible to integrate the job of biocurators in the academic carrier path: A student or postdoctoral fellow may work as a biocurator for several years and then becomes a senior postdoctoral fellow or professor after that. The task of an able biocurator may actually be more academic than some of the researchers who spend most of the time doing routine experiments. It is not fair that the latter type of people should be evaluated better simply because their results are published in the form of journal papers. Biocurators' task is in a manner similar to that of the principal investigators in that they may not spend their time in benches but compose documents based on the results of other laboratory members.

Until the twentieth century, most of the scientific information is provided in the form of books and papers. This is already a thing of the past. In the twenty-first century, databases serve as an equally important venue of publication as journals. In spite of this, we are yet to establish a suitable system to appreciate this type of scientific publication. It is not a matter of politicians and grant agencies but a matter of scientists ourselves. If peer reviewers of grant applications, search committees of faculty members, and individual principal investigators who look for their laboratory staff, change their attitudes to acknowledge the task of biocurators as an important aspect of scientific activity even though they do not publish papers, and regard them as fellow scientists rather than trained technicians, it would become easy to recruit competent biocurators who would add unprecedented functions and values to the digital atlases before they are promoted as an academic faculty personnel.

CONCLUSION

When we see cutting-edge visual databases like Google Earth, we tend to praise the technical achievements of the people who developed amazing database engines and visualization tools, but often forget about the people who made and provided the core contents of the database. Fancy map databases would make no sense without the data obtained through the quiet and persistent efforts of the people in the geographical survey institutes of each country. Development and maintenance of the digital brain atlases confront the same problem of this unconscious neglect to the unostentatious effort for generating core data. Even we ourselves, who work on the development of visual databases, tend to allocate more time and effort to develop and discuss techniques for manipulating data, assuming that the data themselves can be acquired somehow routinely. This is not the case. Whereas Google Earth can buy geographical data from mapping institutes, we have to generate the geographical data of the brain by ourselves. Systematic approach to enable the generation of consistent and unambiguous database records and organizational consideration to pay due appreciation to the effort of the people doing this task would be prerequisites to establish and maintain comprehensive digital brain atlases.

ACKNOWLEDGMENTS

I am grateful to David Osumi Sutherland of the FlyBase, Yoshiki Hotta of the Integrated Database Project, and Shiro Usui of the International Neuroinformatics Coordinating Facility Japan-node for discussion and providing information, and Karl-Friedrich Fischbach, Nicholas J. Strausfeld, J. D. Armstrong and late Kim Kaiser for the organization of and discussion about the Flybrain project.

REFERENCES

Adams, M. D., Celniker, S. E., Holt, R. A., Evans, C. A., Gocayne, J. D., Amanatides, P. G., Scherer, S. E., Li, P. W., Hoskins, R. A., Galle, R. F., George, R. A., Lewis, S. E., Richards, S., Ashburner, M., Henderson, S. N., Sutton, G. G., Wortman, J. R., Yandell, M. D., Zhang, Q., Chen, L. X., Brandon, R. C., Rogers, Y. H., Blazej, R. G., Champe, M., Pfeiffer, B. D., Wan, K. H., Doyle, C., Baxter, E. G., Helt, G., Nelson, C. R., Gabor Miklos, G. L., Abril, J. F., Agbayani, A., An, H. J., Andrews-Pfannkoch, C., Baldwin, D., Ballew, R. M., Basu, A., Baxendale, J., Bayraktaroglu, L., Beasley, E. M., Beeson, K. Y., Benos, P. V., Berman, B. P., Bhandari, D., Bolshakov, S., Borkova, D., Botchan, M. R., Bouck, J., Brokstein, P., Brottier, P., Burtis, K. C., Busam, D. A., Butler, H., Cadieu, E., Center, A., Chandra, I., Cherry, J. M., Cawley, S., Dahlke, C., Davenport, L. B., Davies, P., de Pablos, B., Delcher, A., Deng, Z., Mays, A. D., Dew, I., Dietz, S. M., Dodson, K., Doup, L. E., Downes, M., Dugan-Rocha, S., Dunkov, B. C., Dunn, P., Durbin, K. J., Evangelista, C. C., Ferraz, C., Ferriera, S., Fleischmann, W., Fosler, C., Gabrielian, A. E., Garg, N. S., Gelbart, W. M., Glasser, K., Glodek, A., Gong, F., Gorrell, J. H., Gu, Z., Guan, P., Harris, M., Harris, N. L., Harvey, D., Heiman, T. J., Hernandez, J. R., Houck, J., Hostin, D., Houston,

K. A., Howland, T. J., Wei, M. H., and Ibegwam, C. (2000). The genome sequence of *Drosophila melanogaster*. *Science* 287, 2185–2195.

Armstrong, J. D., Kaiser, K., Müller, A., Fischbach, K. -F., Merchant, N., and Strausfeld, N. J. (1995). Flybrain, an on-line atlas and database of the *Drosophila* nervous system. *Neuron* 15, 17–20.

Armstrong, J. D., and van Hemert, J. I. (2009). Towards a virtual fly brain. *Philos. Transact. A Math Phys. Eng. Sci.* 367, 2387–2397.

Ascoli, G. A., Donohue, D. E., and Halavi, M. (2007). NeuroMorpho.org: a central resource for neuronal morphologies. *J. Neurosci.* 27, 9247–9251.

Bjaalie, J. G., and Grillner, S. (2007). Global neuroinformatics: the International Neuroinformatics Coordinating Facility. *J. Neurosci.* 27, 3613–3615.

Brandt, R., Rohlfing, T., Rybak, J., Krofczik, S., Maye, A., Westerhoff, M., Hege, H. C., and Menzel, R. (2005). Three-dimensional average-shape atlas of the honeybee brain and its applications. *J. Comp. Neurol.* 492, 1–19.

De Schutter, E. (2009). The International Neuroinformatics Coordinating Facility: evaluating the first years. *Neuroinformatics* 7, 161–163.

Dreyer, D., Vitt, H., Dippel, S., Goetz, B., El Jundi, B., Kollmann, M., Huetteroth, W., and Schachtner, J. (2010). 3D standard brain of the red flour beetle *Tribolium castaneum*: a tool to study metamorphic development and adult plasticity. *Front. Syst. Neurosci.* 4, 3. doi:10.3389/neuro.06.003.2010.

El Jundi, B., Heinze, S., Lenschow, C., Kurylas, A., Rohlfing, T., and Homberg, U. (2009a). The locust standard brain: a 3D standard of the central complex as a platform for neural network analysis. *Front. Syst. Neurosci.* 3, 21. doi: 10.3389/neuro.06.021.2009.

El Jundi, B., Huetteroth, W., Kurylas, A. E., and Schachtner, J. (2009b). Anisometric brain dimorphism revisited: Implementation of a volumetric 3D standard brain in *Manduca sexta*. *J. Comp. Neurol.* 517, 210–225.

Fischbach, K. F., and Dittrich, A. P. M. (1989). The optic lobe of *Drosophila melanogaster*. – I. a golgi analysis of wild-type structure. *Cell Tissue Res.* 258, 441–475.

Franklin, K. B. J., and Paxinos, G. (2008). *The Mouse Brain in Stereotaxic Coordinates,* 3rd edn. San Diego, CA: Academic Press.

Guetat, G., Maitre, M., Joly, L., Lai, S. L., Lee, T., and Shinagawa, Y. (2006). Automatic 3-D grayscale volume matching and shape analysis. *IEEE Trans. Inf. Technol. Biomed.* 10, 362–376.

Halavi, M., Polavaram, S., Donohue, D. E., Hamilton, G., Hoyt, J., Smith, K. P., and Ascoli, G. A. (2008). NeuroMorpho.org implementation of digital neuroscience: dense coverage and integration with the NIF. *Neuroinformatics* 6, 241–252.

Hanesch, U., Fischbach, K. F., and Heisenberg, M. (1989). Neuronal architecture of the central complex in *Drosophila melanogaster*. *Cell Tissue Res.* 257, 343–366.

Howe, D., Costanzo, M., Fey, P., Gojobori, T., Hannick, L., Hide, W., Hill, D. P., Kania, R., Schaeffer, M., Pierre, S. S., Twigger, S., White, O., and Rhee, S. Y. (2008). Big data: The future of biocuration. *Nature* 455, 47–50.

Huetteroth, W., El Jundi, B., El Jundi, S., and Schachtner, J. (2010). 3D-reconstructions and virtual 4D-visualization to study metamorphic brain development in the sphinx moth *Manduca sexta*. *Front. Syst. Neurosci.* 4, 7. doi:10.3389/fnsys.2010.00007.

Jahrling, N., Becker, K., Schonbauer, C., Schnorrer, F., and Dodt, H. U. (2010). Three-dimensional reconstruction and segmentation of intact *Drosophila* by ultramicroscopy. *Front. Syst. Neurosci.* 4, 1. doi:10.3389/neuro.06.001.2010.

Jefferis, G. S., Potter, C. J., Chan, A. M., Marin, E. C., Rohlfing, T., Maurer, C. R., Jr., and Luo, L. (2007). Comprehensive maps of *Drosophila* higher olfactory centers: spatially segregated fruit and pheromone representation. *Cell* 128, 1187–1203.

Jenett, A., Schindelin, J. E., and Heisenberg, M. (2006). The virtual insect brain protocol: creating and comparing standardized neuroanatomy. *BMC Bioinformatics* 7, 544.

Kasthuri, N., and Lichtman, J. W. (2007). The rise of the 'projectome'. *Nat. Methods* 4, 307–308.

Katz, P. S., Calin-Jageman, R., Dhawan, A., Frederick, C., Guo, S., Dissanayaka, R., Hiremath, N., Ma, W., Shen, X., Wang, H. C., Yang, H., Prasad, S., Sunderraman, R., and Zhu, Y. (2010). NeuronBank: a tool for cataloging neuronal circuitry. *Front. Syst. Neurosci.* 4, 9. doi:10.3389/fnsys.2010.00009.

Kurylas, A. E., Rohlfing, T., Krofczik, S., Jenett, A., and Homberg, U. (2008). Standardized atlas of the brain of the desert locust, *Schistocerca gregaria*. *Cell Tissue Res.* 333, 125–145.

Kvello, P., Lofaldli, B. B., Rybak, J., Menzel, R., and Mustaparta, H. (2009). Digital, three-dimensional average shaped atlas of the *Heliothis virescens* brain with integrated gustatory and olfactory neurons. *Front. Syst. Neurosci.* 3, 14. doi:10.3389/neuro.06.014.2009.

Laissue, P. P., Reiter, C., Hiesinger, P. R., Halter, S., Fischbach, K. F., and Stocker, R. F. (1999). Three-dimensional reconstruction of the antennal lobe in *Drosophila melanogaster*. *J. Comp. Neurol.* 405, 543–552.

Lein, E. S., Hawrylycz, M. J., Ao, N., Ayres, M., Bensinger, A., Bernard, A., Boe, A. F., Boguski, M. S., Brockway, K. S., Byrnes, E. J., Chen, L., Chen, T. M., Chin, M. C., Chong, J., Crook, B. E., Czaplinska, A., Dang, C. N., Datta, S., Dee, N. R., Desaki, A. L., Desta, T., Diep, E., Dolbeare, T. A., Donelan, M. J., Dong, H. W., Dougherty, J. G., Duncan, B. J., Ebbert, A. J., Eichele, G., Estin, L. K., Faber, C., Facer, B. A., Fields, R., Fischer, S. R., Fliss, T. P., Frensley, C., Gates, S. N., Glattfelder, K. J., Halverson, K. R., Hart, M. R., Hohmann, J. G., Howell, M. P., Jeung, D. P., Johnson, R. A., Karr, P. T., Kawal, R., Kidney, J. M., Knapik, R. H., Kuan, C. L., Lake, J. H., Laramee, A. R., Larsen, K. D., Lau, C., Lemon, T. A., Liang, A. J., Liu, Y., Luong, L. T., Michaels, J., Morgan, J. J., Morgan, R. J., Mortrud, M. T., Mosqueda, N. F., Ng, L. L., Ng, R., Orta, G. J., Overly, C. C., Pak, T. H., Parry, S. E., Pathak, S. D., Pearson, O. C., Puchalski, R. B., Riley, Z. L., Rockett, H. R., Rowland, S. A., Royall, J. J., Ruiz, M. J., Sarno, N. R., Schaffnit, K., Shapovalova, N. V., Sivisay, T., Slaughterbeck, C. R., Smith, S. C., Smith, K. A., Smith, B. I., Sodt, A. J., Stewart, N. N., Stumpf, K. R., Sunkin, S. M., Sutram, M., Tam, A., Teemer, C. D., Thaller, C., Thompson, C. L., Varnam, L. R., Visel, A., Whitlock, R. M., Wohnoutka, P. E., Wolkey, C. K., Wong, V. Y., Wood, M., Yaylaoglu, M. B., Young, R. C., Youngstrom, B. L., Yuan, X. F., Zhang, B., Zwingman, T. A., and Jones, A. R. (2007). Genome-wide atlas of gene expression in the adult mouse brain. *Nature* 445, 168–176.

Livneh, Y., and Mizrahi, A. (2010). A time for atlases and atlases for time. *Front. Syst. Neurosci.* 3, 17. doi:10.3389/neuro.06.017.2009.

Lofaldli, B. B., Kvello, P., and Mustaparta, H. (2010). Integration of the antennal lobe glomeruli and three projection neurons in the standard brain atlas of the moth *Heliothis virescens*. *Front. Syst. Neurosci.* 4, 5. doi:10.3389/neuro.06.005.2010.

Ma, Y., Hof, P. R., Grant, S. C., Blackband, S. J., Bennett, R., Slatest, L., McGuigan, M. D., and Benveniste, H. (2005). A three-dimensional digital atlas database of the adult C57BL/6J mouse brain by magnetic resonance microscopy. *Neuroscience* 135, 1203–1215.

Mai, J. K., Assheuer, J. K., and Paxinos, G. (2004). *Atlas of the Human Brain,* 2nd edn. San Diego, CA: Academic Press.

Markram, H. (2006). The blue brain project. *Nat. Rev. Neurosci.* 7, 153–160.

Mikula, S., Stone, J. M., and Jones, E. G. (2008). BrainMaps.org – Interactive high-resolution digital brain atlases and virtual microscopy. *Brains Minds Media* 3, bmm1426.

Otsuna, H., and Ito, K. (2006). Systematic analysis of the visual projection neurons of *Drosophila melanogaster.* I. Lobula-specific pathways. *J. Comp. Neurol.* 497, 928–958.

Paxinos, G., and Watson, C. (2005). *The Rat Brain in Stereotaxic Coordinates – The New Coronal Set,* 5th edn. San Diego, CA: Academic Press.

Peng, H., Ruan, Z., Long, F., Simpson, J., and Myers, E. (2010). V3D enables real-time 3D visualization and quantitative analysis of large-scale biological image data sets. *Nat. Biotechnol.* 28, 348–353.

Poirier, C., Vellema, M., Verhoye, M., Van Meir, V., Wild, J. M., Balthazart, J., and Van Der Linden, A. (2008). A three-dimensional MRI atlas of the zebra finch brain in stereotaxic coordinates. *Neuroimage* 41, 1–6.

Puelles, L., Martinez-de-la-Torre, M., Paxinos, G., Watson, C., and Martinez, S. (2007). *The Chick Brain in Stereotaxic Coordinates: An Atlas Featuring Neuromeric Subdivisions and Mammalian Homologies*. San Diego, CA: Academic Press.

Rein, K., Zockler, M., Mader, M. T., Grubel, C., and Heisenberg, M. (2002). The *Drosophila* standard brain. *Curr. Biol.* 12, 227–231.

Reiner, A., Perkel, D. J., Bruce, L. L., Butler, A. B., Csillag, A., Kuenzel, W., Medina, L., Paxinos, G., Shimizu, T., Striedter, G., Wild, M., Ball, G. F., Durand, S., Gunturkun, O., Lee, D. W., Mello, C. V., Powers, A., White, S. A., Hough, G., Kubikova, L., Smulders, T. V., Wada, K., Dugas-Ford, J., Husband, S., Yamamoto, K., Yu, J., Siang, C., and Jarvis, E. D. (2004a). Revised nomenclature for avian telencephalon and some related brainstem nuclei. *J. Comp. Neurol.* 473, 377–414.

Reiner, A., Perkel, D. J., Bruce, L. L., Butler, A. B., Csillag, A., Kuenzel, W., Medina, L., Paxinos, G., Shimizu, T., Striedter, G., Wild, M., Ball, G. F., Durand, S., Guturkun, O., Lee, D. W., Mello, C. V., Powers, A., White, S. A., Hough, G., Kubikova, L., Smulders, T. V., Wada, K., Dugas-Ford, J., Husband, S., Yamamoto, K., Yu, J., Siang, C., and Jarvis, E. D. (2004b). The avian brain nomenclature forum: terminology for a new century in comparative neuroanatomy. *J. Comp. Neurol.* 473, E1–E6.

Schambra, U. (2008). *Prenatal Mouse Brain Atlas*. New York, NY: Springer.

Seung, H. S. (2009). Reading the book of memory: sparse sampling versus dense

mapping of connectomes. *Neuron* 62, 17–29.
Sporns, O., Tononi, G., and Kotter, R. (2005). The human connectome: a structural description of the human brain. *PLoS Comput. Biol.* 1, e42. doi:10.1371/journal.pcbi.0010042.
St Pierre, S., and McQuilton, P. (2009). Inside FlyBase: biocuration as a career. *Fly (Austin)* 3, 112–114.
Strausfeld, N. J. (1976). *Atlas of an Insect Brain.* Berlin: Springer-Verlag.
Tanaka, N. K., Awasaki, T., Shimada, T., and Ito, K. (2004). Integration of chemosensory pathways in the *Drosophila* second-order olfactory centers. *Curr. Biol.* 14, 449–457.
Tanaka, N. K., Tanimoto, H., and Ito, K. (2008). Neuronal assemblies of the *Drosophila* mushroom body. *J. Comp. Neurol.* 508, 711–755.
Toga, A. W., and Thompson, P. M. (2001). Maps of the brain. *Anat. Rec.* 265, 37–53.
Tokuno, H., Tanaka, I., Umitsu, Y., Akazawa, T., and Nakamura, Y. (2009). Web-accessible digital brain atlas of the common marmoset (*Callithrix jacchus*). *Neurosci. Res.* 64, 128–131.
Valverde, F. (1998). *Golgi Atlas of the Postnatal Mouse Brain.* Wien: Springer-Verlag.
Van Essen, D. C. (2002). Windows on the brain: the emerging role of atlases and databases in neuroscience. *Curr. Opin. Neurobiol.* 12, 574–579.
Van Horn, J. D., and Toga, A. W. (2009). Is it time to re-prioritize neuroimaging databases and digital repositories? *Neuroimage* 47, 1720–1734.
Woolsey, T. A., Hanaway, J., and Gado, M. H. (2003). *The Brain Atlas: A Visual Guide to the Human Central Nervous System*, 2nd edn. Hoboken, NK: John Wiley & Sons.
Wullimann, M. F., Rupp, B., and Reichert, H. (1996). *Neuroanatomy of the Zebrafish Brain: A Topological Atlas.* Basel: Birkhäuser.
Yap, P. T., Wu, G., Zhu, H., Lin, W., and Shen, D. (2009). TIMER: tensor image morphing for elastic registration. Neuroimage *47*, 549–563.

Conflict of Interest Statement: The author declares that the research was conducted in the absence of any commercial or financial relationships that could be construed as a potential conflict of interest.

Received: 28 December 2009; paper pending published: 30 January 2010; accepted: 31 May 2010; published online: 18 June 2010. Citation: Ito K (2010) Technical and organizational considerations for the long-term maintenance and development of the digital brain atlases and web-based databases. Front. Syst. Neurosci. ***4****:26. doi: 10.3389/fnsys.2010.00026*

frontiers in
SYSTEMS NEUROSCIENCE

REVIEW ARTICLE
published: 22 February 2010
doi: 10.3389/neuro.06.017.2009

A time for atlases and atlases for time

Yoav Livneh[1] and Adi Mizrahi[1,2]*

[1] *Department of Neurobiology, The Alexander Silberman Institute of Life Sciences, The Hebrew University of Jerusalem, Jerusalem, Israel*
[2] *Institute for Life Sciences and Interdisciplinary Center for Neural Computation, The Hebrew University of Jerusalem, Jerusalem, Israel*

Edited by:
Randolf Menzel, Freie Universität Berlin, Germany

Reviewed by:
Jürgen Rybak, Max Planck Institute for Chemical Ecology, Germany
Alexander Borst, Max Planck Institute of Neurobiology, Germany
Randolf Menzel, Freie Universität Berlin, Germany

***Correspondence:**
Adi Mizrahi, Department of Neurobiology, Room 3-223, The Alexander Silberman Inst. of Life Sciences, The Hebrew University of Jerusalem, Edmond J. Safra Campus, Givat Ram, Jerusalem, 91904, Israel.
e-mail: mizrahia@cc.huji.ac.il

Advances in neuroanatomy and computational power are leading to the construction of new digital brain atlases. Atlases are rising as indispensable tools for comparing anatomical data as well as being stimulators of new hypotheses and experimental designs. Brain atlases describe nervous systems which are inherently plastic and variable. Thus, the levels of brain plasticity and stereotypy would be important to evaluate as limiting factors in the context of static brain atlases. In this review, we discuss the extent of structural changes which neurons undergo over time, and how these changes would impact the static nature of atlases. We describe the anatomical stereotypy between neurons of the same type, highlighting the differences between invertebrates and vertebrates. We review some recent experimental advances in our understanding of anatomical dynamics in adult neural circuits, and how these are modulated by the organism's experience. In this respect, we discuss some analogies between brain atlases and the sequenced genome and the emerging epigenome. We argue that variability and plasticity of neurons are substantially high, and should thus be considered as integral features of high-resolution digital brain atlases.

Keywords: brain atlas, stereotypy, *in vivo* imaging, structural plasticity, experience-dependent plasticity, genome, epigenome

INTRODUCTION

Since the days of Ramón y Cajal, it was clearly demonstrated that neurons come in different "flavors". Each neuron within a local circuit may look and function differently even when the neurons are closely packed together. Today we know that differences are evident at almost any scale and any level, ranging from gene expression profiles to the structure of dendritic and axonal arbors. Because it is still not technically possible to study all neurons within a tissue simultaneously, we are subjected to study one or a few neurons at a time in different animals. Since neurons are different, the issue of variability arises. This problem becomes even greater when comparisons are made across studies and across laboratories. To date, there is no common reference frame, and detailed experimental data are rarely shared for purposes of comprehensive comparisons. Therefore, it is desirable to have a shared atlas based on experimental data. When such atlases become available, they could provide a road map for comparative studies across brain regions and species.

In anatomical terms, a new atlas means reviving Cajal's efforts with modern tools, but now taking into consideration not only the two-dimensional dendritic and axonal structures but possibly molecular signatures (Lein et al., 2007), and even complete synaptic connectivity patterns (Lichtman et al., 2008). Furthermore, atlases containing shared data from many research groups would allow in-depth morphological analysis, which could shed light on the relation between arbor structure and function (see e.g., Wen et al., 2009). Indeed, in the past few years there have been a number of efforts to construct high-resolution brain atlases of standardized brains of invertebrates (see e.g., Rein et al., 2002; Brandt et al., 2005; Kurylas et al., 2008). A similar effort has been extremely successful in genetics where the "master atlas" of our era, the genome, has been comprehensively mapped and sequenced. In analogy to the genome, it would then be possible to search the atlas for any combination of axonal projection patterns and/or dendritic arborization of one's favorite neuron. Atlases would not only prompt higher quality data but would be a valuable tool for stimulating new hypotheses and experimental designs.

What should a brain atlas contain? What are the main challenges that arise from the numerous degrees of freedom making up brain circuits? Here, we discuss some advantages and limitations of such futuristic atlases. Specifically, we focus on the limitations imposed by stereotypy and structural plasticity in mature brains and discuss to what extent these would affect future brain atlases of invertebrates and vertebrates alike. We limit our discussion to mature nervous systems. A discussion of atlases in the context of ontogenetic development is equally beneficial (see e.g., Huetteroth et al., also in this issue), however, given space considerations it is out of the scope of this review.

ATLASES AND NEURONAL STEREOTYPY

Several sources of variability call for consideration in future atlases; namely, those arising from inter-neuronal variability within an animal and those arising from inter-animal variability between neurons of the same type. Inter-animal variability has been quantified most powerfully in invertebrates where neurons can be identified individually. One of the first quantitative anatomical reports was carried out on visual neurons of the small crustacean *Daphnia magna* (Macagno et al., 1973). These authors reconstructed axonal projections of identified neurons and revealed that their gross anatomical features are reproducible but that finer details are not. Since then, numerous studies have reported similar observations in a variety of species, using better staining methods and more powerful analytical tools (Mizrahi et al., 2000; Marin et al., 2002; Wong et al.,

2002). In numerous invertebrate systems (e.g. cockroaches, crickets, flies, leeches and honeybees) single neurons can be identified anatomically with relative ease (Coggeshall and Fawcett, 1964; Daley et al., 1981; Johansen et al., 1989; Bodnar et al., 1991; Hammer and Menzel, 1995). Notably, however, anatomical identity may not be generally applicable to all invertebrate species. For example, in the lobster *Panulirus Interruptus* some electrophysiologically identified neurons could not be identified morphologically (Thuma et al., 2009).

What exactly is variable between the morphology of different identified neurons? Quantitative analysis of identified neurons has revealed substantial variations in high-order dendritic and axonal branching patterns, whereas a neuron's morphological identity is based primarily on its low-order or primary branching pattern (Mizrahi et al., 2000). In line with those observations, a rigorous analysis of insect neurons recently showed that anatomical identity is determined by the neuropile area covered by the neurites, and not by the complete branching topology (**Figures 1A,B**; Cuntz et al., 2008). A similar principle might also apply to vertebrate neurons of the same type, but this has not been quantified (see e.g., hippocampal CA1 pyramidal neurons; **Figure 1C**). In the context of atlases, the gross area of neuronal arborization may be used to infer (or reject) potential synaptic partners and possible functions. However, based on projection patterns alone, one cannot deduce either the function or the precise synaptic connectivity patterns of a network with any certainty. To study synaptic connectivity or function, higher resolution methods, such as electron microscopy and/or electrophysiology should be used. This is a major limitation of anatomical atlases which will be hard to overcome.

In vertebrates, and specifically in mammals, the precise nature of stereotypy, variability and synaptic specificity is not known. In principle, stereotypy and variability could have been empirically measured using a similar logic to that used in invertebrate identified neurons. However, unlike invertebrates, there are no known "identified neurons" in the vertebrate CNS as each neuronal subtype may have at least dozens to hundreds of replicas in the circuit (with a known exception – the "Mauthner neurons" in fish; Zottoli, 1978). Moreover, in mammals there is still no consensus on basic anatomical features such as cell numbers, borders between brain regions, cell types and cell subtypes (Bota et al., 2003). Thus, it would be hard to provide compelling statistical evidence for stereotypy and variability in mammalian neurons based on sparse sampling and datasets that might not be composed of homogenous populations of cells. Accordingly, welcome efforts are now underway to establish widely approved classification criteria for defining neuronal subtypes based on anatomical, physiological and molecular characteristics (e.g., Ascoli et al., 2008). These efforts are paving the way for community-approved definitions of vertebrate neuronal subtypes, which would be highly beneficial for future vertebrate brain atlases.

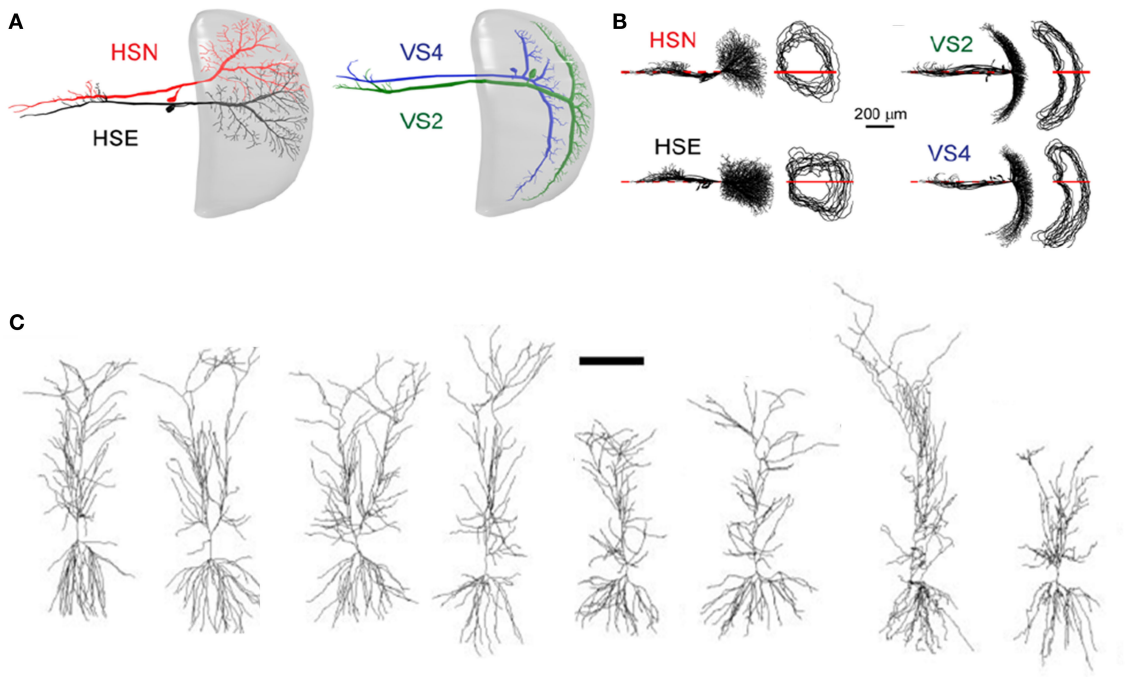

FIGURE 1 | Structural stereotypy in invertebrate and vertebrate neurons. **(A,B)** Identified neurons in the fly visual system. **(A)** Reconstructions of different types of lobula plate tangential cells from the blowfly (HSE, HSN, VS2 and VS4) within the lobula plate (gray). **(B)** Left: Neuronal reconstructions of identified neurons superimposed and sorted according to their cell type. Cells were aligned along their axonal axis (red lines). Right: the corresponding dendrite spanning fields of the reconstructed neurons. Neuronal anatomical identity is determined by the neuropile area that is covered by the neurites, and not by the complete branching topology. **(C)** Qualitative anatomical stereotypy in vertebrate neurons. Reconstructions of eight rat hippocampal CA1 pyramidal cells. Note that the gross field covered by the neurites exhibits a similar trend in all eight neurons. Stereotypy seems to be less robust as compared to invertebrate identified neurons. Scale bar: 200 µm. Panels **(A,B)** are adapted from Cuntz et al. (2008), with permission. Panel **(C)** is adapted from Scorcioni et al. (2004), with permission.

An even more challenging issue is to determine synaptic connectivity patterns between neurons, and include these in atlases. Due to lack of resolution, it is currently impossible to determine the existence of synapses between sets of neurons based on their neurite morphology. The most adequate anatomical method that can show synaptic connectivity is electron microscopy (EM). Recently developed methods, such as "array tomography", are now also providing new tools for exploring the interface between molecular signatures and synaptic connectivity (Micheva and Smith, 2007).

Current efforts, which focus on using EM, are now underway to study synaptic connectivity in dense, highly interconnected, neural tissue. Specifically, EM sampling techniques are being designed to reconstruct "everything" (but primarily synapses) within a volume of tissue (Denk and Horstmann, 2004; see also the early work of Brenner and colleagues on *c.elegans*, by Ward et al., 1975, and the more recent work on *c.elegans* by Chklovskii and colleagues, Chen et al., 2006). This effort has been termed "connectomics" and dares to the challenges imposed by the complexity of the nervous system. There is no doubt that even optimistic connectomists still face serious technical and computational challenges for reconstructing the mammalian connectome. But once these are overcome, the connectome is expected to provide direct empirical data and finite numbers on issues such as inter-animal variability and the level of synaptic specificity in large neural circuits (Lichtman and Sanes, 2008).

Recently, the first connectome in mammals has been solved (the *intermuscularis* muscle connectome in mice; Lu et al., 2009). Notably, this peripheral nervous system connectome was solved by light microscopy rather than by EM (which was possible due to the large size of neuromuscular synapses). Motor units from the same or different animals were compared and an unexpectedly large variability was revealed. Motor unit connectomes from the left and right sides of the same individual were not less different than connectomes of different individuals. This result points to what might be a fundamental difference in organization principles between vertebrate and invertebrate identified neurons (e.g., compare to Goodman, 1978; Mizrahi et al., 2000). In addition, if we assume that the peripheral nervous system represents a more rigid system than the CNS, then connectome variability in the CNS (which is still not known) is expected to be even higher. These results imply that the nervous system in mammals is not as genetically "hard-wired" as it might seem in invertebrates (Bentley, 1975) and may rely on different organization principles during development, and/or adulthood. The mechanisms underlying higher variability in mammalian systems are not clear. While the basic cellular principles of experience-dependent plasticity are not necessarily different in vertebrates and invertebrates, speculatively, experience-dependent plasticity may play a more dominant role in synapse formation in adult mammals, as compared to invertebrates. In this respect, there is still no compelling evidence for mammalian "identified neurons". Thus, anatomical atlases of mammalian species should include multiple examples of each individual neuron they attempt to describe; certainly more than would be needed in invertebrate atlases. Otherwise, the atlas would not be much more useful than any isolated anatomical reference.

ATLASES IN FACE OF STRUCTURAL PLASTICITY

An atlas is a highly useful tool for describing a stereotypical, static system but might not be as useful for highly variable, dynamic systems. The more variable and dynamic the system is, the less likely an atlas will recapitulate it faithfully. Therefore, the extent to which the brain is structurally stereotyped and static determines the constraints and general validity of brain atlases. In biology, neurons stand out in their significant capacity to change and adapt; a capacity usually referred to as "plasticity". There is ample evidence for physiological plasticity. Synapses can potentiate within minutes (Madison et al., 1991; Zucker and Regehr, 2002), receptive fields can rapidly change (Dorris et al., 2000; Gandolfo et al., 2000; Fritz et al., 2003; Geffen et al., 2007) and firing patterns of the same neuronal subtype are rarely the same. On longer time scales (hours to days), neuronal structure is also dynamic (Bhatt et al., 2009). To what extent can we predict one brain from the next in such an ever-changing system? Is structural plasticity an Achilles Heel for brain atlases?

Direct evidence for the degree of structural dynamics is continuously emerging in the last decade, mainly due to advances in genetic labeling and imaging techniques (Young and Feng, 2004). The first studies became possible with the development of the "*thy-1* XFP" transgenic mice (Feng et al., 2000). These publicly available mice have fluorescently labeled neurons that are sparsely scattered throughout the brain and are bright enough so that they could be readily imaged *in vivo*. *In vivo* time-lapse measurements are the experiments of choice for studying structural plasticity since they minimize variability. In principal, digital brain atlases, would be based on averaging across several specimens and across time. Thus, it is possible that many discoveries regarding experience dependant plasticity would still rely on revealing deviations from this average. In this context, the advantage of *in vivo* time-lapse experiments is that they eliminate some of the inter-individual variation discussed above. This allows the detection of smaller, yet significant, changes. Actually, before the era of *in vivo* time-lapse imaging, experimentally explored structural plasticity was limited to large-scale changes (see e.g., Woolley, 1999), missing some of the more subtle differences that are currently being unveiled.

Two papers, using *in vivo* time-lapse imaging, by Trachtenberg et al. (2002) and Grutzendler et al. (2002) prompted a series of experiments that started to reveal the extent of structural plasticity in mature brains in more detail. To date, almost all the available data regarding structural dynamics (at least in mature brains) have been obtained from mammals and particularly from mice (Holtmaat and Svoboda, 2009).

STRUCTURAL STABILITY OF DENDRITES AND AXONS

One consistent observation is that neurites of adult projection neurons are largely stable. In both neocortical pyramidal neurons and olfactory bulb mitral cells only negligible changes were found in dendritic structure over periods of weeks (Grutzendler et al., 2002; Trachtenberg et al., 2002; Mizrahi and Katz, 2003). But unlike projection neurons, neocortical interneurons exhibit structural changes at rates of ~15% over several weeks (Lee et al., 2006). This level of structural plasticity is evident only at specific laminae, suggesting that both the brain region and the cell-type may determine the levels of structural plasticity (Lee et al., 2008). One extreme

example of structural plasticity of dendrites comes from our work on adult-born periglomerular interneurons in the olfactory bulb. Periglomerular interneurons show high levels of dendritic structural plasticity reaching up to 40% per week (**Figure 2A**; Mizrahi, 2007). Notably however, periglomerular interneurons are unique neurons as they are born during adulthood, and are thus relatively immature compared to most other neurons in the brain.

In mammals, axons are thinner than dendrites and more difficult to follow *in vivo*. The few studies that followed axonal morphology over time found that axons are also largely stable. Specifically, time-lapse experiments revealed only ~4% of *de novo* branch formation or elimination per month, with ~25–60% of the branches that exhibited short distance (few micrometers) elongation and/or retraction per month (De Paola et al., 2006). Interestingly, like dendritic dynamics, axonal dynamics vary as a function of cell-type (e.g., thalamocortical axons are less dynamic than intracortical axons; De Paola et al., 2006; Stettler et al., 2006). Together, these results suggest that the extent of dendritic and axonal plasticity varies across cell-types, and should thus be tested for each neuronal population separately.

STRUCTURAL PLASTICITY OF SYNAPSES

In contrast to the relative stability of dendrites and axons, dendritic spines are far more plastic structures (**Figure 2B**). Since new spines are a good approximation of synapses (Knott et al., 2006), this suggests that synaptic connectivity within the mammalian CNS is in an ongoing state of change (Trachtenberg et al., 2002; Zuo et al., 2005; Hofer et al., 2009). Structural plasticity of spines under normal conditions can reach up to 50% per week (Trachtenberg et al., 2002). Interestingly, dendritic spine dynamics also differ between different cell-types and brain regions. For example, in the barrel cortex, the spines of L2/3 pyramidal neurons are less dynamic than those of L5 neurons. L5 pyramidal neurons in the barrel cortex are also more dynamic than L5 pyramidal neurons in the visual

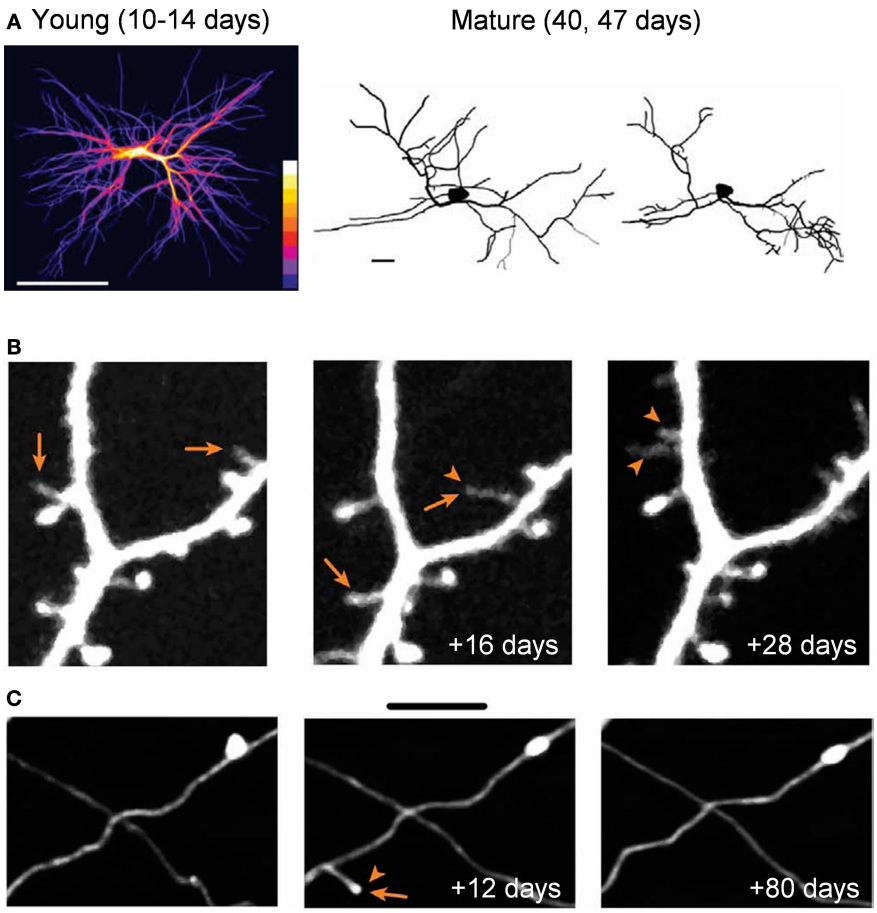

FIGURE 2 | Structural plasticity in the adult mammalian brain. (A) *In vivo* dendritic structural plasticity of adult-born periglomerular interneurons. Left panel: average intensity projection image of 9 imaging sessions of the same developing periglomerular neuron (12 h apart). The color scale bar indicates how many times a dendritic branch was located in a given region (from 1 to 9). Bright colors represent stable dendrites, and dark colors represent dynamic dendrites. Right panel: reconstructions of a mature periglomerular neuron, imaged 7 days apart. Both developing and mature periglomerular neurons exhibit extensive dendritic dynamics. Scale bars: 50 and 10 μm (left and right panel, respectively). **(B,C)** Images from *in vivo* time lapse imaging of dendritic spines **(B)** and axons **(C)** from the neocortex. The images are examples of the same dendritic and axonal segments that were imaged up to 28 or 80 days apart. Note both the addition (arrowhead) and loss (arrows) of dendritic spines **(B)** and axonal segments **(C)**. Scale bars: 5 μm. Panel **(A)** is adapted from Mizrahi (2007), with permission. Panels **(B,C)** are adapted from Holtmaat et al. (2009), with permission.

cortex (Holtmaat et al., 2005). This idea has received additional support from experiments, in which rewiring visual input to the auditory cortex at birth failed to alter dendritic spine dynamics (Majewska et al., 2006). Presynaptic boutons, which are also used as an approximation of synapses, were also found to exhibit cell-type specific dynamics (up to 50% turnover per month; **Figure 2C**; De Paola et al., 2006), further supporting the existence of ongoing changes in CNS synaptic connectivity. Notably, structural dynamics are homeostatically regulated such that the overall morphology is kept constant (e.g., total dendritic branch length, spine density; Trachtenberg et al., 2002; Mizrahi, 2007). This homeostasis might bear functional significance (Samsonovich and Ascoli, 2006).

Structural dynamics may have direct implications on the attempts to reconstruct connectomes (and atlases; see also below). If structural dynamics reflect changes in neuronal connectivity, rather than just strengthening/weakening of synapses between previously connected neurons, then connectomes are also expected to be dynamic. While this issue remains unclear, it might well be that several connectomes would need to be constructed before synaptic connectivity patterns could be inferred with "connectomic precision".

EXPERIENCE-DEPENDENT STRUCTURAL PLASTICITY

The studies discussed above were made with mice housed under normal housing conditions. This prompts the question of whether and how experience might affect structural plasticity. Indeed, several studies have explored this relationship, mainly in primary sensory areas such as the mouse barrel cortex, visual cortex and olfactory bulb (Trachtenberg et al., 2002; Mizrahi and Katz, 2003; Zuo et al., 2005; Mizrahi, 2007; Livneh et al., 2009). In one extreme case, Keck et al. (2008) recently showed that a focal retinal lesion leads to a dramatic increase in spine turnover rate in the visual cortex. Remarkably, within 2 months following the lesion, an almost complete replacement of spines was observed. In a similar study from the same group, Hofer et al. (2009) explored the structural correlates of ocular dominance plasticity (Hubel et al., 1977). In the adult, after the closure of all known developmental critical periods, binocular neurons remain plastic in response to a second monocular deprivation. This occurs only if the animal had previously underwent a first monocular deprivation when it was younger, during the relevant developmental critical period (Hofer et al., 2006). To continue this work, Hofer et al. (2009) correlated these functional changes with the addition of new persistent spines, which may provide the structural changes required for subsequent functional shifts (Hofer et al., 2009). Similarly, functional changes in the barrel cortex due to whisker trimming have also been shown to be correlated with modified structural dynamics (Trachtenberg et al., 2002).

Consistent with structural dynamics under normal housing conditions, different types of neurons seem to undergo different degrees of experience-dependent structural plasticity (Mizrahi and Katz, 2003; Holtmaat et al., 2006; Hofer et al., 2009; Livneh et al., 2009). For example, while L5 visual neocortical neurons undergo experience-dependent structural plasticity, L2/3 neurons do not (Hofer et al., 2009). Recently, we explored experience-dependent structural plasticity of adult-born periglomerular neurons in response to sensory enrichment with a low concentration odor mixture of two simple odors. Enrichment increased the size of these neurons' dendritic tree, as well as their number of putative synapses. Remarkably, this effect was specific only to neurons, which were located in sensory-active regions of the olfactory bulb, even within the same tissue (**Figure 3**; Livneh et al., 2009). These data

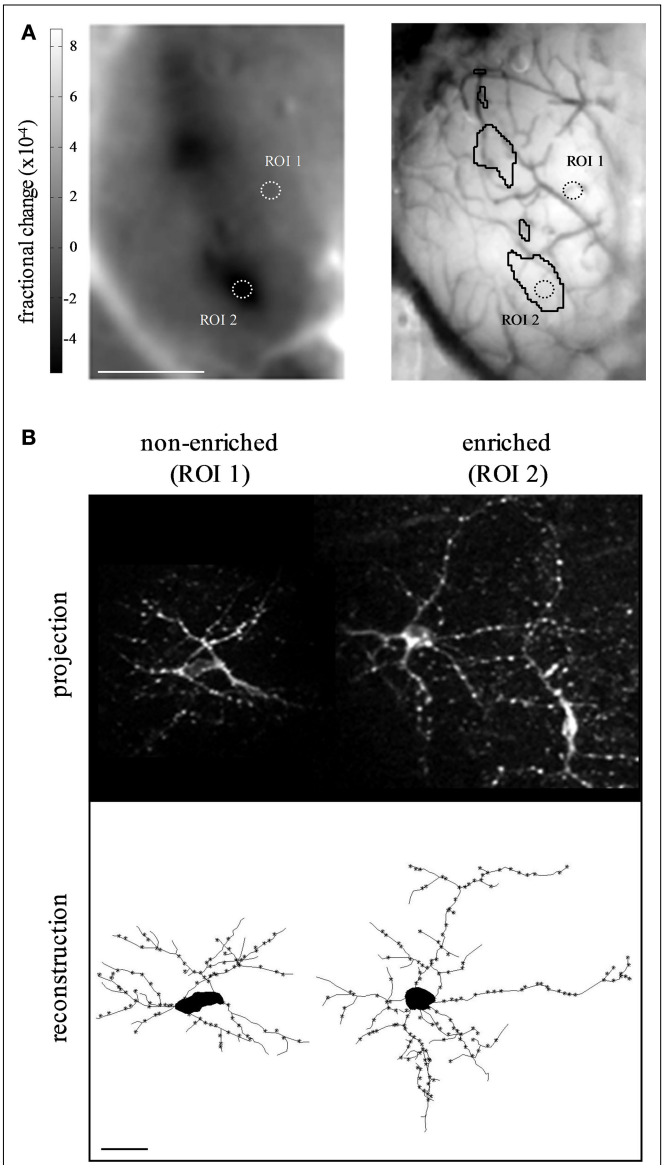

FIGURE 3 | Specificity of experience-dependent plasticity during adult-born neuron development. (A) Intrinsic signal odor map in response to a two-odor mixture (left panel), and the corresponding blood vessel map on the surface of the olfactory bulb (right panel). Sensory-active domains are marked by a black contour in the blood vessel map. Two regions of interest (ROIs), containing the neurons shown in B, are indicated by dotted circles. ROI 1 is in a sensory-non-active domain, while ROI 2 is within a sensory-active domain. Scale bar: 1 mm. **(B)** Two adult-born periglomerular neurons expressing PSD95-GFP as a proxy for synapses from the same experiment shown in A. Left: a periglomerular neuron from a non-enriched domain (non-active, ROI 1), Right: a periglomerular neuron from an enriched domain (active, ROI 2). Top, maximum projection images of the original Z stacks. Bottom, two-dimensional view of the reconstructed neurons at the top. Asterisks mark putative synapses. Scale bar: 20 μm. Sensory enrichment increased both the size of the neurons' dendritic tree and the number of their putative synapses. Adapted from Livneh et al. (2009), with permission.

further support the view that the levels of structural plasticity in different neurons can vary dramatically, even within the same local network.

How can an atlas possibly reflect the continuous structural changes which neurons undergo? One possibility is that there is actually no need to describe structural dynamics in atlases. In most adult animals, structural dynamics, over a time scale of one to several weeks, are usually on the order of 5–20% of the total population. This means that any atlas will be a good approximation (80–95% correct) of a neuron's morphology during its lifetime. A 5–20% error is a figure which might in any case be confounded with inter-individual variability and as such, is satisfactory. However, even a 10% change in synaptic connectivity (morphologically reflected as dendritic spine dynamics) can have dramatic effects on neuronal function. Consequently, small changes in many neurons can lead to substantial changes in the entire network's function (Hofer et al., 2009). Thus, we propose that, as more information becomes available, digital integrated shared atlases could provide not only information regarding the molecular subtype of neurons, their laminar position, and their connectivity; but also their expected structural dynamics.

As discussed above, structural dynamics are also a reflection of (or at least are correlated with) experience-dependent plasticity. Notably, however, experience-dependent plasticity was consistently demonstrated following rather extreme "experience" manipulations (e.g., whisker trimming, retinal lesion, prolonged eye closure, sensory enrichment and nostril occlusion). In line with these extreme manipulations, altered neuronal structural dynamics have been described in pathological conditions, such as ischemia, Alzheimer's disease, and prion disease (Tsai et al., 2004; Zhang et al., 2005; Brown et al., 2007; Fuhrmann et al., 2007). All these experimental manipulations can be viewed as composing a spectrum that ranges from severe brain pathology (in which complete turnover may occur), to learning tasks which supposedly underlie everyday learning (in which only subtle anatomical changes are expected). While experience-dependent structural plasticity has mostly been correlated with extreme and pathological manipulations, it still remains to be determined whether more subtle (i.e., relatively natural) manipulations are also correlated with detectable structural changes (Polley et al., 2004; Megevand et al., 2009). Recent work by Gan and colleagues has correlated motor learning with the formation and selective stabilization of a small fraction of new dendritic spines in the motor cortex. This work suggests that structural plasticity indeed has the potential to underlie a wider array of everyday learning and memory tasks (Yang et al., 2009).

The incorporation of the wide range of structural dynamics into brain atlases is not trivial. This is primarily due to an insufficient amount of information regarding most cell-types. Due to technical limitations, structural plasticity *in vivo* has largely been studied in superficial layers of the mammalian brain like the neocortex and the olfactory bulb. As a result, we actually know very little about most other parts of the CNS with respect to their structural dynamics. One might expect that some regions like the hippocampus or the amygdala, which are associated with numerous processes of learning and memory might be far more structurally plastic than others, but this remains to be seen. Given that the primary sensory regions in the neocortex and the olfactory bulb already show fair levels of structural plasticity and diversity, we are probably (and also literally) only scratching the surface.

As a relatively young field, many questions still remain unresolved regarding structural plasticity in the adult brain. Will deeper brain regions also exhibit ongoing and experience-dependent structural plasticity? Do mature neurons in adult invertebrates or non-mammalian vertebrates also share this capacity for experience- dependent structural plasticity? Is the experience-dependent structural plasticity observed under rather extreme experimental manipulations similar to the plasticity that underlies real life experiences, such as learning? Are most forms of functional plasticity correlated with structural plasticity? Time will tell.

STABILITY AND "PLASTICITY" IN GENOMES AND BRAIN ATLASES

Another recent and well-known atlas of sorts is the sequenced genome. The genomes of more than 180 organisms have now been sequenced (Genome News Network[1])and thus a tremendous amount of data has accumulated in easily-accessible databases. Sequenced genomes allow easy and comprehensive analyses of inter- and intra-species variability, and its relation to pathological conditions. Can high-resolution brain atlases conceptually benefit from the currently more advanced "genome atlas"?

One major lesson to learn from genomes is that it was well worth the effort. The sequencing of the genome and the establishment of shared online genomic databases have greatly advanced our understanding of genome function and evolution. This has allowed for a quantitative assessment of the actual extent of inter-individual genetic variability. Additionally, comparative genomics has enabled the evaluation of the extent and sources of inter-species genetic variability, which has led to a multitude of insights in the field of evolution, and has also advanced our basic understanding of the areas in the genome, which are important for function (protein coding sequences, regulatory elements, etc.; Miller et al., 2004). Furthermore, comparative genomics have facilitated the exploration of the genetic sources of numerous pathological conditions (e.g., Down syndrome; Antonarakis et al., 2004). From a researcher's perspective, the sequenced genome, combined with freely-available online databases, has also expedited scientific progress as it has made many everyday scientific practices considerably easier. In analogy to brain atlases, how variable is the genome? Is genomic variability a constraint?

The most common inter-individual genomic variation is single nucleotide polymorphism (SNP), which has been associated with various traits such as disease susceptibility, and even with perception (Keller et al., 2007; Shastry, 2007). In addition to SNPs, other forms of DNA sequence variation exist, arising for example from inter-individual copy number variation (Beckmann et al., 2007) and from the transposition of transposable DNA elements, which comprise ~20% of mammalian genomes (Lander et al., 2001; Waterston et al., 2002; Gibbs et al., 2004). Inter-individual copy number variation may partially explain inherited and sporadic traits (Beckmann et al., 2007), and the transposition of transposable DNA elements has been shown, for example, to affect the differentiation fate of neuronal precursors (Muotri et al., 2005). Despite these sources of genomic variation, the

[1]http://www.genomenewsnetwork.org

vast majority of the genome sequence is considered to be relatively stable between and within individuals (at least compared to the variability of the nervous system). Indeed, it is commonly thought that the genomes of two randomly selected individuals are ~0.1% different (Shastry, 2007; The Human Genome Project[2]). Notably, in absolute numbers, it is estimated that any two individuals will have several million differences in their genome, a number which emphasizes that this relatively small variability (0.1%) is not negligible at all.

On top of sequence variability, another striking layer of complexity comes from epigenetics. Despite a relatively stable genomic sequence, epigenetic modifications are highly dynamic. At the cellular level, there is accumulating evidence for the impact of epigenetic modifications such as DNA methylation, chromatin remodeling, nucleosome positioning, and histone modifications (most notably methylation and acetylation). These epigenetic modifications affect gene expression, and consequently various cellular processes from stem cell differentiation and cancer to synaptic plasticity (Levenson and Sweatt, 2005; Meshorer and Misteli, 2006; Smith et al., 2007). At the level of the entire organism, epigenetic modifications are gaining increasing experimental attention as well. For example, although monozygotic twins are epigenetically indistinguishable during the early years of life, older monozygotic twins exhibit considerable differences in their overall epigenetic profile (Fraga et al., 2005). Furthermore, epigenetic modifications have been implicated as a possible molecular mechanism for various types of experience-dependent plasticity in both the developing and mature nervous system (Fagiolini et al., 2009; Sweatt, 2009). For example, maternal care has been shown to affect the hypothalamus-pituitary-adrenal stress axis through epigenetic modifications of stress-related genes such as the glucocorticoid receptor (Meaney and Szyf, 2005).

Thus, given the importance of epigenetics and using a similar approach to the Human Genome Project, efforts are now underway to map the human epigenome, starting with DNA methylation (The Human Epigenome Project[3]). This project's official rationale is that epigenetic modifications "…constitute(s) the main and so far missing link between genetics, disease and the environment that is widely thought to play a decisive role in the etiology of virtually all human pathologies[4]." Thus, sequencing the genome has also led to the realization that large-scale mapping of further layers of complexity (e.g., epigenetics) will most likely be equally beneficial. Accordingly, we suggest that high-resolution brain atlases should be analogous to a combination of the genome and the epigenome. But in what way are sequenced genomes and brain atlases analogous?

Despite the notable differences in the extent of inter-and intra-individual variability of these two systems, they are analogous in the sense that the basic components of the system (nucleotides/neurons) are relatively stable. Hence, much will be gained from high-resolution mapping of the system's components and their respective position. However, on top of this relative stability, both systems have developed a remarkable capacity for change (epigenetics/neuronal plasticity). This analogy is further strengthened by the fact that the capacity to change, on top of a relatively constant background, seems to be a general mechanism by which biological systems (from single cells to organisms) maintain normal function, while constantly adapting to their ever-changing environment.

CONCLUDING REMARKS

Efforts to construct high-resolution brain atlases face numerous challenges including inter- and intra-animal variability. Overcoming these challenges will substantially advance our understanding of the organization of neural circuits, and their relation to brain function. In this review, we described structural dynamics (primarily in mammals) as a further layer of complexity, which poses yet another challenge to take into consideration. Digital brain atlases could be a convenient platform for the integration of structural dynamics into pre-existing neuroanatomical (and molecular) data. In this way, seemingly static brain atlases will also be able to capture the dynamic nature of the brain.

ACKNOWLEDGMENTS

We thank E. Meshorer, A. Darvasi, S. Druckmann and members of the Mizrahi lab for useful discussions and for critically commenting on the manuscript.

[2]http://www.ornl.gov/sci/techresources/Human_Genome/home.shtml

[3]http://www.epigenome.org/

[4]http://www.epigenome.org/index.php?page=project

REFERENCES

Antonarakis, S. E., Lyle, R., Dermitzakis, E. T., Reymond, A., and Deutsch, S. (2004). Chromosome 21 and down syndrome: from genomics to pathophysiology. *Nat. Rev. Genet.* 5, 725–738.

Ascoli, G. A., Alonso-Nanclares, L., Anderson, S. A., Barrionuevo, G., Benavides-Piccione, R., Burkhalter, A., Buzsaki, G., Cauli, B., Defelipe, J., Fairen, A., Feldmeyer, D., Fishell, G., Fregnac, Y., Freund, T. F., Gardner, D., Gardner, E. P., Goldberg, J. H., Helmstaedter, M., Hestrin, S., Karube, F., Kisvarday, Z. F., Lambolez, B., Lewis, D. A., Marin, O., Markram, H., Munoz, A., Packer, A., Petersen, C. C., Rockland, K. S., Rossier, J., Rudy, B., Somogyi, P., Staiger, J. F., Tamas, G., Thomson, A. M., Toledo-Rodriguez, M., Wang, Y., West, D. C., and Yuste, R. (2008). Petilla terminology: nomenclature of features of GABAergic interneurons of the cerebral cortex. *Nat. Rev. Neurosci.* 9, 557–568.

Beckmann, J. S., Estivill, X., and Antonarakis, S. E. (2007). Copy number variants and genetic traits: closer to the resolution of phenotypic to genotypic variability. *Nat. Rev. Genet.* 8, 639–646.

Bentley, D. (1975). Single gene cricket mutations: effects on behavior, sensilla, sensory neurons, and identified interneurons. *Science* 187, 760–764.

Bhatt, D. H., Zhang, S., and Gan, W. B. (2009). Dendritic spine dynamics. *Annu. Rev. Physiol.* 71, 261–282.

Bodnar, D. A., Miller, J. P., and Jacobs, G. A. (1991). Anatomy and physiology of identified wind-sensitive local interneurons in the cricket cercal sensory system. *J. Comp. Physiol. A* 168, 553–564.

Bota, M., Dong, H. W., and Swanson, L. W. (2003). From gene networks to brain networks. *Nat. Neurosci.* 6, 795–799.

Brandt, R., Rohlfing, T., Rybak, J., Krofczik, S., Maye, A., Westerhoff, M., Hege, H. C., and Menzel, R. (2005). Three-dimensional average-shape atlas of the honeybee brain and its applications. *J. Comp. Neurol.* 492, 1–19.

Brown, C. E., Li, P., Boyd, J. D., Delaney, K. R., and Murphy, T. H. (2007). Extensive turnover of dendritic spines and vascular remodeling in cortical tissues recovering from stroke. *J. Neurosci.* 27, 4101–4109.

Chen, B. L., Hall, D. H., and Chklovskii, D. B. (2006). Wiring optimization can relate neuronal structure and function. *Proc. Natl. Acad. Sci. U.S.A.* 103, 4723–4728.

Coggeshall, R. E., and Fawcett, D. W. (1964). The Fine Structure of the Central Nervous System of the Leech, Hirudo Medicinalis. *J. Neurophysiol.* 27, 229–289.

Cuntz, H., Forstner, F., Haag, J., and Borst, A. (2008). The morphological identity of insect dendrites. *PLoS Comput. Biol.* 4, e1000251. doi:10.1371/journal.pcbi.1000251.

Daley, D. L., Vardi, N., Appignani, B., and Camhi, J. M. (1981). Morphology of the giant interneurons and cercal nerve projections of the American cockroach. *J. Comp. Neurol.* 196, 41–52.

De Paola, V., Holtmaat, A., Knott, G., Song, S., Wilbrecht, L., Caroni, P., and Svoboda, K. (2006). Cell type-specific structural plasticity of axonal branches and boutons in the adult neocortex. *Neuron* 49, 861–875.

Denk, W., and Horstmann, H. (2004). Serial block-face scanning electron microscopy to reconstruct three-dimensional tissue nanostructure. *PLoS Biol.* 2, e329. doi:10.1371/journal.pbio.0020329.

Dorris, M. C., Pare, M., and Munoz, D. P. (2000). Immediate neural plasticity shapes motor performance. *J. Neurosci.* 20, RC52.

Fagiolini, M., Jensen, C. L., and Champagne, F. A. (2009). Epigenetic influences on brain development and plasticity. *Curr. Opin. Neurobiol.* 19, 207–212.

Feng, G., Mellor, R. H., Bernstein, M., Keller-Peck, C., Nguyen, Q. T., Wallace, M., Nerbonne, J. M., Lichtman, J. W., and Sanes, J. R. (2000). Imaging neuronal subsets in transgenic mice expressing multiple spectral variants of GFP. *Neuron* 28, 41–51.

Fraga, M. F., Ballestar, E., Paz, M. F., Ropero, S., Setien, F., Ballestar, M. L., Heine-Suner, D., Cigudosa, J. C., Urioste, M., Benitez, J., Boix-Chornet, M., Sanchez-Aguilera, A., Ling, C., Carlsson, E., Poulsen, P., Vaag, A., Stephan, Z., Spector, T. D., Wu, Y. Z., Plass, C., and Esteller, M. (2005). Epigenetic differences arise during the lifetime of monozygotic twins. *Proc. Natl. Acad. Sci. U.S.A.* 102, 10604–10609.

Fritz, J., Shamma, S., Elhilali, M., and Klein, D. (2003). Rapid task-related plasticity of spectrotemporal receptive fields in primary auditory cortex. *Nat. Neurosci.* 6, 1216–1223.

Fuhrmann, M., Mitteregger, G., Kretzschmar, H., and Herms, J. (2007). Dendritic pathology in prion disease starts at the synaptic spine. *J. Neurosci.* 27, 6224–6233.

Gandolfo, F., Li, C., Benda, B. J., Schioppa, C. P., and Bizzi, E. (2000). Cortical correlates of learning in monkeys adapting to a new dynamical environment. *Proc. Natl. Acad. Sci. U.S.A.* 97, 2259–2263.

Geffen, M. N., de Vries, S. E., and Meister, M. (2007). Retinal ganglion cells can rapidly change polarity from off to on. *PLoS Biol.* 5, e65. doi:10.1371/journal.pbio.0050065.

Gibbs, R. A., Weinstock, G. M., Metzker, M. L., Muzny, D. M., Sodergren, E. J., Scherer, S., Scott, G., Steffen, D., Worley, K. C., Burch, P. E., Okwuonu, G., Hines, S., Lewis, L., DeRamo, C., Delgado, O., Dugan-Rocha, S., Miner, G., Morgan, M., Hawes, A., Gill, R., Celera, Holt, R. A., Adams, M. D., Amanatides, P. G., Baden-Tillson, H., Barnstead, M., Chin, S., Evans, C. A., Ferriera, S., Fosler, C., Glodek, A., Gu, Z., Jennings, D., Kraft, C. L., Nguyen, T., Pfannkoch, C. M., Sitter, C., Sutton, G. G., Venter, J. C., Woodage, T., Smith, D., Lee, H. M., Gustafson, E., Cahill, P., Kana, A., Doucette-Stamm, L., Weinstock, K., Fechtel, K., Weiss, R. B., Dunn, D. M., Green, E. D., Blakesley, R. W., Bouffard, G. G., De Jong, P. J., Osoegawa, K., Zhu, B., Marra, M., Schein, J., Bosdet, I., Fjell, C., Jones, S., Krzywinski, M., Mathewson, C., Siddiqui, A., Wye, N., McPherson, J., Zhao, S., Fraser, C. M., Shetty, J., Shatsman, S., Geer, K., Chen, Y., Abramzon, S., Nierman, W. C., Havlak, P. H., Chen, R., Durbin, K. J., Egan, A., Ren, Y., Song, X. Z., Li, B., Liu, Y., Qin, X., Cawley, S., Cooney, A. J., D'Souza, L. M., Martin, K., Wu, J. Q., Gonzalez-Garay, M. L., Jackson, A. R., Kalafus, K. J., McLeod, M. P., Milosavljevic, A., Virk, D., Volkov, A., Wheeler, D. A., Zhang, Z., Bailey, J. A., Eichler, E. E., Tuzun, E., Birney, E., Mongin, E., Ureta-Vidal, A., Woodwark, C., Zdobnov, E., Bork, P., Suyama, M., Torrents, D., Alexandersson, M., Trask, B. J., Young, J. M., Huang, H., Wang, H., Xing, H., Daniels, S., Gietzen, D., Schmidt, J., Stevens, K., Vitt, U., Wingrove, J., Camara, F., Mar Alba, M., Abril, J. F., Guigo, R., Smit, A., Dubchak, I., Rubin, E. M., Couronne, O., Poliakov, A., Hubner, N., Ganten, D., Goesele, C., Hummel, O., Kreitler, T., Lee, Y. A., Monti, J., Schulz, H., Zimdahl, H., Himmelbauer, H., Lehrach, H., Jacob, H. J., Bromberg, S., Gullings-Handley, J., Jensen-Seaman, M. I., Kwitek, A. E., Lazar, J., Pasko, D., Tonellato, P. J., Twigger, S., Ponting, C. P., Duarte, J. M., Rice, S., Goodstadt, L., Beatson, S. A., Emes, R. D., Winter, E. E., Webber, C., Brandt, P., Nyakatura, G., Adetobi, M., Chiaromonte, F., Elnitski, L., Eswara, P., Hardison, R. C., Hou, M., Kolbe, D., Makova, K., Miller, W., Nekrutenko, A., Riemer, C., Schwartz, S., Taylor, J., Yang, S., Zhang, Y., Lindpaintner, K., Andrews, T. D., Caccamo, M., Clamp, M., Clarke, L., Curwen, V., Durbin, R., Eyras, E., Searle, S. M., Cooper, G. M., Batzoglou, S., Brudno, M., Sidow, A., Stone, E. A., Payseur, B. A., Bourque, G., Lopez-Otin, C., Puente, X. S., Chakrabarti, K., Chatterji, S., Dewey, C., Pachter, L., Bray, N., Yap, V. B., Caspi, A., Tesler, G., Pevzner, P. A., Haussler, D., Roskin, K. M., Baertsch, R., Clawson, H., Furey, T. S., Hinrichs, A. S., Karolchik, D., Kent, W. J., Rosenbloom, K. R., Trumbower, H., Weirauch, M., Cooper, D. N., Stenson, P. D., Ma, B., Brent, M., Arumugam, M., Shteynberg, D., Copley, R. R., Taylor, M. S., Riethman, H., Mudunuri, U., Peterson, J., Guyer, M., Felsenfeld, A., Old, S., Mockrin, S., and Collins, F. (2004). Genome sequence of the Brown Norway rat yields insights into mammalian evolution. *Nature* 428, 493–521.

Goodman, C. S. (1978). Isogenic grasshoppers: genetic variability in the morphology of identified neurons. *J. Comp. Neurol.* 182, 681–705.

Grutzendler, J., Kasthuri, N., and Gan, W. B. (2002). Long-term dendritic spine stability in the adult cortex. *Nature* 420, 812–816.

Hammer, M., and Menzel, R. (1995). Learning and memory in the honeybee. *J. Neurosci.* 15, 1617–1630.

Hofer, S. B., Mrsic-Flogel, T. D., Bonhoeffer, T., and Hubener, M. (2006). Prior experience enhances plasticity in adult visual cortex. *Nat. Neurosci.* 9, 127–132.

Hofer, S. B., Mrsic-Flogel, T. D., Bonhoeffer, T., and Hubener, M. (2009). Experience leaves a lasting structural trace in cortical circuits. *Nature* 457, 313–317.

Holtmaat, A., Bonhoeffer, T., Chow, D. K., Chuckowree, J., De Paola, V., Hofer, S. B., Hubener, M., Keck, T., Knott, G., Lee, W. C., Mostany, R., Mrsic-Flogel, T. D., Nedivi, E., Portera-Cailliau, C., Svoboda, K., Trachtenberg, J. T., and Wilbrecht, L. (2009). Long-term, high-resolution imaging in the mouse neocortex through a chronic cranial window. *Nat Protoc* 4, 1128–1144.

Holtmaat, A., and Svoboda, K. (2009). Experience-dependent structural synaptic plasticity in the mammalian brain. *Nat. Rev. Neurosci.* 10, 647–658.

Holtmaat, A., Wilbrecht, L., Knott, G. W., Welker, E., and Svoboda, K. (2006). Experience-dependent and cell-type-specific spine growth in the neocortex. *Nature* 441, 979–983.

Holtmaat, A. J., Trachtenberg, J. T., Wilbrecht, L., Shepherd, G. M., Zhang, X., Knott, G. W., and Svoboda, K. (2005). Transient and persistent dendritic spines in the neocortex *in vivo*. *Neuron* 45, 279–291.

Hubel, D. H., Wiesel, T. N., and LeVay, S. (1977). Plasticity of ocular dominance columns in monkey striate cortex. *Philos. Trans. R. Soc. Lond., B, Biol. Sci.* 278, 377–409.

Johansen, J., Halpern, M. E., and Keshishian, H. (1989). Axonal guidance and the development of muscle fiber-specific innervation in *Drosophila* embryos. *J. Neurosci.* 9, 4318–4332.

Keck, T., Mrsic-Flogel, T. D., Vaz Afonso, M., Eysel, U. T., Bonhoeffer, T., and Hubener, M. (2008). Massive restructuring of neuronal circuits during functional reorganization of adult visual cortex. *Nat. Neurosci.* 11, 1162–1167.

Keller, A., Zhuang, H., Chi, Q., Vosshall, L. B., and Matsunami, H. (2007). Genetic variation in a human odorant receptor alters odour perception. *Nature* 449, 468–472.

Knott, G. W., Holtmaat, A., Wilbrecht, L., Welker, E., and Svoboda, K. (2006). Spine growth precedes synapse formation in the adult neocortex *in vivo*. *Nat. Neurosci.* 9, 1117–1124.

Kurylas, A. E., Rohlfing, T., Krofczik, S., Jenett, A., and Homberg, U. (2008). Standardized atlas of the brain of the desert locust, Schistocerca gregaria. *Cell Tissue Res.* 333, 125–145.

Lander, E. S., Linton, L. M., Birren, B., Nusbaum, C., Zody, M. C., Baldwin, J., Devon, K., Dewar, K., Doyle, M., FitzHugh, W., Funke, R., Gage, D., Harris, K., Heaford, A., Howland, J., Kann, L., Lehoczky, J., LeVine, R., McEwan, P., McKernan, K., Meldrim, J., Mesirov, J. P., Miranda, C., Morris, W., Naylor, J., Raymond, C., Rosetti, M., Santos, R., Sheridan, A., Sougnez, C., Stange-Thomann, N., Stojanovic, N., Subramanian, A., Wyman, D., Rogers, J., Sulston, J., Ainscough, R., Beck, S., Bentley, D., Burton, J., Clee, C., Carter, N., Coulson, A., Deadman, R., Deloukas, P., Dunham, A., Dunham, I., Durbin, R., French, L., Grafham, D., Gregory, S., Hubbard, T., Humphray, S., Hunt, A., Jones, M., Lloyd, C., McMurray, A., Matthews, L., Mercer, S., Milne, S., Mullikin, J. C., Mungall, A., Plumb, R., Ross, M., Shownkeen, R., Sims, S., Waterston, R. H., Wilson, R. K., Hillier, L. W., McPherson, J. D., Marra, M. A., Mardis, E. R., Fulton, L. A., Chinwalla, A. T., Pepin, K. H., Gish, W. R., Chissoe, S. L., Wendl, M. C., Delehaunty, K. D., Miner, T. L., Delehaunty, A., Kramer, J. B., Cook, L. L., Fulton, R. S., Johnson, D. L., Minx, P. J., Clifton, S. W., Hawkins, T., Branscomb, E., Predki, P., Richardson, P., Wenning, S., Slezak, T., Doggett, N., Cheng, J. F., Olsen, A., Lucas, S., Elkin, C., Uberbacher, E., Frazier, M., Gibbs, R. A., Muzny, D. M., Scherer, S. E., Bouck, J. B., Sodergren, E. J., Worley, K. C., Rives, C. M., Gorrell, J. H., Metzker, M. L., Naylor, S. L., Kucherlapati, R. S., Nelson, D. L., Weinstock, G. M., Sakaki, Y., Fujiyama, A., Hattori, M., Yada, T., Toyoda, A., Itoh, T., Kawagoe, C., Watanabe, H., Totoki, Y., Taylor, T., Weissenbach, J., Heilig, R., Saurin, W., Artiguenave, F., Brottier, P., Bruls, T., Pelletier, E., Robert, C., Wincker, P., Smith, D. R., Doucette-Stamm, L., Rubenfield, M., Weinstock, K., Lee, H. M., Dubois, J., Rosenthal, A., Platzer, M., Nyakatura,

G., Taudien, S., Rump, A., Yang, H., Yu, J., Wang, J., Huang, G., Gu, J., Hood, L., Rowen, L., Madan, A., Qin, S., Davis, R. W., Federspiel, N. A., Abola, A. P., Proctor, M. J., Myers, R. M., Schmutz, J., Dickson, M., Grimwood, J., Cox, D. R., Olson, M. V., Kaul, R., Shimizu, N., Kawasaki, K., Minoshima, S., Evans, G. A., Athanasiou, M., Schultz, R., Roe, B. A., Chen, F., Pan, H., Ramser, J., Lehrach, H., Reinhardt, R., McCombie, W. R., de la Bastide, M., Dedhia, N., Blocker, H., Hornischer, K., Nordsiek, G., Agarwala, R., Aravind, L., Bailey, J. A., Bateman, A., Batzoglou, S., Birney, E., Bork, P., Brown, D. G., Burge, C. B., Cerutti, L., Chen, H. C., Church, D., Clamp, M., Copley, R. R., Doerks, T., Eddy, S. R., Eichler, E. E., Furey, T. S., Galagan, J., Gilbert, J. G., Harmon, C., Hayashizaki, Y., Haussler, D., Hermjakob, H., Hokamp, K., Jang, W., Johnson, L. S., Jones, T. A., Kasif, S., Kaspryzk, A., Kennedy, S., Kent, W. J., Kitts, P., Koonin, E. V., Korf, I., Kulp, D., Lancet, D., Lowe, T. M., McLysaght, A., Mikkelsen, T., Moran, J. V., Mulder, N., Pollara, V. J., Ponting, C. P., Schuler, G., Schultz, J., Slater, G., Smit, A. F., Stupka, E., Szustakowski, J., Thierry-Mieg, D., Thierry-Mieg, J., Wagner, L., Wallis, J., Wheeler, R., Williams, A., Wolf, Y. I., Wolfe, K. H., Yang, S. P., Yeh, R. F., Collins, F., Guyer, M. S., Peterson, J., Felsenfeld, A., Wetterstrand, K. A., Patrinos, A., Morgan, M. J., de Jong, P., Catanese, J. J., Osoegawa, K., Shizuya, H., Choi, S., and Chen, Y. J. (2001). Initial sequencing and analysis of the human genome. *Nature* 409, 860–921.

Lee, W. C., Chen, J. L., Huang, H., Leslie, J. H., Amitai, Y., So, P. T., and Nedivi, E. (2008). A dynamic zone defines interneuron remodeling in the adult neocortex. *Proc. Natl. Acad. Sci. U.S.A.* 105, 19968–19973.

Lee, W. C., Huang, H., Feng, G., Sanes, J. R., Brown, E. N., So, P. T., and Nedivi, E. (2006). Dynamic remodeling of dendritic arbors in GABAergic interneurons of adult visual cortex. *PLoS Biol.* 4, e29. doi:10.1371/journal.pbio.0040029.

Lein, E. S., Hawrylycz, M. J., Ao, N., Ayres, M., Bensinger, A., Bernard, A., Boe, A. F., Boguski, M. S., Brockway, K. S., Byrnes, E. J., Chen, L., Chen, T. M., Chin, M. C., Chong, J., Crook, B. E., Czaplinska, A., Dang, C. N., Datta, S., Dee, N. R., Desaki, A. L., Desta, T., Diep, E., Dolbeare, T. A., Donelan, M. J., Dong, H. W., Dougherty, J. G., Duncan, B. J., Ebbert, A. J., Eichele, G., Estin, L. K., Faber, C., Facer, B. A., Fields, R., Fischer, S. R., Fliss, T. P., Frensley, C., Gates, S. N., Glattfelder, K. J., Halverson, K. R., Hart, M. R., Hohmann, J. G., Howell, M. P., Jeung, D. P., Johnson, R. A., Karr, P. T., Kawal, R., Kidney, J. M., Knapik, R. H., Kuan, C. L., Lake, J. H., Laramee, A. R., Larsen, K. D., Lau, C., Lemon, T. A., Liang, A. J., Liu, Y., Luong, L. T., Michaels, J., Morgan, J. J., Morgan, R. J., Mortrud, M. T., Mosqueda, N. F., Ng, L. L., Ng, R., Orta, G. J., Overly, C. C., Pak, T. H., Parry, S. E., Pathak, S. D., Pearson, O. C., Puchalski, R. B., Riley, Z. L., Rockett, H. R., Rowland, S. A., Royall, J. J., Ruiz, M. J., Sarno, N. R., Schaffnit, K., Shapovalova, N. V., Sivisay, T., Slaughterbeck, C. R., Smith, S. C., Smith, K. A., Smith, B. I., Sodt, A. J., Stewart, N. N., Stumpf, K. R., Sunkin, S. M., Sutram, M., Tam, A., Teemer, C. D., Thaller, C., Thompson, C. L., Varnam, L. R., Visel, A., Whitlock, R. M., Wohnoutka, P. E., Wolkey, C. K., Wong, V. Y., Wood, M., Yaylaoglu, M. B., Young, R. C., Youngstrom, B. L., Yuan, X. F., Zhang, B., Zwingman, T. A., and Jones, A. R. (2007). Genome-wide atlas of gene expression in the adult mouse brain. *Nature* 445, 168–176.

Levenson, J. M., and Sweatt, J. D. (2005). Epigenetic mechanisms in memory formation. *Nat. Rev. Neurosci.* 6, 108–118.

Lichtman, J. W., Livet, J., and Sanes, J. R. (2008). A technicolour approach to the connectome. *Nat. Rev. Neurosci.* 9, 417–422.

Lichtman, J. W., and Sanes, J. R. (2008). Ome sweet ome: what can the genome tell us about the connectome? *Curr. Opin. Neurobiol.* 18, 346–353.

Livneh, Y., Feinstein, N., Klein, M., and Mizrahi, A. (2009). Sensory input enhances synaptogenesis of adult-born neurons. *J. Neurosci.* 29, 86–97.

Lu, J., Tapia, J. C., White, O. L., and Lichtman, J. W. (2009). The interscutularis muscle connectome. *PLoS Biol.* 7, e32. doi:10.1371/journal.pbio.1000032.

Macagno, E. R., Lopresti, V., and Levinthal, C. (1973). Structure and development of neuronal connections in isogenic organisms: variations and similarities in the optic system of Daphnia magna. *Proc. Natl. Acad. Sci. U.S.A.* 70, 57–61.

Madison, D. V., Malenka, R. C., and Nicoll, R. A. (1991). Mechanisms underlying long-term potentiation of synaptic transmission. *Annu. Rev. Neurosci.* 14, 379–397.

Majewska, A. K., Newton, J. R., and Sur, M. (2006). Remodeling of synaptic structure in sensory cortical areas *in vivo*. *J. Neurosci.* 26, 3021–3029.

Marin, E. C., Jefferis, G. S., Komiyama, T., Zhu, H., and Luo, L. (2002). Representation of the glomerular olfactory map in the *Drosophila* brain. *Cell* 109, 243–255.

Meaney, M. J., and Szyf, M. (2005). Maternal care as a model for experience-dependent chromatin plasticity? *Trends Neurosci.* 28, 456–463.

Megevand, P., Troncoso, E., Quairiaux, C., Muller, D., Michel, C. M., and Kiss, J. Z. (2009). Long-term plasticity in mouse sensorimotor circuits after rhythmic whisker stimulation. *J. Neurosci.* 29, 5326–5335.

Meshorer, E., and Misteli, T. (2006). Chromatin in pluripotent embryonic stem cells and differentiation. *Nat. Rev. Mol. Cell Biol.* 7, 540–546.

Micheva, K. D., and Smith, S. J. (2007). Array tomography: a new tool for imaging the molecular architecture and ultrastructure of neural circuits. *Neuron* 55, 25–36.

Miller, W., Makova, K. D., Nekrutenko, A., and Hardison, R. C. (2004). Comparative genomics. *Annu. Rev. Genomics Hum. Genet.* 5, 15–56.

Mizrahi, A. (2007). Dendritic development and plasticity of adult-born neurons in the mouse olfactory bulb. *Nat. Neurosci.* 10, 444–452.

Mizrahi, A., Ben-Ner, E., Katz, M. J., Kedem, K., Glusman, J. G., and Libersat, F. (2000). Comparative analysis of dendritic architecture of identified neurons using the Hausdorff distance metric. *J. Comp. Neurol.* 422, 415–428.

Mizrahi, A., and Katz, L. C. (2003). Dendritic stability in the adult olfactory bulb. *Nat. Neurosci.* 6, 1201–1207.

Muotri, A. R., Chu, V. T., Marchetto, M. C., Deng, W., Moran, J. V., and Gage, F. H. (2005). Somatic mosaicism in neuronal precursor cells mediated by L1 retrotransposition. *Nature* 435, 903–910.

Polley, D. B., Kvasnak, E., and Frostig, R. D. (2004). Naturalistic experience transforms sensory maps in the adult cortex of caged animals. *Nature* 429, 67–71.

Rein, K., Zockler, M., Mader, M. T., Grubel, C., and Heisenberg, M. (2002). The Drosophila standard brain. *Curr. Biol.* 12, 227–231.

Samsonovich, A. V., and Ascoli, G. A. (2006). Morphological homeostasis in cortical dendrites. *Proc. Natl. Acad. Sci. U.S.A.* 103, 1569–1574.

Scorcioni, R., Lazarewicz, M. T., and Ascoli, G. A. (2004). Quantitative morphometry of hippocampal pyramidal cells: differences between anatomical classes and reconstructing laboratories. *J. Comp. Neurol.* 473, 177–193.

Shastry, B. S. (2007). SNPs in disease gene mapping, medicinal drug development and evolution. *J. Hum. Genet.* 52, 871–880.

Smith, L. T., Otterson, G. A., and Plass, C. (2007). Unraveling the epigenetic code of cancer for therapy. *Trends Genet.* 23, 449–456.

Stettler, D. D., Yamahachi, H., Li, W., Denk, W., and Gilbert, C. D. (2006). Axons and synaptic boutons are highly dynamic in adult visual cortex. *Neuron* 49, 877–887.

Sweatt, J. D. (2009). Experience-dependent epigenetic modifications in the central nervous system. *Biol. Psychiatry* 65, 191–197.

Thuma, J. B., White, W. E., Hobbs, K. H., and Hooper, S. L. (2009). Pyloric neuron morphology in the stomatogastric ganglion of the lobster, *Panulirus interruptus*. *Brain Behav. Evol.* 73, 26–42.

Trachtenberg, J. T., Chen, B. E., Knott, G. W., Feng, G., Sanes, J. R., Welker, E., and Svoboda, K. (2002). Long-term *in vivo* imaging of experience-dependent synaptic plasticity in adult cortex. *Nature* 420, 788–794.

Tsai, J., Grutzendler, J., Duff, K., and Gan, W. B. (2004). Fibrillar amyloid deposition leads to local synaptic abnormalities and breakage of neuronal branches. *Nat. Neurosci.* 7, 1181–1183.

Ward, S., Thomson, N., White, J. G., and Brenner, S. (1975). Electron microscopical reconstruction of the anterior sensory anatomy of the nematode *Caenorhabditis elegans*? 2UU. *J. Comp. Neurol.* 160, 313–337.

Waterston, R. H., Lindblad-Toh, K., Birney, E., Rogers, J., Abril, J. F., Agarwal, P., Agarwala, R., Ainscough, R., Alexandersson, M., An, P., Antonarakis, S. E., Attwood, J., Baertsch, R., Bailey, J., Barlow, K., Beck, S., Berry, E., Birren, B., Bloom, T., Bork, P., Botcherby, M., Bray, N., Brent, M. R., Brown, D. G., Brown, S. D., Bult, C., Burton, J., Butler, J., Campbell, R. D., Carninci, P., Cawley, S., Chiaromonte, F., Chinwalla, A. T., Church, D. M., Clamp, M., Clee, C., Collins, F. S., Cook, L. L., Copley, R. R., Coulson, A., Couronne, O., Cuff, J., Curwen, V., Cutts, T., Daly, M., David, R., Davies, J., Delehaunty, K. D., Deri, J., Dermitzakis, E. T., Dewey, C., Dickens, N. J., Diekhans, M., Dodge, S., Dubchak, I., Dunn, D. M., Eddy, S. R., Elnitski, L., Emes, R. D., Eswara, P., Eyras, E., Felsenfeld, A., Fewell, G. A., Flicek, P., Foley, K., Frankel, W. N., Fulton, L. A., Fulton, R. S., Furey, T. S., Gage, D., Gibbs, R. A., Glusman, G., Gnerre, S., Goldman, N., Goodstadt, L., Grafham, D., Graves, T. A., Green, E. D., Gregory, S., Guigo, R., Guyer, M., Hardison, R. C., Haussler, D., Hayashizaki, Y., Hillier, L. W., Hinrichs, A., Hlavina, W., Holzer, T., Hsu, F., Hua, A., Hubbard, T., Hunt,

A., Jackson, I., Jaffe, D. B., Johnson, L. S., Jones, M., Jones, T. A., Joy, A., Kamal, M., Karlsson, E. K., Karolchik, D., Kasprzyk, A., Kawai, J., Keibler, E., Kells, C., Kent, W. J., Kirby, A., Kolbe, D. L., Korf, I., Kucherlapati, R. S., Kulbokas, E. J., Kulp, D., Landers, T., Leger, J. P., Leonard, S., Letunic, I., Levine, R., Li, J., Li, M., Lloyd, C., Lucas, S., Ma, B., Maglott, D. R., Mardis, E. R., Matthews, L., Mauceli, E., Mayer, J. H., McCarthy, M., McCombie, W. R., McLaren, S., McLay, K., McPherson, J. D., Meldrim, J., Meredith, B., Mesirov, J. P., Miller, W., Miner, T. L., Mongin, E., Montgomery, K. T., Morgan, M., Mott, R., Mullikin, J. C., Muzny, D. M., Nash, W. E., Nelson, J. O., Nhan, M. N., Nicol, R., Ning, Z., Nusbaum, C., O'Connor, M. J., Okazaki, Y., Oliver, K., Overton-Larty, E., Pachter, L., Parra, G., Pepin, K. H., Peterson, J., Pevzner, P., Plumb, R., Pohl, C. S., Poliakov, A., Ponce, T. C., Ponting, C. P., Potter, S., Quail, M., Reymond, A., Roe, B. A., Roskin, K. M., Rubin, E. M., Rust, A. G., Santos, R., Sapojnikov, V., Schultz, B., Schultz, J., Schwartz, M. S., Schwartz, S., Scott, C., Seaman, S., Searle, S., Sharpe, T., Sheridan, A., Shownkeen, R., Sims, S., Singer, J. B., Slater, G., Smit, A., Smith, D. R., Spencer, B., Stabenau, A., Stange-Thomann, N., Sugnet, C., Suyama, M., Tesler, G., Thompson, J., Torrents, D., Trevaskis, E., Tromp, J., Ucla, C., Ureta-Vidal, A., Vinson, J. P., Von Niederhausern, A. C., Wade, C. M., Wall, M., Weber, R. J., Weiss, R. B., Wendl, M. C., West, A. P., Wetterstrand, K., Wheeler, R., Whelan, S., Wierzbowski, J., Willey, D., Williams, S., Wilson, R. K., Winter, E., Worley, K. C., Wyman, D., Yang, S., Yang, S. P., Zdobnov, E. M., Zody, M. C., and Lander, E. S. (2002). Initial sequencing and comparative analysis of the mouse genome. *Nature* 420, 520–562.

Wen, Q., Stepanyants, A., Elston, G. N., Grosberg, A. Y., and Chklovskii, D. B. (2009). Maximization of the connectivity repertoire as a statistical principle governing the shapes of dendritic arbors. *Proc. Natl. Acad. Sci. U.S.A.* 106, 12536–12541.

Wong, A. M., Wang, J. W., and Axel, R. (2002). Spatial representation of the glomerular map in the *Drosophila* protocerebrum. *Cell* 109, 229–241.

Woolley, C. S. (1999). Structural plasticity of dendrites. In Dendrites, G. Stuart, N. Spurston, and M. Hausser, eds (Oxford, Oxford University Press), pp. 339–364.

Yang, G., Pan, F., and Gan, W. B. (2009). Stably maintained dendritic spines are associated with lifelong memories. *Nature* 462, 920–924.

Young, P., and Feng, G. (2004). Labeling neurons *in vivo* for morphological and functional studies. *Curr. Opin. Neurobiol.* 14, 642–646.

Zhang, S., Boyd, J., Delaney, K., and Murphy, T. H. (2005). Rapid reversible changes in dendritic spine structure *in vivo* gated by the degree of ischemia. *J. Neurosci.* 25, 5333–5338.

Zottoli, S. J. (1978). Comparative morphology of the Mauthner cell in fish and amphibians. In Neurobiology of the Mauthner cell, D. S. Faber, and H. Korn, eds (New York, Raven Press) pp. 13–45.

Zucker, R. S., and Regehr, W. G. (2002). Short-term synaptic plasticity. *Annu. Rev. Physiol.* 64, 355–405.

Zuo, Y., Yang, G., Kwon, E., and Gan, W. B. (2005). Long-term sensory deprivation prevents dendritic spine loss in primary somatosensory cortex. *Nature* 436, 261–265.

Conflict of Interest Statement: The authors declare that the research was conducted in the absence of any commercial or financial relationships that could be construed as a potential conflict of interest.

Received: 30 August 2009; paper pending published: 29 October 2009; accepted: 23 November 2009; published online: 22 February 2010.

Citation: Livneh Y and Mizrahi A (2010) A time for atlases and atlases for time. Front. Syst. Neurosci. ***3****:17. doi: 10.3389/neuro.06.017.2009*

frontiers in
SYSTEMS NEUROSCIENCE

ORIGINAL RESEARCH ARTICLE
published: 19 April 2010
doi: 10.3389/fnsys.2010.00009

NeuronBank: a tool for cataloging neuronal circuitry

Paul S. Katz[1]*, Robert Calin-Jageman[1,2], Akshaye Dhawan[3†], Chad Frederick[3], Shuman Guo[3], Rasanjalee Dissanayaka[3], Naveen Hiremath[3], Wenjun Ma[3], Xiuyn Shen[3], Hsui C. Wang[3], Hong Yang[3], Sushil Prasad[3], Rajshekhar Sunderraman[3] and Ying Zhu[3]

[1] *Neuroscience Institute, Georgia State University, Atlanta, GA, USA*
[2] *Department of Pyschology, Dominican University, River Forest, IL, USA*
[3] *Department of Computer Science, Georgia State University, Atlanta, GA, USA*

Edited by:
Randolf Menzel, Freie Universiät Berlin, Germany

Reviewed by:
Gwen Jacobs, Montana State University, USA
Maryann E. Martone, University of California San Diego, USA

****Correspondence:***
Paul S. Katz, Neuroscience Institute, Georgia State University, P.O. Box 5030, Atlanta, GA 30302-5030, USA.
e-mail: pkatz@gsu.edu

†Present Address:
Department of Mathematics and Computer Science, Ursinus College, Collegeville, PA, USA

The basic unit of any nervous system is the neuron. Therefore, understanding the operation of nervous systems ultimately requires an inventory of their constituent neurons and synaptic connectivity, which form neural circuits. The presence of uniquely identifiable neurons or classes of neurons in many invertebrates has facilitated the construction of cellular-level connectivity diagrams that can be generalized across individuals within a species. Homologous neurons can also be recognized across species. Here we describe NeuronBank.org, a web-based tool that we are developing for cataloging, searching, and analyzing neuronal circuitry within and across species. Information from a single species is represented in an individual branch of NeuronBank. Users can search within a branch or perform queries across branches to look for similarities in neuronal circuits across species. The branches allow for an extensible ontology so that additional characteristics can be added as knowledge grows. Each entry in NeuronBank generates a unique accession ID, allowing it to be easily cited. There is also an automatic link to a Wiki page allowing an encyclopedic explanation of the entry. All of the 44 previously published neurons plus one previously unpublished neuron from the mollusc, *Tritonia diomedea*, have been entered into a branch of NeuronBank as have 4 previously published neurons from the mollusc, *Melibe leonina*. The ability to organize information about neuronal circuits will make this information more accessible, ultimately aiding research on these important models.

Keywords: neuroinformatics, identified neurons, invertebrate, mollusc, neuromics, database

INTRODUCTION

The goal of brain atlases is to provide a common structure upon which individual observations can be laid. The finest anatomical scale of a nervous system atlas would be the neurons and synapses, *i.e.* a cellular level wiring diagram. Yet, despite over a hundred years of studying neurons and neuronal interactions, there is no consistent means of representing neurons and neural circuitry. Furthermore, there is no universal electronic repository for that knowledge and thus there is no efficient means to search for information about neuronal circuits across species. Here, the problems associated with creating a neural circuit atlas are defined and a tool called NeuronBank.org is introduced as a step towards addressing these problems.

One challenge with creating an atlas of neuronal wiring is determining what constitutes a particular type of neuron (Masland, 2004; Bota and Swanson, 2007). Mammalian brains have billions of neurons that are thought to fall into a few thousand classes (Bullock, 1993a). It has been known since the work of Cajal that classes or types of neurons form stereotyped neural circuits (Ramon y Cajal, 1995). For example, in the cerebellum, Purkinje neurons receive synaptic input from hundreds of thousands of granule cells and one climbing fiber. However, not all Purkinje neurons are equivalent; they project to different deep cerebellar nuclei and receive input from non-equivalent sets of climbing fibers and granule cells. For a discussion of "equivalent sets" of neurons see chapter 7 in Bullock (1993b).

The quandary of how to classify neurons in mammalian nervous systems is a serious one for understanding the basic wiring of the brain (Masland, 2004; Bota and Swanson, 2007). The problem is becoming more acute because molecular characterization of mammalian neurons is increasing the possible number of neuronal types (Van Hooser et al., 2005; Nelson et al., 2006a,b). Furthermore, new imaging technologies are allowing neuronal wiring diagrams to be very finely specified (Briggman and Denk, 2006; Livet et al., 2007; Smith, 2007; Lichtman et al., 2008; Helmstaedter et al., 2008; Jurrus et al., 2009).

This problem is lessened in some invertebrate nervous systems where individual neurons can be uniquely identified and have similar properties from animal to animal (Croll, 1987; Bullock, 2000). In some invertebrate phyla such as gastropod molluscs and decapod crustaceans, the large size of neurons has facilitated simultaneous intracellular recording from multiple neurons. This has allowed detailed neuronal circuitry to be experimentally determined and related back to behavioral function (Kandel et al., 1967; Brodfuehrer and Thorogood, 2001; Comer and Robertson, 2001; Selverston, 2008; Katz, 2009). Having atlases of the neuronal connectivity in these species is of interest to keep track of the increasingly complex circuitry and cellular properties. Furthermore, creating an atlas of identified neurons in such species can serve as a proving ground for nervous systems with less well-defined neurons.

Homologous neurons and neural circuits can be recognized across species. (Weiss and Kupfermann, 1976; Croll, 1987; Paul, 1991; Newcomb and Katz, 2007). Comparisons of the similarities and differences between species are often difficult to extract from the literature. Yet, there are important reasons why one would want to be able to use information from one species to guide research on neural circuits in other species. For example, the large size of grasshopper neurons allowed their early development to be mapped out and then applied to the much smaller nervous system of the fruit fly (Thomas et al., 1984). A registry of neurons could help sort out homologies and thus help extend findings across taxa.

There are varying degrees to which a neuron can be individually identified (Bullock, 2000). In the extreme, there is one neuron (or a bilaterally symmetric pair) that can be uniquely distinguished from all other neurons in the nervous system. In other cases, there is a small cluster of neurons that appear indistinguishable from each other. In animals that exhibit eutely (constancy of cell number), it is possible to identify every neuron in the nervous system, as has been done for the nematode, *Caenorhabditis elegans*, which has precisely 302 neurons (White et al., 1976, 1986). The small size of *C. elegans* has allowed the entire animal to be serially sectioned and reconstructed with electron microscopy, providing an unrivaled level of detail about the neurons and synapses. With a defined number of neurons, it is a relatively straightforward matter to create a database containing all neurons, *i.e.* its "neurome". WormAtlas.org (Altun et al., 2009) contains all of the neurons along with their synaptic connections, gene expression profile, anatomy, neurotransmitter, and developmental lineage. This type of comprehensive information is not available for any other nervous system. Such knowledge of the neurons and their connectivity is now allowing researchers to address questions related to how neuronal circuitry generates behavior in this animal (De Bono and Maricq, 2005; Schafer, 2005; Karbowski et al., 2007).

The nervous systems in gastropod molluscs are more complex than that of *C. elegans*. There are approximately 8000–10,000 neurons in the central ganglia of opisthobranchs such as *Aplysia californica* and *Tritonia diomedea* (Coggeshall, 1967; Willows et al., 1973). This is two orders of magnitude larger than the nervous system of *C. elegans*, but many orders of magnitude smaller than vertebrate nervous systems. The number of neurons is also at least an order of magnitude less than the number found in insects and other arthropods. Among the 10,000 neurons, some of the larger ones have been individually identified. There are also clusters of neurons that appear similar and thus constitute a type of neuron, such as the sensory neurons in *Aplysia* (Emery and Audesirk, 1978) or *Tritonia* (Getting, 1976). Thus, the gastropod nervous systems provide an interesting test case for creating a neuronal circuitry atlas.

An atlas of neuronal circuitry must have certain features. These would include the ability to represent neurons from different parts of the nervous system and even from the nervous systems of different species. It would also need to be flexible enough to allow new characteristics to be added as our knowledge of neurons grows. Finally, it would need to allow for users to search this information within a species and across species.

One important step towards being able to catalogue and search neurons and neural circuitry is to develop a controlled vocabulary for the characters that apply to neurons. An example of this is the so-called "Petilla" terminology for classifying GABAergic neurons in cerebral cortex, which defines each of the characteristics that might be found in such neurons (Ascoli et al., 2008). A broader approach has been used to create a Neuroscience Information Framework standardized ontology (Bug et al., 2008). This has developed into NeuroLex.org, a semantic web wiki that organizes terms used in neuroscience. Any atlas needs to use terminology that is commonly agreed upon by the community of users.

Another step that is needed to unify knowledge about neuronal circuitry is the development of tools that allow neurons and neuronal connectivity to be catalogued and searched. There are a small number of such repositories in existence that are species-based or phylum-based. For example, as mentioned above, WormAtlas.org catalogues the neurons in the nematode, *C. elegans*. The Brain Architecture Management System (BAMS)[1] has a list of neurons from mammalian nervous systems (Bota et al., 2005). However, the nervous system of *C. elegans* is sufficiently different from the mammalian nervous system that nematode neurons cannot be represented in BAMS and mammalian neurons cannot be represented in WormAtlas. Nematodes and rats are evolutionary distant, so it is not too surprising the ontology for one does not map onto the other in a systematic fashion. Nonethe-less, there are important commonalities such as molecular components (neurotransmitters, receptors, intracellular signaling molecules), physiological properties (plasticity, rhythmicity) and functional design (sensory systems, motor systems). Therefore, it would be of interest to be able to search across species to compare nervous system components and properties the way that one can currently search across species to compare genes and their functions in GenBank[2]

There are several problems that one encounters in trying to represent knowledge about neurons and synapses that are not present for genes. The first is that whereas all genes, regardless of the organism, are strings of nucleotides, there is no uniform definition of what a neuron is (Moroz, 2009). Furthermore, there is debate as to whether complex nervous systems arose independently in different phyla (Nielsen, 1999; Miller, 2009; Moroz, 2009), which would make classification schemes based on homology invalid. However, even if there is deep homology of neuronal cell types (Arendt, 2008; ito-Gutierrez and Arendt, 2009), this does not aid in creating classification schemes because of problems of convergent evolution.

There are many features that can be used to characterize a neuron or a class of neurons: anatomical, electrophysiological, molecular, developmental, and functional. For most neurons, the information about these features is incomplete. New techniques continue to be developed that allow neurons to be categorized along additional dimensions, such as molecular expression patterns. It is virtually impossible at this point in history to fully list all of the possible characteristics of a neuron and its synapses. Therefore, any atlas of neurons and connectivity must by its nature be incomplete.

Yet despite these obstacles, researchers do create circuit diagrams of neurons and their connectivity. For example, **Figure 1** shows the neural circuit mediating the escape swim response of the mollusc

[1]http://brancusi.usc.edu/bkms/

[2]http://www.ncbi.nlm.nih.gov/Genbank/

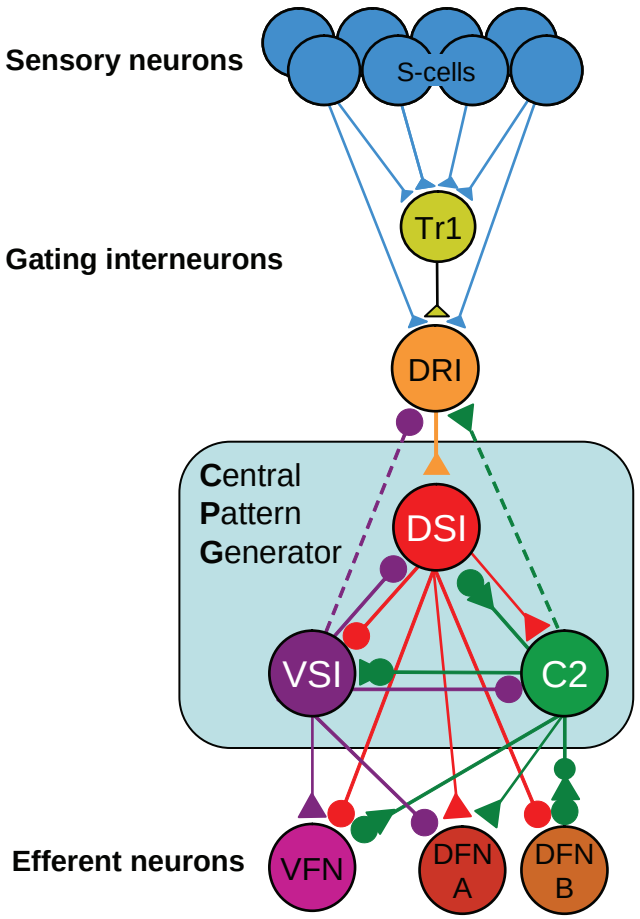

FIGURE 1 | Tritonia swim circuit. This image illustrates fundamental features of a neuronal wiring diagram used in publication. It represents neurons as balls and their synapses as sticks with triangles (excitatory), circles (inhibitory), or combinations of both. The names of the neurons are indicated on the balls.

Tritonia (Katz, 2009). The circuit illustrates the neurons that have been identified as playing a role in this behavior and their synaptic interactions (Getting and Dekin, 1985; Getting, 1989). Even though this neural circuit is relatively simple, it is difficult to represent all of the complexities in one circuit diagram. For example, sometimes neurons are represented as a class; there are three DSIs, but only one is shown on the diagram to make it simpler. The DFN-A and DFN-B neurons are functional classes, not identified neurons. The properties on the neurons and their synapses are not illustrated beyond the fact that some synapses are excitatory and others are inhibitory. Furthermore, by their nature, such circuit diagrams are static; they do not allow readers to explore the circuitry beyond what is presented; there are neurons that feed into this circuit that are not represented here.

In an effort to create a tool that could begin to address some of the needs mentioned, we embarked on the creation of a neural circuit atlas called NeuronBank (Calin-Jageman et al., 2007a). Here, we will explain the fundamental organization of NeuronBank and demonstrate some of its functionality using the *Tritonia* nervous system as an example.

MATERIALS AND METHODS

BASIC ARCHITECTURE OF THE NEURONBANK SYSTEM

The primary challenge in designing NeuronBank was to accommodate species-diversity and continued scientific progress. Meeting these needs required flexibility in both the data model and the user interface, presenting relatively unique challenges for system design. Most current bioinformatics efforts utilize a three-tier architecture: (1) a single relational database provides data to (2) an application layer, which builds an invariant user interface for (3) web clients. In this architecture, changes to the data model must be infrequent because they require developer intervention to update both the database backend and the application layer. Moreover, there is typically only a single data store, so data sharing is not a concern. This type of architecture would not have been suitable for NeuronBank for several reasons. First, different species require different data models and user interfaces. Second, within each species, changes to the data model and user interface are likely to be frequent, making it impractical to require developer intervention. On the other hand, completely separating each species into separate applications would also be untenable. The duplication of effort and the challenges of maintaining interoperability across multiple, independent, yet related systems would override any gain in flexibility in data model and interface.

Our solution was to develop a service-oriented federation of customizable knowledgebases. Individual nodes within the federation (*BranchKBs* – Branch Knowledgebases) are specialized for knowledge of neural circuitry in a single species. New branches can be established using *BranchKB*, a software package that we have developed for creating an online, collaborative knowledgebase of neuronal types and synaptic connectivity. Branches are united by a common framework (*NB-Central* – NeuronBank Central), which enables search and analysis of neural circuits across all species. In this way, we provide the specialization and autonomy necessary to share and analyze knowledge from different species. **Figure 2** shows the overall distributed architecture of NeuronBank.

NB-Central serves two primary roles. First, it creates an environment for invoking and collating services provided by the BranchKBs. This enables a mechanism for searching and analyzing data across all the species represented. Second, it provides a set of web services to the BranchKBs and the clients. These services establish common core functionality, presenting a consistent experience across all branches. One of the major motivations for pursuing a service-based design for both NB-Central and the branches is that this allows for interoperability. Consistent interfaces allow us to support the development of third-party clients and allow for different implementations of the BranchKB using different technologies in the future.

Users interact with this federation via an integrated web client, which consumes resources from both NB-Central and various BranchKBs. Thus, the architectural complexity is masked and the user can seamlessly browse, search, and analyze knowledge from various species that is stored across the federation of NeuronBank branches. The web client features a plug-in architecture, making it possible to utilize different visualization and analysis tools on data from different BranchKBs (**Figure 2**). Moreover, the web service interfaces to BranchKB and NB-Central are open, enabling the development of alternative clients that provide specialized functionality.

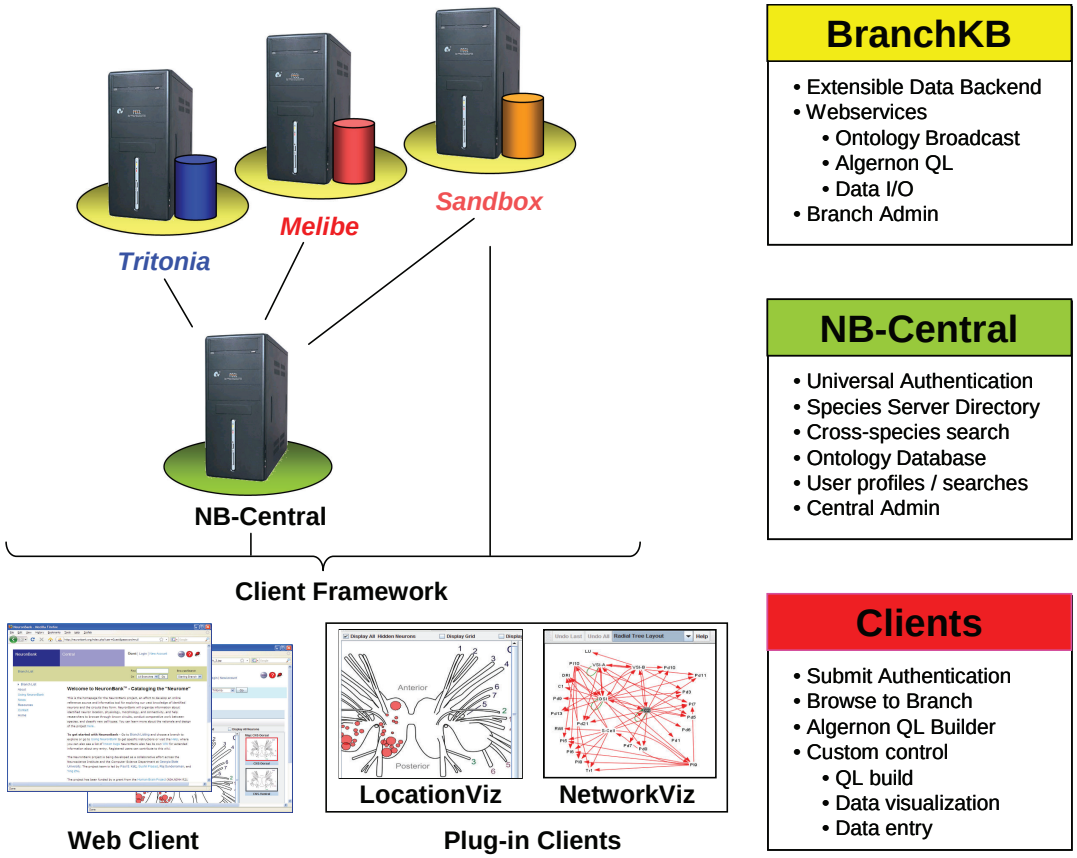

FIGURE 2 | Architecture of NeuronBank.

BRANCHKB

BranchKB is the storage system for each species-specific Branch within NeuronBank. In this respect, BranchKB is similar to the 'database backend' of a traditional web application. However, BranchKB differs from a traditional database in three important respects. First, BranchKB is designed to have a somewhat flexible data model, so that it can be adapted for representing knowledge within a particular species. Second, BranchKB provides services for accessing the current data model, exposing the meta-data required to build a dynamic user interface for that branch. Finally, BranchKB is designed to integrate with NB-Central so that knowledge can be shared across diverse communities.

Flexible data model of neural circuitry

Across all domains, neurons are described by sets of *attributes* (e.g. neurotransmitter, spike shape, and location) and identified by delineating the subset of attributes necessary and sufficient to reliably identify that neuron across different specimens. There is variation, however, in the attributes used to describe neurons in different species or even in different regions of the nervous system of a single species. In addition, new techniques within the neurosciences are constantly adding new attributes that can be used to distinguish neurons. NeuronBank uses a two part hierarchical ontology to represent the knowledge about neurons and connections: (a) a *core ontology* of classes and sub-classes that are applicable to all branches, and (b) an *extensible list of attributes* that can be tailored for a specific branch. All instances have a unique Accession ID that is generated by the system and provides a unique URL.

(a) The core ontology currently consists of root classes for *Neurons*, *Connections*, and *Annotations*. Additional root classes can be added if needed. The core ontology has deliberately been designed to be as simple as possible so that it will be applicable to neural circuits from any species. For example, all neurons have the following four core attributes: Name, Inputs, Outputs, and Annotations. All other properties are represented in the extensible list of attributes. The Inputs, Outputs, and Annotations classes are further sub-classified in a hierarchical manner to represent commonly agreed upon classifications. But, this sub-classification can be changed in the future; it is not a fixed component of NeuronBank. The current core ontology is shown at http://neuronbank.org/help/index.php/Core_Ontology.

(b) The extensible list of attributes allows individual branches of NeuronBank to customize the properties of objects. The NeuronBank application is not affected by any changes made to the extensible list of attributes and provides the

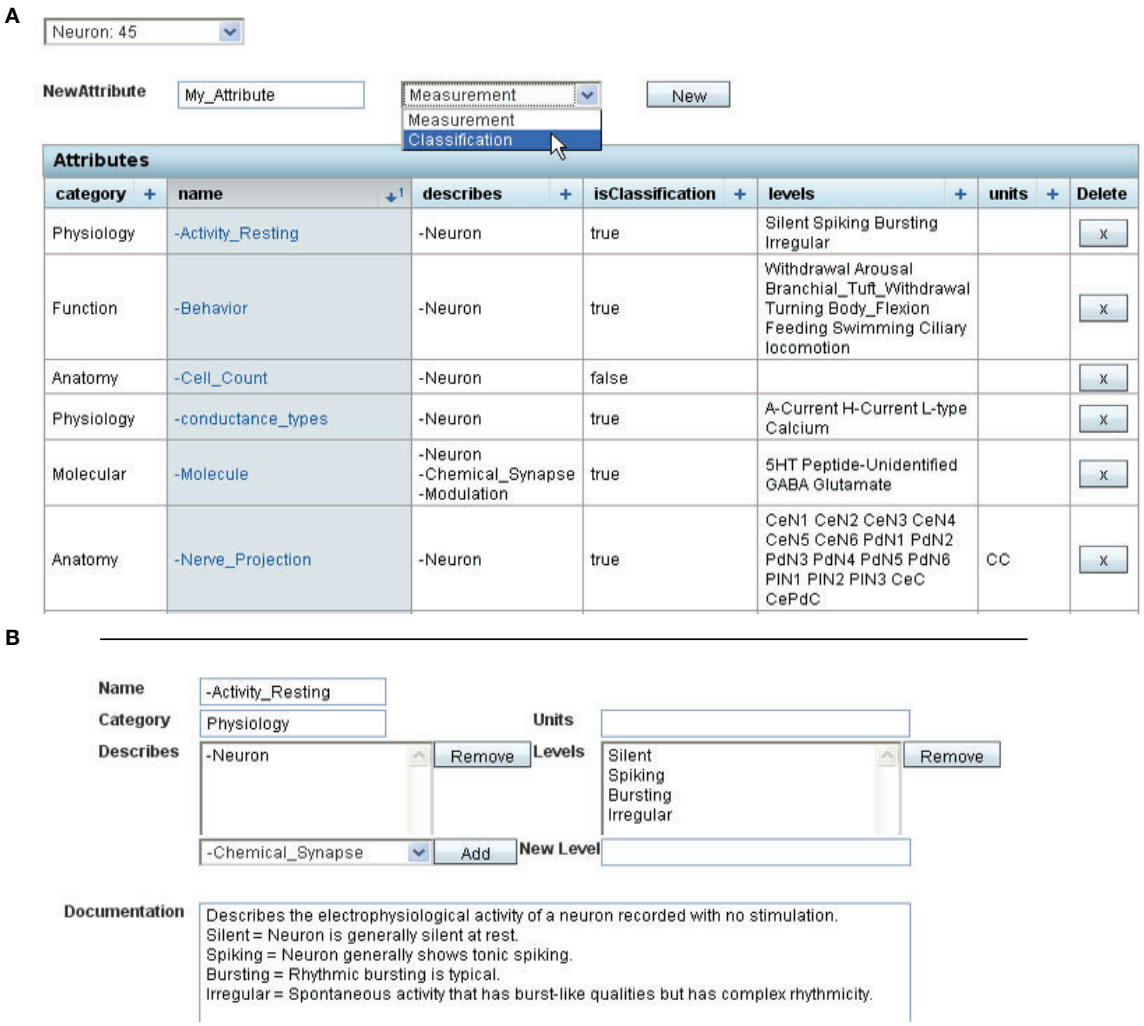

FIGURE 3 | Screenshot showing editing of extensible attributes in the web client. (A). The list of extensible attributes for a neuron is editable. This screenshot shows the first 6 attributes of Neurons in the *Tritonia* extensible list. A new attribute can be added by filling in the name (here "My_Attribute") and choosing whether the attribute is a *Measurement* or a *Classification*. Clicking on the attribute's name allows further editing. **(B)** This is an example of editing the Attribute "Activity_Resting". This is a *classification* with the values Silent, Spiking, Bursting, Irregular. Additional values can be added if they are needed for describing neuronal resting activity.

ability for schema evolution that is typically not available with a relational database system. Changes to the extensible attribute list are made with the attribute editor (**Figure 3**). An attribute can be either a *classification* or a *measurement*. Classification is for attributes with enumerated values, whereas measurement is for attributes that have non-discrete numerical values, sometimes with a standard error.

The administrative editing capability of BranchKB allows each branch to be customized to provide the attributes necessary to describe neurons in that species. As new techniques enable the measurement of additional neural attributes, the data model can be further extended. We envision that communities of neuroscientists interested in a given species will work together to devise the attribute set appropriate for that species.

Meta-data for dynamic user interfaces

Although a dynamic interface was a design requirement for web and plug-in clients, it has significant implications for the design of BranchKB. Specifically, BranchKB must enable clients to retrieve not only data but also the current data model. Thus, each BranchKB exposes functions that enable client applications to retrieve the current class structure, the attributes that apply to a particular class, and the attribute values that are valid for a particular instance. These functions are made available through a set of web services so that each customized instance of BranchKB maintains a consistent set of interfaces for various clients (see below).

NB-CENTRAL

NB-Central is a hub that unifies the diverse branches into a coherent federation. First, it provides a common set of web services to the BranchKBs. These services impart common core functionality,

eliminating duplication of effort and generating a consistent experience across all branches. Second, NB-Central creates an environment for invoking and collating services provided by the BranchKBs. This enables a mechanism for searching and analyzing data across all of the species represented. By drawing on existing work in the fields of web services and distributed architectures, we have designed NB-Central as a unifying mechanism for managing heterogeneous, dispersed resources. The specific functions of NB-Central are as follows:

(1) Branch Directory. NB-Central maintains a master list of online BranchKBs, periodically polls their status, and provides information to clients about each branch.
(2) User Authentication and profiles. NB-Central provides a single-point authentication system; each BranchKB invokes this service to check a user's credentials and establish his/her privileges. Thus, a logon can be executed from any point in the federation. In addition to Branch-level permissions, NB-Central stores all user-profile information and provides secure access to this information via a web service. This enables a user's preferences and privileges to be available to all BranchKBs.
(3) Cross-branch searching. Despite the heterogeneity across BranchKBs, it is essential to enable comparative work across species. NB-Central works in concert with the federation of BranchKBs to provide this function by exposing a web service for cross-species search. This service accepts a query and then passes it on to each available BranchKB. NB-Central collates the results and returns them back to the user. Thus, NB-Central provides a single point to access data throughout the federation.

USER ROLES

NeuronBank has just four types of users: Branch Administrators, Branch Editors, Registered Users, and Unregistered Users. All users have full access to read the knowledge in the federation. They can search, browse, and export this knowledge. They can be anonymous or register with NB-Central to enable stored searches, favorites, and other user services. Registered users can modify the Help Wiki and the NeuronBank Wiki (see below). Branch Editors curate the customizations, which specialize the Branches. Specifically, Branch Editors create, edit, and document the specialized data model, *i.e.* the extensible list of attributes for describing neurons in that species. They can add new neurons, annotate existing knowledge, elucidate new properties of existing neurons, etc. Branch Administrators have all of the access of Branch editors, but also perform user management for their Branch.

WEB CLIENT

NeuronBank web client is the primary user interface for the NeuronBank federation. It invokes web services of both NB-Central and the various BranchKBs. The primary functions of the web client are to enable knowledge access (browsing and searching), knowledge entry (create, edit, and delete), knowledge analysis (visualization) ontology curation (customizing species-specific neuron attributes), and user administration.

To accommodate the heterogeneity in data models across different BranchKBs, the interfaces for accessing, editing, and analyzing knowledge must be dynamic and built on-the-fly from meta-data retrieved from the relevant BranchKB. Moreover, visualization and analysis needs vary across branches. To achieve a high level of flexibility, the web client utilizes a plug-in system. A software plug-in is a program that extends the capability of the main program. The plug-in programs interact with the main program through services such as Application Programming Interfaces (API) or data exchange protocols. The plug-in system provides much flexibility and extensibility, allowing third parties to develop small programs for their specific applications. Different plug-ins can be invoked on data from different BranchKBs. Additional plug-ins can be developed for general use or to meet specialized needs for a particular branch. The current NeuronBank includes two plug-in programs: LocationViz and NetworkViz. These two programs retrieve neuron data from the knowledgebase through a standard data exchange protocol, and then display the neuron location or circuit information in 2D maps.

IMPLEMENTATION TECHNOLOGIES

BranchKB

We implemented BranchKB as a set of Java-based web-services and servlets. As a knowledge store, we used the Protégé knowledge-management system[3]. Protégé is a mature, open-source Java-based knowledgebase system (Musen et al., 1994; Noy et al., 2003). It provides a class/instance/attribute data store that can be accessed via both a Java API and an extensible query language called Algernon. Protégé knowledgebases can be stored in a number of formats, including MySQL database tables. Finally, Protégé knowledgebases can be imported and exported to a variety of formats, including RDF and XML. Import and export formats can also be extended via a plug-in architecture. Protégé provides native support for both a dynamic data model and meta-data access. This enabled us to rapidly prototype BranchKB.

NB-Central

Similar to BranchKB, we implemented NB-Central as a set of Java-based web services and servlets. As the data model for user and branch information is relatively stable and simple, we used a conventional relational database backend (mySQL 5.0).

Web and plug-in clients

We implemented our web client as a Java Server Faces (JSF) web application hosted on Apache Tomcat application server. JSF is a stable, well-supported web-application technology. It features a free and full-featured IDE (Sun Developer Studio). The Visualization clients were implemented as Java applets.

Servers

We use Dell PowerEdge servers with dual Xeon processors running Fedora Red Hat Operating System. We currently maintain both a test server and a production server. Each runs Apache web server, Apache Tomcat application server, mySQL, Protégé and PHP. NB-Central currently resides on the same server as our two BranchKBs, along with our help system, public website, code versioning repository, and developer documentation system. The

[3]protege.stanford.edu

public website is implemented using Exponent, which requires a mySQL database and PHP scripting system. The Wikis use the popular MediaWiki package.

RESULTS

To illustrate the interactions between system components and provide more insight into operation of our federated architecture, we will walk through the use of NeuronBank. Currently, we have implemented most of the functionality envisioned for general users, but have only prototyped the functions for Branch Editors and Administrators, which we grant for the Sandbox branch upon request. Our progress has been sufficient, however, to deploy our first Branches for public testing and to populate them with all the known neurons and connection in two species, *Tritonia diomedea*, which now has 45 neurons and *Melibe leonina*, which has only 4 published neurons.

BRANCH LISTING

This interface from the web client presents a directory of branches, allowing users to quickly identify the species catalogued in the federation, the status of each branch, and their permissions on each branch (**Figure 4**). From here, users can jump directly into a branch to view, edit, or analyze knowledge within that species. This simple interface masks considerable complexity. The web client dynamically builds this interface by invoking the Branch-directory web service on NB-central.

DYNAMIC SEARCH INTERFACES

One of the most important aspects for any knowledge management system is an effective search interface. We have implemented five types of search functions in NeuronBank v1.0:

(1) Text searches. Text strings can be searched for from any page in NeuronBank using the "Find" function, which is located on the navigation bar (**Figures 4*i*, 5***i***).
(2) Browse neurons. A simple browse function allows users in one click to view all of the neurons in that branch (**Figure 5*ii***).
(3) Form-based searches. We have implemented a more powerful querying system using *Algernon*[4], a powerful LISP-based query language (**Figure 5*iii***), which enables path-based searches. (e.g., find all the neurons with chemical synapses where the presynaptic neuron is involved with the behavior "swimming" **Figure 5**). Creating queries directly in Algernon is relatively complex and would not be suitable for most users. Therefore, we developed a form-based interface for the web that allows users to construct ad-hoc Algernon queries. The primary novelty of this interface is that it builds the search interface dynamically to match the current data model of a selected branch. Specifically, the web client retrieves the current class structure from a selected BranchKB. When a class is selected as part of a search, the client retrieves from the BranchKB the attributes that can apply to that class and the paths leading away from that class. Thus, a single search interface on the client can generate queries for any BranchKB, despite substantial heterogeneity in their data models. Once the user has designed a query, the client constructs an equivalent Algernon statement and executes the search.
(4) Cross-Branch searches. Each branch stores knowledge for a different species using a slightly different data model. Normally, this would make it difficult to conduct a search efficiently across multiple Branches. However, each BranchKB presents a consistent interface via web services. This enabled us to further generalize the dynamic search interface in the web client. Specifically, the same query can be submitted to all BranchKBs in the federation using the same interface. Cross branch searches can be conducted using the "Find" text search or the form-based query.
(5) Anatomical searches. One of the important distinguishing characteristics of a neuron is its location within a nervous system. However, given the incommensurable body plans of distantly related organisms—no single coordinate or mapping system could possibly represent anatomical locations across species. To overcome this problem, we have

[4]http://userweb.cs.utexas.edu/users/qr/algy/

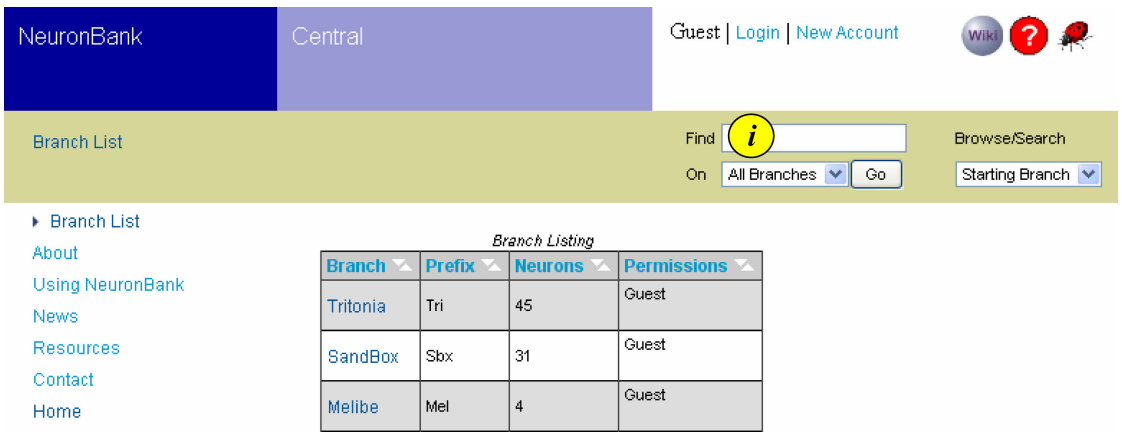

FIGURE 4 | Branch List. Screen shot showing the Branch List and the navigation bar at the top. The branch list is dynamically generated to show the active branches, the number of neurons in each branch and the permissions of the user for each branch. Text searches can be initiated from the navigation bar (*i*).

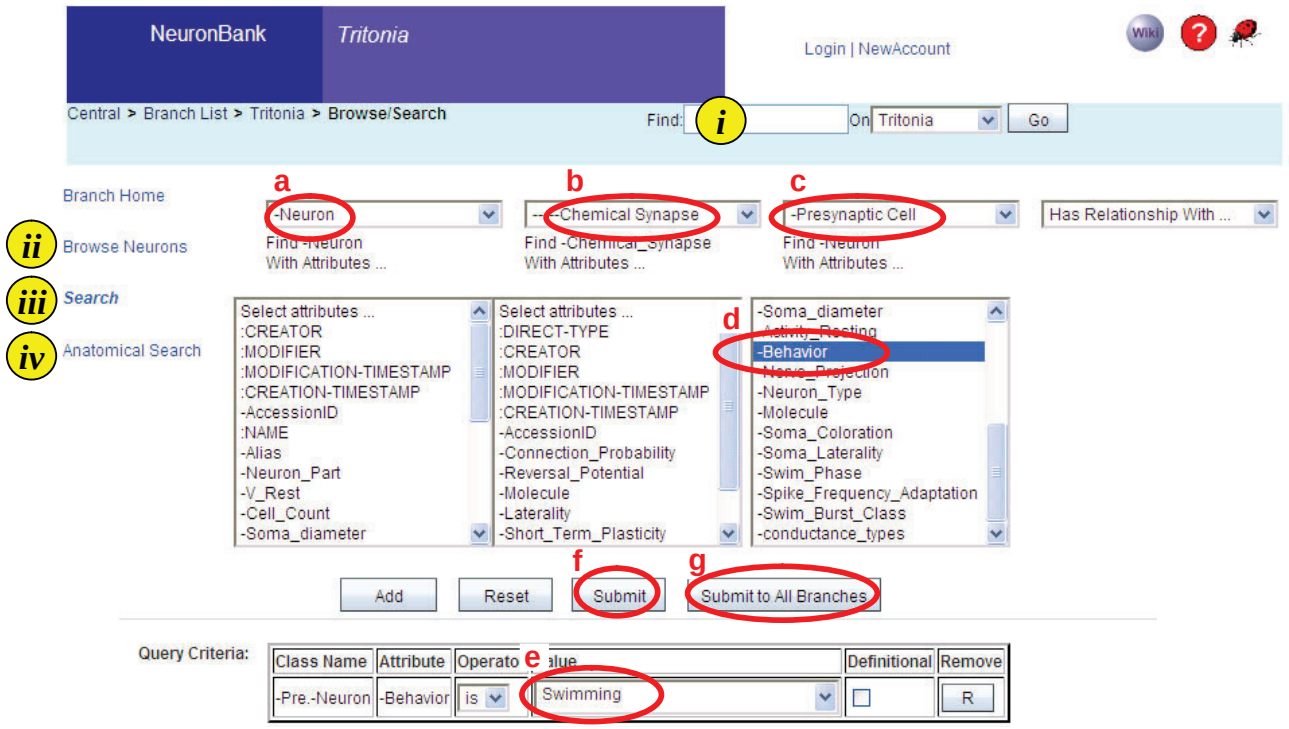

FIGURE 5 | Screen shot of a search on the *Tritonia* branch. Four types of searching are available *i.* Text string, *ii.* Browsing, *iii.* Form-based search, *iv.* Anatomical search. In a form-based search shown, the user has created a query for a neuron (a) with a chemical synapse (b) where the presynaptic cell (c) has an attribute of "-behavior" (d) and the value of that attribute is "Swimming" (e). This query can be submitted to the *Tritonia* branch (f) or it can be submitted to all branches (g).

supplemented the web client with a LocationViz plug-in. This embedded JAVA applet visualizes the somatic locations of neurons in 2-dimensions on an anatomical plane. This representation system is sufficient for a variety of species in which soma location can be indicated relative to a set of standard brain views or slices. For example, in *Tritonia*, neurons can be located based on standardized views of the dorsal and ventral surface of the brain. The LocationViz plug-in can accept a different set of reference views for each BranchKB, thus enabling the same plug-in to visualize anatomical information over many branches. For species in which this form of representation is *not* sufficient (e.g. mammals), a different visualization plug-in will need to be developed.

FIRST PUBLIC BRANCHES

We have deployed the first branches of NeuronBank for public use: the *Tritonia* and *Melibe* branches. These branches contain the published information about the neurons and synaptic connectivity in the molluscs, *Tritonia diomedea* and *Melibe leonina*, which are model neuronal systems (Thompson and Watson, 2005; Katz, 2009). The branches serve as a convenient test for establishing a branch because the number of publications related to identification of neurons and connections is relatively small (<15 for both) and the community of researchers is also small (7 independent labs). It took less than 2 weeks for one person to enter all of the information about neurons and synaptic connections in *Tritonia* into our test server. We had a second person repeat the process and again found that it took less than 2 weeks of moderate work to input all 44 neurons and their connections. We then had students, post-docs, and other *Tritonia* researchers search the knowledgebase for errors in content. We immediately found one omission; a user noticed that we had neglected to include Neuron Pd14 (Tri0002792). This oversight illustrates the need for NeuronBank; the description of this neuron was buried in a paper (Murray and Willows, 1996) and thus not apparent to most researchers. It was the author of that paper who noticed the omission from NeuronBank. We have also used the *Tritonia* branch as an outlet for publication of a neuron that we identified, but have not published in a journal, the LU neuron (Tri0002823).

AN EXAMPLE SEARCH

To illustrate the features of the system, we will walk through a form-based search. Let's say you are on the *Tritonia* branch and want to search for all neurons that make a chemical synapse with a presynaptic neuron that is involved with the behavior "swimming". **Figure 5** shows the pull-menus that would be used to construct this query. One drawback of this system is that it takes some knowledge of the meaning of the attributes to construct appropriate queries. Future implementations will allow the user access to definitions of all of the attributes as well as their links in NeuroLex.org.

The query can be submitted to the current branch (*Tritonia*) or it can be submitted to all branches (**Figure 5f,g**). Generalizing a search across the federation presents two problems. (1) How is the client to discover available BranchKBs? (2) How should the client

collate results across the federation? These problems are overcome by NB-Central, which acting as a hub for the federation generates the Algernon query and invokes the search web services across all the branches. The results are then displayed in a table (**Figure 6**), which shows how many hits were found in each branch. This query had 37 results in *Tritonia*, 4 in the Sandbox branch, and one in the *Melibe* branch.

The results within a branch are displayed in one of three formats: List, Location, or Network (**Figure 7**). The List format presents the components of the query, allowing users to easily trace the inference chain performed on the knowledgebase. For example, the results of the query shown in **Figure 7A** include the Neuron, the Chemical synapse, and the Presynaptic Neuron. Clicking on any entry in this table will take the user to the respective object in the Branch.

The Location format (**Figure 7B**) is generated with the LocationViz plug-in, which is also used for Anatomical searches. Users can click on the plotted neurons to quickly access their detailed information. This plug-in is also used by Branch Editors to mark or edit the soma location of an identified neuron.

The Network format (**Figure 7C**) is generated by another plug-in, NetworkViz. A major function of NeuronBank is to catalog synaptic connectivity. As most neurons have many synaptic partners, a simple list of inputs and outputs is overwhelming. Typically, a network diagram provides a more intuitive display of a neuron's local circuitry. The NetworkViz plug-in provides a complete network graph of search results and also the local partners of individual neurons. Users can re-arrange the nodes in the network and link into the detail pages of displayed neurons and connections. We have not yet implemented search and edit modes for this plug-in. This plug-in was developed with the Prefuse.org visualization toolkit, a free (BSD license), Java-based toolkit that provides optimized data structures for graphs, a host of layout and visual encoding techniques, and support for dynamic queries, integrated search, and knowledgebase connectivity.

Each of the neurons is represented as a node connected by arrows to other neurons. This network diagram was dynamically generated from the information in the *Tritonia* branch. Thus, we have created a system that can automatically generate neuronal circuit diagrams. In this case, the entire swim central pattern generator and its immediate outputs were pulled from the knowledgebase. Right clicking on any neuron or synapse will open the detail page for that item.

Results from

Branch	Query Status	No. of Results
Tritonia	Query Complete	37
SandBox	Query Complete	3
Melibe	Query Complete	1

FIGURE 6 | Cross branch query results. The query from **Figure 5** was submitted to all branches. The number of results obtained from each branch is displayed in the column on the right. Clicking on the name of the branch takes the user to the results for that branch.

AN EXAMPLE NEURON

The detail page for one neuron (DSI) is shown in **Figure 8**. This page demonstrates more of the features incorporated into both BranchKB and the web client. The top left panel shows the attributes of DSI and the values of those attributes. Some of the attributes (**Figure 8, #1**) are core attributes, such as the *Accession ID*, which is used in an automated Return URL (**Figure 8, #2**) that links directly to this record. This accession ID has now been cited in published papers (Calin-Jageman et al., 2007b; Hill and Katz, 2007; Katz, 2007, 2009; Sakurai et al., 2007; Hill et al., 2008; Sakurai and Katz, 2008, 2009), allowing readers of those papers access to the information about the neuron stored in NeuronBank. This table also shows a number of extensible attributes. (**Figure 8, #3**), such as soma coloration and behavior, which are specific to *Tritonia*. The location of the cell body indicated on a map, was

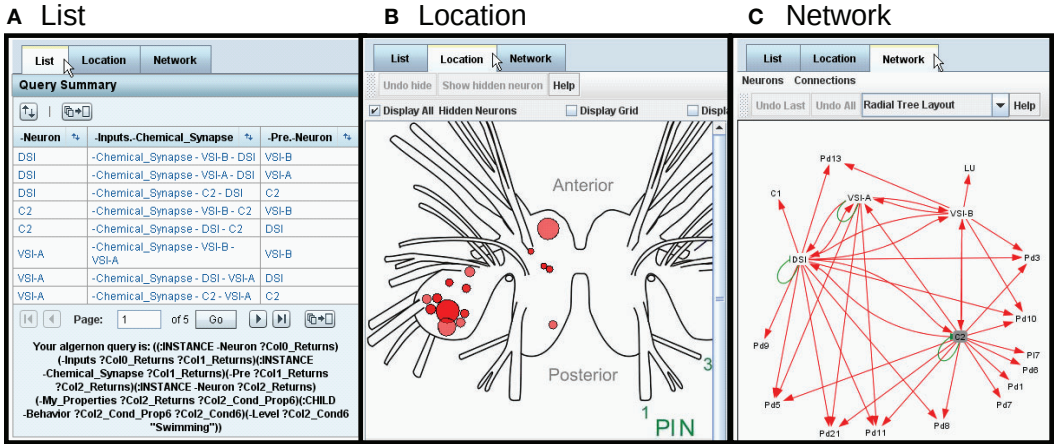

FIGURE 7 | Three ways to view the results: List, Location, and Network (tabs). (A) The List view shows all parts of the search result as clickable items. **(B)** The Location view displays the neuron cell bodies on a map of the nervous system. **(C)** The Network view displays the results in the form of a synaptic wiring diagram. Red arrows represent chemical synapses and green arrows represent electrical connections.

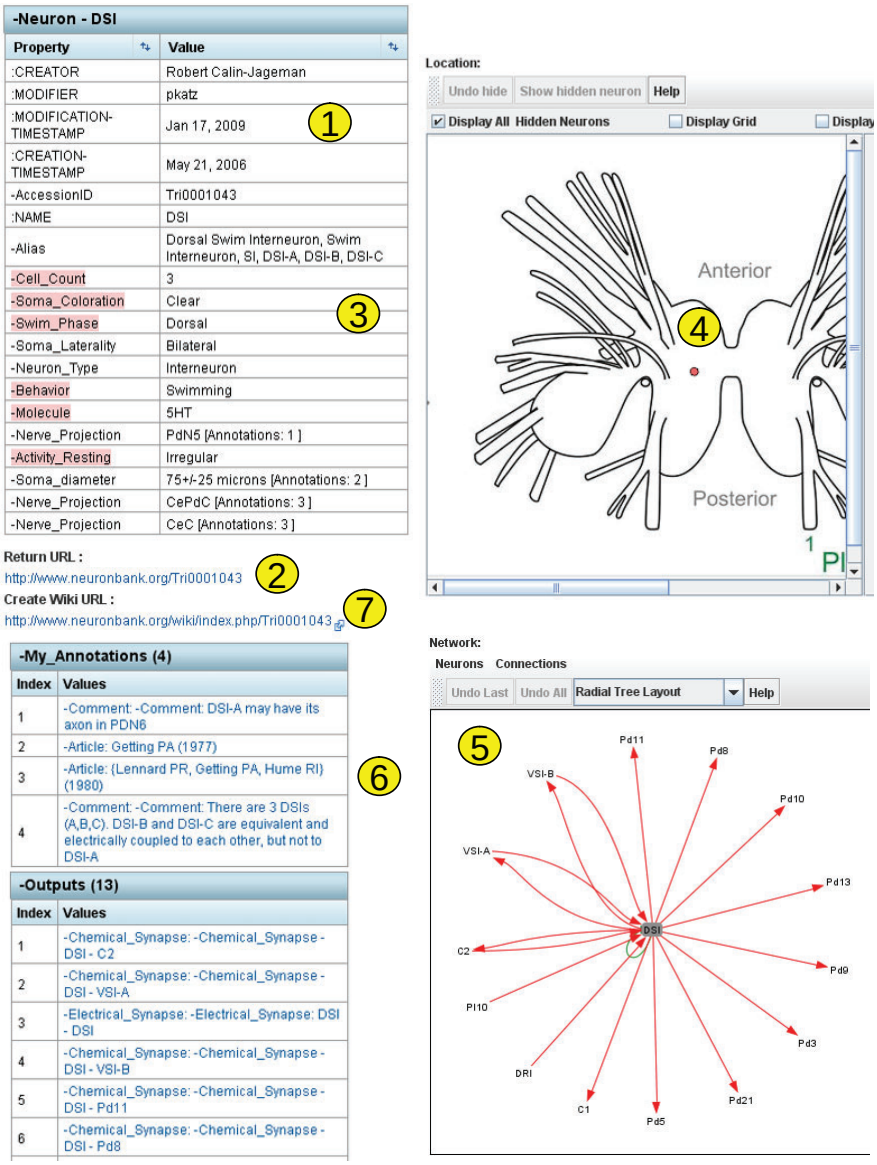

FIGURE 8 | Detail page dynamically generated for DSI.

dynamically generated by LocationViz (**Figure 8, #4**). All input and output synapses are graphically represented in a dynamic format by NetworkViz (**Figure 8, #5**). The detail page contains annotations that document the sources of information and provide additional comments (**Figure 8, #6**). Finally, a link is provided to the entry for this neuron in the NeuronBank Wiki (**Figure 8, #7**), which is explained below.

NEURONBANK WIKI

In parallel to the NeuronBank Branches, we have created a Wikipedia-like NeuronBank Wiki. A link to the Wiki appears at the top of each page. All objects in NeuronBank have an Accession ID, which automatically reserves a unique wiki page URL. This wiki is used for a less constrained description of objects in NeuronBank. The wiki page for DSI is shown in **Figure 9**.

The NeuronBank Wiki has several functions that are synergistic with the NeuronBank knowledgebase. It can be used for information that does not fit a class of NeuronBank objects. In fact, neurons from species that don't have Branches yet can and do have NeuronBank Wiki entries[5]. Unlike the BranchKBs, the NeuronBank Wiki is open to be edited by any registered user of NeuronBank. It can serve as a Neuromics Encyclopedia. We have had success in using the NeuronBank Wiki as a means to gather information from researchers for ultimate incorporation into a NeuronBank branch. We have also used the wiki for educational purposes. Students can initiate pages about neurons, which can be read and released by instructors. Some of the student-initiated pages can be seen at http://neuronbank.org/wiki/index.php/Category:Biol6102_student_pages.

[5]www.neuronbank.org/wiki/index.php/GPR

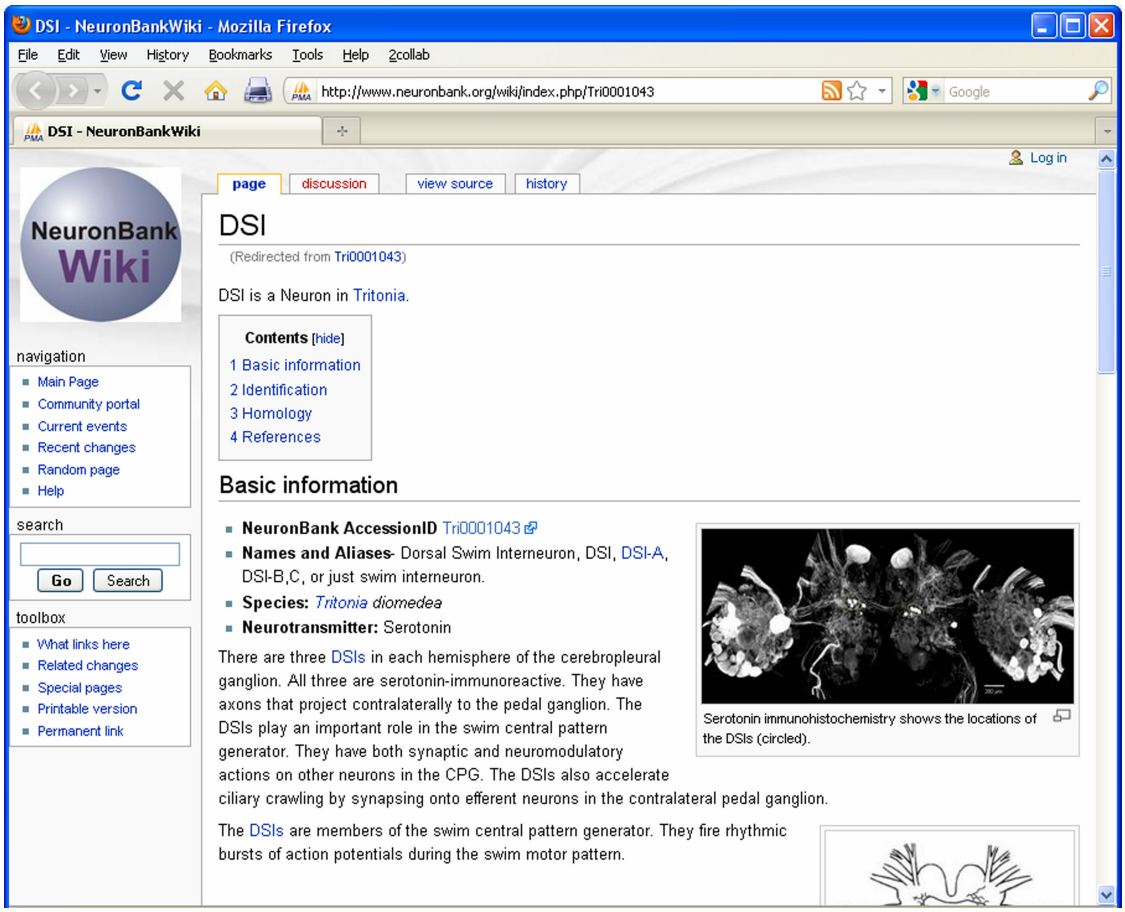

FIGURE 9 | Screen shot of the NeuronBank Wiki page for DSI.

DISCUSSION

NeuronBank is a first generation neural circuit atlas that fulfills many of the necessary criteria. NeuronBank users access a web interface that hides the complexity of the underlying structure of NeuronBank. The different branches are unified by NB-Central. The information about each species is housed in a separate data store, which is accessed through BranchKB. Each branch allows for a flexible representation of neurons; new attributes can be added at any time and incorporated in the extensible list of attributes. NeuronBank can represent neurons from different species even if those nervous systems have different characteristics. The extensible attribute list allows the different branches of NeuronBank to be customized. Plug-in architecture allows data stored in the database to be visualized differently. Currently, there are two plug-ins: one for cell soma location (LocationViz) and the other for neural circuit visualization (NetworkViz). Additional plug-ins can be developed as the need arises. Finally, NeuronBank provides a number of different means to search the information in the database within a species and across species.

The detailed records for each neuron provide complete tables of attributes, all source information, and visualization of anatomical location and synaptic connectivity. This functionality can be readily tested on the *Tritonia* branch accessible from NeuronBank.org. One immediate advantage of having this system online is that information about *Tritonia* neurons is now accessible with a simple Google search, such as "DSI NeuronBank", greatly increasing the accessibility of this information for both research and education.

The NeuronBank wiki is a unique contribution in that it acts to bridge the gap between the unstructured wiki, which is difficult to search, and the very structured database, which has a less familiar appearance to many users. Each entry in NeuronBank has a reserved wiki page. Similarly every object in the NeuronBank knowledgebase also has a unique AccessID, which defines a unique URL. This allows the wiki to link back to objects in the knowledgebase. Searching the knowledgebase can then link the user to information that is presented in an encyclopedic format on the wiki.

The wiki has the potential to become the source of input to a NeuronBank branch. Users can input information into the wiki, which can be monitored by editors who then incorporate that information into the formal knowledgebase.

NeuronBank and the NeuronBank Wiki have potential as an educational tool. Already there are several dozen pages that have been contributed to the NeuronBank wiki by students in courses and in laboratories. These pages can be edited by the community to provide encyclopedic references for neurons and neuronal features. Students who are learning about the neural circuits represented in NeuronBank can have a reference source for neuron identification.

NeuronBank also serves as a neural registry. As more neurons are identified, their characteristics can be compared against those in the registry to determine if they represent a new class of neurons. This may accelerate the investigation of research on neural circuits. Research involving the identification of neurons has slowed considerably since gastropod nervous systems were first examined with electrophysiology in the 1960s. In *Tritonia*, most of the neurons that are known today, were identified by 1973 (Willows et al., 1973). Only three neuronal identifications were published in the last decade (Frost et al., 2001, 2003). However, lab books contain additional neurons that have been uniquely identified. Generally, unless a functional story is associated with the identification of a neuron, it is not possible to publish that identification in a journal. Therefore, having an outlet for publication of incremental knowledge is crucial for the continued advancement of the field.

FUTURE DIRECTIONS

The current version of NeuronBank should still be considered a prototype because the components supporting data entry, user management, and ontology curation are extremely rudimentary and have not yet been made available for public use. Moreover, some additional features remain to be implemented for general users. For example, the form based search, although powerful, is awkward to use and must be replaced by a more user-friendly search interface.

One issue to be resolved is how to maintain common ontologies across species to enable cross-species searches. One possible solution is to register all terms in a common lexicon, such as Neurolex.org. As long as the terms are consistent in their meaning and usage, then it ought to be possible to keep the various branches in alignment. Curation policies will need to be implemented.

A bigger problem with tools such as this is to get community buy in. There needs to be a critical mass of information already available before scientists will begin to use the tool. So, an initial investment needs to be made in creating branches and wiki pages. Recent initiatives by the International Neuroinformatics Coordinating Facility (INCF)[6] promise to increase the awareness and use of informatic tools such as NeuronBank.

ACKNOWLEDGMENTS

Jason Pamplin, John Propper, Hao Tian, Piyaphol Phoungphol, Janaka Balasooriya, and Yan Chen for their contributions to NeuronBank. We thank Joshua Lillvis and Arianna Tomvacakis for their helpful suggestions on an earlier version of this manuscript. We are grateful to Akira Sakurai for helping with the figures. Supported by NIH R21 MH76753, NSF IIS-0827418, and seed grants from Georgia State University.

[6]http://www.incf.org/

REFERENCES

Altun, Z. F., Herndon, L. A., Crocker, C., Lints, R., and Hall, D. H. (2009). Available at: www.wormatlas.org.

Arendt, D. (2008). The evolution of cell types in animals: emerging principles from molecular studies. *Nat. Rev. Genet.* 9, 868–882.

Ascoli, G. A., onso-Nanclares, L., Anderson, S. A., Barrionuevo, G., avides-Piccione, R., Burkhalter, A., Buzsaki, G., Cauli, B., Defelipe, J., Fairen, A., Feldmeyer, D., Fishell, G., Fregnac, Y., Freund, T. F., Gardner, D., Gardner, E. P., Goldberg, J. H., Helmstaedter, M., Hestrin, S., Karube, F., Kisvarday, Z. F., Lambolez, B., Lewis, D. A., Marin, O., Markram, H., Munoz, A., Packer, A., Petersen, C. C., Rockland, K. S., Rossier, J., Rudy, B., Somogyi, P., Staiger, J. F., Tamas, G., Thomson, A. M., Toledo-Rodriguez, M., Wang, Y., West, D. C., and Yuste, R. (2008). Petilla terminology: nomenclature of features of GABAergic interneurons of the cerebral cortex. *Nat. Rev. Neurosci.* 9, 557–568.

Bota, M., Dong, H. W., and Swanson, L. W. (2005). Brain architecture management system. *Neuroinformatics* 3, 15–48.

Bota, M., and Swanson, L. W. (2007). The neuron classification problem. *Brain Res. Rev.* 56, 79–88.

Briggman, K. L., and Denk, W. (2006). Towards neural circuit reconstruction with volume electron microscopy techniques. *Curr. Opin. Neurobiol.* 16, 562–570.

Brodfuehrer, P. D., and Thorogood, M. S. E. (2001). Identified neurons and leech swimming behavior. *Prog. Neurobiol.* 63, 371–381.

Bug, W. J., Ascoli, G. A., Grethe, J. S., Gupta, A., Fennema-Notestine, C., Laird, A. R., Larson, S. D., Rubin, D., Shepherd, G. M., Turner, J. A., and Martone, M. E. (2008). The NIFSTD and BIRNLex vocabularies: building comprehensive ontologies for neuroscience. *Neuroinformatics* 6, 175–194.

Bullock, T. H. (1993a). How are more complex brains different? One view and an agenda for comparative neurobiology. *Brain Behav. Evol.* 41, 88–96.

Bullock, T. H. (1993b). *How Do Brains Work*? Boston: Birkhauser.

Bullock, T. H. (2000). Revisiting the concept of identifiable neurons. *Brain Behav. Evol.* 55, 236–240.

Calin-Jageman, R. J., Dhawan, A., Yang, H., Wang, H.-C., Tian, H., Phounghol, P., Frederick, C., Balasooriya, J., Chen, Y., Prasad, S. K., Sunderraman, R., Zhu, Y., and Katz, P. S. (2007a). "Development of NeuronBank: A Federation of Customizable Knowledge Bases of Neuronal Circuitry," in *Proceedings of the Ist IEEE International Workshop on Service Oriented Technologies for Biological Databases and Tools, IEEE Services Computing Workshops* (SOBDAT/SCW 2007). Salt Lake City, UT.

Calin-Jageman, R. J., Tunstall, M. J., Mensh, B. D., Katz, P. S., and Frost, W. N. (2007b). Parameter space analysis suggests multi-site plasticity contributes to motor pattern initiation in Tritonia. *J. Neurophysiol.* 98, 2382–2398.

Coggeshall, R. E. (1967). A light and electron microscope study of the abdominal ganglion of *Aplysia californica*. *J. Neurophysiol.* 30, 1263–1287.

Comer, C. M., and Robertson, R. M. (2001). Identified nerve cells and insect behavior. *Prog. Neurobiol.* 63, 409–439.

Croll, R. P. (1987). "Identified neurons and cellular homologies," in *Nervous Systems in Invertebrates*, ed. M. A. Ali MA (New York: Plenum Publishing Corp.), 41–59.

De Bono, M., and Maricq, A. V. (2005). Neuronal substrates of complex behaviors in C. elegans. *Annu. Rev. Neurosci.* 28, 451–501.

Emery, D. G., and Audesirk, T. E. (1978). Sensory cells in Aplysia. *J. Neurobiol.* 9, 173–179.

Frost, W. N., Hoppe, T. A., Wang, J., and Tian, L. M. (2001). Swim initiation neurons in Tritonia diomedea. *Am. Zool.* 41, 952–961.

Frost, W. N., Tian, L. M., Hoppe, T. A., Mongeluzi, D. L., and Wang, J. (2003). A cellular mechanism for prepulse inhibition. *Neuron* 40, 991–1001.

Getting, P. A. (1976). Afferent neurons mediating escape swimming of the marine mollusc, *Tritonia*. *J. Comp. Physiol.* 110, 271–286.

Getting, P. A. (1989). "A network oscillator underlying swimming in *Tritonia*," in *Neuronal and Cellular Oscillators*, ed. J. W. Jacklet (New York: Marcel Dekker, Inc), 215–236.

Getting, P. A., and Dekin, M. S. (1985). "*Tritonia* swimming: a model system for integration within rhythmic motor systems," in *Model Neural Networks and Behavior Selverston*, ed. A. I. Selverston (New York: Plenum Press), 3–20.

Helmstaedter, M., Briggman, K. L., and Denk, W. (2008). 3D structural imaging of the brain with photons and electrons. *Curr. Opin. Neurobiol.* 18, 633–641.

Hill, E. S., and Katz, P. S. (2007). Role of membrane potential in calcium signaling during rhythmic bursting in tritonia swim interneurons. *J. Neurophysiol.* 97, 2204–2214.

Hill, E. S., Sakurai, A., and Katz, P. S. (2008). Transient enhancement of spike-evoked calcium signaling by a serotonergic interneuron. *J. Neurophysiol.* 100, 2919–2928.

ito-Gutierrez, E., and Arendt, D. (2009). CNS evolution: new insight from the mud. *Curr. Biol.* 19, R640–R642.

Jurrus, E., Hardy, M., Tasdizen, T., Fletcher, P. T., Koshevoy, P., Chien, C. B., Denk, W., and Whitaker, R. (2009). Axon tracking in serial block-face scanning electron microscopy. *Med. Image Anal.* 13, 180–188.

Kandel, E. R., Frazier, W. T., Waziri, R., and Coggeshall, R. E. (1967). Direct and common connections among identified neurons in Aplysia. *J. Neurophysiol.* 30, 1352–1376.

Karbowski, J., Schindelman, G., Cronin, C. J., Seah, A., and Sternberg, P. W. (2007). Systems level circuit model of *C. elegans* undulatory locomotion: mathematical modeling and molecular genetics. *J. Comput. Neurosci.* 24, 253–276.

Katz, P. S. (2007). Tritonia. *Scholarpedia J.* 2, 3504.

Katz, P. S. (2009). Tritonia swim network. *Scholarpedia J.* 4, 3638.

Lichtman, J. W., Livet, J., and Sanes, J. R. (2008). A technicolour approach to the connectome. *Nat. Rev. Neurosci.* 9, 417–422.

Livet, J., Weissman, T. A., Kang, H., Draft, R. W., Lu, J., Bennis, R. A., Sanes, J. R., and Lichtman, J. W. (2007). Transgenic strategies for combinatorial expression of fluorescent proteins in the nervous system. *Nature* 450, 56–62.

Masland, R. H. (2004). Neuronal cell types. *Curr. Biol.* 14, R497–R500.

Miller, G. (2009). Origins. On the origin of the nervous system. *Science* 325, 24–26.

Moroz, L. L. (2009). On the independent origins of complex brains and neurons. *Brain Behav. Evol.* 74, 177–190.

Murray, J. A., and Willows, A. O. D. (1996). Function of identified nerves in orientation to water flow in Tritonia diomedea. *J. Comp. Physiol. A* 178, 201–209.

Musen, M. A., Eriksson, H., Gennari, J. H., Tu, S. W., and Puerta, A. R. (1994). PROTEGE-II: a suite of tools for development of intelligent systems from reusable components. *Proc. Annu. Symp. Comput. Appl. Med. Care* 1065.

Nelson, S. B., Hempel, C., and Sugino, K. (2006a). Probing the transcriptome of neuronal cell types. *Curr. Opin. Neurobiol.* 16, 571–576.

Nelson, S. B., Sugino, K., and Hempel, C. M. (2006b). The problem of neuronal cell types: a physiological genomics approach. *Trends Neurosci.* 29, 339–345.

Newcomb, J. M., and Katz, P. S. (2007). Homologues of serotonergic central pattern generator neurons in related nudibranch molluscs with divergent behaviors. *J. Comp. Physiol. A Neuroethol. Sens. Neural. Behav. Physiol.* 193, 425–443.

Nielsen, C. (1999). Origin of the chordate central nervous system – and the origin of chordates. *Dev. Genes Evol.* 209, 198–205.

Noy, N. F., Crubezy, M., Fergerson, R. W., Knublauch, H., Tu, S. W., Vendetti, J., and Musen, M. A. (2003). Protege-2000: an open-source ontology-development and knowledge-acquisition environment. *AMIA Annu. Symp. Proc.* 953.

Paul, D. H. (1991). Pedigrees of neurobehavioral circuits: Tracing the evolution of novel behaviors by comparing motor patterns, muscles, and neurons in members of related taxa. *Brain Behav. Evol.* 38, 226–239.

Ramon y Cajal, S. (1995). *Histology of the Nervous System of Man and Vertebrates [English translation]*. Oxford: Oxford University Press.

Sakurai, A., Calin-Jageman, R. J., and Katz, P. S. (2007). The potentiation phase of spike timing-dependent neuromodulation by a serotonergic interneuron involves an increase in the fraction of transmitter release. *J. Neurophysiol.* 98, 1975–1987.

Sakurai, A., and Katz, P. S. (2008). "A serotonergic interneuron evokes both state-dependent and state-independent neuromodulatory actions," in *Neuroscience Meeting Planner Washington* (DC: Society for Neuroscience) 574.3.

Sakurai, A., and Katz, P. S. (2009). State-, timing-, and pattern-dependent neuromodulation of synaptic strength by a serotonergic interneuron. *J. Neurosci.* 29, 268–279.

Schafer, W. R. (2005). Deciphering the neural and molecular mechanisms of *C. elegans* behavior. *Curr. Biol.* 15, R723–R729.

Selverston, A. (2008). Stomatogastric ganglion. *Scholarpedia J.* 3, 1661.

Smith, S. J. (2007). Circuit reconstruction tools today. *Curr. Opin. Neurobiol.* 17, 601–608.

Thomas, J. B., Bastiani, M., Bate, M., and Goodman, C. S. (1984). From grasshopper to *Drosophila*: a common plan for neuronal development. *Nature* 310, 203–207.

Thompson, S., and Watson, W. H. III (2005). Central pattern generator for swimming in Melibe. *J. Exp. Biol.* 208, 1347–1361.

Van Hooser, S. D., Heimel, J. A., and Nelson, S. B. (2005). Functional cell classes and functional architecture in the early visual system of a highly visual rodent. *Prog. Brain Res.* 149, 127–145.

Weiss, K. R., and Kupfermann, I. (1976). Homology of the giant serotonergic neurons (metacerebral cells) in Aplysia and pulmonate molluscs. *Brain Res.* 117, 33–49.

White, J. G., Southgate, E., Thomson, J. N., and Brenner, S. (1976). The structure of the ventral nerve cord of *Caenorhabditis elegans*. *Philos. Trans. R. Soc. Lond., B, Biol. Sci.* 275, 327–348.

White, J. G., Southgate, E., Thomson, J. N., and Brenner, S. (1986). The structure of the nervous system of the nematode *Caenorhabditis elegans*. *Philos. Trans. R. Soc. Lond., B, Biol. Sci.* 314, 1–340.

Willows, A. O. D., Dorsett, D. A., and Hoyle, G. (1973). The neuronal basis of behavior in *Tritonia*. I. Functional organization of the central nervous system. *J. Neurobiol.* 4, 207–237.

Conflict of Interest Statement: The authors declare that the research was conducted in the absence of any commercial or financial relationships that could be construed as a potential conflict of interest.

Received: 14 November 2009; paper pending published: 27 February 2010; accepted: 31 March 2010; published online: 19 April 2010.

*Citation: Katz PS, Calin-Jageman R, Dhawan A, Frederick C, Guo S, Dissanayaka R, Hiremath N, Ma W, Shen X, Wang HC, Yang H, Prasad S, Sunderraman R and Zhu Y. (2010) NeuronBank: a tool for cataloging neuronal circuitry. Front. Syst. Neurosci. **4**:9. doi: 10.3389/fnsys.2010.00009*

frontiers in
SYSTEMS NEUROSCIENCE

ORIGINAL RESEARCH ARTICLE
published: 03 February 2010
doi: 10.3389/neuro.06.021.2009

The locust standard brain: a 3D standard of the central complex as a platform for neural network analysis

Basil el Jundi[1], Stanley Heinze[1†], Constanze Lenschow[1†], Angela Kurylas[1], Torsten Rohlfing[2] and Uwe Homberg[1]*

[1] *Fachbereich Biologie, Tierphysiologie, Philipps-Universität Marburg, Marburg, Germany*
[2] *Neuroscience Program, SRI International, Menlo Park, CA, USA*

Edited by:
Randolf Menzel, Freie Universitat Berlin, Germany

Reviewed by:
Jürgen Rybak, Max Planck Institute for Chemical Ecology, Germany
Hanna Mustaparta, Norwegian University of Science and Technology, Norway

***Correspondence:**
Uwe Homberg, Fachbereich Biologie, Tierphysiologie, Philipps-Universität Marburg, D-35032 Marburg, Germany.
e-mail: homberg@staff.uni-marburg.de

†Present address:
Stanley Heinze, Department of Neurobiology, University of Massachusetts Medical School, Worcester, Massachusetts 01605, USA; Constanze Lenschow, Fachbereich Biologie, Freie Universität Berlin, Germany.

Many insects use the pattern of polarized light in the sky for spatial orientation and navigation. We have investigated the polarization vision system in the desert locust. To create a common platform for anatomical studies on polarization vision pathways, Kurylas et al. (2008) have generated a three-dimensional (3D) standard brain from confocal microscopy image stacks of 10 male brains, using two different standardization methods, the Iterative Shape Averaging (ISA) procedure and the Virtual Insect Brain (VIB) protocol. Comparison of both standardization methods showed that the VIB standard is ideal for comparative volume analysis of neuropils, whereas the ISA standard is the method of choice to analyze the morphology and connectivity of neurons. The central complex is a key processing stage for polarization information in the locust brain. To investigate neuronal connections between diverse central-complex neurons, we generated a higher-resolution standard atlas of the central complex and surrounding areas, using the ISA method based on brain sections from 20 individual central complexes. To explore the usefulness of this atlas, two central-complex neurons, a polarization-sensitive columnar neuron (type CPU1a) and a tangential neuron that is activated during flight, the giant fan-shaped (GFS) neuron, were reconstructed 3D from brain sections. To examine whether the GFS neuron is a candidate to contribute to synaptic input to the CPU1a neuron, we registered both neurons into the standardized central complex. Visualization of both neurons revealed a potential connection of the CPU1a and GFS neurons in layer II of the upper division of the central body.

Keywords: iterative shape averaging, virtual insect brain, single-cell registration, central complex, desert locust, digital neuroanatomy, standard brain, 3D

INTRODUCTION

Many insects are able to perceive the pattern of polarized light in the blue sky (Horváth and Varjú, 2004). Studies on bees and ants have shown that these insects use the celestial polarization pattern for spatial orientation and navigation (Wehner, 1992). These and other insect species detect the plane of skylight polarization (*E*-vector) with a specialized dorsal rim area (DRA) of their compound eye (Labhart and Meyer, 1999; Mappes and Homberg, 2004). Photoreceptors in the DRA are highly sensitive to polarized light and send axonal projections to distinct dorsal regions of the lamina and medulla (Blum and Labhart, 2000; Homberg and Paech, 2002). Polarization-sensitive (POL) interneurons have been studied in the brain of the field cricket (Labhart, 1988; Labhart et al., 2001; Sakura et al., 2008) and in the desert locust *Schistocerca gregaria* (Vitzthum et al., 2002; Pfeiffer et al., 2005; Kinoshita et al., 2007; Pfeiffer and Homberg, 2007; Heinze and Homberg, 2009; Heinze et al., 2009).

In locusts, POL-neurons innervate specific, mostly small and distinct neuropils in the brain that are specialized for integration and processing of polarized-light information. These neuropils are connected by distinct fiber bundles and can be regarded as elements of a polarization vision pathway in the locust brain (Homberg, 2004). Neurons of a small ventral layer of the anterior lobe of the lobula (ALo) receive polarization information from the dorsal rim area of the medulla (DRMe) and send these signals to the anterior optic tubercle (AOTu) in the central brain. Only neurons of the lower unit of the AOTu are sensitive to polarized light (Pfeiffer et al., 2005). These neurons integrate signals from the sky polarization and chromatic contrast and compensate their *E*-vector tuning for diurnal changes in solar elevation (Pfeiffer and Homberg, 2007). Polarization information is transmitted from the AOTu to two distinct regions of the lateral accessory lobe, the median olive (MO) and the lateral triangle (LT) (Homberg et al., 2003). From these areas, neurons transfer polarization information to a final processing stage of the polarization vision pathway, the central complex.

Abbreviations: 3D, Three-dimensional; aCa, Accessory calyx; AL, Antennal lobe; aL, Anterior lip; ALo, Anterior lobe of the lobula; aMe, Accessory medulla; AOTu, Anterior optic tubercle; CBU, Upper division of the central body; CBL, Lower division of the central body; CPU, Columnar neuron of the CBU and PB; CL, Columnar neuron of the CBL; CLSM, Confocal laser scanning microscope; CC, Central complex; DLo, Dorsal lobe of the lobula; DRA, Dorsal rim area; DRMe, Dorsal rim area of the medulla; DS, Dorsal shell; GAM, Goat anti-mouse; GAR, Goat anti-rabbit; GFS, Giant fan-shaped (neuron); ILo, Inner lobe of the lobula; ISA, Iterative shape averaging (method); LAL, Lateral accessory lobe; lAOTu, Lower unit of the anterior optic tubercle; LH, Lateral horn; LT, Lateral triangle; MB, Mushroom body; Me, Medulla; MN, Midbrain neuropil; MO, Median olive; NGS, Normal goat serum; No, Nodulus; NoL, Lower unit of the nodulus; NoU, Upper unit of the nodulus; OLo, Outer lobe of the lobula; PB, Protocerebral bridge; PBS, Phosphate-buffered saline; PBT, PBS containing 0.3% Triton X-100; pCa, Primary calyx; Pe, Pedunculus; POL, Polarization-sensitive; TB, Tangential neuron of the PB; TL, Tangential neuron of the CBL; uAOTu, Upper unit of the anterior optic tubercle; VIB, Virtual insect brain (method); VS, Ventral shell

The central complex comprises a group of neuropils spanning the midline of the brain and consists of the protocerebral bridge (PB), the upper (CBU) and lower (CBL) divisions of the central body, and a pair of postero-ventral neuropils, termed noduli (No).

Studies in *Drosophila* suggest a role of the central complex in walking and leg coordination (Strauss and Heisenberg, 1993; Strauss, 2002; Poeck et al., 2008), flight control (Ilius et al., 1994), spatial orientation (Strauss, 2002; Neuser et al., 2008), and memory for visual object parameters (Liu et al., 2006; Wang et al., 2008). Together with evidence from locusts for a prominent role in sky compass orientation (Vitzthum et al., 2002; Heinze and Homberg, 2007), the central complex can be regarded as an integration center for multisensory information that is relevant to spatial memory and spatial orientation in diverse behaviours. One of the key features of the central complex is a highly modular neuroarchitecture. The CBU and CBL are organized into sets of clearly defined horizontal layers (Homberg, 1991; Müller et al., 1997) and the CBU, CBL and PB, in addition, into arrays of 16 regular vertical modules, called columns (Williams, 1975). Three major classes of cell types have been distinguished in the central complexes of locusts and other insects: (i) tangential neurons arborize in various areas outside the central complex and provide signaling input to distinct layers (Strausfeld, 1976; Hanesch et al., 1989); (ii) pontine neurons interconnect defined columns of the CBU in a regular way (Hanesch et al., 1989; Siegl et al., 2009), and (iii) columnar neurons provide signaling output from columnar domains to follower neurons in the lateral accessory lobes (LALs) (Hanesch et al., 1989; Heinze and Homberg, 2008). A subset of at least 13 different types of columnar and tangential neurons in the locust central complex are sensitive to polarized light (Vitzthum et al., 2002; Heinze and Homberg, 2009; Heinze et al., 2009), and many of these contribute to a topographic representation of *E*-vectors underlying the columnar neuroarchitecture of the PB (Heinze and Homberg, 2007).

For a deeper understanding of information processing in the neuronal network of the central complex, detailed knowledge about the synaptic connections between the different cell types is essential. An important step towards this goal is the generation of a high-quality three-dimensional (3D) anatomical atlas of the brain in which individual variations in shape, position and size of brain structures have been eliminated. This standard atlas can then serve as a platform to pool and simultaneaously visualize neurons from different preparations. Improvements in 3D imaging, processing, and computational capacity have permitted the creation of 3D standard brain atlases of the fruit fly, *Drosophila melanogaster* (Rein et al., 2002), the honey bee, *Apis mellifera* (Brandt et al., 2005), the desert locust, *Schistocerca gregaria* (Kurylas et al., 2008), and the moths, *Manduca sexta* (el Jundi et al., 2009) and *Heliothis virescens* (Kvello et al., 2009). For generation of these atlases, two different standardization methods have been established. The Virtual Insect Brain (VIB) protocol (Jenett et al., 2006) was used for the *Drosophila* and *Manduca* standard brains, whereas the Iterative Shape Averaging (ISA) method (Rohlfing et al., 2001) was used for the *Apis* and *Heliothis* standard brains. The VIB standard brains of *Drosophila* and *Manduca* were used primarily to compare volumes of brain areas between sexes. In contrast, the ISA brain of the honey bee was created to register single neurons from individual brains into a common standard. To reveal the limitations and advantages of the ISA and VIB procedures, both techniques were applied in comparison for the generation of a standard brain of the desert locust (Kurylas et al., 2008).

In this study we review the ISA and VIB standard brains of the desert locust and compare their advantages and limitations. As our goal is the analysis of neural connections in the central-complex network, we determined the ISA standardization method as the more appropriate one. To facilitate accurate representation of central-complex neurons, it is essential to have available an atlas of higher spatial resolution than is typically available for the whole brain. We, therefore, created a new, high-resolution ISA standard atlas of the central complex and immediately adjacent neuropils associated with the central complex. We show herein that this new 3D standard central complex is a highly suitable platform to investigate potential connections between central-complex neurons.

In the current work, we focus our attention to the columnar cell type CPU1a (Vitzthum et al., 2002). Previous analyses suggested that CPU1a neurons receive input from single columns of the PB and from a pair of columns of the CBU (Heinze and Homberg, 2008). In addition to polarized-light input, which is most likely provided in the PB arborizations (Heinze et al., 2009), the CPU1a neuron receives input in the CBU columns which is probably polarization-independent. A candidate neuron to provide synaptic input in the CBU is the tangential giant fan-shaped (GFS) neuron (Williams, 1972; Homberg, 1994), which arborizes in the CBU. To investigate possible connections between both neurons, we reconstructed a GFS and a CPU1a neuron in 3D and registered both into the standard central complex. The visualization of both neurons in the standard central complex reveals potential connections between these neurons in layer II of the CBU.

MATERIALS AND METHODS

ANIMALS

Desert locusts (*Schistocerca gregaria)* were reared under crowded conditions at 28°C on a 12:12 light/dark cycle. Only adult gregarious male locusts (1–3 weeks after imaginal moult) were used for reconstructions of the central complexes.

STANDARDIZED CENTRAL COMPLEX

Immunocytochemistry

Brains were dissected out of the head capsule and were fixed over night in 4% formaldehyde/0.1 M phosphate-buffered saline (4% FA/PBS, pH 7.4) at 4°C. They were then embedded in gelatine/albumin and sectioned from anterior to posterior with a vibrating-blade microtome (Leica VT1200 S, Leica Microsystems, Wetzlar, Germany) into 250-µm thick frontal sections. Brain sections were rinsed in 0.1 M PBS containing 0.3% Triton X-100 (PBT) for 1 h at room temperature and were preincubated (4°C, over night) in 5% normal goat serum (NGS; Jackson ImmunoResearch, Westgrove, PA, USA) in 0.1 M PBT containing 0.02% sodium azide. For visualization of distinct brain areas, all specimens were incubated with a monoclonal mouse antibody against the presynaptic vesicle protein synapsin I (SYNORF1, Klagges et al., 1996, kindly provided by Dr. E. Buchner, Würzburg) for 4–6 days at 4°C. Anti-synapsin was diluted 1:50 in 0.1 M PBT containing 1% NGS and 0.02% sodium azide. To distinguish the layers of the central body, a rabbit antibody against

serotonin was added to the primary antibody solution (1:20,000; Diasorin, Dietzenbach, Germany). After extensive rinsing, sections were incubated with goat anti-mouse (GAM) antibody conjugated to Cy5 and goat anti-rabbit (GAR) antibody conjugated to Cy2 (both 1:300; Jackson ImmunoResearch, Westgrove, PA, USA) in 0.1 M PBT, 1% NGS and 0.02% sodium azide for up to 3 days at 4°C. After rinsing, preparations were dehydrated in an ascending ethanol series (30–100%, 15 min each) and were cleared with a solution of 1:1 ethanol/methyl salicylate (15 min) followed by methyl salicylate (at least 40 min). Brain sections were embedded between two coverslips in Permount (Fisher Scientific, Pittsburgh, PA, USA). Compression of the preparations was prevented by spacers (Zweckform, Oberlaindern, Germany).

CLSM image acquisition

The brain sections were scanned using a confocal laser scanning microscope (CLSM, Leica TCS SP2) with a 20× oil objective (HC PL APO 20×/0.70 lmm Corr CS, Leica, Bensheim, Germany). The fluorescent signal of Cy5 was detected with a HeNe laser (633 nm). In addition, the sections were also scanned with an Ar laser (488 nm) to detect the serotonin staining signal (Cy2). The sections were scanned with 1024 × 1024 pixels per stack in xy direction (pixel size in xy direction: 1 × 1 μm) and 1 μm step size in z direction. Sections were scanned from anterior and posterior.

Image processing and reconstruction

The image stacks of the central complex and surrounding neuropils obtained from the brain sections were processed using Amira 4.1.2 software (Visage Imaging, Fürth, Germany). Because the central complex and surrounding neuropils extended across several brain sections we first aligned the corresponding image data. Pairs of image stacks from adjacent brain sections were opened in Amira and the matching optical slices in both stacks of data were selected. These optical slices were exactly overlapped with the *TransformEditor* by translation in *x*, *y* and *z* direction and by rotation of the image stacks. The image stacks were then connected using the module *Merge*. The resulting image data showed a detailed representation of staining for synapsin and serotonin of the central complex and surrounding brain areas.

For 3D reconstructions, *Labelfield* files were created with the same dimensions (voxel size and resolution) as the corresponding merged image stacks. Using the *Segmentation Editor*, reconstructions of selected neuropils were performed. All neuropils were labeled based on the anti-synapsin image stacks except for layers II and III of the CBU. These layers could not be distinguished in the synapsin channel and were, therefore, reconstructed using the corresponding anti-serotonin image stacks. Regions of interest were labeled in 3D in several optical slices and contiguous 3D structures were reconstructed using the tool *Wrap*.

Standardization of the central complex

We used 20 sectioned brains from male locusts to generate a 3D standardized central complex using the ISA method. For an exact registration of the neuropils of interest it was essential to mask the areas surrounding the central complex and LALs in the image stacks with the module *Arithmetic*. In some of the image stacks we corrected the tonal value using Adobe Photoshop 8 (Adobe Systems, San Jose, CA, USA) Furthermore, due to computer memory limitations, it was necessary to downsample the image stacks and the labelfield files with the module *Resample* to a voxel size of 2 × 2 × 2 μm.

For registration of the central complexes the central-complex image stacks and corresponding labelfields were exported to 3D image files in Analyze format. The overall registration procedure was controlled by a shell script, which used command-line driven registration tools developed by one of the authors (TR) and available in source code as part of the Computational Morphometry Toolkit (http://nitrc.org/projects/cmtk/). To reduce the time for image registration and transformation of the 20 central complexes, standardization of the central complex was calculated on a Linux-based cluster provided by Philipps-University of Marburg.

Analogous to the whole-brain procedure, CLSM images of the central complexes were first globally registered to a chosen reference specimen using an affine registration. Then, the iterative averaging and non-rigid transformation procedure was repeated four times. After completion of the averaging process, corresponding standardized 3D reconstructions of the labeled central-complex structures were created by applying the final transformation parameter to the label image stacks that corresponded to the standardized CLSM images. For an accurate standardization of the image stacks, the registration parameters were optimized and refined after repeated visual inspection of the results.

CENTRAL-COMPLEX NEURONS

Staining and immunocytochemistry

Central-complex neurons were injected iontophoretically with 4% Neurobiotin (Vector, Burlingame, CA) through glass microelectrodes with a resistance of 50–180 MΩ. The Neurobiotin was injected with a continuous depolarizing current of 1–3 nA for 1–5 min. The brains were dissected out of the head capsule and were fixed over night in 4% paraformaldehyde at 4°C. Both preparations were processed further as described by Heinze and Homberg (2008). Briefly, after fixation and rinsing, the brains were incubated at 1:1000 with Cy3-streptavidin (Dianova, Hamburg, Germany) in 0.1 M PBT for 3 days. After rinsing in buffer, they were dehydrated in an ascending ethanol series (25%–100%, 15 min each), transferred to ethanol/methyl salicylate (1:1, 15 min), and cleared in methyl salicylate for 35 min. Brains were mounted in Permount between two glass cover slides.

After scanning with the CLSM (10× oil objective) the embedded brains were incubated in xylene (2–4 h) to remove the embedding medium. Brains were rehydated in a descending ethanol series (100%–20%, 15 min. each) and were embedded in gelatine/albumin over night at 4°C. They were sectioned with the vibrating-blade microtome in 130–140-μm thick frontal sections. The sections were rinsed in 0.1 M PBS (4 × 15 min) and, after preincubation in 5% NGS in 0.1 M PBT at 4°C over night, were incubated for 6 days in anti-synapsin (1:50) and Cy3-streptavidin (1:1000) in 0.1 M PBT containing 1% NGS. After washing in 0.1 M PBT for 2 h, the sections were treated with Cy5-GAM (1:300), Cy3-streptavidin (1:1000) and 1% NGS in 0.1 M PBT for up to 3 days at 4°C. After rinsing, the preparations were dehydrated in an ascending ethanol series (30%–100%, 15 min. each) and were cleared with 1:1

ethanol/methyl salicylate (15 min.) followed by methyl salicylate (at least 40 min.). Sections were finally embedded in Permount between two coverslips.

Reconstruction and registration

The dye-injected neurons and the corresponding anti-synapsin stainings were scanned with the CLSM using a 20× or 40× objective (HCX PL APO 40×/1.25–0.75 Oil CS) at a resolution of 1024 × 1024 pixels (voxel size in xy direction: 0.22–0.35 × 0.22–0.35 µm) and a distance of 0.5 µm between optical slices. For neuron reconstructions in 3D we used the *SkeletonTree* tool in Amira 4.1.2 (Schmitt et al., 2004; Evers et al., 2005). Because of the limited computational capacity it was not possible to merge the scanned image stacks of the neurons with the anti-synapsin staining at high resolution. Therefore, we oriented all individual image stacks to the correct position with respect to each other using the *TransformEditor* and saved their positions with the module *ApplyTransform.* Reconstructions of the neurons were performed by opening image stacks consecutively and reconstructing the particular part of the neurons. For reconstruction of the corresponding neuropils the anti-synapsin-labeled image stacks were also transformed to their exact position, downsampled to a voxel size of 1 × 1 × 1 µm, and then merged into a single image stack. The nomenclature for central-complex neuropils and layers follows Heinze and Homberg (2008), the nomenclature for the lateral accessory lobe structures is based on Homberg (1994).

The reconstructed neurons were registered into the standardized central complex and into the standard locust brain of Kurylas et al. (2008). For registration of the neurons we registered distinct neuropils of the individual central complex into the standardized central complex and the standard brain using Amira 4.1.2. Neuropils of the individual central complex were first registered into the standard central complex and the standard brain using an affine transformation, computed by the *AffineRegistration* module. Afterwards, an elastic registration of the neuropils was performed using the module *ElasticRegistration*. The transformation parameters of the registrations were then applied to the neurons using the modules *ApplyTransform* and *ApplyDeformation*. Because of limited computational capacity it was not possible to register all neuropils in one process into the standard central complex. Therefore, we registered only two neuropils into the standard central complex in each case and then applied the registration parameters for the registration of the corresponding part of the neuron. Finally, all registered neuron parts were connected.

Visualization

To visualize our data we used several tools in Amira. The 3D surface views of the reconstructed neuropils were generated with the module *SurfaceGen* and were visualized with the tool *SurfaceView.* Direct volume rendering displays of the CLSM analogous image data of the standard central complex were created with the tool *Voltex*. To hide irrelevant structures surrounding the standardized neuropils and to distinguish the neuropils we masked the image data with the module *Arithmetic.* To this end, we used the standardized neuropil labelfield as a mask and removed surrounding synapsin-immunostained regions. Reconstructed neurons of the central complex were visualized with the *SkeletonView.* Volume data of the neuropils were calculated with the module *TissueStatistics*. Neuropil sizes were measured by the *Measuring* tool. Statistical analysis of these data was performed in SPSS 11.5 (Chicago, IL, USA) for Windows.

RESULTS

STANDARD ATLAS OF THE LOCUST BRAIN

As a basis for further analysis of the neuroarchitecture of the locust brain and, in particular, for better understanding of neural networks associated with polarization vision and sky compass orientation Kurylas et al. (2008) have previously established a standard atlas of the locust brain, based on data from ten male locust brains. Like other standard insect brains (Rein et al., 2002; Brandt et al., 2005) the reconstructions of the brains used for the registration process were based on staining against a synaptic neuropil marker. We briefly review the major findings of that study to illustrate the necessity for higher resolution standard atlases of particular brain areas of interest. In total, 33 distinct neuropils were reconstructed and registered for the standard locust brain (**Figure 1**). Seven neuropils were registered in the optic lobe: the medulla proper (Me) was distinguished from two associated neuropils, the DRMe, which receives polarized-light information from the DRA of the compound eye (Homberg, 2004), and the accessory medulla (aMe). Four subunits were distinguished in the lobula complex: the anterior (ALo), the dorsal (DLo), the inner (ILo) and the outer lobe of the lobula (OLo). In the median protocerebrum, the lateral horn (LH), the AOTu, the mushroom body, and the central complex were reconstructed. The AOTu is subdivided into an upper unit (uAOTu), which receives visual input from the optic lobe, and a lower unit (lAOTu), which is innervated by POL neurons (Pfeiffer et al., 2005). The mushroom bodies (MB) were divided into the combined pedunculus (Pe)-lobes, the accessory calyx (aCa), and the primary calyx (pCa). In the central complex (CC) in the center of the brain, the PB, the upper division of the central body (CBU), the lower division of the central body (CBL), and the paired noduli (No) were distinctly registered. Below the MB the deutocerebral antennal lobes (AL) were the most ventral neuropils reconstructed in the brain. Although several brain regions, such as the tritocerebrum, the LALs, or the antennal mechanosensory and motor center, were reconstructed in some individual brains, they were not included in the standard brains due to difficulties in reproducibly identifying their boundaries to adjacent brain structures. These neuropils and brain regions were assigned to a common, artificial "midbrain neuropil" structure for standardization (Kurylas et al., 2008).

For creation of a visual 3D standard brain, two methods have been established: The Virtual Insect Brain protocol (VIB; Jenett et al., 2006) and the Iterative Shape Averaging method (ISA, Rohlfing et al., 2001). Both methods were applied to create a standardized brain of the locust (**Figures 1A,B**). For an evaluation of both standardization procedures the relative distances to the center of the brain and the relative volumes of the standardized brains were compared to the mean distances and volumes of the ten individual brains (Kurylas et al., 2008). In the VIB standard brain, neuropil volumes showed lower deviation from the mean volumes compared with the ISA standard brain. In contrast, the ISA standard brain showed higher invariance in relative distances, displayed brain structures more distinctly and showed higher sym-

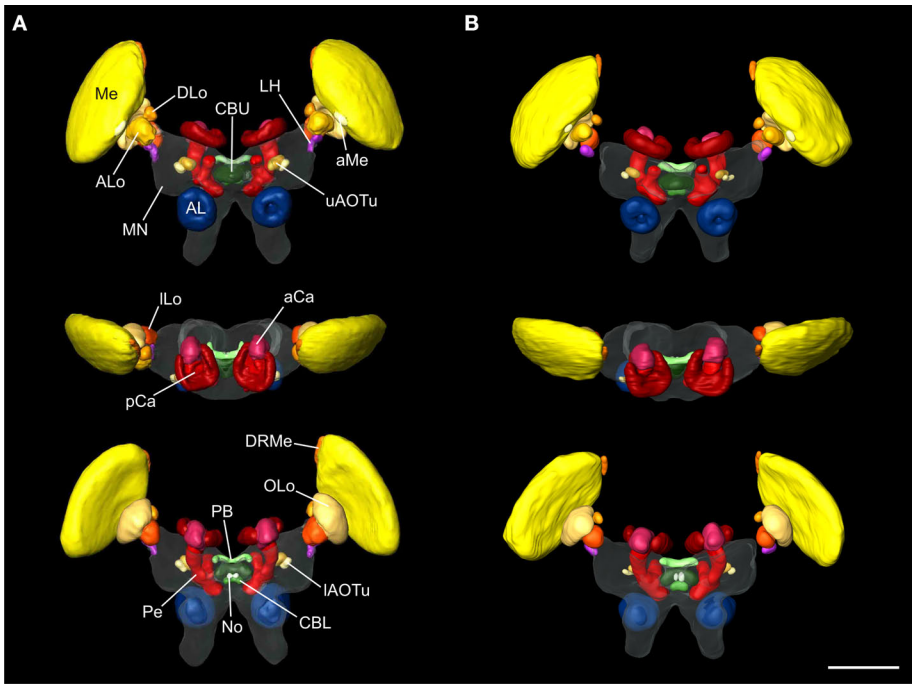

FIGURE 1 | Visual comparison of the 10-animal ISA and VIB whole standard brains of the desert locust *Schistocerca gregaria*. Surface reconstruction of 33 distinct neuropils plus a "midbrain neuropil" (MN, transparent) **(A)** ISA standard brain in anterior (top), dorsal (middle), and posterior (bottom) view (aCa, accessory calyx; AL, antennal lobe; ALo, anterior lobe of the lobula; aMe, accessory medulla; CBL, lower division of the central body; CBU, upper division of the central body; DLo, dorsal lobe of the lobula; DRMe, dorsal rim area of the medulla; lLo, inner lobe of the lobula; lAOTu, lower unit of the anterior optic tubercle; LH, lateral horn; Me, medulla; No, noduli; OLo, outer lobe of the lobula; PB, protocerebral bridge; pCa, primary calyx; Pe, pedunculus; uAOTu, upper unit of the anterior optic tubercle). **(B)** VIB standard brain viewed from anterior (top), dorsal (middle), and posterior (bottom) sides. Visualization of the "midbrain neuropil" is based on average image data (modified from Kurylas et al., 2008, **Figures 5A–C**, right panel). The color coding of the neuropils is consistent with Brandt et al. (2005). Scale bar: 600 µm.

metry in brain structures than the VIB standard. Therefore, the VIB standard brain is ideal for comparative volume analysis at the level of neuropils, whereas the standardized ISA brain is more useful as a platform to register and combine the morphologies of individual neurons (Kurylas et al., 2008). The small relative size of some neuropils of interest, like the noduli, layers of the central complex, or the subunits of the AOTu posed a severe limitation to both atlases. These neuropils were represented by only small numbers of voxels. To analyze and to fit neuron branches faithfully into subunits of the central complex, we therefore decided to create an ISA standard of the locust central complex and associated brain areas at a higher image resolution.

THE STANDARD CENTRAL COMPLEX

For detailed reconstruction and identification of central-complex subunits, scanning of whole brains was not feasible due to limitations in focal depth of the 10× microscope objective. Therefore, a new set of 20 brains was dissected and sectioned in 250 µm-thick sections, followed by scanning and reconstruction of the regions of interest. In total, we reconstructed and standardized 22 neuropils and layers in the central complex. Analogous to whole-mount brains, reconstructions were based on anti-synapsin immunostaining, except for reconstruction of the layers of the CBU. The CBU consists of three layers (layers I–III) from anterior to posterior (Homberg, 1991). Based on anti-synapsin staining, the boundary between layers I and II was well defined (**Figure 2A**), but layers II and III could not be distinguished. The boundary between layers II and III was instead determined by serotonin immunostaining (Homberg, 1991; Heinze and Homberg, 2008; Siegl et al., 2009; **Figure 2B**). Although layers I and II can be further subdivided into the dorsal sublayers Ia and IIa and the ventral sublayers Ib and IIb (Homberg, 1991), their precise boundaries are fuzzy (Heinze and Homberg, 2008), and these sublayers were, therefore, not included in the standardized central complex. The CBL was reconstructed as a single neuropil. It is located anterior of the posterior groove and consists of six layers (Müller et al., 1997). These layers were not well defined in synapsin- or serotonin immunostaining and were hence not reconstructed individually. Postero-dorsal to the CB we reconstructed the protocerebral bridge (PB, **Figure 2B**). Although the CBU, CBL, and the PB are divided into 16 columns (Williams, 1975; Heinze and Homberg, 2007), it was not possible to reveal these substructures based on synapsin- or serotonin immunostaining. The paired noduli are located posterior to the CB (**Figure 2D**) and consist of upper (NoU) and lower units (NoL). The upper unit shows three sublayers termed nodular layer I (NoUI), II (NoUII) and III (NoUIII) from dorsal to ventral. All subunits and layers of the noduli were reconstructed individually based on distinct anti-synapsin staining. Anterior to the ventral groove and dorsal to the CBU we reconstructed the anterior lip (aL), a neuropil that is directly connected to the central complex (**Figure 2A**). Two other

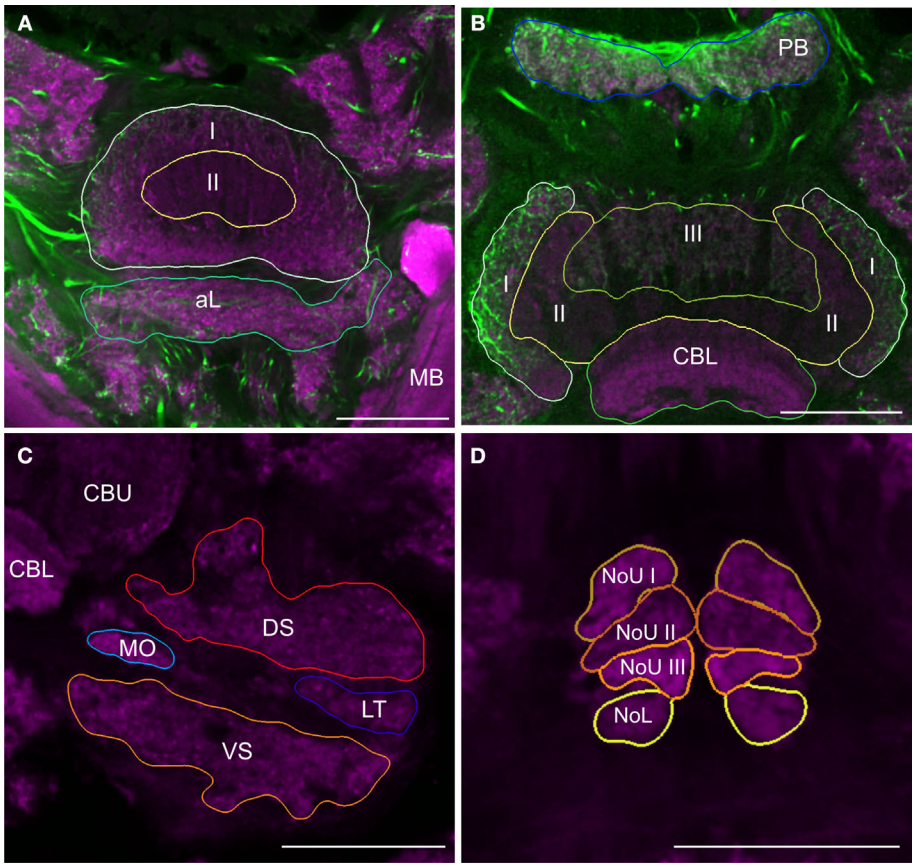

FIGURE 2 | Images from frontal sections through the central complex and lateral accessory lobe at different levels based on immunostaining for synapsin *(magenta)* and serotonin *(green)*. (A) Optical slice through layer I (I) and II (II) of the upper division of the central body and the anterior lip (aL) at the level of the mushroom bodies (MB). **(B)** Axial slice through the protocerebral bridge (PB), layer I (I), II (II) and III (III) of the upper division of the central body and the lower division of the central body (CBL). **(C)** Frontal section through the lateral accessory lobe, ventrolateral of the upper (CBU) and the lower (CBL) division of the central body. The lateral accessory lobe is subdivided into the dorsal shell (DS), the ventral shell (VS), the median olive (MO), and the lateral triangle (LT). **(D)** Confocal image through the upper and the lower units of the noduli (NoL). The upper units of the noduli are subdivided into layers I–III (NoU I, II, III). Scale bars: 100 µm.

structures that are closely associated with the central complex are the paired lateral accessory lobes (LALs; **Figure 2C**). The LALs are located posterior of the medial lobes of the MB and ventrolateral of the central complex. They consist of four well-defined subunits (Homberg, 1994). Most prominent are a large dorsal shell extending anteriorly around the medial lobe of the mushroom body and a large ventral shell (VS). Both major subunits are separated by fibers in the isthmus tracts, which give rise to two further subunits, the LT and the MO.

For standardization, we reconstructed 20 individual adult male central complexes. Based on the results from Kurylas et al. (2008) and our aim to create a visual standardized model of these 22 neuropils for neural network analysis, we created the standard central complex using the ISA method (Rohlfing et al., 2001). For standardization, one of the 20 brains had to be used as an initial affine registration template. Because the template brain determines the absolute scale of the ultimate standard atlas, we chose the brain with the smallest differences in neuropil distances from the mean distances of all brains to the brain center. Optical slices of this template brain are shown in **Figure 2**. The ISA method created a fuzzy initial standardized atlas of the central complex based on affine registrations, followed by four iterations of averaging and non-rigid transformations. During registration in the iterative procedure the image stacks of the standard central complex converged into increasingly accurate alignment, and neuropil structures became increasingly sharp and well defined. The final outputs of the ISA procedure were an averaged intensity image (CLSM) stack and an "averaged" label image stack of the reconstructions of the neuropils. The average intensity image of the ISA standard central complex is shown in **Figures 3A,B** as a direct volume rendering visualization. A 3D surface visualization of the reconstructed structures in the standard brain is shown in **Figures 3C–G** from different perspectives. The mean shape property of standardized structures generated by the ISA method has been demonstrated previously through a comparison of the degree of deformation between two individual brains and between the standard brain and an individual brain (Brandt et al., 2005; Kurylas et al., 2008). The ISA standard central complex, therefore, represents a "typical" central complex in terms of shape and appearance and provides a reliable, high-resolution reference coordinate space for registration and analysis of central-complex neurons of the desert locust.

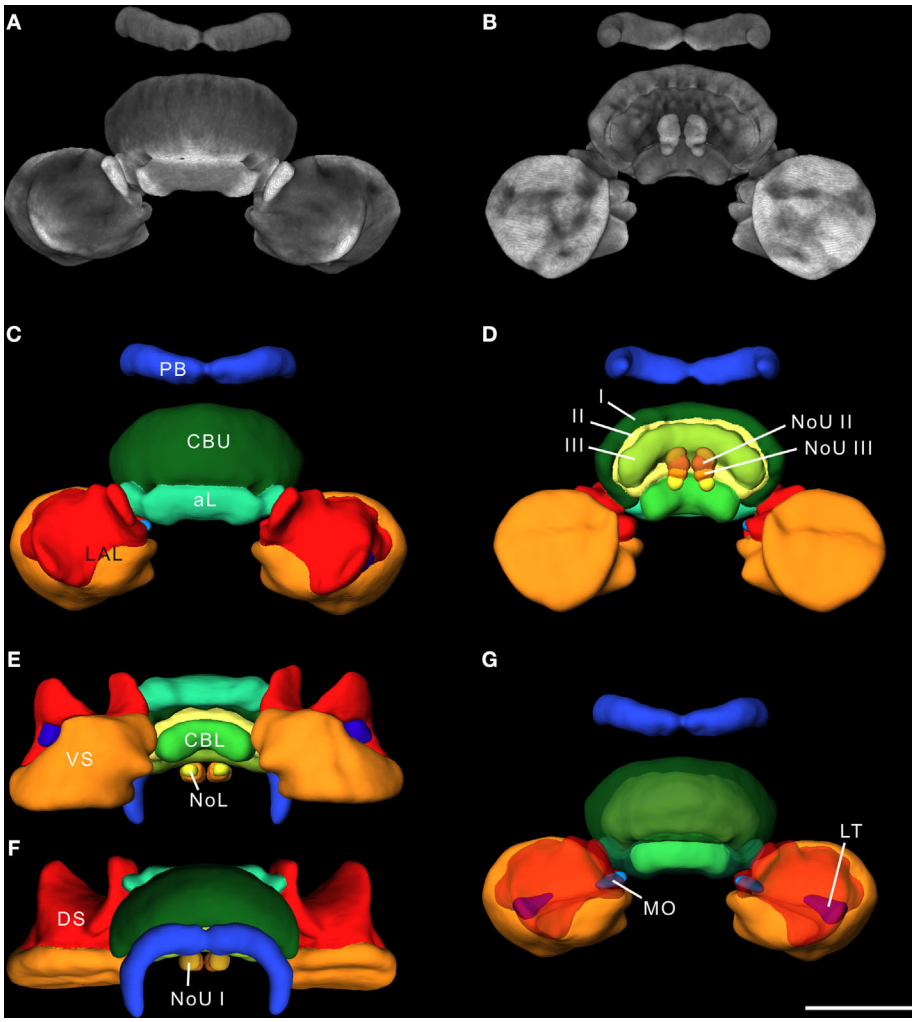

FIGURE 3 |The 20-animal standard central complex calculated using the ISA method. (A,B) 3D reconstruction of the standardized image stack by direct volume rendering. For visualization, synapsin labeling in brain areas surrounding the image data was deleted. **(A)** 3D visualization of the standardized CLSM image stack from anterior. **(B)** Posterior view of the standard central complex image data. **(C–G)** Surface reconstruction of all 22 segmented neuropils from different perspectives. **(C)** Anterior view **(D)** posterior view **(E)** ventral view **(F)** dorsal view **(G)** anterior view with transparent layer I of the upper division of the central body and dorsal shells. I, II, III, layers I–III of the upper division of the central body; aL, anterior lip; CBL, lower division of the central body; CBU, upper division of the central body; DS, dorsal shell; LAL, lateral accessory lobe; LT, lateral triangle; MO, median olive; NoL, lower unit of the nodulus; NoU I, II, III, layers I–III of the upper units of the noduli; PB, protocerebral bridge; VS, ventral shell. Scale bar: 200 µm.

Comparison of volumes and sizes of central-complex subdivisions between the standard brain and the standardized central complex revealed significantly smaller mean neuropil volumes of the PB and CBL (student *t*-test; two tailed; **Figure 4A**) in the sections than in the whole-mount brains. The CBU ($p = 0.062$) and the No ($p = 0.551$) were not significantly smaller. These differences in mean volumes probably resulted from larger tissue shrinkage of the brain sections and perhaps from differences in image resolution between the whole-mounts and the brain sections. Although the mean sizes of the PB and CBL were significantly different, the corresponding sizes in the ISA whole brain atlas do not reflect this (**Figure 4A**). Similarly, the sizes of the neuropils between the standard central complex and the central-complex neuropils in the whole-brain ISA standard do not exhibit the same differences (**Figure 4B**).

CPU1A NEURON

The POL columnar CPU1 and CPU2 neurons are among the largest columnar cell types of the central complex. To further analyze the neural connections of these neurons, we reconstructed a subtype of CPU1 neurons termed CPU1a in 3D, based on high-resolution image stacks obtained with a 20× and a 40× oil objective (**Figure 5**). The somata of all CPU1 neurons are located in the pars intercerebralis; the neurons have arborizations in the PB, the central body, and in one or both LALs (Heinze and Homberg, 2008). CPU1a neurons have arborizations in a single ipsilateral column of the PB and in two adjacent contralateral columns of the CBU. Axonal ramifications are concentrated in the contralateral LAL (**Figure 5A**). The reconstructed neuron has its cell body in the anterior pars intercerebralis and, judged from the location of its arborization domain in the PB, densely arborizes in the

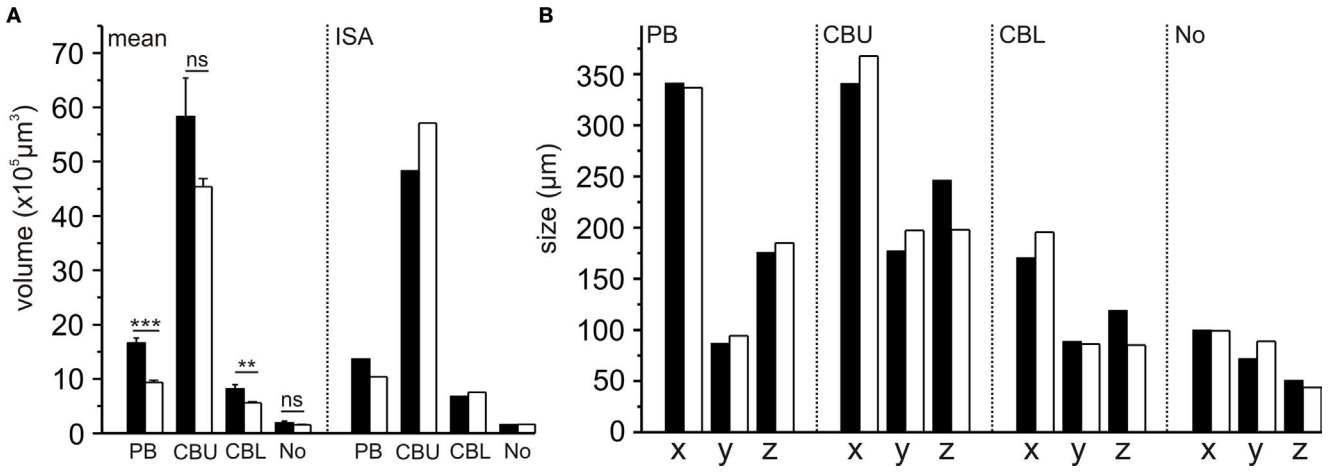

FIGURE 4 | Comparison of volumes and sizes of central-complex subdivisions between the 10-animal standard whole brain (*black bars*; from Kurylas et al., 2008) and the 20-animal standard central complex (*white bars*, this work). (A) Comparison of the means and ISA neuropil volumes (bars: standard error; ***$p < 0.001$; **$p < 0.01$; ns, not significant). **(B)** Comparison of neuropil sizes in the ISA standard brain and in the ISA standard central complex. CBL, lower division of the central body; CBU, upper division of the central body; No, noduli; PB, protocerebral bridge; *x, y, z* neuropil sizes in *x, y,* and *z* directions.

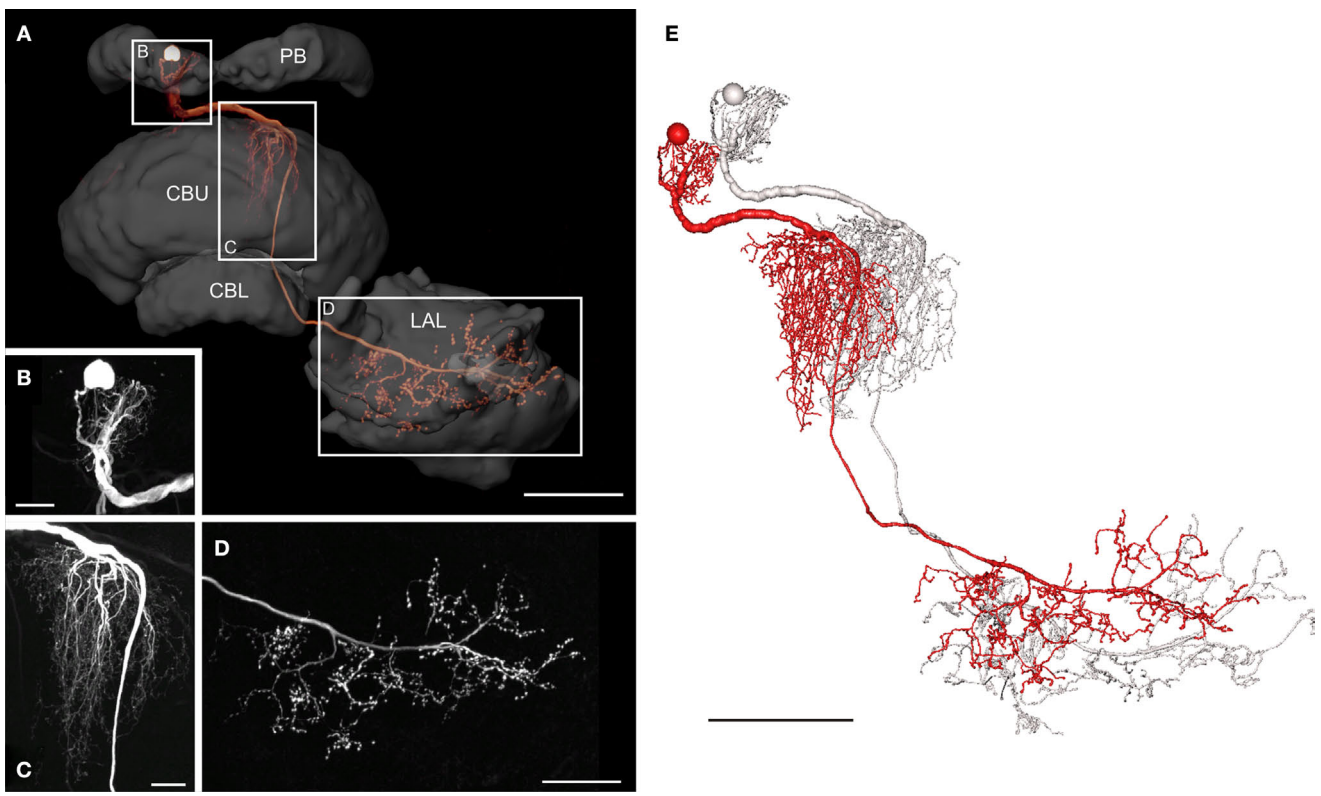

FIGURE 5 | Morphology of a CPU1a neuron. (A) Anterior view of a 3D volume rendering visualization of the CPU1a neuron and reconstruction of several neuropils of the central complex and lateral accessory lobe. CBL, lower division of the central body; CBU, upper division of the central body; LAL, lateral accessory lobe; PB, protocerebral bridge. Boxes show areas enlarged in **B–D**. **(B)** Location of cell body and arborizations in column R7 of the PB; maximum intensity projection of a confocal image stack. **(C)** Maximum intensity projections of ramifications of the CPU1 cell in two columns of the CBU, viewed from anteriorly. **(D)** Maximum intensity projection of optical slices of the arborizations in the ventral shell of the left LAL shown in anterior view. **(E)** 3D reconstruction of the CPU1a neuron before (*red*) and after affine and elastic registration (*grey*). Scale bars: **(A,E)** 100 µm; **(B,C)** 20 µm; **(D)** 50 µm.

second innermost column (column R7) of the right PB hemisphere (Williams, 1975; Heinze and Homberg, 2008; **Figure 5B**). The primary neurite leaves the PB on the anterior side and runs ventrally to the CB. The neurite crosses the hemisphere via the z-bundle between the PB and the CB and enters the CBU at its dorsal contralateral side. There, the CPU1a cell gives rise to a large tree of smooth dendritic arborizations, extending through two adjacent columns of the CBU (**Figure 5C**). The main neurite projects ventrally along the anterior face of the CBU, continues between layer I of the CBU and the anterior lip, and enters the ventral groove. Anterior to the CBL, the axonal fiber joins the isthmus tract and invades the contralateral LAL. Varicose and beaded ramifications are confined to the VS of the LAL (**Figure 5D**). The 3D reconstructions of the neuron before (*red*) and after transformation (*grey*) for registration into the standard central complex are shown in **Figure 5E**.

The distribution of smooth and beaded terminal fiber specializations suggests that the CPU1a neuron receives synaptic input from column R7 of the PB and from two columns of the CBU and sends this information to the VS of the LAL. In the PB the CPU1a neuron most likely receives polarization information (Heinze and Homberg, 2007). In addition to polarization vision input, CPU1a neurons likely receive input from unknown sources in the CBU. To determine candidate neurons to provide this input, we reconstructed the GFS neuron, a tangential neuron with ramifications in the CBU.

GIANT FAN-SHAPED NEURON

The GFS neuron (Williams, 1972; Homberg, 1994) is a tangential neuron of the central body. Tangential neurons connect various brain regions to the PB or to particular layers of the CB. The soma of the GFS neuron lies posterior to the LAL in the ventro-median protocerebrum (**Figure 6A**). The main neurite runs dorsally through the ventro-median protocerebrum and enters the ipsilateral LAL through the posterior surface of the VS. In the LAL the GFS neuron has smooth ramifications, especially in the dorsal shell and less prominently in the VS (**Figure 6C**), but not in the LT and MO. Additional dendritic processes extend around the medial lobe of the mushroom body toward anterior regions of the brain and arborize with fine terminals in the ipsilateral anteromedian protocerebrum (**Figures 6D and 7A**). Finally, a few dendritic processes extend to lateral aspects of the anterior lip (**Figure 7A**). The main neurite runs through the LAL dorsally from the isthmus tract toward the CB. Laterally from the CBL, it bends posteriorly and enters the posterior groove. Here the main neurite gives rise to eight major side branches. They enter eight

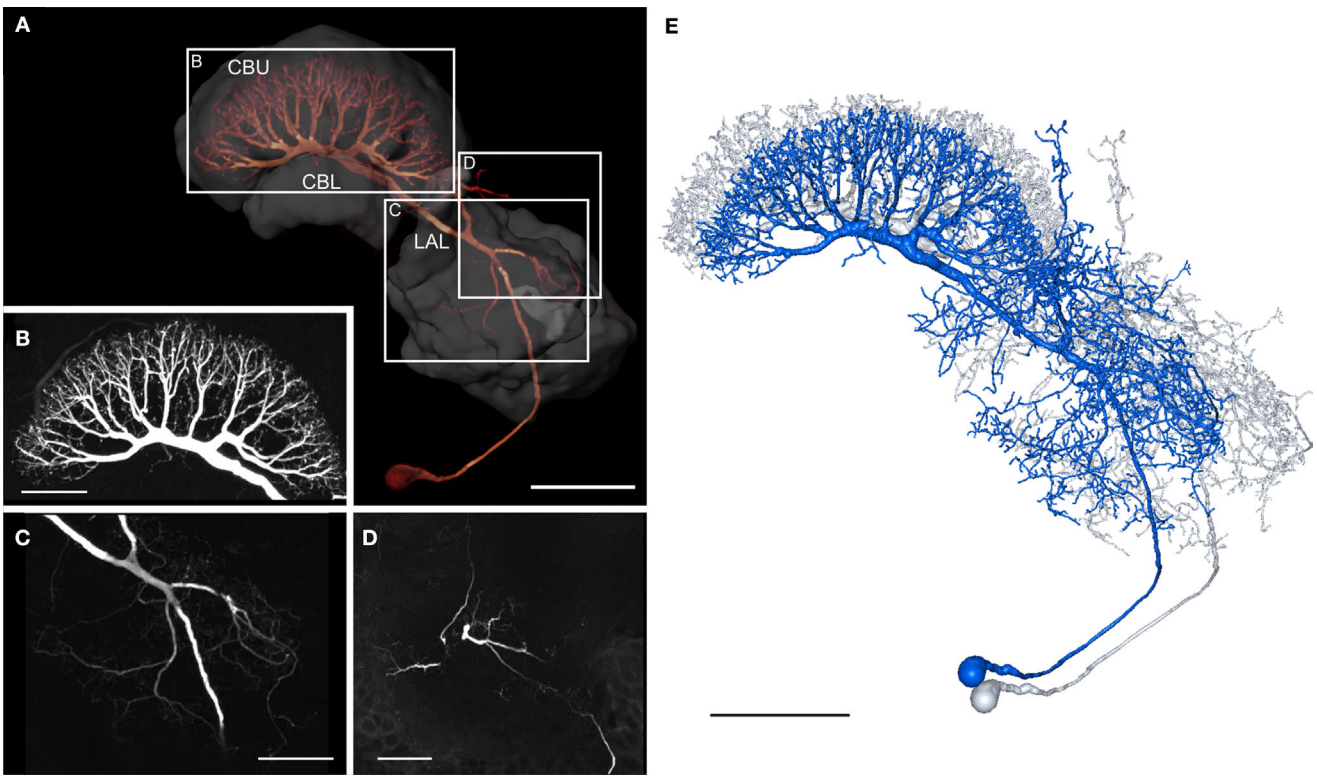

FIGURE 6 | Morphology of the giant fan-shaped (GFS) neuron. **(A)** Anterior view of the GFS neuron by direct volume rendering. Reconstructions of central-complex neuropils and the lateral accessory lobe are shown transparently. CBL, lower division of the central body; CBU, upper division of the central body; LAL, lateral accessory lobe. Boxes show areas enlarged in **B–D**. **(B)** Maximum intensity projection of the arborization tree in the CBU, anterior view. **(C)** Maximum intensity projection of a confocal image stack from anterior showing ramification in the left LAL. **(D)** Maximum intensity projections of optical slices showing arborizations in the anterior median protocerebrum, anterior view. **(E)** 3D reconstruction of the GFS neuron before (*blue*) and after registration (*grey*). Scale bars: **(A,E)** 100 µm; **(B–D)** 50 µm.

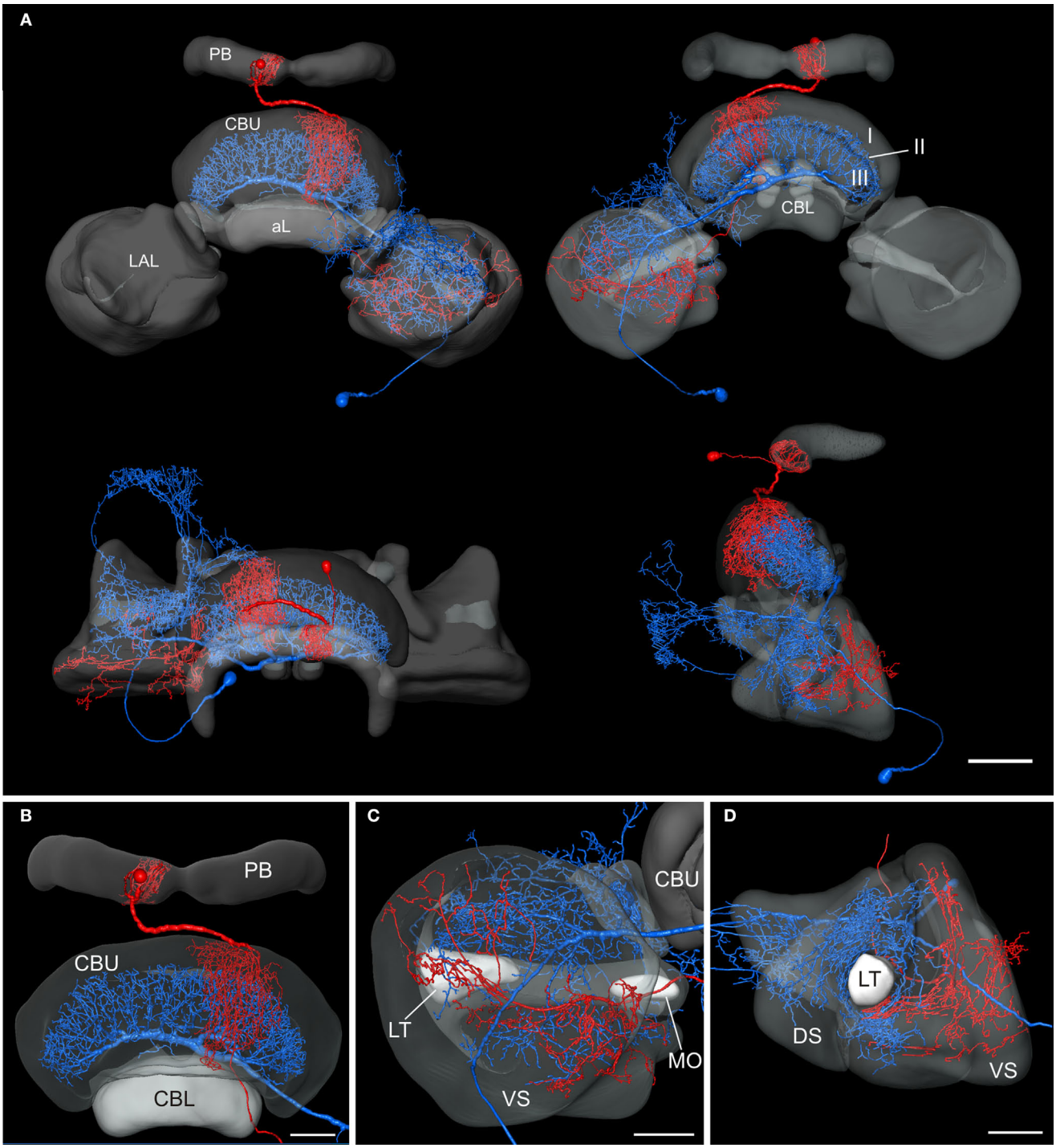

FIGURE 7 | Registration of the CPU1a (*red*) and GFS (*blue*) neurons into the 3D standard central complex. (A) Anterior view (top left), posterior view (top right), dorsal view (bottom left) and lateral view (bottom right). **(B)** Anterior view showing arborizations in the upper division of the central body (*CBU*) and in the protocerebral bridge (*PB*). **(C)** Posterior view of the standardized right lateral accessory lobe with processes of the CPU1a and GFS neurons. **(D)** Ventrolateral view of the lateral accessory lobe. I, II, III, layers I–III of the upper division of the central body; aL, anterior lip; CBL, lower division of the central body; DS, dorsal shell; LAL, lateral accessory lobe; LT, lateral triangle; MO, median olive; VS, ventral shell. Scale bars: **(A)** 100 µm; **(B–D)** 50 µm.

pairs of columns of the CBU and ramify into highly varicose fiber processes, concentrated in layer II (**Figure 6B**). The 3D reconstructions of the GFS neuron before (*blue*) and after registration (*grey*) are shown in **Figure 6E**.

NEURONS IN THE STANDARD CENTRAL COMPLEX

To analyze whether the tangential GFS neuron is a candidate to provide synaptic input to the columnar CPU1a cell, we registered both cells into the standardized central complex (**Figure 7**). For an

exact fit of the two neurons into the virtual central-complex atlas, corresponding brain areas of the individual brains were reconstructed (**Figures 5A and 6A**) and were registered into the standard central complex. For registration of the neuropils we used an affine registration followed by a non-rigid elastic registration. The transformation and deformation parameters were then applied to the reconstructed neurons to visualize both neurons in the standard central complex (**Figure 7A**). The ramifications in column R7 of the PB of the registered CPU1a neuron indicate high accuracy of the registration process (**Figure 8C**, arrow). The CPU1a neuron shows arborizations only in the VS of the LAL of the standard central complex, as is observed in the original brain. The GFS cell, in contrast, innervates the ventral and dorsal shells of the LAL, however, with the majority of ramifications in the dorsal shell (**Figure 7C**), again as observed in the original brain. As in the individual brains, both registered neurons do not enter the LT and the MO (**Figures 7C,D**). To investigate whether the output region of the GFS neuron and the input region of the CPU1a cell co-localize, we analyzed the CBU ramifications in detail. The CPU1a cell shows ramifications in layer I of the CBU (**Figure 7B**) and fewer arborizations in layers II and III of the CBU (**Figure 8D**). Neurites of the GFS neuron, in contrast, do not enter layer I, but show highest concentration of arborizations in layer II of the CBU (**Figure 8D**). Although the CPU1a cell shows fewer arborizations in layer II, processes of both neurons clearly overlap in layer II of the CBU (**Figures 7A and 8D**). This co-localization of input processes of the CPU1a cell and output areas of the GFS neuron shows that the GFS neuron is a candidate to contribute to synaptic input to CPU1a neurons in layer II of the CBU.

DISCUSSION

COMPARISON OF VIB AND ISA STANDARDS

Kurylas et al. (2008) have generated two whole standard brains of the desert locust, one following the VIB protocol (Jenett et al., 2006) and the second using the ISA method (Rohlfing et al., 2001). Both standardization methods were performed with the

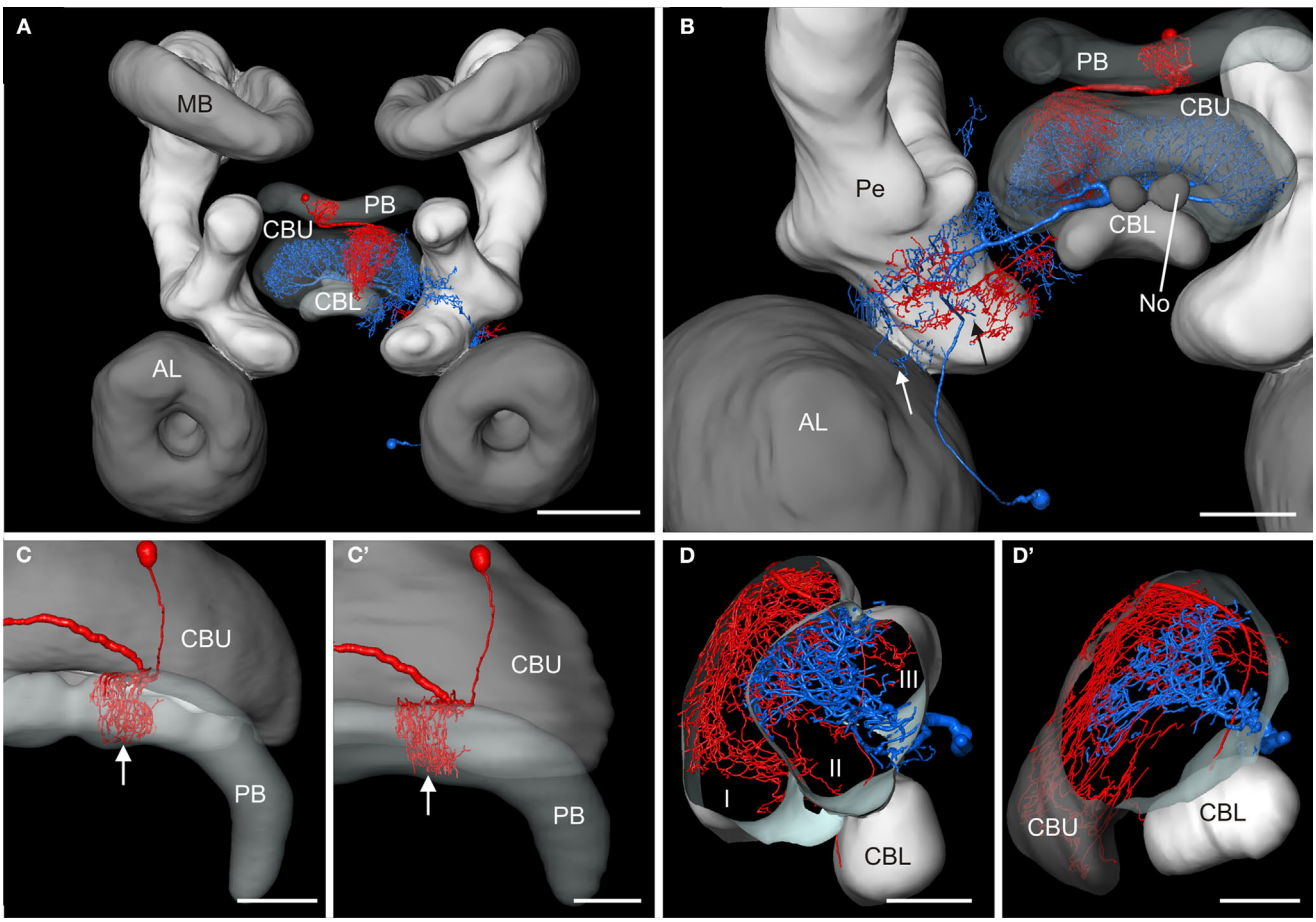

FIGURE 8 | Registration of the CPU1a *(red)* and GFS *(blue)* neurons into the ISA standard brain and into the standard central complex. (A) Anterior view of the central brain of the standard brain showing the central complex, the mushroom bodies (MB) and the antennal lobes (AL). **(B)** Postero-lateral view of the central standard brain. Arrows indicate displacement of arborizations of the GFS neuron into the pedunculus (Pe) and antennal lobe. **(C,C')** Dorsal view showing cell body and ramifications of the CPU1a neuron in column R7 (white arrows) of the protocerebral bridge (PB) registered into the standard central complex **(C)** and into the central complex neuropils of the standard brain **(C')**. **(D,D')** Oblique sagittal sections through the central body of the standardized central complex (section thickness: 42 µm, **D**) and the standard brain (section thickness: 54 µm, **D'**) illustrating common projections of both neurons in layer II of the upper division of the central body. I, II, III, layers I–III of the upper division of the central body; CBL, CBU lower, resp. upper division of the central body; No, nodulus. Scale bars: **(A)** 200 µm; **(B)** 100 µm; **(C–D')** 50 µm.

same set of ten brain preparations. For future applications it was particularly interesting to analyze advantages and limitations of both methods. Standard brains also exist for the fruit fly (Rein et al., 2002), the moths *Manduca sexta* (el Jundi et al., 2009) and *Heliothis virescens* (Kvello et al., 2009), and the honeybee (Brandt et al., 2005). Whereas the *Drosophila* and *Manduca* standards were generated using the VIB method, the honeybee and *Heliothis* standard brains are based on the ISA method. The standard brains of *D. melanogaster* and of *M. sexta* were primarily developed to compare volumes of brain neuropils. Accordingly, standard volumes were calculated and compared between the sexes (Rein et al., 2002; el Jundi et al., 2009). An additional motivation for the *Drosophila* standard brain was the prospect to quantitatively compare volumes of brain areas between wildtype and genetically manipulated flies. The honeybee and *Heliothis* standard brains were instead created to register neurons from different preparations into a common anatomical framework (Brandt et al., 2005; Kvello et al., 2009).

A comparison of the two locust standard brains showed that the VIB method creates an ideal standard brain for inter- and intraspecific volume comparisons, because it keeps neuropil volumes unchanged. This is not surprising, because the calculation of the standard or mean volumes does not depend on the process of registration. Instead, the VIB protocol calculates mean volumes of all segmented neuropils based on the labelfields before the brains are registered. The most meaningful result of the VIB protocol is the image stack of all registered segmented neuropils, as shown in Jenett et al. (2006, **Figure 4**), Kurylas et al. (2008, **Figures 5D–F**) and el Jundi et al. (2009, **Figures 4D,F**). The 3D surface view of the standard brain is a threshold representation of this registered image stack.

The ISA method, in contrast, generated the more exact visual standard atlas regarding positions and shapes of the neuropils and bilateral symmetry of the brain (Kurylas et al., 2008). The ISA script registers the brains based on intensity image stacks (here, CLSM). After registration, deformation parameters are applied to the corresponding label fields to create a 3D model of standard brain structures. In contrast to the VIB method, which is easy to use through a step-by-step script in Amira, the ISA standard brain has to be calculated outside Amira, currently via a shell script. Both methods require choosing an individual brain as a template for the registration procedure. Whereas in the visual standard brain of the VIB method the positions of the neuropils are highly dependent on this template brain, the spatial relationships of neuropil positions in the ISA standard are largely independent from this template but their orientations may be affected (el Jundi et al., 2009). During the initial, affine registration stage of the ISA method, the brains are also scaled depending on the template brain (Rohlfing et al., 2004; el Jundi et al., 2009) to minimize anatomical differences (Kuß et al., 2007; Kurylas et al., 2008). To minimize these possible sources of bias, Kurylas et al. (2008) calculated for all brains the relative distances of neuropils to the brain center and chose the brain with the lowest deviations from the mean distances as the template brain.

THE STANDARD CENTRAL COMPLEX

In this work, we have generated a standardized central complex of the desert locust brain based on 20 individual central complexes. The central complex is involved in the control of locomotion and flight and plays an important role in spatial orientation in response to polarized light. In locusts it is the final processing stage in the polarization vision pathway (Heinze and Homberg, 2007) and is probably the main integration site of polarization information from both eyes (Heinze et al., 2009). The central complex is innervated by a large variety of neuronal cell types (Heinze and Homberg, 2008, 2009), whose roles in information processing and integration are largely unknown. To generate an anatomical platform for analysis of central-complex neurons from different brains, we used the ISA method based on Kurylas et al. (2008) and, for the first time, implemented this technique for the registration of only one brain area. This required masking of the regions surrounding the central complex in the CLSM image stacks. To hide the surrounding brain regions of the stacks we used the corresponding label fields with the module *Arithmetic*, after we enlarged the label fields by about 15 voxels in all directions and removed irrelevant regions.

A limitation of the locust standard brain of Kurylas et al. (2008) is the relative low resolution of images ($5.9 \times 5.9 \times 3$ µm). Thereby, it was unfeasible to increase the number of reconstructed neuropils in the central brain. As a result, the subdivisions of the LALs, the anterior lip, and the layers of the CBU and noduli were not included into the standard whole brain. However, most of these structures are crucially involved in polarized-light signaling and are, thus, innerved by POL neurons (LAL: Vitzthum et al., 2002; Pfeiffer et al., 2005; CBU: Heinze and Homberg, 2007, 2009; No: Heinze and Homberg, 2009). Especially the LALs are an important processing stage for polarized-light signals. They receive polarized-light input from the AOTu (Homberg, 2004) and send this information to the central complex (Vitzthum et al., 2002). In addition, they receive polarized-light information from the central complex and transfer it to descending pathways (Homberg, 1994; Heinze and Homberg, 2009).

The absence of these neuropils in the standard whole brain resulted in substantial imprecision during transformation of the two neurons (**Figure 8**). As a result of the absence of the LAL in the standard whole brain, ramifications of the GFS neuron in the DS and VS were displaced into the Pe and the antennal lobe (**Figure 8B**, arrows). In contrast, the arborizations of the CPU1a- and GFS neurons in the central-complex neuropils of the standard whole brain show that it is an adequate atlas for neurons that ramify in reconstructed brain areas (**Figures 8C',D'**). Nevertheless, the additional information provided by the additionally reconstructed neuropils and layers is indispensable for precise fitting of neurons into these compartments.

For future studies it will be important to incorporate the ISA standard central complex into the ISA whole-brain standard. To do this, we have to face the potential problem that the registration of the central complex atlas is based on brain sections, whereas the construction of the whole-brain standard was performed through a whole-mount protocol (Kurylas et al., 2008). Compared to whole-mount preparations, which show already noticeable tissue shrinkage (Bucher et al., 2000; Ott, 2008), morphological distortions may be even larger in brain sections. Comparisons of mean volumes showed that the CBL and PB are significantly smaller in the standard central complex than in the standard brain, whereas the slightly smaller sizes of the CBU and

No are not significant. Interestingly, these differences between mean volumes are not reflected when comparing the volumes of the ISA standards (**Figure 4A**). Both, the ISA volumes and the overall dimensions of the central-complex neuropils are similar in the standard brain and the standard central complex (**Figures 4A,B**). Taken together, the similar ISA volumes and sizes are a promising basis for our next goal to register the standardized central complex into the standard brain.

A similar potential problem arises when transforming neurons into the standard central complex. For detailed neuronal reconstructions, an adequate resolution of the CLSM image stacks is necessary. Owing to the limited working distance of the 20× and 40× objectives, the individual neurons of the central complexes were imaged from 130–140-µm brain sections. These sections may differ in shrinkage artifacts from the 250-µm brain sections used for the standardized central complex. For registration of the neurons into the standard central complex it was, therefore, necessary to transform, scale, and deform the cells in a fitting process. To do this, defined neuropils of the individual central complexes were registered into the standardized central complex, and the same transformation parameters of the registrations were then applied to the neurons.

THE POLARIZATION VISION NETWORK IN THE CENTRAL COMPLEX

The central complex comprises a group of highly modular midline neuropils in the insect brain. The topographic representation of zenithal *E*-vector tunings in the columns of the PB of the locust strongly suggests that coding of solar azimuth is a major aspect of the functional role of the central complex (Heinze and Homberg, 2009; Heinze et al., 2009). Based on anatomical and physiological data, a flow of information processing in the polarization vision network of the central complex has been suggested (Heinze and Homberg, 2008, 2009; Heinze et al., 2009). Tangential neurons TL2 and TL3 represent the input neurons of the polarization vision network in the central complex. They receive their inputs in the LT and MO of the LAL and send axonal projections to the CBL (Vitzthum et al., 2002). Columnar CL1 neurons connect the CBL to the PB and, together with tangential TB neurons of the PB, are most likely involved in generating the compass-like representation of *E*-vectors in the PB (Heinze and Homberg, 2007). Processed polarization information is, finally, transferred via CPU1 and CPU2 cells to the LALs and is then transmitted indirectly to descending neurons.

CPU1 AND GFS NEURONS

In addition to polarized light, a brain area involved in spatial orientation and memory has to integrate a variety of other inputs, including landmark information, motivational input, and feedback from ongoing motor activity (Heinze et al., 2009). This may lead to suppression of output if motivation for spatially-oriented behavior is low or to a context-dependent ratio of activation of motor centers in the right and left hemispheres of the nervous system for a spatial motor task. Because of their morphology, polarity, and hierarchy in the polarization vision system, the CPU1- and the conditionally POL CPU2 cells (Heinze and Homberg, 2009) are ideal candidates to receive modulatory input, in addition to solar azimuth coding. CPU1/2 cells most likely receive their polarized-light input in the PB (Heinze and Homberg, 2009; Heinze et al., 2009), but have a second, even larger dendritic input region in the CBU. Two principal subclasses of CPU neurons have axonal projections to one (CPU1) or to both (CPU2) LALs (Heinze and Homberg, 2008). Three subtypes of CPU1 cells are distinguished based on ramifications in the ipsilateral (CPU1a,c) or contralateral (CPU1b) hemisphere of the PB (Heinze and Homberg, 2008). Whereas in all CPU1 neurons the ramifications in the PB are limited to single columns, the arborizations in the CBU either extend over several columns (CPU1b), are confined to two to three columns (CPU1a), or occur in a single column (CPU1c). Thus, the ratio between the polarization and non-polarization inputs may be defined through anatomical broadening in the CBU. In contrast, ramifications of all CPU1 and CPU2 cells invade layers I–III of the CBU but decline in density from layer I to III.

Co-registration suggests that the GFS neuron is a promising candidate to provide input to CPU1a neurons and perhaps to all types of CPU1/2 neurons. Spiking activity in CPU1a cells is modulated by the *E*-vector of polarized light (Vitzthum et al., 2002). CPU1 cells receive polarized-light input from both eyes and have zenith-centered receptive fields extending over 120° (Heinze et al., 2009). The GFS neuron, by contrast, is not sensitive to polarized light (Heinze, 2009), but is weakly inhibited by frontally presented unpolarized light (Homberg, 1994). The GFS neuron responds more strongly to movement stimulation in the ipsilateral field of view, is phasically excited by frontal wind stimulation, and shows strong activity bursts associated with tethered flight (Homberg, 1994; Müller, 1997; Heinze, 2009). Interestingly, CPU1a cells also respond to frontal light with an inhibition of spiking (Vitzthum et al., 2002). Taken together, these data support the hypothesis that the GFS neuron transfers non-polarized visual input and perhaps flight-associated excitation to the CPU1/2 cells.

In addition to the GFS neuron, a variety of other tangential neurons of the CBU, such as TU1 and TU2 cells (Homberg et al., 1999), are possible candidates to provide synaptic input to CPU cells. Registering further neurons into the standard central complex will allow us to explore the neuronal connectivities in the central-complex network with increasing depth and complexity, and to formulate hypotheses on neural pathways and novel physiological properties of particular cell types that can then be tested in subsequent recordings. Our current achievements of a common platform for the whole brain and, with higher resolution, for the central complex provide an ideal basis for this enterprise.

ACKNOWLEDGMENTS

We are grateful to Dr. Thomas Gebhardt for providing the Linux cluster and help in Linux, and to Erich Buchner for providing the anti-synapsin antibody. We thank Ulrike Träger for helpful suggestions on the manuscript and Karl Heinz Herklotz for maintaining the locust cultures. This work was supported by DFG grants HO 950/14 and HO 950/16 to Uwe Homberg. Torsten Rohlfing was supported by NIAAA under grant AA013521-INIA and NIBIB under Grant EB008381. Registration tools and scripts for Iterative Shape Averaging are available in source code as part of the Computational Morphometry Toolkit from http://www.nitrc.org/projects/cmtk/.

REFERENCES

Blum, M., and Labhart, T. (2000). Photoreceptor visual fields, ommatidial array, and receptor axon projections in the polarisation-sensitive dorsal rim area of the cricket compound eye. *J. Comp. Physiol. A* 186, 119–128.

Brandt, R., Rohlfing, T., Rybak, J., Krofczik, S., Maye, A., Westerhoff, M., Hege, H. C., and Menzel, R. (2005). Three-dimensional average-shape atlas of the honeybee brain and its applications. *J. Comp. Neurol.* 492, 1–19.

Bucher, D., Scholz, M., Stetter, M., Obermayer, K., and Pflüger, H. J. (2000). Correction methods for three-dimensional reconstructions from confocal images: I. Tissue shrinking and axial scaling. *J. Neurosci. Methods* 100, 135–143.

el Jundi, B., Huetteroth, W., Kurylas, A. E., and Schachtner, J. (2009). Anisometric brain dimorphism revisited: implementation of a volumetric 3D standard brain in *Manduca sexta*. *J. Comp. Neurol.* 517, 210–225.

Evers, J. F., Schmitt, S., Sibila, M., and Duch, C. (2005). Progress in functional neuroanatomy: precise automatic geometric reconstruction of neuronal morphology from confocal image stacks. *J. Neurophysiol.* 93, 2331–2342.

Hanesch, U., Fischbach, K. F., and Heisenberg, M. (1989). Neuronal architecture of the central complex in *Drosophila melanogaster*. *Cell Tissue Res.* 257, 343–366.

Heinze, S. (2009). Characterization of Polarization Sensitive Neurons of the Central Complex in the Brain of the Desert Locust (*Schistocerca gregaria*). PhD Thesis, Philipps University Marburg, Marburg.

Heinze, S., Gotthardt, S., and Homberg, U. (2009). Transformation of polarized light information in the central complex of the locust. *J. Neurosci.* 29, 11783–11793.

Heinze, S., and Homberg, U. (2007). Maplike representation of celestial *E*-vector orientations in the brain of an insect. *Science* 315, 995–997.

Heinze, S., and Homberg, U. (2008). Neuroarchitecture of the central complex of the desert locust: intrinsic and columnar neurons. *J. Comp. Neurol.* 511, 454–478.

Heinze, S., and Homberg, U. (2009). Linking the input to the output: new sets of neurons complement the polarization vision network in the locust central complex. *J. Neurosci.* 29, 4911–4921.

Homberg, U. (1991). Neuroarchitecture of the central complex in the brain of the locust *Schistocerca gregaria* and *S. americana* as revealed by serotonin immunocytochemistry. *J. Comp. Neurol.* 303, 245–254.

Homberg, U. (1994). Flight-correlated activity changes in neurons of the lateral accessory lobes in the brain of the locust *Schistocerca gregaria*. *J. Comp. Physiol. A* 175, 597–610.

Homberg, U. (2004). In search of the sky compass in the insect brain. *Naturwissenschaften* 91, 199–208.

Homberg, U., Hofer, S., Pfeiffer, K., and Gebhardt, S. (2003). Organization and neural connections of the anterior optic tubercle in the brain of the locust, *Schistocerca gregaria*. *J. Comp. Neurol.* 462, 415–430.

Homberg, U., and Paech, A. (2002). Ultrastructure and orientation of ommatidia in the dorsal rim area of the locust compound eye. *Arthropod Struct. Dev.* 30, 271–280.

Homberg, U., Vitzthum, H., Müller, M., and Binkle, U. (1999). Immunocytochemistry of GABA in the central complex of the locust *Schistocerca gregaria*: identification of immunoreactive neurons and colocalization with neuropeptides. *J. Comp. Neurol.* 409, 495–507.

Horváth, G., and Varjú, D. (2004). Polarization Patterns in Nature and Polarized Light in Animal Vision. Berlin, Heidelberg, New York, Springer Verlag.

Ilius, M., Wolf, R., and Heisenberg, M. (1994). The central complex of *Drosophila melanogaster* is involved in flight control: studies on mutants and mosaics of the gene ellipsoid body open. *J. Neurogenet.* 9, 189–206.

Jenett, A., Schindelin, J. E., and Heisenberg, M. (2006). The virtual insect brain protocol: creating and comparing standardized neuroanatomy. *BMC Bioinformatics* 7, 544.

Kinoshita, M., Pfeiffer, K., and Homberg, U. (2007). Spectral properties of identified polarized-light sensitive interneurons in the brain of the desert locust *Schistocerca gregaria*. *J. Exp. Biol.* 210, 1350–1361.

Klagges, B. R. E., Heimbeck, G., Godenschwege, T. A., Hofbauer, A., Pflugfelder, G. O., Reifegerste, R., Reisch, D., Schaupp, M., Buchner, S., and Buchner, E. (1996). Invertebrate synapsins: a single gene codes for several isoforms in *Drosophila*. *J. Neurosci.* 16, 3154–3165.

Kurylas, A. E., Rohlfing, T., Krofczik, S., Jenett, A., and Homberg, U. (2008). Standardized atlas of the brain of the desert locust, *Schistocerca gregaria*. *Cell Tissue Res.* 333, 125–145.

Kuß, A., Hege, H. C., Krofczik, S., and Borner, J. (2007). Pipeline for the creation of surface-based averaged brain atlases. In Proceedings of Winter School of Computer Graphics 2007, 1, 17–24.

Kvello, P., Løfaldli, B. B., Rybak, J., Menzel, R., and Mustaparta, H. (2009). Digital, three-dimensional average shaped atlas of the *Heliothis virescens* brain with integrated gustatory and olfactory neurons. *Front. Syst. Neurosci.* 3:14. doi: 10.3389/neuro.06.014.2009.

Labhart, T. (1988). Polarization-opponent interneurons in the insect visual system. *Nature* 331, 435–437.

Labhart, T., and Meyer, E. P. (1999). Detectors for polarized skylight in insects: a survey of ommatidial specializations in the dorsal rim area of the compound eye. *Microsc. Res. Tech.* 47, 368–379.

Labhart, T., Petzold, J., and Helbling, H. (2001). Spatial integration in polarization-sensitive interneurones of crickets: a survey of evidence, mechanisms and benefits. *J. Exp. Biol.* 204, 2423–2430.

Liu, G., Seiler, H., Wen, A., Zars, T., Ito, K., Wolf, R., Heisenberg, M., and Liu, L. (2006). Distinct memory traces for two visual features in the *Drosophila* brain. *Nature* 439, 551–556.

Mappes, M., and Homberg, U. (2004). Behavioral analysis of polarization vision in tethered flying locusts. *J. Comp. Physiol. A* 190, 61–68.

Müller, M. (1997). Anatomische und funktionelle Charakterisierung der unteren Einheit des Zentralkörpers im Gehirn der Heuschrecke Schistocerca gregaria. Doctoral Thesis, Universität Regensburg, Germany.

Müller, M., Homberg, U., and Kühn, A. (1997). Neuroarchitecture of the lower division of the central body in the brain of the locust (*Schistocerca gregaria*). *Cell Tissue Res.* 288, 159–176.

Neuser, K., Triphan, T., Mronz, M., Poeck, B., and Strauss, R. (2008). Analysis of a spatial orientation memory in *Drosophila*. *Nature* 453, 1244–1247.

Ott, S. R. (2008). Confocal microscopy in large insect brains: Zinc–formaldehyde fixation improves synapsin immunostaining and preservation of morphology in whole-mounts. *J. Neurosci. Methods* 172, 220–230.

Pfeiffer, K., and Homberg, U. (2007). Coding of azimuthal directions via time-compensated combination of celestial compass cues. *Curr. Biol.* 17, 960–965.

Pfeiffer, K., Kinoshita, M., and Homberg, U. (2005). Polarization-sensitive and light-sensitive neurons in two parallel pathways passing through the anterior optic tubercle in the locust brain. *J. Neurophysiol.* 94, 3903–3915.

Poeck, B., Triphan, T., Neuser, K., and Strauss, R. (2008). Locomotor control by the central complex in *Drosophila* – An analysis of the *tay bridge* mutant. *Dev. Neurobiol.* 68, 1046–1058.

Rein, K., Zöckler, M., Mader, M. T., Grübel, C., and Heisenberg, M. (2002). The *Drosophila* standard brain. *Curr. Biol.* 12, 227–231.

Rohlfing, T., Brandt, R., Maurer, C. R. Jr, and Menzel, R. (2001). Bee brains, B-splines and computational democracy: Generating an average shape atlas. Proceedings of the IEEE Workshop on Mathematical Methods in Biomedical Image Analysis, MMBIA, Kauai, Hawaii. 187–194.

Rohlfing, T., Brandt, R., Menzel, R., and Maurer, C. R. (2004). Evaluation of atlas selection strategies for atlas-based image segmentation with application to confocal microscopy images of bee brains. *Neuroimage* 21, 1428–1442.

Sakura, M., Lambrinos, D., and Labhart, T. (2008). Polarized skylight navigation in insects: model and electrophysiology of e-vector coding by neurons in the central complex. *J. Neurophysiol.* 99, 667–682.

Schmitt, S., Evers, J. F., Duch, C., Scholz, M., and Obermayer, K. (2004). New methods for the computer-assisted 3-D reconstruction of neurons from confocal image stacks. *Neuroimage* 23, 1283–1298.

Siegl, T., Schachtner, J., Holstein, G. R., and Homberg, U. (2009). NO/cGMP signalling: L-citrulline and cGMP immunostaining in the central complex of the desert locust *Schistocerca gregaria*. *Cell Tissue Res.* 337, 327–340.

Strausfeld, N. J. (1976). Atlas of an Insect Brain. Heidelberg, Springer.

Strauss, R. (2002). The central complex and the genetic dissection of locomotor behaviour. *Curr. Opin. Neurobiol.* 12, 633–638.

Strauss, R., and Heisenberg, M. (1993). A higher control center of locomotor behavior in the *Drosophila* brain. *J. Neurosci.* 13, 1852–1861.

Vitzthum, H., Müller, M., and Homberg, U. (2002). Neurons of the central complex of the locust *Schistocerca gregaria* are sensitive to polarized light. *J. Neurosci.* 22, 1114–1125.

Wang, Z., Pan, Y., Li, W., Jiang, H., Chatzimanolis, L., Chang, J., Gong, Z., and Liu, L. (2008). Visual pattern memory requires foraging function in the central complex of *Drosophila*. *Learn. Mem.* 15, 133–142.

Wehner, R. (1992). Arthropods. In Animal Homing, F. Papi, ed. (London, Chapman and Hall), pp. 45–144.

Williams, J. L. D. (1972). Some Observations on the Neuronal Organisation of the Supra-Oesophageal Ganglion in *Schistocerca gregaria* Forskål with Particular Reference to the Central Complex. PhD Thesis, University of Wales, Cardiff

Williams, J. L. D. (1975). Anatomical studies of the insect central nervous system: a ground-plan of the midbrain and an introduction to the central complex in the locust, *Schistocerca gregaria* (Orthoptera). *J. Zool.* 176, 67–86.

Conflict of Interest Statement: The authors declare that the research was conducted in the absence of any commercial or financial relationships that could be construed as a potential conflict of interest.

Received: 04 September 2009; paper pending published: 29 October 2009; accepted: 19 December 2009; published online: 03 February 2010.

*Citation: el Jundi B, Heinze S, Lenschow C, Kurylas A, Rohlfing T, and Homberg U (2010) The locust standard brain: a 3D standard of the central complex as a platform for neural network analysis. Front. Syst. Neurosci. **3**:21. doi: 10.3389/neuro.06.021.2009*

frontiers in
SYSTEMS NEUROSCIENCE

ORIGINAL RESEARCH ARTICLE
published: 13 July 2010
doi: 10.3389/fnsys.2010.00030

The digital bee brain: integrating and managing neurons in a common 3D reference system

Jürgen Rybak[1,2]*, Anja Kuß[3], Hans Lamecker[3], Stefan Zachow[3], Hans-Christian Hege[3], Matthias Lienhard[4], Jochen Singer[1], Kerstin Neubert[4] and Randolf Menzel[1]

[1] *Institute for Biology – Neurobiology, Free University Berlin, Berlin, Germany*
[2] *Max Planck Institute for Chemical Ecology, Jena, Germany*
[3] *Zuse Institute Berlin, Berlin, Germany*
[4] *Max Planck Institute for Molecular Genetics, Berlin, Germany*

Edited by:
Raphael Pinaud, University of Rochester, USA

Reviewed by:
Kevin Daly, West Virginia University, USA
Sarah Farris, West Virginia University, USA
Carsten Duch, Arizona State University, USA

****Correspondence:***
Jürgen Rybak, Department of Evolutionary Neuroethology, Max-Planck-Institut for Chemical Ecology, Hans-Knöll Strasse 8, D-07745 Jena, Germany.
e-mail: jrybak@ice.mpg.de

The honeybee standard brain (HSB) serves as an interactive tool for relating morphologies of bee brain neurons and provides a reference system for functional and bibliographical properties (http://www.neurobiologie.fu-berlin.de/beebrain/). The ultimate goal is to document not only the morphological network properties of neurons collected from separate brains, but also to establish a graphical user interface for a neuron-related data base. Here, we review the current methods and protocols used to incorporate neuronal reconstructions into the HSB. Our registration protocol consists of two separate steps applied to imaging data from two-channel confocal microscopy scans: (1) The reconstruction of the neuron, facilitated by an automatic extraction of the neuron's skeleton based on threshold segmentation, and (2) the semi-automatic 3D segmentation of the neuropils and their registration with the HSB. The integration of neurons in the HSB is performed by applying the transformation computed in step (2) to the reconstructed neurons of step (1). The most critical issue of this protocol in terms of user interaction time – the segmentation process – is drastically improved by the use of a model-based segmentation process. Furthermore, the underlying statistical shape models (SSM) allow the visualization and analysis of characteristic variations in large sets of bee brain data. The anatomy of neural networks composed of multiple neurons that are registered into the HSB are visualized by depicting the 3D reconstructions together with semantic information with the objective to integrate data from multiple sources (electrophysiology, imaging, immunocytochemistry, molecular biology). Ultimately, this will allow the user to specify cell types and retrieve their morphologies along with physiological characterizations.

Keywords: confocal microscopy, neuron reconstruction, image registration, brain atlas, statistical shape model, neural networks, ontology, *Apis mellifera*

INTRODUCTION

Analysis of the structure of neural networks requires the selective staining of the participating neurons, their three-dimensional (3D) reconstruction, and the integration of these reconstructions into a common reference frame, an anatomical atlas. Insects have rather small brains that can be captured in full using confocal microscope imaging. Unsurprisingly, significant advances have been made in attempts to create digital atlases of whole insect brains (see the other contributions to this special issue).

Neurons that participate in neural networks are normally stained in separate preparations. Even if double or triple staining is performed in one brain, a whole network can only be reconstructed using data collected from multiple preparations. An ideal frame for the precise composition of multiple reconstructions would be an atlas of the whole brain that contains a large number of landmarks for warping different brains into one reference (e.g., Toga and Mazziotta, 2002). We developed and tested the suitability of this approach by creating a standard atlas of the bee brain (the honeybee standard brain: HSB, Brandt et al., 2005). The HSB atlas can be used to successfully reconstruct components of a neural network from separately acquired neurons and to visualize their spatial relations.

To create digital standard insect brains, two standardization methods have been employed: (1) The iterative shape method (ISA), which eliminates individual shape variability (Rohlfing et al., 2001; Brandt et al., 2005; Kvello et al., 2009). (2) The virtual insect brain (VIB) protocol, which allows a comparative volume analysis of brain neuropils, developmental studies, and studies on neuronal plasticity and genetic differences (Rein et al., 2002; Kurylas et al., 2008; el Jundi et al., 2009). We favored the ISA standard, which is derived by averaging across multiple individual brains. Analyses of other procedures, for example, selecting an individual representative brain, have shown that the averaging procedure is best suited to the registration of neurons collected from different brains (Kurylas et al., 2008).

Abbreviations: AL, antennal lobe; br, basal ring of the calyx; ca, calyx; CB, central body; co, collar of the calyx; d, dorsal; DL, dorsal lobe; HSB, honeybee standard brain; K, Kenyon cell; l, lateral; l-ACT, lateral antennocerebralis tract; lc, lateral calyx; lh, lateral horn; li, lip of the calyx; LPL, lateral protocerebral lobe; Lo, lobula; m, median; m-ACT, median antennocerebralis tract; MB, mushroom body; mc, medial calyx; Me, Medulla; Oe, esophagus; p, posterior; pe, peduncle; PL, protocerebral lobe; PN, projection neuron; SSM, statistical shape model; SOG, subesophageal ganglion; v, ventral

The averaging method applied in the HSB is based on ideas of Ashburner (2000) and Guimond et al. (2000), who derive an average-shape image through an iteration of one affine registration, followed by multiple elastic registrations (Rohlfing et al., 2001, 2004). To create an initial average image, the method first registers all images to an (arbitrarily chosen) initial reference using affine registration. The method then registers all images non-rigidly to this average, generating a new average, and so forth. The underlying idea is that after several such iterations the average converges to the shape centroid of the population, which is, up to affine components (position, orientation, scaling, and shearing), independent of the choice of the initial reference image (Guimond et al., 2000, for more details on applying these methods for creating the honeybee standard brain: see Brandt et al., 2005).

The first step towards filling the atlas with structural information about neurons requires the semi-automatic segmentation of the neurons of interest and their related neuropils. The neuropil segmentations are spatially registered onto structures of the atlas. Then, the transformation coordinates produced by registration are used to fit neurons from different experiments into the atlas. Protocols for integrating genetically labeled neuron populations and single cell reconstructions into brain atlases have been described (e.g., Jenett et al., 2006; Kuß et al., 2007; Rybak et al., 2009). These protocols provide the electronic resources and tools for reconstructing neurons (Schmitt et al., 2004; Evers et al., 2005) as well as registration techniques that enable spatial normalization of structures using geometric warping algorithms (Rohlfing et al., 2001; Toga and Mazziotta, 2002; Westerhoff, 2003; Maye et al., 2006).

To facilitate the segmentation process, a statistical shape model (SSM) was developed. In order to develop the SSM a method was used that is based on successful procedures for automatic segmentation of medical imaging data (Lamecker et al., 2004; Kainmüller et al., 2007, 2009; Seim et al., 2008). The method integrates *a priori* information about variable neuropil shapes as imaged from confocal microscope imaging data (Neubert, 2007; Singer et al., 2008). Features in the imaging data are compared to intensity profiles of the confocal gray-value data, which have been learned by the model from a training data set. These comparisons are used to adapt all neuropil boundaries contained in the SSM to individual neuropil boundaries in the present imaging data.

In this study, emphasis was placed on the strategy of standardizing and optimizing the registration process and the subsequent fitting procedures of neuronal data. These issues are important to make the HSB usable for researchers at other labs. The applicability of statistical shape atlases that contain information about brain structures and their variability are discussed.

Furthermore, we introduce an ontology-based approach integrates vast amounts of data from various experimental sources in a structured way into a single coherent database.

The HSB atlas and examples of registered neurons can be downloaded and visualized at http://www.neurobiologie.fu-berlin.de/beebrain/

MATERIALS AND METHODS

All animals (workerbee foragers, *Apis mellifera carnica)* were taken from the hives at the Institute for Neurobiology, Free University, Berlin, Germany.

HISTOLOGY

Synaptic neuropil background staining

Neuropil background staining used for the HSB is described in detail in (Brandt et al., 2005). In brief, brains were dissected in phosphate buffered saline (PBS) and fixed in 4% para-formaldehyde (PFA) for 2 h. After blocking in 10% normal goat serum (NGS; Jackson ImmunoResearch, Westgrove, PA, USA) in PBS-Triton X-100 (Sigma)), they were incubated for 5 days in synaptic antibodies (primary antisera NC46 and SYNORF1 each diluted 1:30 in NGS-PBS-TritonX-100 (SYNORF1, Klagges et al., 1996, and NC46 were kindly provided by Dr. E. Buchner, Würzburg). Afterwards, the brains were incubated for 3–5 days with Cy3 conjugated mouse anti-rabbit secondary antibody (Jackson ImmunoResearch; dilution 1:200 in NGS-PBS-TritonX-100). Brains were dehydrated and cleared in methylsalicylate.

Lucifer yellow histology

For preparations that were utilized for construction of the SSM Lucifer yellow was used as a neuropil background stain. Brains were fixed in 4% para-formaldehyde (pFA) (Sigma) for either 2 h at room temperature or overnight at 4°C. After washing, brains were dehydrated in ascending ethanol series, and cleared in methylsalicylate. 4% Lucifer yellow was added either to the fixative at a dilution of 1:500 or to PBS-TritonX treated overnight.

Ethyl gallate histology (Wigglesworth, 1957)

Brains were fixed for 4 h in 2.5% glutaraldehyde in cacodylate buffer. After several washes in buffer, brains were osmicated in 2% OsO_4 in cacodylate buffer for 1 h in the dark. Tissue was then transferred to 0.5% ethyl gallate (Merck) in distilled water for 1–4 h. The solution was changed until the blue-gray color disappeared. After thorough washing in distilled water, the specimens were dehydrated and embedded in Durcupan (Fluca). Ethyl gallate preparations were sectioned at 10–25 µm.

Confocal microscopy

Whole-mount brains used for creating the SSM were counterstained with Lucifer yellow and imaged sequentially with the Leica TCS-SP2 confocal microscope using a 10× dry or 10× oil Leica objective (HC PL APO 10 × /0.4, Leica, Bensheim, Germany). For Lucifer yellow-stained tissue, the Ar-Kr 488-nm laser line was used at a voxel resolution of approximately 1.5 × 1.5 × 3 µm. The dye-filled neurons were excited using the 543-nm line (detected with an emission spectrum of 550–620 nm) or the 633-nm line (detected with an emission spectrum of 650–750 nm) of the HeNe laser. For high-resolution scans of intracellularly stained neurons, we used the 20× oil (HC PL APO 20 × /0.70) 40× oil HCX PL APO CS 40.0×/1.25) and 63× oil objectives (HCX PL APO 63×/1.32–0.60) (Leica, Bensheim, Germany). Depending on the zoom factor (1–4) the voxel resolution was approximately 0.1–0.4 × 0.1–0.4 × 1 µm. In all confocal scans we used a pixel resolution of 1024 × 1024 in *xy* axes and an 8 bit intensity resolution. Because of the refractive index mismatch in the optical path, dry lenses usually introduce a shortening of distances in the *z* axis. According to Bucher et al. (2000), shortening can be considered as a linear scaling in the *z* direction. Therefore, the scaling factor from preparations that were scanned with dry lenses is estimated to be 1.6. (refraction index: methylsalicylate = 1.51, oil = 1.54, air = 1).

TRACING OF NEURONS

All confocal scans were digitized as double channels after which each channel was analyzed separately using the three-dimensional visualization and segmentation modules in Amira (version 4.1; Visage Imaging, Berlin; San Diego, CA, USA). Tracing and reconstruction of the neurons, including topology, lengths, and diameters, were performed using a module that integrates methods presented in (Schmitt et al., 2004; Evers et al., 2005). Traced single neurons, which were Amira data SkeletonTree format, were converted to the LineSet format and then triangulated to meshed surfaces. These surface files were exported as wavefront (obj) files. Wavefront files of neurons and neuropil surfaces were imported with the Adobe 3D Reviewer to Adobe Acrobat Pro Extended (Adobe Systems, Inc.). The images in the PDF version of this manuscript can be viewed by using the 3D viewer mode of the Acrobat Reader (version 9 and higher, which is freely available at http://get.adobe.com/de/reader/.

SEGMENTATION OF NEUROPILS

Semi-automatic segmentation

Image segmentation was performed semi-automatically using Amira 4.1. The segmentation results were image stacks of type LabelField. LabelFields assign a label, which represents a distinct (brain) structure, to each voxel.

In most cases, no image preprocessing on the raw images was necessary, except for an adjustment of the gray-scale window. In some cases, Gaussian smoothing and unsharp masking from Amira's DigitalFilters tool were applied to enhance faint contours. Image stacks were then loaded into the interactive segmentation editor. Using the segmentation editor's BrushTool, the neuropil areas of interest were traced manually, slice by slice. To facilitate and speed up this manual segmentation process, a method that automatically interpolates segmentations between image slices was applied. In a post-processing step, connected areas of voxels containing only a small number of voxels were eliminated with the RemoveIslands tool. Finally, the LabelFields were smoothed (SmoothLabels).

An image series showing the brain neuropils of the HSB with superimposed LabelFields using the ColorWash module is provided in the **Movie 1** in supplementary material. The final segmentations were supervised by a segmentation expert (curator of the HSB, JR). Depending on the staining quality of the tissue, an experienced user needs a minimum of 8–10 h to reconstruct all neuropils defined for the HSB.

REGISTRATION INTO THE HSB

Registration and transformation of neurons into the HSB

To fit a neuron into the HSB, two steps are applied. First, the neuron's related neuropils are registered to corresponding parts of the HSB. This requires an affine and a subsequent elastic registration, which respectively result in a 9-degree of freedom transformation matrix and a deformation field (VectorField). Second, the registration resulted are used to transform the neuron's geometric representation (SkeletonTree or LineSet).

The affine and the elastic registration procedures use a metric that takes the spatial correspondence of two label fields into account. Similarity measures were used as label consistency. The affine registration procedure further uses a hierarchical optimization algorithm going from coarser to finer resolution.

A description of the registration process and parameter settings can be found in the Amira User Guide (Visage Imaging, Berlin; San Diego, CA, USA). A detailed protocol is found in the section "Registration protocol" of supplementary material (see also Kuß et al., 2007).

Registration using landmarks

Histological sections stained with ethyl gallate were registered into the HSB using the LandmarkWarp module of Amira. The corresponding anatomical locations in the histological sections and the gray-value dataset of the HSB were defined by two sets of landmarks.

THE STATISTICAL SHAPE MODEL

A SSM captures the mean shape and the geometric variability of a given set of input geometries by a limited number of parameters and can therefore be used for automated and robust image segmentation. The SSM of the bee brain applied in this work was presented in Lienhard (2008). A detailed description of the procedure and references to other approaches can be found in Lamecker (2008). Our strategy for the creation of an SSM from three-dimensional image data includes several steps: (1) Triangular surfaces were reconstructed from 16 manually labeled image stacks of central neuropils of the worker bee. In contrast to the previously presented HSB, the neuropil counter stain was achieved using 5% Lucifer yellow. Most labels for neuropils were chosen as defined in the HSB (Brandt et al., 2005). The median and lateral calyces of each mushroom body were segmented without subdivisions. The optic and antennal lobes were not included in this model. A subdivision of the calyces into lip, collar, and basal ring was not performed. (2) Point-to-point correspondences were established between all training surfaces, i.e., vertices with the same index share the same anatomical position on each training surface. To achieve this, all surfaces were equally partitioned into regions (patches), which represent homologous biological compartments. A reference surface triangulation was then mapped onto each training shape using surface parameterization techniques (Lamecker et al., 2003). (3) After alignment of all training shapes to one reference, principal component analysis was applied on the set of shape vectors representing the surfaces' vertex coordinates. This process generated the SSM representing the average shape plus a linear combination of the most characteristic modes of shape variation (shape modes) contained in the training set.

The SSM allows a highly compact representation of shape variations among a large number of individuals. The most challenging step in the SSM generation is the identification of corresponding points (step 2). Our approach is interactive as it involves manual specification of patch boundaries. Yet, this allows the production of accurate SSMs even for very complex geometries with large deformations and arbitrary topologies, as in the case of the bee brain.

SSM-based automated image segmentation

Image segmentation can be automated by using *a priori* knowledge, particularly about geometrical shapes and intensity profiles. The general idea is to roughly position an SSM in the imaging data and subsequently vary the shape parameters (weights of the shape modes) and the spatial location until the SSM matches the object in the imaging data as closely as possible (Lamecker, 2008). The intensity distributions of the underlying imaging data are evaluated around

the current SSM, and the surface of the SSM is displaced according to a set of given rules leading to the displacement model, which will be discussed in the next section. From the computed displacement, new shape weights or new locations are computed. This procedure guarantees that the segmentation indeed represents a plausible shape (robustness). In order to overcome possible mismatches due to individual variations not captured by the SSM, a post-processing step usually provides some fine tuning for accuracy (Kainmüller et al., 2007, 2009; Seim et al., 2008). Apart from the SSM itself, the main ingredient is a rule for displacing the SSM according to the underlying imaging data to be segmented. This is provided by the displacement model.

The displacement model

A simple method for computing displacements of the surface model in the imaging data is to determine a normal displacement for each vertex of the model such that the new vertex position coincides with a strong gradient in the imaging data. Here, the only assumption made is that object boundaries in the imaging data are reflected by significant local variations in the image intensity. In the case of confocal imaging of bee brains more information about the imaging process can be included in order to refine this model. Such extensions have been proposed by Neubert (2007) and Singer (2008) for different imaging protocols.

Segmentation performance

Accuracy. Cross-validation tests are used to estimate how reliably the SSM-based segmentation of the bee brain performs in practice. In the leave-one-out test one image is removed from the training set, and a calculation is performed to determine how accurately a reduced SSM, which is constructed from the remaining images, can be adapted to that removed image. The ability of the model to describe arbitrary shapes is described as completeness or generality. In order to estimate the quality of the displacement models (intensity profile analysis) leave-all-in tests were performed. In contrast to the leave-one-out test, the known image is not removed from the SSM. This way the performance of the displacement strategy can be measured, separated from the quality of the SSM itself.

Performance measures. Measures for the mean and maximal surface distance were calculated using the Amira SurfaceDistance module. This module computes several different distance measures between two surfaces. The following measures were computed from the histogram of these values: mean distance and standard deviation; root mean square distance; maximum distance (Hausdorff distance); medial distance; area deviation (percentage of area that deviates more than a given threshold).

RESULTS

CONFOCAL MICROSCOPY

Because the registration process is based on label fields, the neuropils have to be stained in such a way that neuropil borders can be identified and segmented. We first applied an antibody against synapsin which nicely stains neuropils dense in synapses, and thus contrasts its border to surrounding tissue (Brandt et al., 2005). A simpler method involves imaging the autofluorescence of the tissue induced by glutaraldehyde. One could also enhance the autofluorescence using dyes such as Lucifer yellow. Lucifer yellow staining, though reduced in contrast compared to the synapsin antibody staining, allows more rapid and easier histological processing. It further detects neuronal structures in much more detail than autofluorescence, and results in homogenous staining throughout the brain.

The challenge for transforming neurons into the common frame of the HSB (**Figure 1**) is to segment the complete Gestalt of each neuron at low resolution together with its spatial relations to adjacent structures (often gained by high-resolution microscopy) such that a warping algorithm allows for precise matching between samples from different individual brains.

In **Figure 2** several examples of neurons are shown, each stemming from a different preparation, and each having been separately transformed into the HSB. To capture all parts of a neuron at different resolutions, several confocal scans were necessary. This poses the problem of registering several label fields leading to subsequent errors during realignment of all parts of the neuron that accumulate during the registration processes, which may induce artifacts at the edges of the label fields (Maye et al., 2006). The strategy used for each of the examples of **Figure 2** was to first scan an overview of the brain containing the whole neuron, and then reconstruct the main parts of the neuron. Afterwards, the neuron's regions of interest, for example, the dendritic tree of the L3 neuron, were reconstructed from high-resolution scans (**Figure 2B**), downscaled, aligned, and merged to the main neuron reconstructed from low resolution scans. Deviations that are caused by using several independent regions of the same neuron in several steps of registration are kept to a minimum. As a result, the spatial accuracy of the warping process is enhanced. This iterative procedure allows us to compose compounds of registrations at different levels of resolution, for example, the target areas of olfactory and mechanosensory interneurons (Ai et al., 2009) in subregions of the protocerebral lobe (arrows in **Figure 2A**) together with registrations at high resolution of their fine structures for the analysis of their local topological features (**Figures 2C,D**). The movie

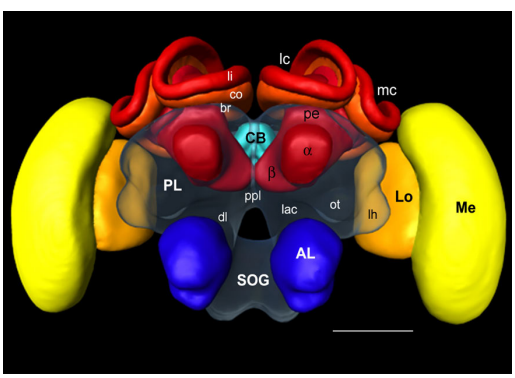

FIGURE 1 | Surface reconstruction of the honeybee standard brain (HSB). Neuropil areas defined in the HSB are shown in different colors. Components of the midbrain area (protocerebral lobes, PL, and subesophageal ganglion, SOG) are fused and shown in transparency. Subcompartments of the protocerebral lobe and mushroom bodies are indicated in lower case letters. Scale: 300 µm. PL: protocerebral lobe; ppl: posterior protocerebral lobe, Lo: lobula; Me: medulla, li: lip, co: collar, br: basal ring, lh: lateral horn, ot: optic tubercle, lac: lateral accessory lobe, mc: median calyx, lc: lateral calyx, pe: peduncle, α: alpha-lobe, β: beta-lobe, SOG: suboesophageal ganglion.

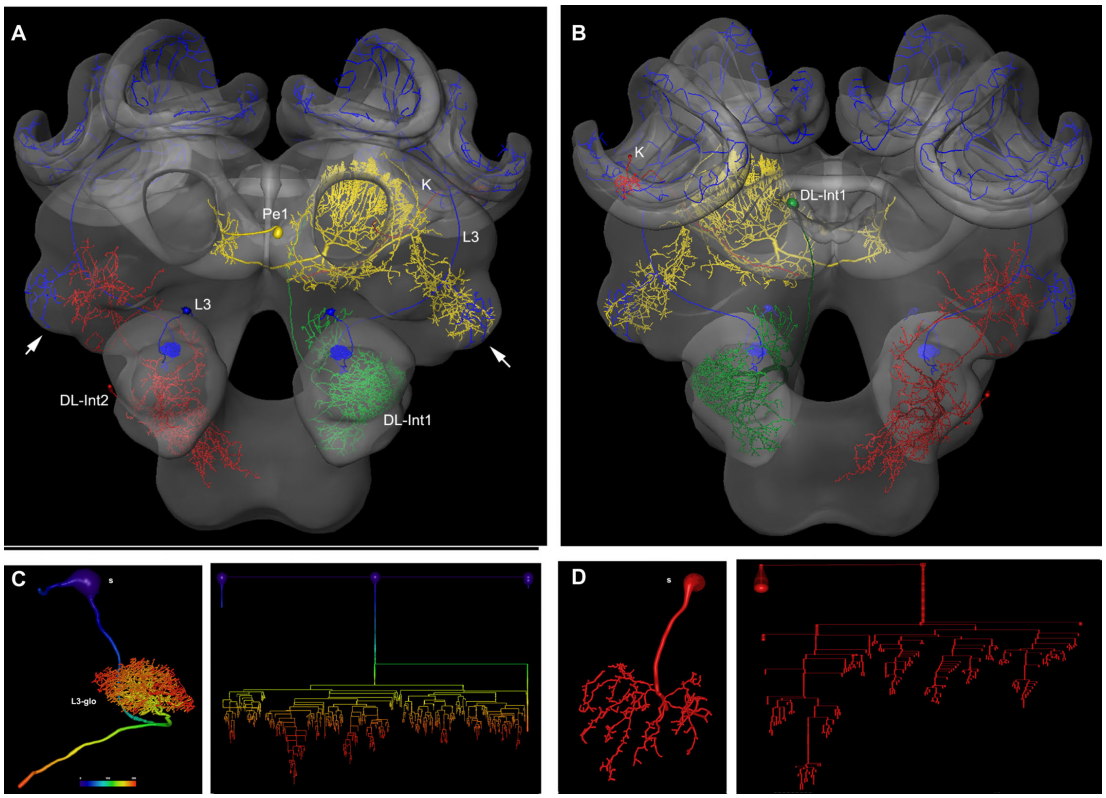

FIGURE 2 | Olfactory (L3: blue) mechanosensory (dorsal lobe interneuron 1 and 2: DL_Int1, green, DL_Int2, red) and central interneurons (Pe1, yellow) registered into HSB. A mirror image is exhibited for the L3. **(A)** frontal view **(B)** caudal view. The projection areas in the lateral protocerebral lobe are compared (arrows). They occupy either separate neuropil areas: L3 and DL_Int2, or L3 and Pe1 overlap. **(A)** The L3 neuron projects to the lateral horn (arrows) and mushroom body calyces (MC, LC). The axonal terminals of the L3 neuron form microdomains in the lip region of the calyces and overlap with the dendritic fields of Kenyon cells (K, in B). Scale: 50 µm. **(C, D)** Neuron reconstruction and dendrogram of the respective neurons derived from high-resolution confocal scans. In **(C)** the neuronal distance is indicated in color. See false-color coded bar. (see also **movies** of supplementary material S3).

of supplementary material S3 and the interactive viewing mode in the PDF file (**Figure 2A**) allows visualization of the neurons' spatial relationships.

Estimating the accuracy of the registration process is a difficult task. Certainly, the process involves numerous steps, which are prone to induce inaccuracies (see above). For example, the histological procedure may induce variable distortions due to local shrinkage differences that are not fully compensated by the affine and elastic registration. The experimenter may not segment correctly; the number of label fields (and, thus, the number of registrations steps) and thus distortions of the reconstructed surfaces of neuropils and neurons will lead to incorrect locations of the transformed neuron in the HSB. In addition, the neuropils and neurons themselves will differ from animal to animal, and it is this variability that determines the fundamental limit regarding the reliability of any brain atlas – besides the methodological problems. Therefore, it is not possible to derive a measure of reliability in the composition of neurons registered sequentially into the brain atlas. The best way of checking the spatial accuracy of such neurons is by comparing the relative positions of the neuron to the neuropil border lines in the original preparation to the situation after the registration process. We provide circumstantial evidence for the reliability of the segmentation and registration process by describing an example in which we compared the locations of intracellularly stained neurons with cross sections in high-resolution ethyl gallate-stained paraffin sections using two different registration methods.

INTEGRATING DATA COLLECTED BY DIFFERENT HISTOLOGICAL METHODS

In **Figure 3** a registered olfactory projection neuron (L5) is visualized together with a registered ethyl gallate section showing midbrain regions (mushroom bodies, central body, and protocerebral lobe). The ethyl gallate method (Wigglesworth, 1957) provides detailed information about the neural architecture revealing the composition of neuropils, somata, and tracts, thus capturing the spatial context information. A whole series of ethyl gallate-stained sections was first used to identify the median and lateral antennocerebralis tracts (ACTs) in a correlative light and electron microscopy study (Rybak, 1994). Our future goal is to integrate data from these histological procedures into the HSB. Here, we demonstrate the spatial accuracy of the registration process. A horizontal ethyl gallate section was warped into the HSB using a landmark-based registration by finding corresponding points or landmarks in the HSB and the histology section (**Figure 3**). Separately, a single stained L3 axon, which was transformed to the HSB using a

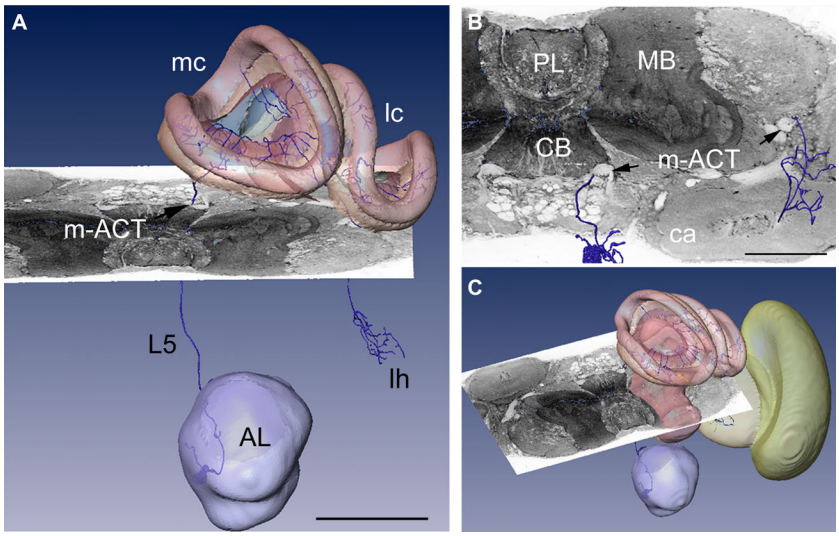

FIGURE 3 | Visualization of the neural architecture of the midbrain from two different preparations using landmark and label field registration techniques. **(A)** The L5 projection neuron (in blue) of the median antenno-cerebralis tract (m-ACT) connects the antennal lobe with the mushroom body calyx (MC, LC) and lateral horn (LH), L5 axon (black arrow). **(B)** The m-ACT can be identified in a cross section as the ascending and descending protocerebral part (m-ACT, black arrows). The spatial locations of the two registrations demonstrate the spatial accuracy of fitting neuronal data into the HSB. **(C)** The histological ethyl gallate section is located at around 300 µm from the calycal surface (horizontal plane). Scale: 200 µm, CB: central body, MB: mushroom body, PL: protocerebral lobe.

label field registration, runs through the corresponding ascending and descending parts of the median ACT (m-ACT) as seen in the ethyl gallate section (**Figures 3A–C**). The spatial accuracy of the registration process is indeed very high, and allows identification of m-ACT neurons in the median and lateral antenno-cerebralis tract (l-ACT) even at the single neuron level (see black arrows in **Figure 3B**).

ANALYZING PUTATIVE SYNAPTIC CONNECTIONS

Fitting neurons into the HSB can be achieved with a certain degree of accuracy with regard to spatial relationships, but thus far cannot replace studies on synaptic connectivity. This must be achieved by electron microscopy (e.g., Ganeshina and Menzel, 2001) or by some approximation in confocal co-localization studies on the light microscopy level. Combining high-resolution confocal laser scanning microscopy with precise three-dimensional dendritic surface reconstruction (Schmitt et al., 2004) allows for automated co-localization analysis in order to map the distribution of potential synaptic contacts onto dendritic trees or axon terminals (Evers et al., 2005; Meseke et al., 2009).

This technique was used to estimate the distribution of putative GABAergic synaptic contacts on the dendrites of the Pe1 neuron, a single identified mushroom body extrinsic neuron (Mauelshagen, 1993; Rybak and Menzel, 1998, **Figure 4**). GABA-like immunoreactivity has been shown for the A3 feedback neurons (Schäfer and Bicker, 1986; Grünewald, 1999). These neurons also innervate the mushroom body lobes and peduncle and may provide local inhibitory input to the Pe1 neuron (**Figure 4B**, green label). In **Figure 4D** the distribution of putative inhibitory input synapses onto the Pe1 dendritic tree is highlighted by red dots, indicating a distance of GABA-like immunoreactivity profiles of up to about 300 nm (Okada et al., 2007).

To achieve the accuracy required for neuronal connectivity estimates, the development of higher resolution atlases that define subregions of the brain and allow their integration into a common coordinate system is needed. An example is given in this special issue of Frontiers in Neuroscience by el Jundi et al. (2010) who constructed a high-resolution atlas of the central complex of *Locusta* and determined the spatial relations of two central complex neurons.

THE STATISTICAL SHAPE MODEL (SSM)

Advantage of the SSM

The accurate and reliable localization of region boundaries during the registration process is a prerequisite for fitting neurons into any Standard Atlas. This is true for manual (or semi-automatic) and fully automatic segmentation techniques, though the advantage of the latter is that the level of human expert interaction is reduced. Labeling performed by different individuals often leads to variable results. A model-based auto-segmentation of neuropil boundaries utilizes *a priori* knowledge about the 3D shape of an object, in our case the bee brain, and characteristic features of the imaging data. Such a model provides a measure of the variability of the object set and can therefore be used to analyze and quantify morphological volumetric changes in neuropiles of the adult animal.

An SSM of the central bee brain (excluding the antennal and optic lobes) was calculated from 16 training shapes, resulting in 17 shape modes. These were extended to 32 shapes (31 shape modes) by mirroring the right and left brain hemisphere along the neuraxis in each preparation. Each training shape was manually segmented by labeling the neuropil boundaries of the confocal imaging data stained with Lucifer yellow. Triangulated polygonal surfaces were reconstructed from the labeled images and simplified to 150000 triangles. The surfaces were then affinely aligned using

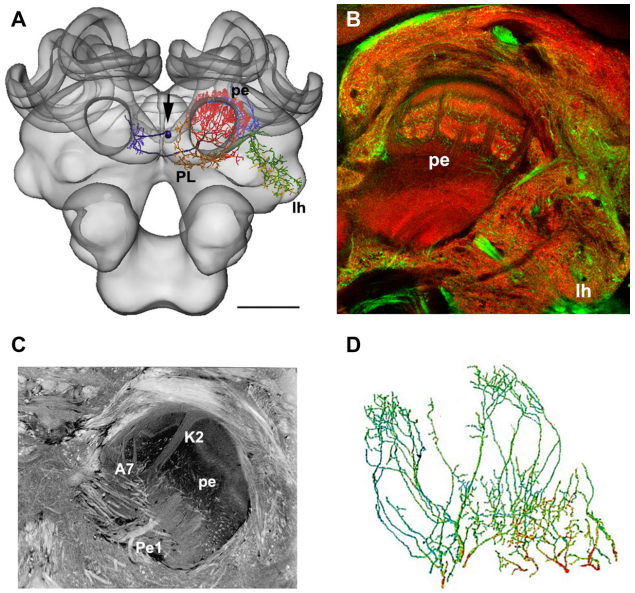

FIGURE 4 | (A) The Pe1 neuron fitted into the HSB (skeleton view). Different parts of the neuron are colored according to their innervation of subneuropils in the central bee brain. **(B)** GABA-IR in the bee brain. Double labeling of GABA-IR-like (green) and synapsin staining (synorf1, red). The optical section cuts the mushroom body at the transition zone between the α-lobe and peduncle (pe), lh: lateral horn of the protocerebral lobe. **(C)** A histological section of the central bee brain stained with ethyl gallate reveals the neural architecture of the mushroom bodies at the transition from the α-lobe to the peduncle. The large axon diameter of the Pe1 is identified as a single unique neuron. A7: type 7 α-lobe extrinsic neuron, K2: strand of Kenyon cells type 2, PE: peduncle. **(D)** The finger-like dendritic protrusions of an intracellularly marked and reconstructed PE1 neuron branch all over the cross section of the mushroom body at the border line between the β-lobe and the peduncle. These branches are organized in two regions (the proximal domain 1 and the distal domain 2) where the Pe1 is postsynaptic. Red dots indicate close appositions of GABA-IR profiles (arrows), which are more numerous in domain 1. Scale bars: **(A)** 200 µm.

the geometrical center as a reference point, and then transferred to a common coordinate system. In order to map the surfaces of the training shape in a proper way, certain conditions are required for creating the surfaces (for details see Lienhard, 2008). In order to achieve a correct model of a biological structure, one needs to find the corresponding anatomical points on all training shapes. To determine correspondences, surfaces were divided into 89 regions according to shape features and anatomical landmarks (**Figure 5A**). A principal component analysis provided a linear model of the shape variability of the training set (**Figure 5B**, see also the **Movie** in section **"The statistical shape model"** of supplementary material).

In order to place the SSM of the central bee brain roughly into the confocal images an affine registration was used applying a non-deformable model that contained only brain regions that represent borders to exterior structures. A positioning algorithm recomputed rotation, scaling, and translation parameters using characteristic image features of brain tissues. In order to reduce noise in the low-contrast Lucifer yellow stain a non-linear isotropic filter was applied to the data (Weickert, 1997; Lamecker et al., 2004).

The SSM-based segmentation algorithm, as described in the section "Methods", was applied until no further improvement could be achieved, meaning that the change of the shape between consecutive iterations fell under a defined threshold. The displacement vectors were computed via analyzing 1D profiles of image intensities along surface normals at each vertex (**Figure 5D**). Based on these displacements the SSM was iteratively adapted (see **Figures 5C,D** and the movie in section **"Automatic segmentation"** of supplementary material). The process of initial positioning and the adjustment of the model in an exemplary training dataset image (LY12) are shown in **Figure 6**.

Application of the segmentation algorithm on the training set images results in an average surface distance of 4.06 ± 0.95 µm of the fitted model to the manual segmented shapes. A leave-one-out test simulating new image data yields to a distance of 8.82 ± 1.02 µm. In comparison, two manual segmentations of the same imaging data lead to a mean surface distance of 4.79 µm.

The SSM and displacement algorithm was also tested with confocal data not contained in the training set that was used for creation of the shape model. We used extracted parts of the SSM in combination with the displacement model in order to automatically segment the mushroom body neuropil in high-resolution confocal scans (**Figure 7A**). **Figure 7B** shows the results for a single section using either the whole mushroom body calyces (red intersects) or the calyces (yellow intersects) to auto-segment the structures. Slightly better results were achieved using the reduced model of the calyx (arrows in **Figure 7B**). **Figures 7C,D** shows manually segmented neuropil borders in comparison to the automatic segmentation. **Figure 8** provides a direct comparison of the HSB and SSM. The mean surface distance between HSB and SSM amounts to 8.5 µm. Particularly large distances were found at the median calyx (MC) and subesophageal ganglion (SOG), possibly indicating stronger shrinkage dependencies induced by the different histological procedures. It takes an experienced segmentor around 8 h to manually segment those central brain structures used for the SSM.

In contrast, a further evaluation of the quality of automatic segmented bee brains and the estimated post-processing times amounts currently to approximately 3–4 h by an experienced segmenter.

HIERARCHICAL STRUCTURE LABELING AND BROWSING

The HSB created so far contains only geometric and topological information about neurons and neuropils. For many applications, semantic information also needs to be integrated. This semantic information includes information about the hierarchical organization of brain structures and information about relations between structures. An example would be the description of the anatomical proximity of neuron A and neuron B and the possible communication between them. Often neurobiologists have this knowledge, but the information needs to be made explicit.

In recent years, the development of ontologies has been an appropriate choice for capturing and representing semantic information in many fields, including biology. In the information sciences, an ontology is a formal representation of concepts or structures and relations among those structures in a defined application domain. Visually, ontologies can be described as graphs in which structures are represented by nodes and relationships between structures by edges. In ontology modeling, there are two different types of nodes:

Table 1 | The most important relations used in our bee brain ontology to describe spatial, morphological and, connectional properties.

Relation	Inverse relation	Description
hasPart	isPart	Model hierarchical organization of brain structures.
isInstanceOf	–	Models class membership.
adjacentTo	–	Models spatial adjacency.
hasSomaLocation	isSomaLocation	Model locations of neuron
hasAxonTerminals Location	isAxonTerminals Locations	parts soma, axon, and their
hasAxonPrimary Location	isAxonPrimary Location	terminals, and dendrites.
hasDendritesLocation	isDendritesLocation	
hasTract	isTract	Assign tracts.

classes and instances. Classes describe common concepts, such as *brain*. An instance of such a class could be, for example, the *brain of animal A*. Relations appear among classes, among instances, and among classes and instances. Relations can have different types, as for example the type *isA*. With these basic tools we can create the statement *brain of animal A isA brain*.

To support the understanding and analysis of structural and functional characteristics of brain structures, ontologies need to fulfill several requirements. An ideal brain ontology would include a complete set of structural parts and neuron types. It would also contain axonal projections between regions and neuron types, and it would include morphological, connectional, and functional properties of these particular neurons. According to Bota and Swanson (2008), an ideal ontology would be species specific. These authors also state that the development of such an ontology is a long-term goal for a community project. Indeed, we consider our attempts as an early step only.

Our ontology uses predefined classes of the foundational model of anatomy (FMA) (Rosse and Mejino, 2003). The most important of these are *Cell*, *Cell_Part*, *Organ*, and *Organ_Part* where *Cell* and

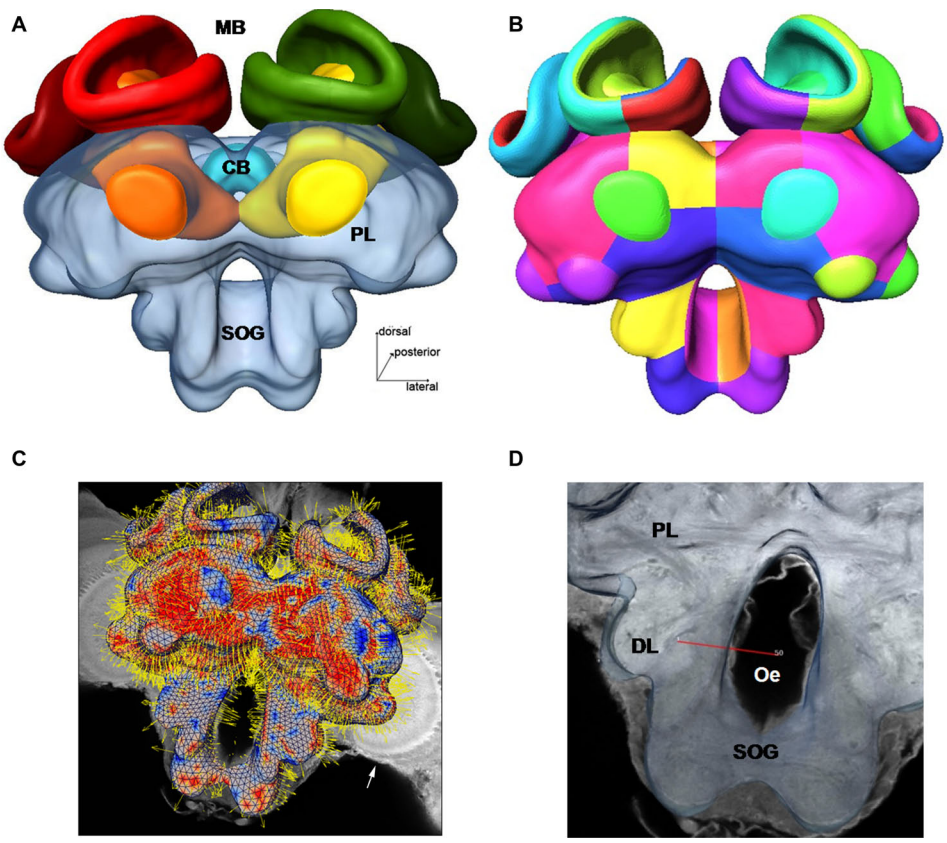

FIGURE 5 | (A) The surface of the statistical shape model (SSM) of the central honeybee brain (with exception of the antennal and optic lobes) derived from 16 segmented worker bee brains. The calyx regions of the mushroom bodies are not subdivided. **(B)** Patch decomposition: in order to find correspondence among the set of training data the surface of each segmented brain is subdivided into 89 patches (colored regions). **(C)** Position of the displacement of the bee brain model in the imaging data. Displacement vectors are shown as yellow arrows, blue color indicates the displacement vectors point outwards, red means they point inwards. The white arrow indicates one orthogonal slice of the 3D confocal image stack to which the model adapts. **(D)** A protocerebral region close to the esophagus is shown to demonstrate matching of the SSM (in transparency) to the corresponding gray-value confocal image. The red line marks the intensity profile (length 100 µm) along the vertex normals (adapted from Lienhard, 2008; Singer, 2008) for **(A)**: see also S4 movie in supplementary material.

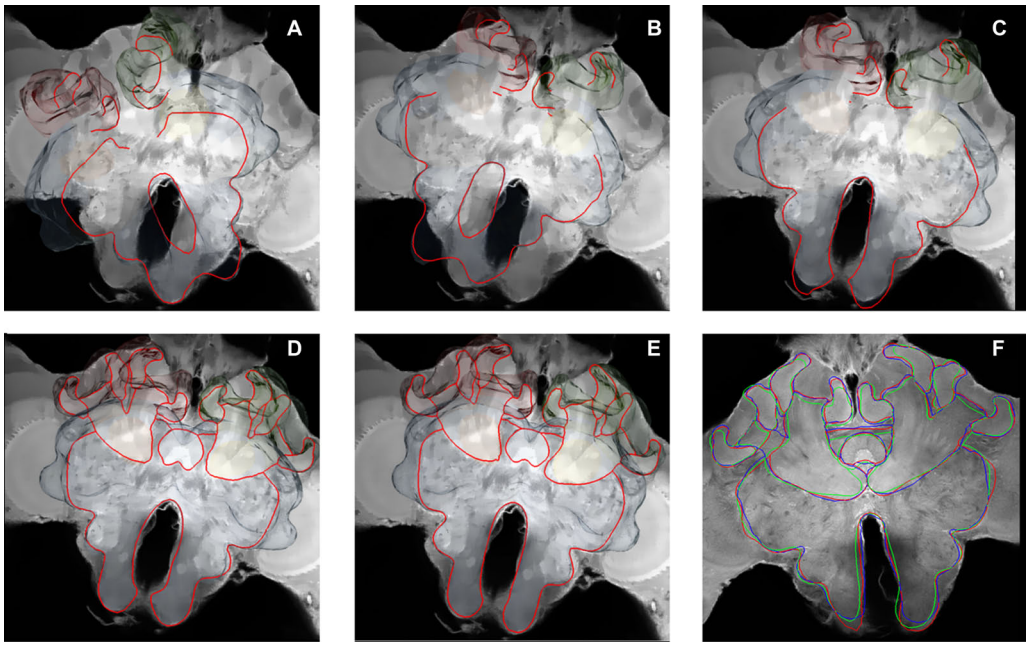

FIGURE 6 | Evaluation of the statistical shape model (SSM) and the displacement algorithm. The auto-segmentation process illustrated by a leave-all-in segmentation of preparation LY-12 (Lucifer yellow background stain) with the SSM. **(A)** Initial position of the average shape of the lateral mushroom body. **(B, C)** Result of the initial global positioning of a simplified SSM (which consists of just one individual surface). **(D–F)** Result of the optimization of the position and shape parameters in red. The result of the original manual segmentation is shown in blue. The result of the automatic segmentation process using a leave-one-out test is shown in green. (From Singer, 2008). See also S5 movie in supplementary material.

Cell_Part only consider neurons and *Organ* and *Organ_Part* only consider neuropils of the bee brain. We further restrict our relations to describe spatial, morphological and, if available, connectional properties. **Table 1** lists the most important relations used in our bee brain ontology. **Figure 9** shows a scheme of how classes, instances and relations are connected using the Pe1 neuron as an example (see also **Figures 2 and 4**). The editor Protégé was used to create the ontology. Currently, the ontology contains 100 classes attached to 600 instances, and 1300 relations of 17 types. Integrated are several neuron types including the location representation of their somata, axons, and dendrites. This ontology has been linked to the reconstructions of the HSB by assigning the reconstructions' ID and file name to appropriate instances of the ontology. This step enables ontology-based browsing of the atlas (Kuß et al., 2008, 2009).

In a first usage approach of the ontology-linked HSB, we addressed the automatic creation of meaningful visualizations. Good visualizations transport a large amount of information and form an important communication medium. This information can be used to present research results, to communicate with research partners or to teach neurobiology. Often the process of creating such meaningful and expressive visualizations is time-consuming and requires sound knowledge of the visualization software used. In our approach, the user only selects a structure to be visualized and a predefined query, such as "Show overview". Then, an algorithm automatically creates a visualization that contains the selected structure highlighted as a focus object and further structures forming the context. This works as follows: Each predefined query owns a set of relation types considered to be relevant. Starting at the selection, the algorithm then looks within the ontology for other structures in the vicinity of the selection that may be of interest for the desired visualization. Only structures connected via a relation type relevant to the query are of interest.

DISCUSSION

The motivation for creating a digital atlas of the bee brain originated from the experience that a large amount of information is lost when single, intracellularly marked neurons are drawn on paper traced in camera lucida projections or just photographed. Neurons are three-dimensional entities embedded in a network of other neurons, and it is this information that is required in the future to interpret functional properties of neurons and neural networks in relation to their structure and connectivity (Abel et al., 2001; Müller et al., 2002; Krofczik et al., 2008). Insect brains are small enough to be scanned fully with confocal microscopy at a reasonable resolution. Therefore, no border problem appears, or at least it is reduced to the spatially limited connections with the ventral chord. Furthermore, many neurons in the insect brain are individually identifiable, and quite a number of them have already been identified (e.g. Hammer, 1993; Mauelshagen, 1993; Menzel, 2001; Heinze and Homberg, 2008; Homberg, 2008; see also this issue). Often neural tracts or compositions of local neurons consist of a few hundred neurons allowing for the possibility that in the not too distant future all neurons of a particular neuropil or part of the brain will be described in their morphology. In that case one would need this "description" in a digital 3D format so that the full power of mass data computation can be applied to visualize zoom

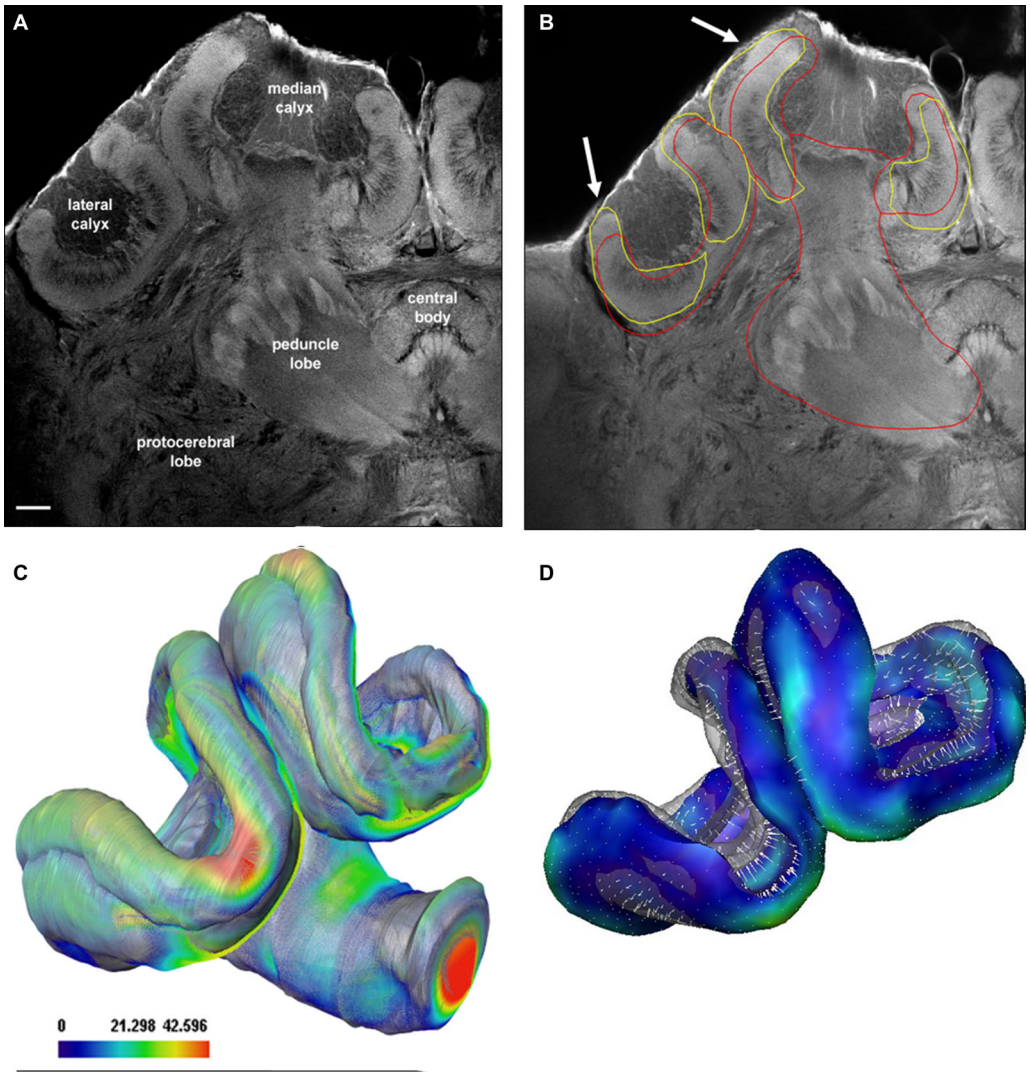

FIGURE 7 | Evaluation of the auto-segmentation process using a reduced shape model for confocal imaging data. (A) Confocal Lucifer yellow image of the median and left brain hemisphere scanned with a 20× oil objective. **(B)** Result of the automatic segmentation process. Arrows indicate refinement of automatic segmentation using isolated neuropils: yellow lines when only the calyx was used, red line when the whole mushroom bodies were used. **(C, D)** Surface representations of shape differences between manually (transparent) and automatically segmented (solid) labels. The mean surface distance of the manually segmented and the automatically segmented surface is 11 µm using the mushroom body model of the SSM as compared to 10.5 µm using the calyx model. Scale bar in **(C):** surface distance in µm.

determine potential connectivity patterns, to derive quantitative measures of distances, diameters, branching patterns, potential synaptic sites, and relate structures to functional components such as distribution of transmitters, receptors, channels, and intracellular molecules. At the moment we are far from getting even close to these goals, but important groundwork has been done, and one can hope that the time-consuming (and tedious) steps towards reaching these goals, such as manual segmentation, correction of errors, complicated procedures during registration, neuron tracing, (see Maye et al., 2006) will soon be overcome or become less cumbersome (for an review on automated registration and neuron tracing methods, see Peng, 2008). Apart from the aesthetic pleasure one experiences in visualizing single neurons and their compositions within the 3D atlas, right now the reward gained from creating the brain atlas and filling it with useful information is limited to understanding the spatial relationship. But this will soon change, because the information stored in the framework of the atlas will allow us to pose new questions, to discover novel patterns of neural connections, to assemble and organize large amounts of information, and to relate function to structure as proposed by us as well as other authors (e.g. Namiki and Kanzaki, 2008; Staudacher et al., 2009).

We began our project by creating an average atlas from 20 bee brains whose 22 neuropils were segmented manually and then used for the averaging process. The composition of these neuropils made it possible to calculate rigid and elastic transformations that provided enough information for faithful registration of neurons. The average-shape property ensures that the deformation applied

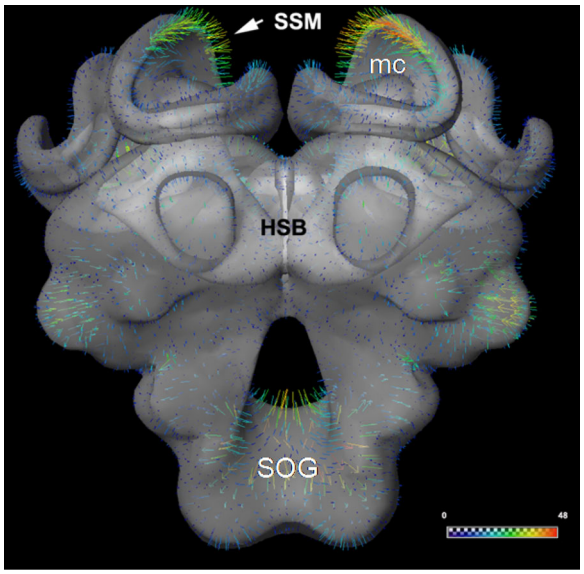

FIGURE 8 | A comparison of the iterative average shape brain (HSB) and the statistical shape model (SSM). The mean surface distance measured after rigid registration of HSB onto the SSM amounts to 8.5 µm. Only the surface model of the HSB is shown here, and the surface distances between HSB and SSM are indicated by colored vectors (arrow and false-color scale bar). Note the particularly large distance at the median calyx (MC) and subesophageal ganglion (SOG), which might be due to the stronger shrinkage process caused by the different histological procedures employed for the two models (see section "Methods" and text).

to the individuals remains small. Furthermore, manual segmentation as applied in our first approach is subject to noise, i.e., contouring between slices varies according to criterion variability of the experimenter. Averaging several such noisy label images reduces random parts of the contours, thus increasing the reliability of the standard. We have shown (Rohlfing et al., 2001; Brandt et al., 2005) that the non-rigid registration is able to increase the distinctness of inner structures such as tracts and strata even though the algorithm does not "know" about those structures, because it is applied on the label images without interior structures. We deduced from our observations that registration fidelity is sufficient for the spatial scale level of the standard brain. This result also makes us optimistic that a non-rigid registration of neuropil boundaries to the standard yields a reliable and reasonably accurate estimate of the "true" position of a co-stained neuron within the standard.

As pointed out above, it is not easy to evaluate how accurate the registrations of neurons are using the average neuropil borders as guiding posts. When a neuron runs close to the border of a neuropil used for registration a small deviation from its relative position becomes very important, that is the neuron lies either inside or outside the particular neuropil. We have observed these inaccuracies, and they can be corrected by repeating the segmentation and registration processes (see section **"Registration protocol"** of supplementary material). Preparation artifacts due to dissecting of the specimen and histological processing can lead to distortion effects that are only partly corrected by the registration algorithm. Further inaccuracies are due to surface reconstruction (smoothing) from segmented label fields, and to cropping of areas of interest. For the latter the edges of cut regions are not well defined for the individual brain and the standard reference and are therefore difficult to operate for the registration algorithm (Maye et al., 2006).

The question of whether two close neurons are potentially in synaptic contact is much more difficult to answer and may well be beyond the scope of the registration process. Double markings in the same brain combined with electron microscopy will also be necessary in the future to prove such contacts, but the registration process already provides conclusive evidence that will either provide the motivation to start such a demanding project or forsake it altogether (e.g., Hohensee et al., 2008; Meseke et al., 2009). We provided one example to document that registered neurons are so precisely embedded in the histology of high-resolution light microscopy cross sections (**Figure 3**) that one may well conclude that their location relative to surrounding neurons is down to the precision of a few microns. In a similar approach single-cell labeling was used in combination with non-rigid registration techniques to estimate the synaptic density and spatial relationship of *Drosophila* olfactory interneurons (projection neurons) in central brain areas (Jefferis, 2007). Using intensity-based image registration for averaging the brains, they estimated the accuracy of registration up to a few microns. Greater accuracy might not be possible because the protocols always depend on neurons from different brains, and the variance of neuron Gestalt from brain to brain will limit the resolution.

A general problem with neuron reconstructions relates to the fact that high-resolution imaging microscopy requires lenses whose working distance is often not large enough to cover the whole dendritic tree of the respective neuron, whereas low resolution images are necessary to connect parts of the same neuron or different neurons. Physical sections, e.g., vibrotome offer a solution to this problem, but consecutive sections need to be aligned such that the neuron can be fully reconstructed and registered into the atlas (el Jundi et al., 2009, 2010).

So far we have registered 50 neurons into the HSB, a small proportion indeed of the approximately 950000 neurons of the bee brain (Witthöft, 1967). However, even this small number calls for more sophisticated means of visualization, selection of combinations of neurons and ways of highlighting particular properties of the network arising from these neurons (potential contacts, estimated information flow, combination with data from, for example, immunocytochemistry and electron microscopy, electrophysiology, and Ca-imaging).

THE STATISTICAL SHAPE ATLAS

An atlas derived from an averaging process (as the HSB, **Figure 1**) contains a large amount of information about spatial relations of structures. It is highly suggestive to use this information for one of the most time-consuming, difficult and tedious steps, the segmentation process of the structures (neuropils) necessary for the registration of any individual brain. We took up this argument and implemented a procedure, a model-based auto-segmentation, originally developed for the analysis of shape variability and modeling of structures in medical imaging (Lamecker, 2008). This method was adapted and applied to

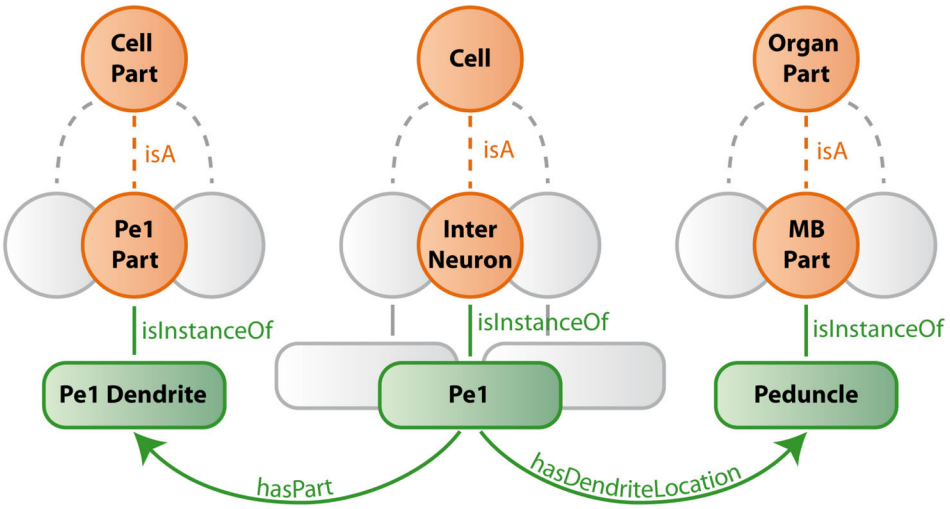

FIGURE 9 | Schematic description of bee brain ontology (with the Pe1 neuron as an example). Orange circles symbolize classes which represent summarizing concepts of structures with similar properties. Green rounded squares symbolize instances of classes which are connected by green edges (relations) to each other. Gray structures indicate that only a small selection is presented.

the central bee brain to generate a SSM (**Figure 5**) that reflects the shape variability of a restricted set of 16 bee brains. In combination with a displacement model (Kainmüller et al., 2007, 2009; Lamecker, 2008), based on evaluation of intensity gradients within the confocal images, the SSM allows automatic neuropil segmentation (**Figures 5–7**). Our approach was combined with alterations in the histological procedure. Lucifer yellow was used instead of synaptic antibodies as a neuropil background stain. Furthermore, only a selected part of the brain was used (the central brain excluding the antennal lobes). Lucifer yellow treatment during the histological procedure provides us with the same information as the antibody, but is faster and the results in more homogenously stained neuropils. The focus on the central brain allowed us to test the power of the approach for the most important and most complex structures of the bee brain, the mushroom bodies (**Figures 4 and 7**). An automatic procedure for segmenting neuropils provides the following additional advantages: (1). *A priori* knowledge about the 3D shape of the objects in question, in our case, the bee brain with its characteristic features of the image data. (2). Measures about the variability of the object set, and thus provides us with information which can be used to analyze and quantify any changes induced during development or on the basis of different genetic backgrounds (as described by Kurylas et al.,, 2008; el Jundi et al., 2010 for the VIB). (3). Information useful for across-species investigations in order to analyze evolutionary changes by comparative analysis of brain structures at least in closely related groups (e.g., hymenoptera, Gronenberg, 2001; beewolf, Rybak et al., 2003).

We found that SSM can well be used to detect neuropil borders in these preparations. Nevertheless there are deviations in the automatic segmentation process (see **Figure 7**). An analysis of the post-processing time by a segmentation expert shows that one still saves considerable time and gains accuracy (Rybak, personal observation).

A quantitative comparison of HSB and SSM (**Figure 8**) reveals that the volume of the HSB is smaller relative to the SSM. Stronger shrinkage of the HSB might be due to the prolonged incubation time required for the synaptic antibody procedure (1 week). Nevertheless, since shape differences in segmented brains by either the synaptic antibodies or the Lucifer yellow method seem to be small, it is reasonable to take segmented data used for the HSB and include it into the enlarged model of the SSM. Moreover, all imaging data used for the HSB were segmented by experts, thus providing very reliable definitions of the neuropil boundaries, and the quality of the SSM will be enhanced by adding the HSB dataset, since shape variability represented by the enlarged SSM will capture a higher number of histological procedures used for insect preparations (i.e., fixation, incubation of antibodies, use of fluorescent dyes).

One disadvantage of the current HSB is that it is closed to improvements and adaptations, which will certainly result from more appropriate histological procedures such as the shift from antibody staining of neuropil borders to easy-to-use fluorescent dyes. Working with the SSM will allow us to create a novel form of HSB that grows with each brain, and which adapts stepwise any morphological changes with histological procedures. Thus, enlarging the set of brains included in the SSM by already segmented brains used for the HSB and by developing more elaborated displacement algorithms based on intensity profile analysis will allow us to create such a new atlas based on many more brains, particularly in the context of different experiments (electrophysiology, immunocytochemistry, etc). Additionally, combining a shape atlas with proper registration techniques will allow us to use such an atlas, initially created to replace manual segmentation (for the label field registration of neurons). Once the deformation field that fits the SSM model to a confocal image is calculated it can be used to integrate the neuron into the average-shape atlas. Such an approach can forego and eventually replace the label field registration as in the current HSB.

ACKNOWLEDGMENTS

We thank Alvar Prönneke for his help in evaluating the SSM Vincent Dercksen for landmark registration and Dirk Drenske for help with the 3D-PDF. We are particularly grateful to Gisela Manz and Astrid Klawitter for help with the reconstructions. We would also like to thank Daniel Münch and Hiro Ai for providing data for **Figures 2 and 4**.

NOTE

An Interactive three-dimensional view of the Honeybee Standard Brain and integrated neurons for **Figures 1,2A and 4A** can be found in the 3D PDF file in the supplementary section. In order to utilises the 3D tools requires viewing with Adobe Acrobat Reader 8.0 or greater.

GLOSSARY

Labelfield There are two ways to represent segmentations of images: either boundaries are added to an image that enclose sets of pixels that are considered to belong together, or to pixels/voxels a label (a specific ID) is assigned that represents a particular object. In Amira the label field representation is used.

Ontology In the information sciences, an ontology is a formal representation of concepts or structures and relations among those structures in a defined application domain. They represent semantic information using a controlled vocabulary. Visually, ontologies can be described as graphs in which structures are presented by nodes and relationships between structures are represented by edges.

Registration The process of computing a coordinate transformation that maps the coordinates of one image onto the anatomically equivalent point in another image.

Segmentation Classification of regions (intensity values) within the image data and partition of homogenous regions. The use of a single threshold means binarization of the image, i.e., separation of background and structure of interest. Segmentation may separate many structures within the image (connected components or segments of the image).

Transformation Mathematical operation that moves, rotates, scales, and/or even deforms an object in such a way, that it will be aligned to another similar one.

Warping Reformatting of an image under a deformation given by a non-rigid coordinate transformation. This is also known as also elastic or free-form deformation.

Glossary on the Internet: http://en.wikipedia.org/wiki/Image_registration.
http://life.bio.sunysb.edu/morph/glossary/gloss1.html.
http://life.bio.sunysb.edu/morph/glossary/gloss2.html.

SUPPLEMENTARY MATERIAL

The Supplementary Material for this article can be found online at http://www.frontiersin.org/systemsneuroscience/paper/10.3389/fnsys.2010.00030/

SUPPLEMENT 1: COLORWASH HSB movies in wmv format

These movies show confocal images of the honeybee brain in frontal, horizontal and sagittal directions. Neuropils were stained with synaptic antibodies. The colored label fields of brain neuropils as defined for the Honey Bee Standard Brain (HSB, Brandt et al., 2005) are superimposed. Note that some neuropil areas that are not defined in the HSB are labeled. Abbreviations: AL: antennal lobe, a: alpha-lobe, b: beta-lobe, CB: central body, li: lip, co: collar, br: basal ring, Me: medulla, Lo: lobula, PL: protocerebral lobe, SOG: subesophageal ganglion. MC: median calyx, LC: lateral calyx. ot: optic tubercle,, pb: protocerebral bridge, DL: dorsal lobe, lac: lateral accessory lobe, pe: peduncle, lh: lateral horn.

SUPPLEMENT 2 pdf

Registration Protocol that describes the incorporation of neuronal morphologies into the Honeybee Standard brain (HSB).

SUPPLEMENT 3 movies in mpg format

a The spatial relationship of olfactory L3 neuron (blue), mechanosensory (DL and 2: green and red, respectively) and central interneuron Pe1 (yellow) after transformation to the Honeybee Standard Brain (HSB).
b the same movie in stereo mode

SUPPLEMENT 4 movie in wmv format

The Statistical Shape Model: Visualization of the central brain and morphological variations of the mushroom bodies and protocerebral neuropils (for more details: see text and Lienhard, 2008).

SUPPLEMENT 5 movie in wmv format

Displacement model: Positioning and Displacement of the central brain model in the image data. Reddish-white flickering indicates the deformation of the model during the adjustment of the SSM to the image data.

REFERENCES

Abel, R., Rybak, J., and Menzel, R. (2001). Structure and response patterns of olfactory interneurons in the honeybee, *Apis mellifera*. *J. Comp. Neurol.* 437, 363–383.

Ai, H., Rybak, J., Menzel, R., and Itoh, T. (2009). Response characteristics of vibration-sensitive interneurons related to Johnston's organ in the honeybee, *Apis mellifera*. *J. Comp. Neurol.* 515, 145–160.

Ashburner, J. (2000). *Computational Neuroanatomy*. Dissertation, University College, London.

Bota, M., and Swanson, L. W. (2008). BAMS neuroanatomical ontology: design and implementation. *Front. Neuroinformatics* 2, 2. doi:10.3389/neuro.11.002.2008/.

Brandt, R., Rohlfing, T., Rybak, J., Krofczik, S., Maye, A., Westerhoff, M., Hege, H. C., and Menzel, R. (2005). Three-dimensional average-shape atlas of the honeybee brain and its applications. *J. Comp. Neurol.* 492, 1–19.

Bucher, D., Scholz, M., Stetter, M., Obermayer, K., and Pflüger, H. J. (2000). Correction methods for three-dimensional reconstructions from confocal images. I. Tissue shrinking and axial scaling. *J. Neurosci. Methods* 100, 135–143.

el Jundi, B., Huetteroth, W., Kurylas, A. E., and Schachtner, J. (2009). Anisometric brain dimorphism revisited: implementation of a volumetric 3D standard brain in *Manduca sexta*. *J. Comp. Neurol.* 517, 210–225.

el Jundi, B., Heinze, S., Lenschow, C., Kurylas, A., Rohlfing, T., and Homberg, U. (2010). The locust standard brain: a 3D standard of the central complex as a platform for neural network analysis. *Front. Syst. Neurosci.* 3:21. doi: 10.3389/neuro.06.021.2009.

Evers, J. F., Schmitt, S., Sibila, M., and Duch, C. (2005). Progress in functional neuroanatomy: precise automatic geometric reconstruction of neuronal morphology from confocal image stacks. *J. Neurophysiol.* 93, 2331–2342.

Ganeshina, O., and Menzel, R. (2001). GABA-immunoreactive neurons in the mushroom bodies of the honeybee: an electron microscopic study. *J. Comp. Neurol.* 437, 335–349.

Gronenberg, W. (2001). Subdivisions of hymenopteran mushroom body

calyces by their afferent supply. *J. Comp. Neurol.* 435, 474–489.

Grünewald, B. (1999). Morphology of feedback neurons in the mushroom body of the honeybee, *Apis mellifera*. *J. Comp. Neurol.* 404, 114–126.

Guimond, A., Meunier, J., and Thirion, J. P. (2000). Average brain models: a convergence study. *Comput. Vis. Image Underst.* 77, 192–210.

Hammer, M. (1993). An identified neuron mediates the unconditioned stimulus in associative olfactory learning in honeybees. *Nature* 366, 59–63.

Heinze, S., and Homberg, U. (2008). Neuroarchitecture of the central complex of the desert locust: intrinsic and columnar neurons. *J. Comp. Neurol.* 511, 454–478.

Homberg, U. (2008). Evolution of the central complex in the arthropod brain and its association with the visual system. *Arthropod Struct. Dev.* 37, 347–362.

Hohensee, S., Bleiss, W., and Duch, C. (2008). Correlative electron and confocal microscopy assessment of synapse localization in the central nervous system of an insect. *J. Neurosci. Methods* 168, 64–70.

Jefferis, G. S., Potter, C. J., Chan, A. M., Marin, E. C., Rohlfing, T., Maurer, C. R., and Luo, L. (2007). Comprehensive maps of *Drosophila* higher olfactory centers: spatially segregated fruit and pheromone representation. *Cell* 128, 1187–1203.

Jenett, A., Schindelin, J. E., and Heisenberg, M. (2006). The virtual insect brain protocol: creating and comparing standardized neuroanatomy. *BMC Bioinformatics* 7, 544.

Kainmüller, D., Lange, T., and Lamecker, H. (2007). "Shape constrained automatic segmentation of the liver based on a heuristic intensity model," in *Proceeding MICCAI: 3D Segmentation in the Clinic: A Grand Challenge,* eds T. Heimann, M. Styner, and B. van Ginneken, 109–116.

Kainmüller, D., Lamecker, H., Seim, H., Zinser, and M., Zachow, S. (2009). "Automatic extraction of mandibular nerve and bone from cone-beam CT data," in *Medical Image Computing and Computer Assisted Intervention (MICCAI), Lecture Notes in Computer Science* Vol. 5762 (New York: Springer), 76–83.

Klagges, B. R. E., Heimbeck, G., Godenschwege, T. A., Hofbauer, A., Pflugfelder, G. O., Reifegerste, R., Reisch, D., Schaupp, M., Buchner, S., and Buchner, E. (1996). Invertebrate synapsins: a single gene codes for several isoforms in *Drosophila*. *J. Neurosci.* 16, 3154–3165.

Krofczik, S., Menzel, R., and Nawrot, M. P. (2008). Rapid odor processing in the honeybee antennal lobe network. *Front. Comput. Neurosci.* 2, 9. doi:10.3389/neuro.10.009.2008.

Kuß, A., Hege, H. C., Krofczik, S., and Börner, J. (2007). "Pipeline for the creation of surface-based averaged brain atlases," In *Proceedings of WSCG 2007 – the 15th International Conference in Central Europe on Computer Graphics, Visualization and Computer Vision, Vol. 15* (Plzen, Czech Republic), 17–24.

Kuß, A., Prohaska, S., Meyer, B., Rybak, J., and Hege, H. C. (2008). Ontology-based visualisation of hierarchical neuro-anatomical structures. *Proc. Vis. Comp. Biomed.*, eds. C. P. Botha et al., 177–184.

Kuß, A., Prohaska, S., and Rybak, J. (2009). Using ontologies for the visualization of hierarchical neuroanatomical structures. *Front. Neuroinformatics.* Conference Abstract: 2nd INCF Congress of Neuroinformatics. doi: 10.3389/conf.neuro.11.2009.08.017

Kurylas, A. E., Rohlfing, T., Krofczik, S., Jenett, A., and Homberg, U. (2008). Standardized atlas of the brain of the desert locust, *Schistocerca gregaria*. *Cell Tissue Res.* 333, 125–145.

Kvello, P., Løfaldli, B., Rybak, J., Menzel, R., and Mustaparta, H. (2009). Digital, three-dimensional average shaped atlas of the *Heliothis virescens* brain with integrated gustatory and olfactory neurons. *Front. Syst. Neurosci.* 3, 14. doi:10.3389/neuro.06.014.2009.

Lamecker, H. (2008). *Variational and Statistical Shape Modeling for 3D Geometry Reconstruction*. Ph.D. thesis, Publisher: Dr. Hut Verlag, ISBN 978-3-89963-878-3.

Lamecker, H., Lange, T., Seebass, M., Eulenstein, S., Westerhoff, M., and Hege, H. G. (2003). "Automatic segmentation of the liver for preoperative planning of resections," in *Proceedings of Medicine Meets Virtual Reality (MMVR)*, eds J. D. Westwood et al. Studies in Health Technologies and Informatics 94, 171–174.

Lamecker, H., Seebass, M, Hege, H. G., and Deuflhard, P. (2004). "A 3d statistical shape model of the pelvic bone for segmentation," in *Proceedings of SPIE – Medical Imaging: Image Processing,* eds J. M. Fitzpatrick and M. Sonka. Vol. 5370, 1341–1351.

Lienhard, M. (2008). *Aufbau und Analyse Eines Statistischen Formmodells des Gehirns der Honigbiene Apis mellifera*. BSc Free University of Berlin.

Mauelshagen, J. (1993). Neural correlates of olfactory learning in an identified neuron in the honey bee brain. *J. Neurophysiol.* 69, 609–625.

Maye, A., Wenckebach, T. H., and Hege, H.-C. (2006). Visualization, reconstruction, and integration of neuronal structures in digital brain atlases. *Int. J. Neurosci.* 116, 431–459.

Menzel, R. (2001). Searching for the memory trace in a mini-brain, the honeybee. *Learn. Mem.* 8, 53–62.

Meseke, M., Evers, J. E., and Duch, C. (2009). Developmental changes in dendritic shape and synapse location tune single-neuron computations to changing behavioral functions. *J. Neurophysiol.* 102, 41–58.

Müller, D., Abel, R., Brandt, R., Zöckler, M., and Menzel, R. (2002). Differential parallel processing of olfactory information in the honeybee, *Apis mellifera L. J. Comp. Physiol. A*, 188, 359–370.

Namiki, S., and Kanzaki, R. (2008). Reconstructing the population activity of olfactory output neurons that innervate identifiable processing units. *Front. Neural Circuits* 2, 1. doi: 10.3389/neuro.04.001.

Neubert, K. (2007). *Model-Based Autosegmentation of Brain Structures in the Honeybee, Apis mellifera*. BSc. Free University of Berlin.

Okada, R., Rybak, J., Manz, G., and Menzel, R. (2007). Learning-related plasticity in PE1 and other mushroom body-extrinsic neurons in the honeybee brain. *J. Neurosci.* 27, 11736–11747. doi: 10.1523/JNEUROSCI.2216-07.2007.

Peng, H. (2008). Bioimage informatics: a new area of engineering biology. *Bioinformatics* 24, 1827–1836.

Rein, K., Zöckler, M., Mader, M. T., Grübel, C., and Heisenberg, M. (2002). The drosophila standard brain. *Curr. Biol.* 12, 227–231.

Rohlfing, T., Brandt, R., Maurer, C. R. Jr., and Menzel, R. (2001). "Bee brains, B-splines and computational democracy: generating an average shape atlas," in *Proceedings of the IEEE Workshop on Mathematical Methods in Biomedical Image Analysis* (MMBIA, Kauai, Hawaii), 187–194.

Rohlfing, T., Brandt, R., Menzel, and C. R. Maurer, Jr. (2004). Evaluation of atlas selection strategies for atlas-based image segmentation with application to confocal microscopy images of bee brains. *NeuroImage* 21, 1428–1442.

Rosse, C., and Mejino, J. (2003). A reference ontology for bioinformatics: the foundational model of anatomy. *J. Biomed. Inform.* 36, 478–500.

Rybak, J. (1994). Die strukturelle Organisation der Pilzkörper und synaptische Konnektivität protocerebraler Interneuronen im Gehirn der Honigbiene, *Apis mellifera*. Eine licht- und elektronenmikroskopische Studie. Dissertation, Freie Universität Berlin, Berlin.

Rybak, J., Groh, C., Meyer, C., Strohm, E., and Tautz, J. (2003). "3-D reconstruction of the beewolf brain, *Philanthus triangulum F.*," in *Proceedings of the 29th Göttingen Neurobiology Conference*, eds N. Elsner and H. Zimmermann, 856.

Rybak, J., and Menzel, R. (1998). Integrative properties of the Pe1-neuron, a unique mushroom body output neuron. *Learn. Mem.* 5, 133–145.

Rybak, J., Kuss, A., Holler, W., Brandt, R., Hege, H. G., Nawrot, M., and Menzel, R. (2009). The honeybee standard brain HSB – a versatile atlas tool for integrating data and data exchange in the neuroscience community. Eighteenth Annual Computational Neuroscience Meeting: CNS*2009, Berlin, Germany. 18–23 July. *BMC Neurosci.* 10 (Suppl. 1), 1. doi: 10.1186/1471-2202-10-S1-P1.

Schäfer, S., and Bicker, G. (1986). Distribution of GABA-like immunoreactivity in the brain of the honeybee. *J. Comp. Neurol.* 246, 287–300.

Schmitt, S., Evers, J. F., Duch, C., Scholz, M., and Obermayer, K. (2004). New methods for the computer-assisted 3-d reconstruction of neurons from confocal image stacks. *Neuroimage* 23, 1283–1298.

Seim, H., Kainmüller, D., Heller, M., Kuß, A., Lamecker, H., Zachow, S., and Hege, H. G. (2008). Automatic segmentation of the pelvic bones from CT data based on a statistical shape model. *Eurographics Workshop on Visual Computing for Biomedicine (VCBM)* (Delft, Netherlands), 93–100.

Singer, J. (2008). *Entwicklung einer Anpassungsstrategie zur Autosegmentierung des Gehirns der Honigbiene Apis mellifera mittels eines statistischen Formmodells*. BSc. Free University of Berlin.

Singer, J., Lienhard, M., Seim, H., Kainmüller, D., Kuß, A., Lamecker, H., Zachow, S., Menzel, R., and Rybak, J. (2008). Model-based autosegmentation of the central brain of the honeybee, *Apis mellifera*, using active shape models. *Front. Neuroinform. Conference Abstract: Neuroinformatics.* doi: 10.3389/conf.neuro.11.2008.01.064.

Staudacher, E. M., Huetteroth, W., Schachtner, J., and Daly, K. C. (2009). A 4-dimensional representation of antennal lobe output based on an ensemble of characterized projection neurons. *J. Neurosci. Methods* 180, 208–223.

Toga, A. W., and Mazziotta, J. C. (Eds.). (2002). *Brain Mapping,* 2nd Edn. San Diego, CA: Academic Press.

Westerhoff (né Zöckler), M. (2003). *Visualization and Reconstruction of 3D Geometric Models from Neurobiological Confocal Microscope Scans*. Ph.D. thesis, Fachbereich Mathematik und Informatik, Free University of Berlin.

Wigglesworth, V. B. (1957). The use of osmium in the fixation and staining of tissues. *Proc. R. Soc. [Biol.]* 147, 185–199.

Witthöft, W. (1967). Absolute Anzahl und Verteilung der Zellen im Hirn der Honigbiene. *Z. Morphol*. Tiere 61, 160–184.

Weickert, J. (1997). "A review of nonlinear diffusion filtering," in *Scale-Space Theories in Computer Vision,* eds B. T. Haar Romeny, L. Florack, J. Koenderink, and M. Viergever. *Lecture Notes in Computer Science*, Vol. 1252, 3–28.

Conflict of Interest Statement: The authors declare that the research was conducted in the absence of any commercial or financial relationships that could be construed as a potential conflict of interest.

*Received: 11 December 2009; paper pending published: 13 January 2010; accepted: 16 June 2010; published online: 13 July 2010. Citation: Rybak J, Kuß A, Lamecker H, Zachow S, Hege H-C, Lienhard M, Singer J, Neubert K and Menzel R (2010) The digital bee brain: integrating and managing neurons in a common 3D reference system. Front. Syst. Neurosci. **4**:30. doi: 10.3389/fnsys.2010.00030*

frontiers in
SYSTEMS NEUROSCIENCE

ORIGINAL RESEARCH ARTICLE
published: 26 October 2009
doi: 10.3389/neuro.06.014.2009

Digital, three-dimensional average shaped atlas of the *Heliothis virescens* brain with integrated gustatory and olfactory neurons

Pål Kvello[1], Bjarte Bye Løfaldli[1], Jürgen Rybak[2], Randolf Menzel[2] and Hanna Mustaparta[1]*

[1] *Department of Biology, Norwegian University of Science and Technology, Trondheim, Norway*
[2] *Institut für Biologie-Neurobiologie, Freie Universität Berlin, Berlin, Germany*

Edited by:
Raphael Pinaud,
Rochester University, USA

Reviewed by:
Sylvia Anton,
Institut National de la Recherche Agronomique, France
Kevin Daly,
West Virginia University, USA
C. G. Galizia,
Universität Konstanz, Germany

Correspondence:
Hanna Mustaparta,
Department of Biology, Norwegian University of Science and Technology, Neuroscience Unit, MTFS, Olav Kyrres gt. 9, 7489 Trondheim, Norway.
e-mail: hanna.mustaparta@bio.ntnu.no

We use the moth *Heliothis virescens* as model organism for studying the neural network involved in chemosensory coding and learning. The constituent neurons are characterised by intracellular recordings combined with staining, resulting in a single neuron identified in each brain preparation. In order to spatially relate the neurons of different preparations a common brain framework was required. We here present an average shaped atlas of the moth brain. It is based on 11 female brain preparations, each stained with a fluorescent synaptic marker and scanned in confocal laser-scanning microscope. Brain neuropils of each preparation were manually reconstructed in the computer software Amira, followed by generating the atlas using the Iterative Shape Average Procedure. To demonstrate the application of the atlas we have registered two olfactory and two gustatory interneurons, as well as the axonal projections of gustatory receptor neurons into the atlas, visualising their spatial relationships. The olfactory interneurons, showing the typical morphology of inner-tract antennal lobe projection neurons, projected in the calyces of the mushroom body and laterally in the protocerebral lobe. The two gustatory interneurons, responding to sucrose and quinine respectively, projected in different areas of the brain. The wide projections of the quinine responding neuron included a lateral area adjacent to the projections of the olfactory interneurons. The sucrose responding neuron was confined to the suboesophageal ganglion with dendritic arborisations overlapping the axonal projections of the gustatory receptor neurons on the proboscis. By serving as a tool for the integration of neurons, the atlas offers visual access to the spatial relationship between the neurons in three dimensions, and thus facilitates the study of neuronal networks in the *Heliothis virescens* brain. The moth standard brain is accessible at http://www.ntnu.no/biolog/english/neuroscience/brain

Keywords: insect, taste, olfaction, neuron, three-dimensional reconstruction

INTRODUCTION

Challenged by the need to integrate the rapidly growing data in neuroscience, digital brain atlases have become an important tool serving as a database for neural structures with their three dimensional spatial information. The intention is to provide common frameworks into which data from different brain preparations can be registered and spatially related. As the scientific record includes data from many animal species, digital brain atlases of several vertebrates and invertebrates have been made (Toga and Thompson, 2001; Rein et al., 2002; Toga, 2002; Van Essen, 2002; Brandt et al., 2005; Kurylas et al., 2008; Jundi et al., 2009). In insects, three dimensional digital brain atlases have been generated for four species; the population-based quantitative atlas of the fruit fly *Drosophila melanogaster* (Rein et al., 2002), the average shaped standard atlas of the honeybee *Apis mellifera* (Brandt et al., 2005) and the locust *Schistocerca gregaria* (Kurylas et al., 2008), and the recently made standard brain atlas of the hawkmoth *Manduca sexta* (Jundi et al., 2009). In creating the locust brain atlas two procedures were used for comparison, the Virtual Insect Brain (VIB) procedure initially developed for standardisation of the fruit fly neuroanatomy (Jenett et al., 2006) and the Iterative Shape Averaging (ISA) procedure developed to generate the honeybee standard brain (Rohlfing et al., 2001; Brandt et al., 2005). This study concluded that the VIB procedure using a global and a local rigid transformation followed by a local nonrigid transformation preserves anatomical variability, whereas the ISA procedure using an affine transformation followed by iterative nonrigid registrations reduces the variability.

The digital brain atlases of these four insects are based on common neuropil substrates like the protocerebrum including the optic lobes, the central body and the mushroom bodies, the deutocerebrum with the antennal lobes, and the tritocerebrum. Additional structures included in two or three of the atlases are the protocerebral bridge, anterior optic tubercles, lateral horns and the suboesophageal ganglion, the latter fused with the brain in the fly, the honeybee and the moth. These structures are involved in visual, olfactory and gustatory information processing as well as associative learning and memory formation. They are linked by neurons mediating information from one structure to the next where the information is further processed, thus forming networks within and between the different brain structures. In order to

understand how the neuronal networks operate, it is critical to clarify the connectivity between physiologically and morphologically characterised neurons in the circuits. Revealing such details is a very elaborate process requiring a preparation accessible for *in vivo* recordings of identifiable neurons. Particularly suited for these examinations are the insects. Their nervous system is easily accessible for intracellular electrophysiological recordings. Combined with staining the entire morphology of the neurons can be precisely determined and three dimensionally visualised in the individual brain. In addition the brain is small enough to be studied as a whole, avoiding the problem of cutting neurons projecting out of a section. The number of identified neurons is large and growing, like neurons of the visual system in the fly *Calliphora vicina* and the locust *Schistocerca gragaria* (Borst and Haag, 2002; Heinze and Homberg, 2007), the olfactory system in a number of species (Kanzaki et al., 1989; Heinbockel et al., 1999; Lei et al., 2001; Müller et al., 2002; Reisenman et al., 2005; Rø et al., 2007; Yamagata et al., 2007) auditory system of the crickets (Poulet and Hedwig, 2006) the mushroom bodies in the honeybee (Mauelshagen, 1993; Rybak and Menzel, 1998) as well as neuromodulatory neurons and descending neurons (Kanzaki et al., 1991; Hammer, 1993; Bräunig and Pflüger, 2001). Consequently the need for a standardized brain model as a tool for organizing and analyzing data has been substantial in many species. In addition to the three dimentional digital standard atlases providing common frames for integrating neurons in the entire brain, separate atlases of the antennal lobes have been made in a number of species, including heliothine moths (Rospars and Chambille, 1981; Flanagan and Mercer, 1989; Stocker et al., 1990; Galizia et al., 1999; Laissue et al., 1999; Rospars and Hildebrand, 2000; Chiang et al., 2001; Berg et al., 2002; Sadek et al., 2002; Reischig and Stengl, 2002; Smid et al., 2003; Greiner et al., 2004; Huetteroth and Schachtner, 2005; Masante-Roca et al., 2005; Skiri et al., 2005a; Iyengar et al., 2006; Jefferis et al., 2007). These atlases are valuable tools for studying the neuronal network involved in processing olfactory information (Namiki and Kanzaki, 2008; Staudacher et al., 2009).

The moth, *Heliothis virescens*, is a major pest insect in agriculture and an object for extensive research in many areas, including chemosensory coding, learning and memory (Hartlieb, 1996; Mustaparta, 2002; Skiri et al., 2005b; Jørgensen et al., 2006, 2007a,b; Kvello et al., 2006). The generation of a standard brain atlas of *H. virescens* is particularly motivated by the already large amount of data on the olfactory and the gustatory system. Tuning of olfactory receptor neurons according to biologically relevant odorants, pheromones as well as plant odorants have been described (Berg et al., 1998; Mustaparta and Stranden, 2005; Røstelien et al., 2005). Projections of the primary axons in particular glomeruli of the antennal lobe are shown for the pheromone system by functional tracing (Berg et al., 1998). Antennal lobe projection neurons have been anatomically described according to glomerular innervation and axonal tracts (Rø et al., 2007), studies that are being followed up in ongoing investigations focusing on the physiology of morphologically characterised neurons.

Whereas the central olfactory pathways have been described in this as well as in many insect species, only scarce knowledge exists about the central gustatory pathways in two insect species, the fly *Sarcophaga bullata* (Mitchell and Itagaki, 1992) and in the locust *Locusta migratoria* (Rogers and Newland, 2003). *H. virescens* is emerging as one of few model insects in elucidating the gustatory pathways. The axonal projections of the gustatory receptor neurons have been traced to defined areas of the suboesophageal ganglion and tritocerebrum (Jørgensen et al., 2006; Kvello et al., 2006), and intracellular recordings combined with staining of individual gustatory neurons in the CNS have been made from a large number of neurons (unpublished). Particularly interesting is the connection between the gustatory and the olfactory systems which forms the neuronal basis for associative learning of odorants and tastants. In order to integrate the existing and future data, as well as to spatially relate neurons of any brain compartment, a common framework of the entire *H. virescens* brain is needed. Using standard brain atlases to integrate identified neurons of different preparations offers easy visual access to the relative position of the neurons in three dimensions and thus promotes an understanding of their functional relationship. Therefore, in the search for neuronal networks in any animal species, a standard brain atlas is a valuable tool.

In this paper we present a digital standard brain atlas of the moth *Heliothis virescens*. Since the purpose is to relate spatial information between different preparations it is important to minimize individual variability. We therefore chose to generate the standard brain using the ISA procedure. To demonstrate its application we have registered two olfactory and two gustatory interneurons, as well as the axonal projections of the gustatory receptor neurons on the antennae and proboscis into the model using the procedure described by Brandt et al. (2005). The presented average standard brain atlas of this moth will be used as a tool for investigating and visualising the neural networks underlying gustatory and olfactory coding as well as appetitive and aversive learning and memory formation. The moth standard brain is accessible at http://www.ntnu.no/biolog/english/neuroscience/brain

MATERIALS AND METHODS

INSECTS

The moths, *Heliothis virescens* (Heliothinae; Lepidoptera; Noctuidae) were imported as pupae from a laboratory culture at Novartis Crop Protection, Basel, Switzerland. Before emerging the pupae were separated according to sex and placed in a glass container (height: 18 cm, width: 12 cm, depth: 17 cm) covered by a perforated plexiglass. The container with pupae was kept in a Refritherm 6 E incubator (Struers) at a reversed photoperiod (14-h light and 10-h dark) and at a temperature of 22–23°C. When emerged, the adults were placed into a plexiglass cylinder (height: 20 cm, diameter: 10 cm) covered by a perforated lid. The moths were fed *ad. lib.* on a 0.15 M sucrose solution. Experiments were performed on adult female moths 3- to 5-days after emerging.

THE STANDARD BRAIN

Preparations

Female moths were mounted in plastic tubes with the head immobilized by dental wax (Kerr Corporation, Romulus, MI, USA). After removing cephalic scales and mouthparts, the moths were decapitated. The brains were dissected in Ringer solution and fixed in 4% paraformaldehyde in a phosphate-buffered saline (PBS: 684 mM NaCl, 13 mM KCl, 50.7 mM Na2HPO4 and 5 mM

KH2PO4, pH 7.2) over night at 4°C. After a 10-min rinse in PBS, preparations were dehydrated in an increasing ethanol series (50%, 70%, 90%, 96%, 100%, 10 min each), degreased in xylol for 5 min, and rehydrated in a decreasing ethanol series (100%, 96%, 90%, 70%, 50%, 10 min each). The brains were then washed for 10 min in PBS, and incubated for 30 min in 1 mg/ml collagenase solution (Collagenase Type I, Invitrogen Norge AS) at 36°C. Subsequently the brains were preincubated in 10% normal goat serum (NGS; Sigma, St. Louis, MO, USA) in a PBS solution containing 0.1% Triton X (PBSX) for 30 min at room temperature. The brains were further incubated with a monoclonal antibody against the synaptic protein synapsin (SYNORF 1, kindly provided by Dr. E. Buchner, Würzburg, Germany), diluted 1:10 in PBSX and 10% NGS for 48 h at 4°C. After the preparations had been rinsed five times each for 20 min in PBS, they were incubated for 24 h with a Cy5-conjungated goat anti-mouse secondary antibody (Jackson Immunoresearch; dilution 1:500 in PBSX) at 4°C. The incubation was followed by rinsing in PBS, five times for 20 min, before the brains were dehydrated in increasing ethanol series. Finally the brains were cleared in methyl salicylate and mounted as whole mounts in double-sided aluminium slides.

Visualization of brain preparations

The stained whole-mount brain preparations were visualized with a laser-scanning confocal microscope (LSM 510 META Zeiss, Jena, Germany) using a C-Apochromat 10×/0.45NA water objective. The fluorescent dye (Cy5) was exited by a 633 nm line of argon laser. Due to the large size of the brain, each preparation was scanned in two partially overlapping tiles with a resolution of 1024 × 1024 pixels in the xy-plane and an interslice distance of 3 µm (voxel size of 0.75 µm × 0.75 µm × 3 µm). The resulting two stacks of optical sections per brain were resampled in order to make the size of the files manageable for the computer, then merged and filtered by the computer software Amira 4.1 (Mercury Computer Systems, San Diego, CA, USA). To compensate for the refraction indexes of the mountant and that of the water objective, the *z*-axis dimension was multiplied by a factor of 1.3. The final voxel size of each stack consequently increased to 1.1 µm × 1.1 µm × 3.9 µm.

Reconstruction of brain structures

The gray value image stacks acquired from the confocal microscope were elaborately examined section by section and brain structures of interest were manually labelled using the segmentation editor in Amira (**Table 1**). In this process any group of voxels belonging to a particular brain structure was given a unique label resulting in a stack of label images corresponding to the underlying confocal images. As a prerequisite to the subsequent registration and averaging process corresponding structures of the different brain preparations were given the same label. These label images were subsequently used to perform conventional volumetric analyzes, to reconstruct polygonal surface models and to generate the average standard brain atlas. The volume of each labelled structure was calculated by the "TissueStatistics" tool in Amira 4.1. Other conventional volumetric analyses, like mean volume, relative volume, standard deviations and relative standard deviation, were performed using Microsoft office Excel (2003).

Averaging brain structures

Creating the average standard brain followed the ISA method according to the description for the honeybee *Apis mellifera* and the locust *Schistocerca gregaria* (Rohlfing et al., 2001; Brandt et al., 2005; Kurylas et al., 2008). One brain was first selected as a template. Then the label images of the other brain preparations were affine registered to the label images of the template brain followed by making an average. Then the affine registered brain preparations and the template were elastically registered to the average followed by the generation of a second average. This was repeated by a second elastic registration of the previous elastic registered preparations to the

Table 1 | Volumetric analysis of the 16 reconstructed brain structures included in the standard brain atlas. Calculations for the medulla, lobula and lobula plate are based on 10 brains, whereas the remaining structures are based on 11. Mean volume (Mean V), relative volume (Rel. V), standard deviation (SD) and relative standard deviation (Rel. SD).

Structure	Mean *V* (µm³)	Rel. *V* (%)	SD (µm³)	Rel. SD (%)
Right antennal lobe	4.34×10^6	2.95	4.95×10^5	11.37
Left antennal lobe	4.31×10^6	2.92	5.15×10^5	11.96
Central body	1.69×10^6	1.14	3.05×10^5	18.07
Right calyx	2.38×10^6	1.61	3.15×10^5	13.22
Left calyx	2.38×10^6	1.61	3.24×10^5	13.61
Right peduncle and lobe	1.41×10^6	0.96	4.34×10^5	30.76
Left peduncle and lobe	1.34×10^6	0.91	3.89×10^5	28.93
Right anterior optic tubercle	4.98×10^5	0.34	1.26×10^5	25.37
Left anterior optic tubercle	5.00×10^5	0.34	1.24×10^5	24.77
Midbrain region	9.31×10^7	63.12	1.52×10^7	16.32
Right medulla	1.30×10^7	8.79	1.07×10^6	8.24
Left medulla	1.27×10^7	8.63	1.05×10^6	8.26
Right lobula	3.61×10^6	2.44	2.52×10^5	6.98
Left lobula	3.40×10^6	2.30	3.34×10^5	9.82
Right lobula plate	1.47×10^6	1.00	2.83×10^5	19.23
Left lobula plate	1.38×10^6	0.94	3.22×10^5	23.33

second average brain. Thus, the affine registration compensating for position, rotation and global size differences was performed only once whereas the elastic registration compensating for local differences in shape was performed twice. To verify the average shape property of the ISA-generated standard brain atlas, three dimentional polygonal surface models of the standard brain and each individual brain were made. They were subsequently aligned with respect to position, orientation and size before the shape differences between them were calculated. The calculations were performed using the surface distance tool in Amira 4.1 which measured the average distance between corresponding points on the surface of the different brain preparations.

INTERNEURONS

Preparation

The insects were mounted in a plastic tube with the head exposed. Wax was used to immobilize the head and the mouthparts. For recording from the olfactory neurons, the antennae were fastened to the wax with tungsten cramps. The cuticle between the eyes was removed, exposing the antennal lobes and the protocerebrum. Large trachea, intracranial- and antennal muscles were removed to eliminate brain movements. When recording from gustatory interneurons the antenna and the uncoiled proboscis were fastened to the wax with tungsten cramps. The labium was cut off and the underlying trachea removed. Subsequently the left eye was cut off and the preparation tilted in order to expose the left side of the SOG and tritocerebrum. To facilitate insertion of the microelectrode the neurolemma was removed with a tungsten hook and the preparation was superfused with ringer solution.

Stimulation, recordings and staining

The taste stimuli used in the experiments were sucrose (1 M, Sigma-Aldrich), quinine hydrochloride (0.1 M, VWR), distilled water, and tactile touch, previously found to elicit responses in separate receptor neurons (Jørgensen et al., 2007a). The stimuli were applied to the sensilla as droplets on a glass rod. The olfactory stimuli were applied as air puffs (0.8 ml/500 ms) through glass cartridges, each containing the odorants applied to a filter paper. The two neurons included were tested for 100 µg of each of 12 primary plant odorants (Hexanol, (3Z)-Hexen-1-ol, (3Z)-Hexenyl acetate, Ocimene, racemic- Linalool, Geraniol, (+)-3-Carene, trans-Verbenol, Methyl benzoate, 2-Phenylethanol, (-)-Germacrene D, Farnesene) (Røstelien et al., 2005). Neuronal activity in the antennal lobe and the SOG was recorded intracellularly with a glass microelectrode containing 0.2 M K^+-acetate solution with 4% dye (Micro-Ruby or Micro-Emerald, Invitrogen). After stimulation with tastants and odorants the neurons were stained by passing a 1–3 nA depolarizing current of 2 Hz with 0.2 s duration. Complete labelling of the neurons required dye injection for 5–10 min. After current injection, the dye was allowed to diffuse over night at 4°C. The brains were dissected in Ringer solution. The "olfactory" preparation was fixed in 4% paraformaldehyde in PBS similar to the standard brain preparations. The two "gustatory" preparations were also fixed in a solution of 4% paraformaldehyde in PBS, but additionally added 0.5% glutaraldehyde as an alternative and less time consuming way of visualizing neuropile structures. All three preparations were left over night at 4°C. To amplify the staining of the labelled neurons the brains were incubated in Streptavidin-Cy3 (Micro-Ruby stained preparations) and Streptavidin-Cy2 (Micro-Emerald stained preparations) (Jackson immunoresearch, West Grove, PA, USA; diluted 1:200 in PBS) over night at 4°C. After 10 min rinse in PBS the "olfactory" preparation went through the same protocol as the preparations used for the standard brain, starting with preincubation in 10% normal goat serum (NGS; Sigma, St. Louis, MO, USA) in a PBS solution containing 0.1% Triton X (PBSX) for 30 min at room temperature. Finally, all preparations were dehydrated in increasing ethanol series and cleared in methyl salicylate.

Visualization

The brains were mounted as whole mounts on double-sided aluminium slides and the stained neurons were examined with a confocal laser-scanning microscope (LSM 510 META, Zeiss, Jena, Germany) using a C-Apochromat 10×/0.45NA water objective, a C-Achroplan 40×/0.8NA water objective and a Plan-Neofluar 20×/0.5 dry lens objective. The two fluorescent dyes were exited by different lasers. Micro-emerald was excited by a Titanium Sapphire laser of 780 nm and a 488 nm argon laser, both filtered through a bandpass filter BP 500–550 IR. Micro-ruby was excited by a 543 nm Helium Neon laser and filtered through a bandpass filter BP 565–615 IR. The Titanium Sapphire laser was used for two-photon microscopy increasing the resolution in the *z*-axis which enabled us to better distinguish among overlapping neurites. The brains were scanned frontally with an interslice distance of 0.5–3 µm and an optical resolution in the *y*- and *x*-axis of 1024 × 1024 pixels. The neurons were scanned in several tiles and the tiles were manually merged in Amira. To compensate for the refraction indexes of the mountant and that of the water and dry lens objective, the *z*-axis dimension was multiplied by a factor of 1.3 and 1.6, respectively.

Reconstruction and registration of neurons into the average standard brain atlas

The gray value image stacks acquired from the confocal microscope were examined section by section and the neurons were semi-automatically reconstructed using the skeleton tool (Evers et al., 2004; Schmitt et al., 2004), which was implemented as a custom module in Amira 3.1. Registration of the neurons into the standard brain atlas followed the same procedure as described by Brandt et al. (2005). Selected brain structures in the "neuron-preparations" were reconstructed as label images. The selection only included brain structures corresponding to the structures in the standard brain atlas. Then, the label images in the "neuron-preparations" were affine- and elastically registered to the label images of the standard brain. The resulting transformation parameters for the brain structures were subsequently applied to the reconstructed neurons. The same procedure was followed for integrating the previously described gustatory receptor neurons (Jørgensen et al., 2006; Kvello et al., 2006).

RESULTS

RECONSTRUCTION

For creating the standard brain of the moth *Heliothis virescens* we selected the 11 best out of 72 female brain preparations. The selection was mainly based on the staining quality and the preservation

of brain structures. Brain neuropils with high synaptic density were clearly stained with the antibody SYNORF 1 against synapsin, as visualized in the confocal microscope images (**Figure 1**).

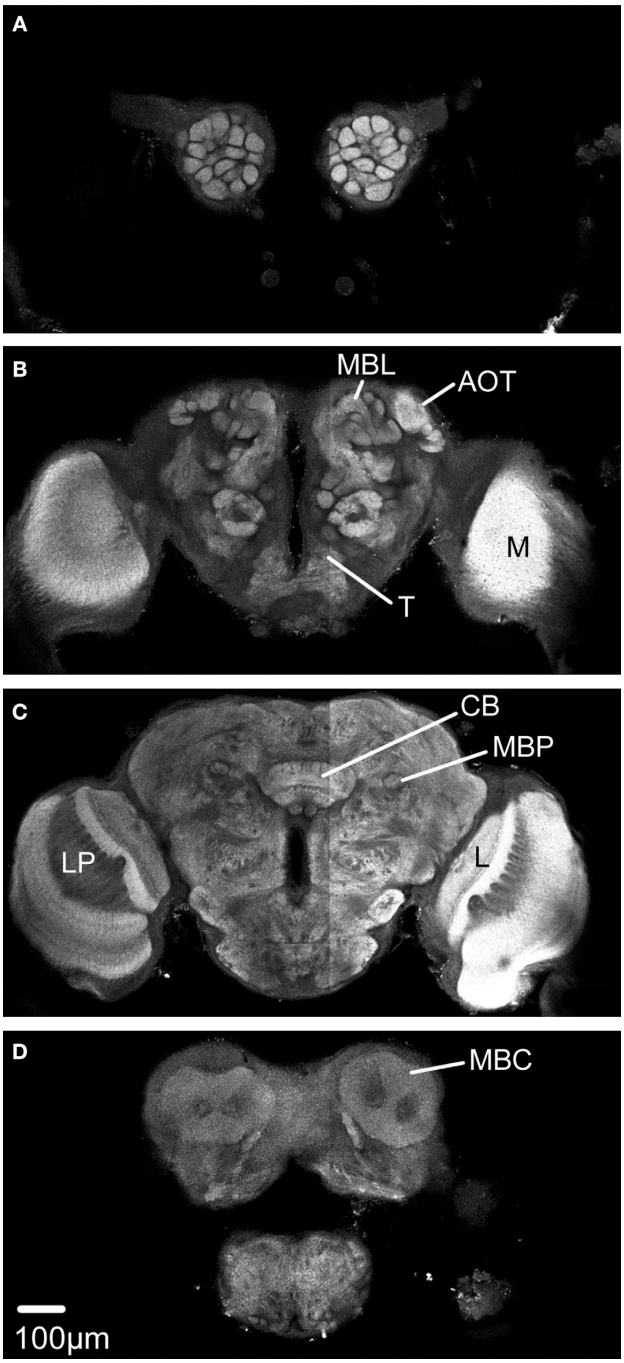

FIGURE 1 | Confocal images of the *Heliothis virescens* brain immunostained with the synaptic marker SYNORF 1. Sections from anterior to posterior at depths 30 µm, 100 µm, 162 µm and 246 µm. **(A)** Right and left antennal lobes with olfactory glomeruli. **(B–D)** Anterior optic tubercle (AOT), mushroom body lobes (MBL), tritocerebrum (T), central body (CB), medulla (M), lobula (L), Lobula plate (LP), mushroom body peduncle (MBP) and mushroom body calyces (MBC). Light intensity difference is due to merging of two image stacks with different light intensities.

Based on distinguishable structures, each of the 11 brain preparations was divided into 16 anatomical regions that were separately labelled (**Table 1**).

In one of the 11 preparations the optic lobes were excluded because of mechanical damage. However, the medial part of this brain was included because of its high staining quality. Because some neuropil structures could not be clearly distinguished in these whole mount preparations, they were included in a larger region. Thus, the region termed "Midbrain region" includes the protocerebral lobes with the lateral horns, the lateral accessory lobes, the protocerebral bridge and a small, previously not described structure located posterior to the antennal lobe glomeruli and merging into the protocerebrum. The midbrain region also includes the antennal mechanosensory and motor centre of the deutocerebrum, the tritocerebrum and the suboesophageal ganglion (SOG) (**Figures 2A,B**).

The calyces of the mushroom bodies could be clearly distinguished from the surrounding protocerebrum and labelled as one distinct structure (**Figures 2C,D**). The pedunculus and the lobe system of the mushroom bodies were difficult to completely separate and were therefore included as a single labelled region (**Figures 2E,F**). The central body and the anterior optic tubercles could be distinguished and were assigned to separate labels (**Figures 2G–J**). Among the lateral protocerebral structures comprising the optic lobes we included the medulla, the lobula and the lobula plate as separate labels (**Figures 2K,L**). Among the deutocerebral structures we have collectively assigned the antennal lobe glomeruli as one labelled region (**Figures 2M,N**). As a prerequisite to the subsequent registration process corresponding structures of the different preparations were given the same label. From the constructed label files a complete three dimensional surface reconstruction of one brain was made, shown in **Figure 3**.

Conventional volumetric analyzes including means and standard deviations of the absolute and relative volumes were performed on the label images of each anatomical region in all 11 brain preparations (**Table 1**).

AVERAGING

After constructing the label images of all 11 brain preparations one brain was selected as a template into which the other were registered and subsequently averaged. The selection of the template brain was based on staining quality and shape. Before starting the ISA procedure the label images were divided into three major compartments, the right optic lobe, the left optic lobe and the remaining medial brain structures. The registration and averaging procedures were subsequently performed separately on each compartment. The procedures were repeated according to the ISA method. The three average label image stacks resulting from the second elastic registration were selected as the standard brain. A three dimentional polygonal surface model of each major compartment was created (**Figure 4**).

To verify the average shape property of the standard brain which we defined as the brain shape being most similar to the 11 individual brains, we calculated the shape difference between them. The calculations were performed using the surface distance tool in Amira 4.1 which measured the mean distance between corresponding points on the surface of the different brain preparations.

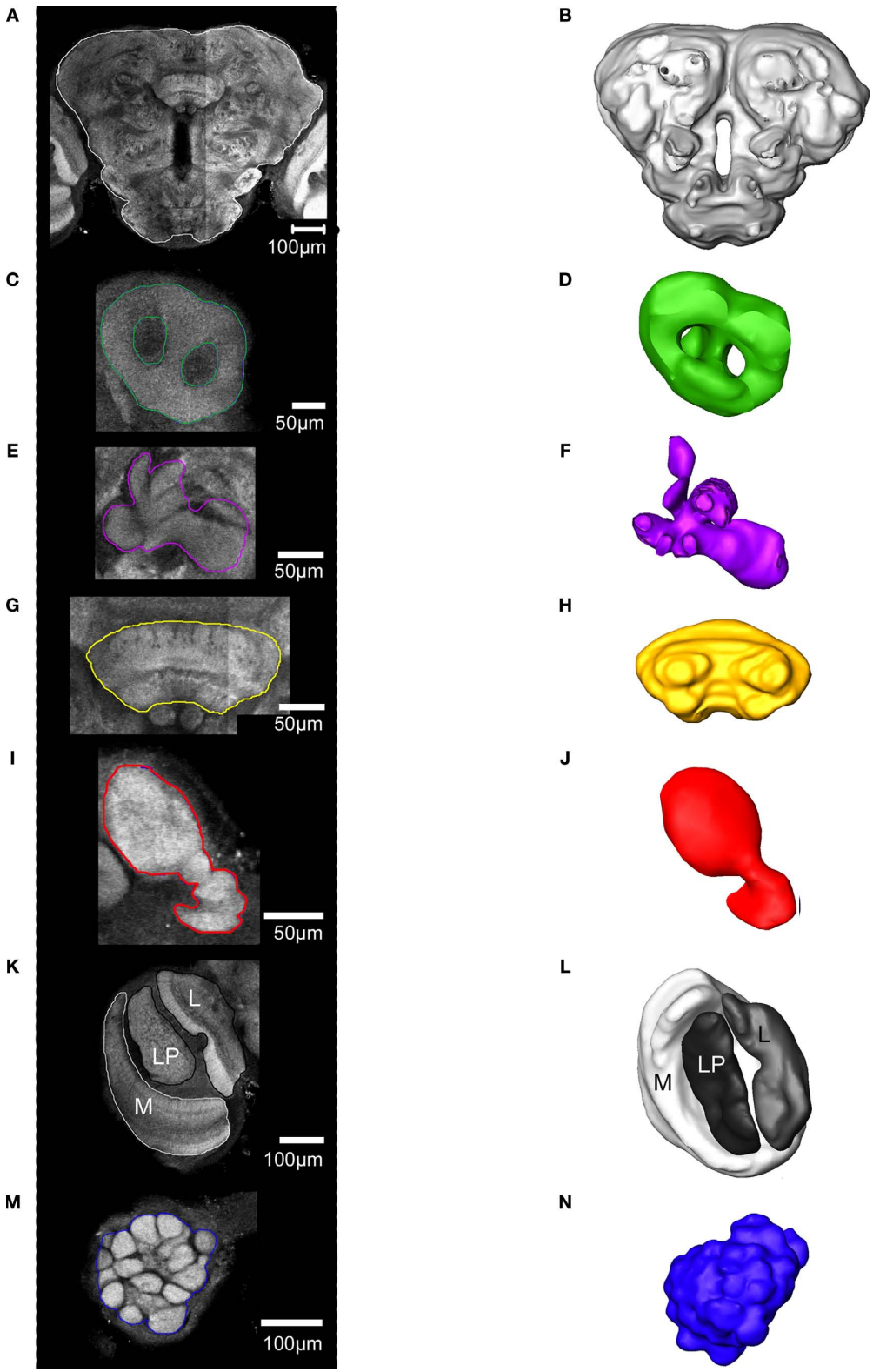

FIGURE 2 | The structures included in the *Heliothis virescens* standard brain atlas visualized by confocal images including their labelled outline (left) and surface reconstructions (right). The images are from a single brain preparation. **(A,B)** Midbrain region. **(C,D)** Mushroom body calyx. **(E,F)** Mushroom body peduncle and lobes. **(G,H)** Central body. **(I,J)** Anterior optic tubercle. **(K,L)** Optic lobe neuropils including the medulla (M), lobula plate (LP) and lobula (L). **(M,N)** Antennal lobe glomeruli. Light intensity difference is due to merging of two image stacks with different light intensities.

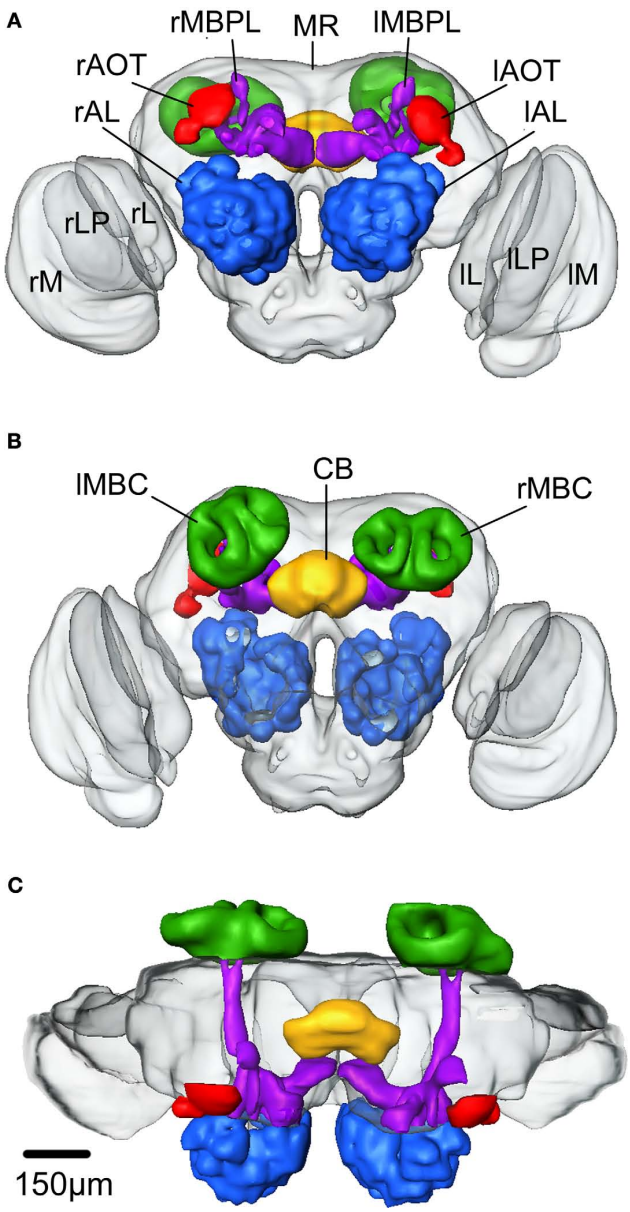

FIGURE 3 | Surface reconstruction of an individual brain of *Heliothis virescens*. (A) Anterior view. **(B)** Posterior view. **(C)** Dorsal view. Midbrain region (MR), right mushroom body calyces (rMBC), right mushroom body peduncle and lobes (rMBPL), central body (CB), right anterior optic tubercle (rAOT), right antennal lobe (rAL), right medulla (rM), right lobula plate (rLP), right lobula (rL), left mushroom body calyces (lMBC), left mushroom body peduncle and lobes (lMBPL), left anterior optic tubercle (lAOT), left antennal lobe (lAL), left medulla (lM), left lobula plate (lLP), left lobula (lL).

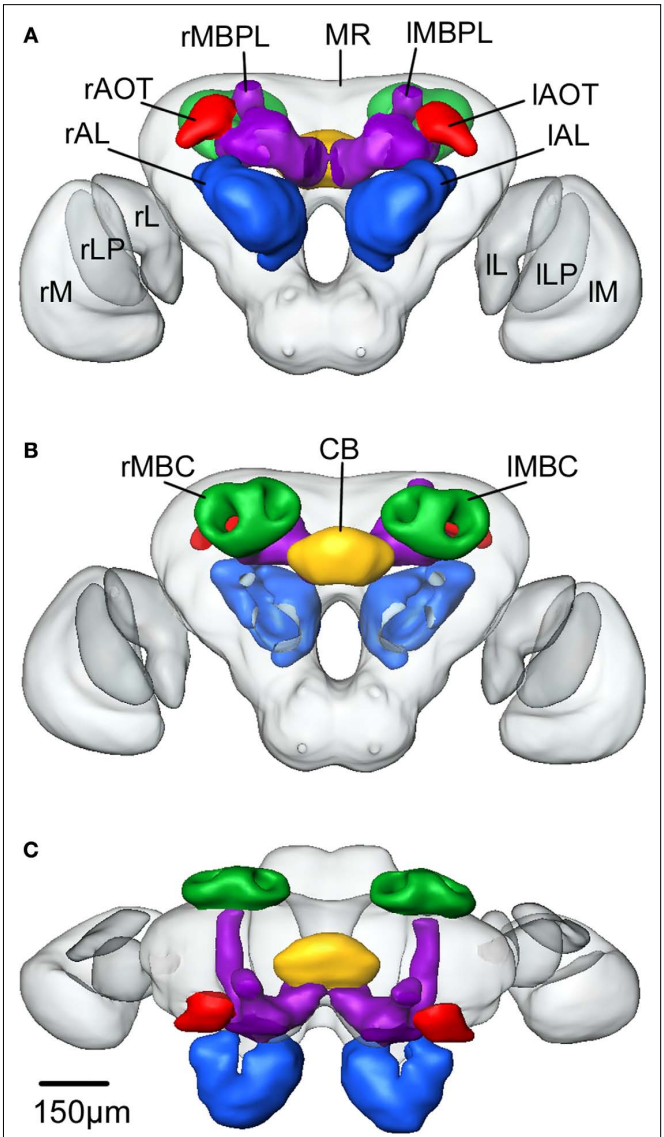

FIGURE 4 | The average standard brain of *Heliothis virescens*. (A) Anterior view. **(B)** Posterior view. **(C)** Dorsal view. Midbrain region (MR), right mushroom body calyces (rMBC), right mushroom body peduncle and lobes (rMBPL), central body (CB), right anterior optic tubercle (rAOT), right antennal lobe (rAL), right medulla (rM), right lobula plate (rLP), right lobula (rL), left mushroom body calyces (lMBC), left mushroom body peduncle and lobes (lMBPL), left anterior optic tubercle (lAOT), left antennal lobe (lAL), left medulla (lM), left lobula plate (lLP), left lobula (lL).

All the brains were compared with each other and with the standard after they had been aligned with respect to position, rotation and global size (rigid and iso-scaling transformations). The calculations were performed separately on each of the three major compartments (**Figure 5**).

As shown in **Figure 5**, on average the standard brain is a true average brain, fulfilling the average shape requirements for the standard brain atlas.

FITTING SINGLE NEURONS INTO THE STANDARD BRAIN ATLAS

To demonstrate the application of the average standard brain atlas we have registered four intracellularly recorded and stained interneurons into the model, two olfactory and two gustatory neurons. To visualize the gustatory input region we have also registered the previously described axonal projections of the antennal and the proboscis gustatory receptor neurons (Jørgensen et al., 2006; Kvello et al., 2006). The two olfactory interneurons were stained simultaneously during one recording, a phenomenon often observed for antennal lobe projection neurons. The olfactory function was manifested as exitation to several of the tested odorants in repeated

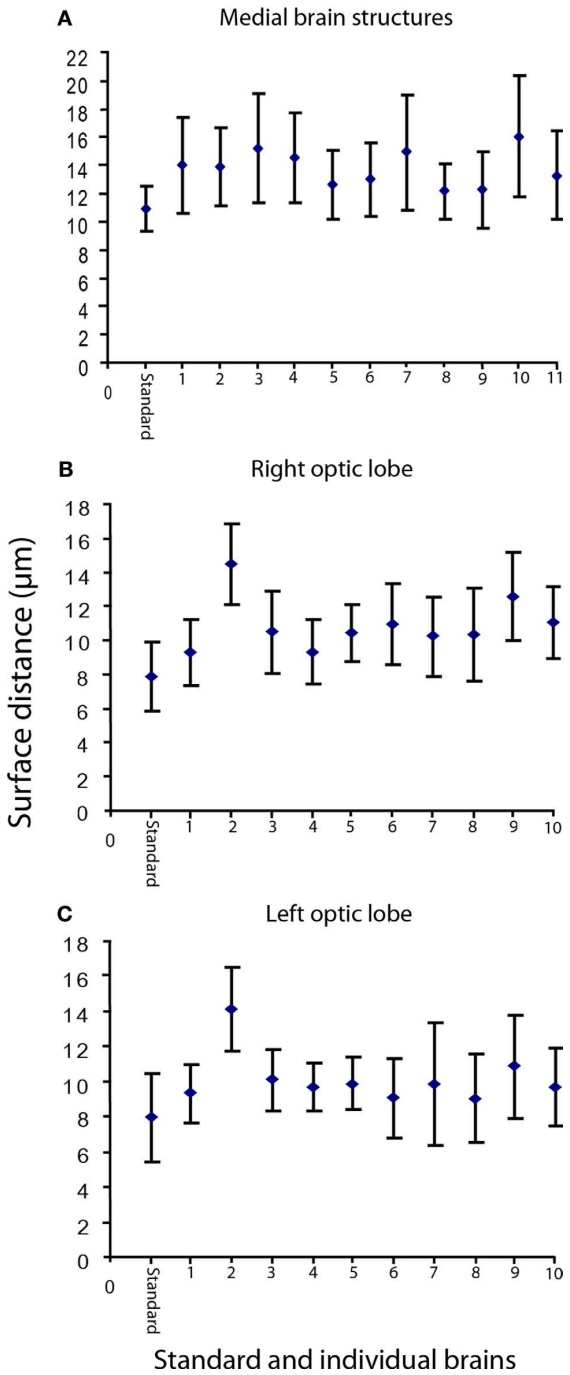

FIGURE 5 | The mean surface distance between the standard brain and the individual brains, as well as between each individual brain and the other brains. (A) The mean distance between the standard (the medial brain structures) and the 11 individual brains is 11.0 µm, whereas the mean distance between the individual brains range from 12.2 to 16.1 µm. **(B)** The right optic lobe. The mean distance between the standard and the 10 individual brains is 8.0 µm, whereas the mean distance between the individual brains range from 9.3 to 14.5 µm **(C)** The left optic lobe. The mean distance between the standard and the 10 individual brains is 8.0 µm, whereas the mean distance between the individual brains range from 9.1 to 14.2 µm. On average the standard brain is more similar to each individual brain than the individual brains are to each other. The vertical bars show the standard deviation.

stimulation. The axons closely followed each other all the way from the left antennal lobe to the calyces of the ipsilateral mushroom body and laterally in the protocerebral lobe (**Figure 6**).

The two neurons densely innervated the same glomerulus (**Figure 6A**), but no connections to the somata were identified. The axons followed the inner antenno-cerebral tract, each giving off four branches projecting in partially overlapping areas of the mushroom body calyces (**Figures 6B–D**). They continued anterior laterally in the protocerebral lobe, extending several branches into an area posterior dorsally of the lateral horn. One branch of both axons extended into the lateral horn (**Figures 6C,D**). The lateral area of the protocerebral lobes also received gustatory information, as shown by one neuron (**Figure 7A**).

This neuron was excited by quinine and tactile stimulation of the right antenna. The excitation was strongest to quinine appearing as two bursts, similar to the quinine responses of the receptor neurons (Jørgensen et al., 2007a). The response to sucrose stimulation did not exceed the mechanosensory response. The dendrites arborised in the dorsal SOG/tritocerebrum and the axon projected in wide areas of the protocerebral lobes. To elucidate whether the axonal projections of the gustatory- and the olfactory interneurons laterally in the protocerebral lobes are overlapping or separated, they were registered into the standard brain atlas (**Figures 7B–D**). The registration revealed two closely, but separated projection areas (smallest distance 34 µm); the gustatory area located anterior-ventrally to the olfactory area.

The other gustatory interneuron, with excitatory responses to repeated application of sucrose to the proboscis (latency: 47 ms), was confined to the SOG (**Figure 8**), the terminal area of the gustatory receptor neurons on the antennae and the proboscis.

The interneuron showed no response to sucrose stimulation of the antennae. The dendrites arborized extensively in the left, lateral SOG with branches extending from the anterior surface of the neuropil to the most posterior part (**Figures 8A–D**). The axon ran contra laterally in a medial commissure before bifurcating in one lateral and one ventral branch. Both branches turn in posterior direction ramifying extensively throughout the right, ventro lateral SOG, each ramification ending in a large beaded terminal. The soma was located dorso medially, close to the oesophagus (**Figure 8C**). To indicate possible connections between the gustatory receptor neurons and the interneuron, the antennal and the proboscis gustatory receptor neurons were registered into the standard brain atlas together with the interneuron. Overlap with the dendritic arborisations of the interneuron only occurred with the proboscis receptor neuron projections, as shown in **Figures 8C,D** by the single axon of category two described in Kvello et al. (2006). In fact, direct contact occurred between a few of the neurites. No overlap with the antennal gustatory receptor neurons was found.

DISCUSSION

The results present a digital, three dimensional average standard brain atlas of *Heliothis virescens*, based on brain preparations of 3- to 5-days-old females. Since the aim is to use this atlas as a common framework into which identified neurons of different brain preparations will be transformed, the important feature is a minimized difference between the standard model and any individual brain. Both from nature and experimental procedures, the individual brain

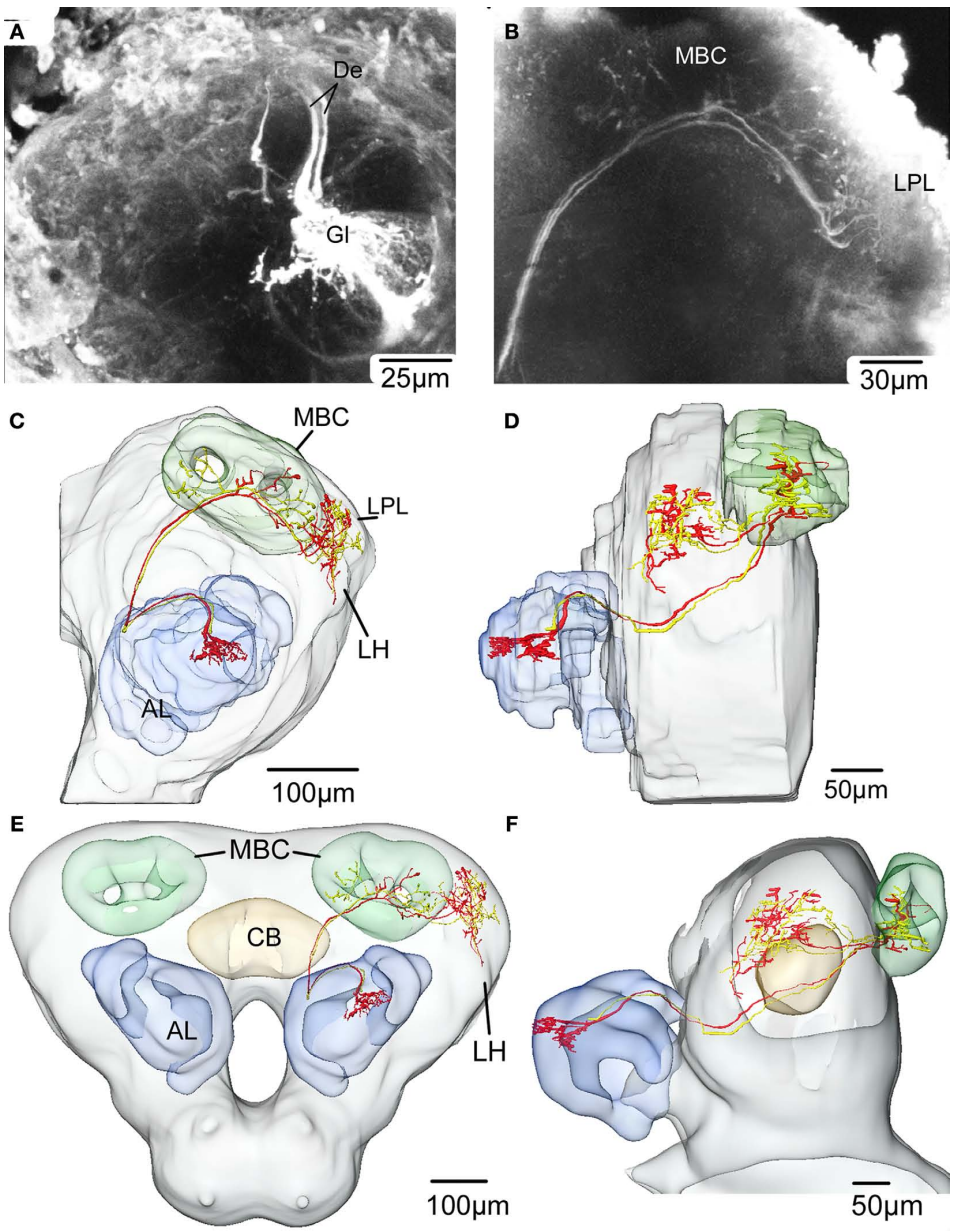

FIGURE 6 | Confocal images and registration of two antennal lobe projection neurons (simultaneously stained) into the average standard brain atlas of *Heliothis virescens*. (A) Confocal image of a section showing Micro-Ruby stained dendrites (De) of two antennal lobe projection neurons innervating a single glomerulus (Gl). Their branching pattern within the glomerulus could not be distinguished. **(B)** Confocal image showing the projections of the two neurons in the mushroom body calyces and in the lateral part of the protocerebral lobe. **(C,D)** Reconstruction of the left protocerebral lobe with the two neurons innervating one glomerulus (Gl) of the antennal lobe (AL), the mushroom bodies calyces (MBC) and the lateral protocerebral lobe (LPL) in a frontal view **(C)** and lateral view **(D)**. One branch of both axons extends into the lateral horn (LH). **(E,F)** The two neurons registered into the standard brain atlas in a frontal view **(E)** and lateral view **(F)**. Central body (CB).

preparations differ slightly, not only in size and orientation, but also in shape of the whole brain as well as brain structures exemplified by the 11 individual preparations in this study (**Table 1**, **Figure 5**). The ISA procedure takes this variability into account in the rigid and the elastic registrations as well as in the averaging procedures, resulting in a brain model with minimized differences to the individual brains (**Figure 5**), as previously demonstrated for the honeybee and the locust brain models (Brandt et al., 2005; Kurylas et al., 2008).

The procedure used and the structures selected for making the moth standard brain atlas are in general the same as for the honeybee brain, with a few modifications. The division of the moth brain into three compartments compensated for individual differences of the optic lobe orientations. The segregation allowed the use of 11 specimen for the midbrain region and 10 for the optic lobes because of mechanical damage. The selection of structures was based on staining quality, significance as landmarks and relevance

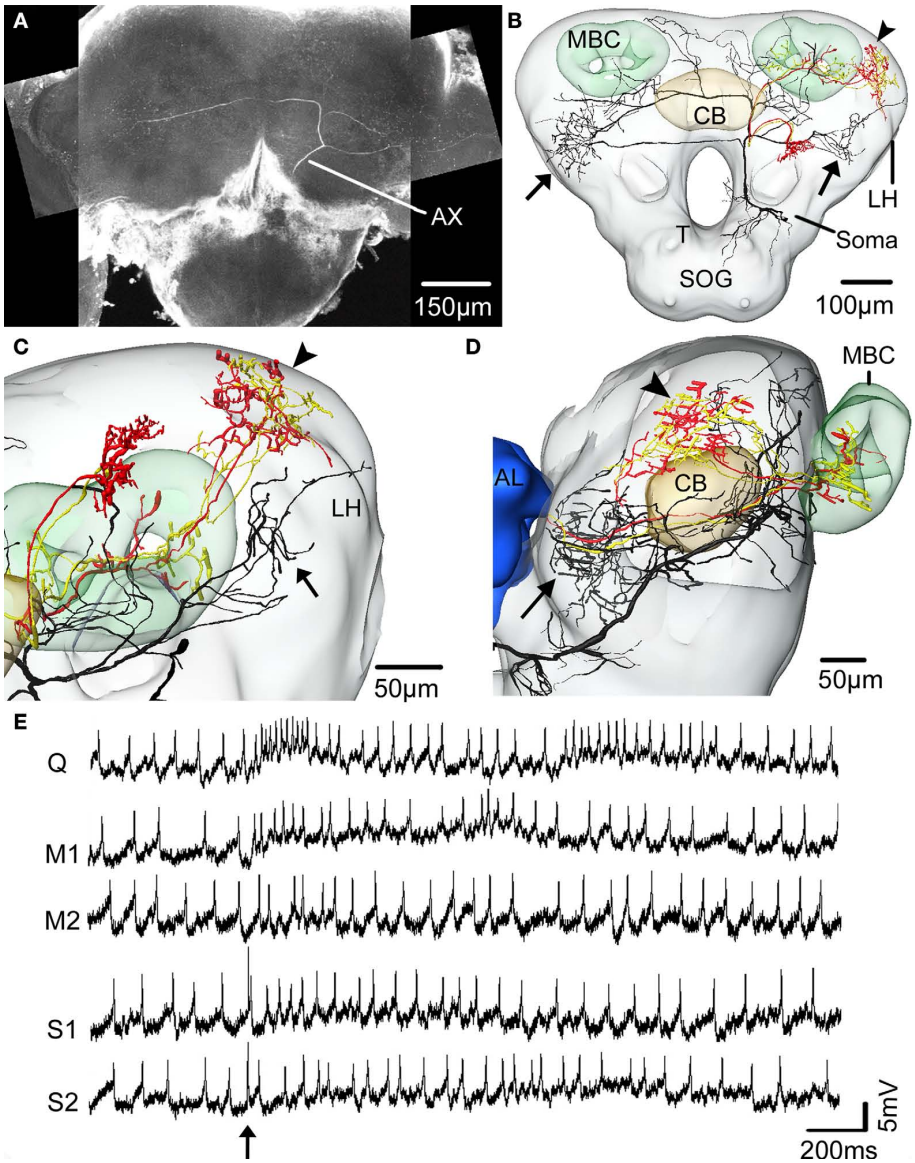

FIGURE 7 |The spatial relationship between a single gustatory interneuron and the two antennal lobe projection neurons visualised in the standard brain atlas of *Heliothis virescens*. (A) Confocal image of a brain section showing the gustatory interneuron stained with Micro-Emerald. Axon (Ax). **(B)** Reconstruction of the gustatory interneuron (black) and the two antennal lobe projection neurons (yellow and red) registered into the standard brain atlas (frontal view with selected brain structures). Mushroom body calyces (MBC), Central body (CB), Lateral horn (LH), Suboesophageal ganglion (SOG), Tritocerebrum (T). **(C,D)** Magnified sections of the lateral parts of the left protocerebral lobe in a frontal view **(C)** and a lateral view **(D)**. The segregated axonal projections of the gustatory interneuron and the antennal lobe projection neurons appear. Arrows point to the axonal projections of the gustatory interneuron and the arrowheads to the axonal projections of the antennal lobe projection neurons. Antennal lobe (AL). **(E)** Electrophysiological recordings from the interneuron during stimulation of the right antenna with quinine (Q), mechanosensory stimuli (M1, M2) and sucrose (S1, S2). Arrow points to the stimulus onset.

with respect to chemosensory coding and learning. Structures of the optic lobes like the medulla, lobula and lobula plate were well stained and also necessary to make the brain model complete. The well stained central body and the anterior optic tubercles are important landmarks in the midbrain. The antennal lobe glomeruli, the mushroom bodies, and the lateral parts of the protocerebral lobes are involved in processing olfactory information (Rø et al., 2007), and the SOG/tritocerebrum in processing gustatory information (Jørgensen et al., 2006; Kvello et al., 2006). However, the staining quality of these structures varied, either because of how well the antibody penetrated the tissue or because of different synaptic density. As a result the weakly stained structures were collectively assigned to one large label (Midbrain region) whereas the well stained structures were given a unique label.

The antennal lobe glomeruli with high synaptic density appeared as distinct stained structures, easily distinguished from the dark surroundings. They were collectively assigned as one label, separate from the remaining antennal lobe. This differs from the standard brain of the fruit fly, honeybee and the locust where the whole antennal lobe was assigned as one label (Rein et al., 2002; Brandt et al.,

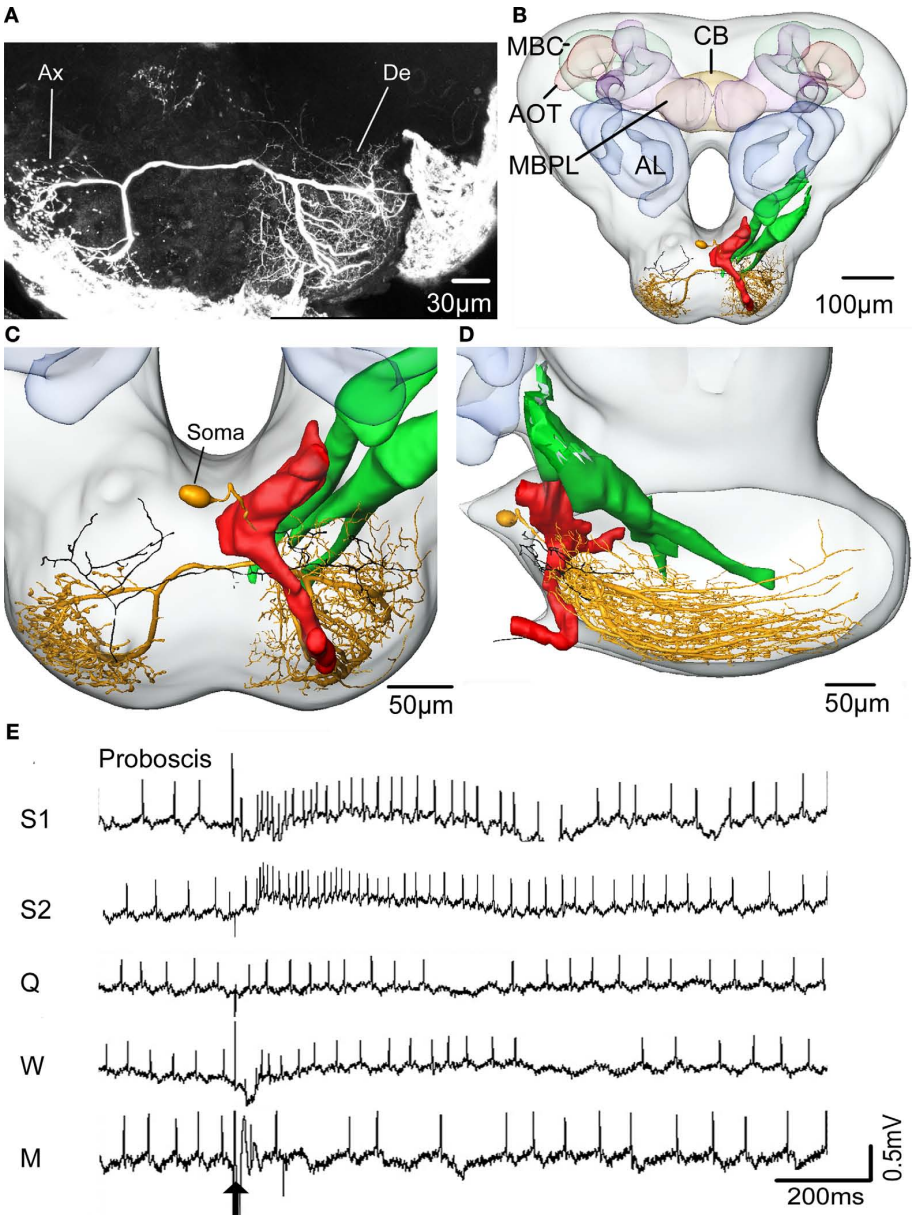

FIGURE 8 | The spatial relationship between a single gustatory interneuron and the axonal projections of the antennal and proboscis gustatory receptor neurons visualized in the standard brain atlas of the *Heliothis virescens*. **(A)** Confocal image of a section of the suboesophageal ganglion with a Micro-Ruby stained gustatory interneuron. Axon (Ax), Dendrite (De). **(B)** The gustatory interneuron (yellow) and the axonal projections of the antennal (green) and proboscis (red and black) gustatory receptor neurons registered into the standard brain atlas (frontal view with a few selected structures) Mushroom body calyces (MBC), Anterior optic tubercle (AOT), Mushroom body peduncle and lobes (MBPL), Antennal lobe (AL), Central body (CB). **(C,D)** Magnified section of the suboesophageal ganglion in a frontal view **(C)** and a lateral view **(D)**. The axon terminals of the proboscis gustatory receptor neuron (black) overlap the dendritic arborisations of the gustatory interneuron with direct contact between a few of the neurites. **(E)** Electrophysiological recordings from the interneuron during stimulation of the proboscis with sucrose (S1, S2), quinine (Q), water (W) and a mechanosensory stimulus (M). Arrow points to the stimulus onset.

2005; Kurylas et al., 2008). One reason for the separate glomerular labelling in the moth brain atlas was the difficulties in determining the borderline between the antennal lobe and the protocerebrum. In addition, the antennal lobe glomeruli have a larger surface relative to the volume as compared to the whole antennal lobe, which is an advantage when registering neurons into the atlas. The particular registration algorithm developed for label images use information that lies in the borderline of the label images (Rohlfing et al., 2001). A larger surface gives the algorithm more information and consequently improves the precision when registering neurons into the brain atlas. Finally, we also want to emphasize the glomeruli, being of particular interest since they relay information from olfactory sensory neurons to the second order neurons. We did not find it practical to include each of the 66 glomeruli as separate labels because

we have already made three dimensional atlases of the antennal lobe glomeruli of this species (Berg et al., 2002; Skiri et al., 2005a). At present, the separate antennal lobe atlas seems necessary for identifying the glomeruli innervated by a neuron, since this needs a detailed analysis of the relative position of the glomeruli. If practical and technically possible the atlas of the antennal lobe glomeruli may be registered into the standard brain atlas in the future.

The mushroom bodies were divided into the calyces and the peduncle/lobe system. These two compartments were easily distinguished, but a further division into their sub-compartments proved unreliable. Consistent with previous studies of *H. virescens* (Rø et al., 2007) and *Spodoptera littoralis* (Sjöholm et al., 2005) we could not distinguish any accessory calyx from the primary calyces. Such a division of the calyces, described in the moth *Manduca sexta*, may reflect a functional difference between the species (Homberg et al., 1988; Nighorn et al., 2001). Because of the difficulties of separating the mushroom body peduncle and the lobe system in the *H. virescens* brain these structures were included in the same label like in the other insect brain atlases (Rein et al., 2002; Brandt et al., 2005; Kurylas et al., 2008; Jundi et al., 2009). As shown in *Heliothis virescens* and *Spodoptera littoralis* the peduncle fuses anteriorly with the lobe system dividing into a dorsal α lobe and a medial β lobe, both intimately associated with the γ lobe (Sjøöholm et al., 2005; Rø et al., 2007). Specific to Lepidoptera is the Y lobe which was vaguely observed in a few preparations and therefore was not included in the standard atlas.

The SOG, tritocerebrum and protocerebral lobes, including the lateral accessory lobes, the protocerebral bridge and the lateral horns did not appear distinct and therefore were collectively included into the midbrain region label. In the same label we also included the particular structure located posterior to the antennal lobe glomeruli merging into the protocerebral lobes without a distinct borderline. The SOG, tritocerebrum and protocerebral lobes are also included in the same label in the honeybee and the fruit fly brain atlases. In these species as in the moth, the three structures are highly interconnected and seem to lack an area with high synaptic density where a reliable distinction can be made (Rein et al., 2002; Brandt et al., 2005). This differs from the locust where the SOG (not included in the standard locust brain atlas) is a distinct ganglion connected to the brain by the circumoesophageal connectives (Burrows, 1996). The lateral horn is another structure treated differently among the five insect brain atlases. In *H. virescens*, they were weakly stained and therefore included in the same label as the SOG, tritocerebrum and protocerebral lobes like in the honeybee and M. sexta (Brandt et al., 2005; Jundi et al., 2009). This differs from the fruit fly and the locust where the lateral horns were given a unique label (Rein et al., 2002; Kurylas et al., 2008). The midbrain region is by far the largest structure in the standard moth brain atlas. Its shape results in a relative small surface which is disadvantageous when registering neurons into the structure. Therefore, the central body and the anterior optic tubercles, located within the midbrain region, serve as important landmarks. These two structures appeared quite distinct in all 11 preparations. Especially the central body is a stable landmark because its location in the middle of the brain keeps it protected from distortion by external factors.

The application of the average standard brain atlas is demonstrated by the four registered interneurons, as well as the axonal projections of the gustatory receptor neurons shown in **Figures 7 and 8**. The olfactory interneurons showed the typical morphology of inner-tract antennal lobe projection neurons (Rø et al., 2007), with dendrites innervating a single glomerulus of the antennal lobe, and axons projecting via the inner antenno-cerebral tract to the calyces of the mushroom body involved in olfactory learning and memory (Menzel, 2001; Heisenberg, 2003), and to the lateral parts of the median protocerebrum considered to be a premotoric area (**Figure 6**). Interestingly, axonal projections of the quinine responding neuron were identified in a separate, but closely located area of the olfactory projections. Because of the absence of distinct landmarks in this brain region the standard brain atlas proved particularly valuable in visualizing and distinguishing these target areas of the gustatory- and olfactory projections (**Figures 7B–D**). However, registration of more neurons into the standard brain atlas combined with electrophysiology is needed to verify whether the projection areas of the two chemosensory modalities are completely separated or partly overlapping in this area of the brain. The atlas also proved valuable in visualising possible connections between the sucrose responding interneuron and the receptor neurons in the SOG (**Figure 8**). The direct contact between the intermingled dendritic branches of one gustatory interneuron and the projections of the proboscis gustatory receptor neuron suggest input from the proboscis. In contrast the non overlapping projections of the antennal gustatory receptor neuron indicate no antennal input. This was in fact shown physiologically by the excitatory responses of the interneuron to sucrose stimulation of the proboscis, but not of the antennae. Furthermore, the short and constant latency of the response indicate monosynaptic connections (Burrows and Newland, 1994; Newland, 1999). The axon projected contra laterally relative to the dendritic arborizations, terminating in the ventro lateral SOG where motorneurons of the mouthparts presumably are located. Thus, this neuron may receive direct synaptic input from the sucrose receptor neurons on the proboscis and feed into motor neurons involved in feeding.

The standard brain atlas is a valuable tool for visualising the spatial relationship between neurons from different brain preparations, detecting regions of overlap among the neurites, and thus to make predictions about neuronal connectivity. The procedure of rigid and elastic registration is particularly suited as an objective way to integrate neurons from different preparations into the digital standard brain atlas. The average property of the atlas ensures that the neurons undergo a minimal deformation in the registration procedure. In combination with physiological data the atlas provides an important tool for investigating and visualising the neural networks underlying gustatory and olfactory coding as well as appetitive and aversive learning and memory formation.

ACKNOWLEDGMENTS

The project was financed by the Norwegian University of Science and Technology and the Royal Norwegian Society of Sciences and Letters. We thank Prof. Erich Buchner (Universität Würzburg, Würzburg, Germany) for providing antibodies, Dr. Robert Brandt (Mercury Computer Systems, Berlin, Germany) and Anja Kuss (Zuse-Institute Berlin) for help with Amira, Dr. Sabine Krofczik (Freie Universität Berlin) for staining protocols and Gisela Manz (Freie Universität Berlin) for advices during the intracellular recordings.

REFERENCES

Berg, B. G., Almaas, T. J., Bjaalie, J. G., and Mustaparta, H. (1998). The macroglomerular complex of the antennal lobe in the tobacco budworm moth *Heliothis virescens*: specified subdivision in four compartments according to information about biologically significant compounds. *J. Comp. Physiol. A* 183, 669–682.

Berg, B. G., Galizia, C. G., Brandt, R., and Mustaparta, H. (2002). Digital atlases of the antennal lobe in two species of tobacco budworm moths, the oriental Helicoverpa assulta (male) and the American *Heliothis virescens* (male and female). *J. Comp. Neurol.* 446, 123–134.

Borst, A., and Haag, J. (2002). Neural networks in the cockpit of the fly. *J. Comp. Physiol. A* 188, 419–437.

Brandt, R., Rohlfing, T., Rybak, J., Krofczik, S., Maye, A., Westerhoff, M., Hege, H. C., and Menzel, R. (2005). Tree-dimensional average-shape atlas of the honeybee brain and its applications. *J. Comp. Neurol.* 492, 1–19.

Bräunig, P., and Pflüger, H.-J. (2001). The unpaired median neurons of insects. *Adv. In Insect Phys.* 28, 185–266.

Burrows, M. (1996). The Neurobiology of an Insect Brain. New York, Oxford University Press.

Burrows, M., and Newland, P. L. (1994). Convergence of mechanosensory afferents from different classes of exteroceptors onto spiking local interneurons in the locust. *J. Neurosci.* 14, 3341–3350.

Chiang, A.-S., Liu, Y.-C., Chiu, S. L., Hu, S. H., Huang, C.-Y., and Hsieh, C.-H. (2001). Three-dimensional mapping of brain neuropils in the cockroach, *Diploptera punctata. J. Comp. Neurol.* 440, 1–11.

Evers, J. F., Schmitt, S., Sibila, M., and Duch, C. (2004). Progress in functional neuroanatomy: precise automatic geometric reconstruction of neuronal morphology from confocal image stacks. *J. Neurophysiol.* 93, 2331–2342.

Flanagan, D., and Mercer, A. R. (1989). An atlas and 3-D reconstruction of the antennal lobes in the worker honey bee, *Apis mellifera* L. (*Hymenoptera: Apidae*). *Int. J. Insect Morphol. Embryol.* 18, 145–159.

Galizia, C. G., McIlwrath, S. L., and Menzel, R. (1999). A digital three-dimensional atlas of the honeybee antennal lobe based on optical sections acquired by confocal microscopy. *Cell Tissue Res.* 295, 383–394.

Greiner, B., Gadenne, C., and Anton, S. (2004). Three-dimensional antennal lobe atlas of the male moth, *Agrotis ipsilon*: a tool to study structure-function correlation. *J. Comp. Neurol.* 475, 202–210.

Hammer, M. (1993). An identified neuron mediates the unconditioned stimulus in associative olfactory learning in honeybees. *Nature* 366, 59–63.

Hartlieb, E. (1996). Olfactory conditioning in the moth *Heliothis virescens. Naturwissenschaften* 83, 87–88.

Heinbockel, T., Christensen, T. A., and Hildebrand, J. G. (1999). Temporal tuning of odor responses in pheromone-responsive projection neurons in the brain of the sphinx moth *Manduca sexta. J. Comp. Neurol.* 409, 1–12.

Heinze, S., and Homberg, U. (2007). Maplike representation of celestial E-vector orientations in the brain of an insect. *Science* 315, 995–997.

Heisenberg, M. (2003). Mushroom body memoir: from maps to models. *Nat. Rev. Neurosci.* 4, 266–275.

Homberg, U., Montague, R. A., and Hildebrand. J. G. (1988). Anatomy of antenno-cerebral pathways in the brain of the sphinx moth *Manduca sexta. Cell Tissue Res.* 254, 255–281.

Huetteroth, W., and Schachtner, J. (2005). Standard three-dimensional glomeruli of the *Manduca sexta* antennal lobe: a tool to study both developmental and adult neuronal plasticity. *Cell Tissue Res.* 319, 513–524.

Iyengar, B. G., Chou, C. J., Sharma, A., and Atwood, H. L. (2006). Modular neuropile organization in the Drosophila larval brain facilitates identification and mapping of central neurons. *J. Comp. Neurol.* 499, 583–602.

Jefferis, G. S. X. E., Potter, C. J., Chan, A. I., Marin, E. C., Rohlfing, T., Maurer, C. R., and Luo, L. Q. (2007). Comprehensive maps of Drosophila higher offactory centers: Spatially segregated fruit and pheromone representation. *Cell* 128, 1187–1203.

Jenett, A., Schindelin, J. E., and Heisenberg, M. (2006). The Virtual Insect Brain protocol: creating and comparing standardized neuroanatomy. *BMC Bioinformatics* 7, 544.

Jørgensen, K., Almaas, T. J., Marion-Poll, F., and Mustaparta, H. (2007a). Electrophysiological characterization of responses from gustatory receptor neurons of sensilla chaetica in the Moth *Heliothis virescens. Chem. Senses* 32, 863–879.

Jørgensen, K., Stranden, M., Sandoz, J. C., Menzel, R., and Mustaparta, H. (2007b). Effects of two bitter substances on olfactory conditioning in the moth *Heliothis virescens. J. Exp. Biol.* 210, 2563–2573.

Jørgensen, K., Kvello, P., Almaas, T. J., and Mustaparta, H. (2006). Two closely located areas in the suboesophageal ganglion and the tritocerebrum receive projections of gustatory receptor neurones located on the antennae and the proboscis in the moth *Heliothis virescens. J. Comp. Neurol.* 496, 121–134.

Jundi, B. E., Huetteroth, W., Kurylas, A. E., and Schachtner, J. (2009). Anisometric brain dimorphism revisited: implementation of a volumetric 3D standard brain in *Manduca sexta. J. Comp. Neurol.* 517, 210–225.

Kanzaki, R., Arbas, E. A., and Hildebrand, J. G. (1991). Physiology and morphology of descending neurons in pheromone-processing olfactory pathways in the male moth *Manduca sexta. J. Comp. Physiol. A* 169, 1–14.

Kanzaki, R., Arbas, E. A., Strausfeld, N. J., and Hildebrand, J. G. (1989). Physiology and morphology of projection neurons in the antennal lobe of the male moth *Manduca sexta. J. Comp. Physiol. A* 165, 427–453.

Kurylas, A. E., Rohlfing, T., Krofczik, S., Jenett, A., and Homberg, U. (2008). Standardized atlas of the brain of the desert locust, *Schistocerca gregaria. Cell Tissue Res.* 333, 125–145.

Kvello, P., Almaas, T. J., and Mustaparta, H. (2006). A confined taste area in a lepidopteran brain. *Arthropod Struct. Dev.* 35, 35–45.

Laissue, P. P., Reiter, C., Hiesinger, P. R., Halter, S., Fischbach, K. F., and Stocker, R. F. (1999). Three-dimensional reconstruction of the antennal lobe in *Drosophila melanogaster. J. Comp. Neurol.* 405, 543–552.

Lei, H., Anton, S., and Hansson, B. S. (2001). Olfactory protocerebral pathways processing sex pheromone and plant odor information in the male moth *Agrotis segetum. J. Comp. Neurol.* 432, 356–370.

Masante-Roca, I., Gadenne, C., and Anton, S. (2005). Three-dimensional antennal lobe atlas of male and female moths, *Lobesia botrana* (Lepidoptera : Tortricidae) and glomerular representation of plant volatiles in females. *J. Exp. Biol.* 208, 1147–1159.

Mauelshagen, J. (1993). Neural correlates of olfactory learning paradigms in an identified neuron in the honeybee brain. *J. Neurophysiol.* 69, 609–625.

Menzel, R. (2001). Searching for the memory trace in a mini-brain, the honeybee. *Learn. Mem.* 8, 53–62.

Mitchell, B. K., and Itagaki, H. (1992). Interneurons of the subesophageal ganglion of *Sarcophaga bullata* responding to gustatory and mechanosensory stimuli. *J. Comp. Physiol. A* 171, 213–230.

Müller, D., Abel, R., Brandt, R., Zöckler, M., and Menzel, R. (2002). Differential parallel processing of olfactory information in the honeybee, *Apis mellifera* L. *J. Comp. Physiol. A* 188, 359–370.

Mustaparta, H. (2002). Encoding of plant odour information in insects: peripheral and central mechanisms. *Entomol. Exp. Appl.* 104, 1–13.

Mustaparta, H., and Stranden, M. (2005). Olfaction and learning in moths and weevils living on angiosperm and gymnosperm hosts. *Recent Adv. Phytochem.* 39, 269–292.

Namiki, S., and Kanzaki, R. (2008). Reconstructing the population activity of olfactory output neurons that innervate identifiable processing units. *Front. Neural Circuits* 2, 1. doi: 10.3389/neuro.01.028.2009.

Newland, P. L. (1999). Processing of gustatory information by spiking local interneurons in the locust. *J. Neurophysiol.* 82, 3149–3159.

Nighorn, A., Simpson, P. J., and Morton, D. B. (2001). The novel guanylyl cyclase MsGC-I is strongly expressed in higher-order neuropils in the brain of *Manduca sexta. J. Exp. Biol.* 204, 305–314.

Poulet, J. F. A., and Hedwig, B. (2006). The cellular basis of a corollary discharge. *Science* 311, 518–522.

Rein, K., Zöckler, M., Mader, M. T., Grübel, C., and Heisenberg, M. (2002). The Drosophila standard brain. *Curr. Biol.* 12, 227–231.

Reischig, T., and Stengl, M. (2002). Optic lobe commissures in a three-dimensional brain model of the cockroach *Leucophaea maderae*: a search for the circadian coupling pathways. *J. Comp. Neurol.* 443, 388–400.

Reisenman, C. E., Christensen, T. A., and Hildebrand, J. G. (2005). Chemosensory selectivity of output neurons innervating an identified, sexually isomorphic olfactory glomerulus. *J. Neurosci.* 25, 8017–8026.

Rø, H., Müller, D., and Mustaparta, H. (2007). Anatomical organization of antennal lobe projection neurons in the moth *Heliothis virescens. J. Comp. Neurol.* 500, 658–675.

Rogers, S. M., and Newland, P. L. (2003). The neurobiology of taste in insects. *Adv. In Insect Phys.* 141–204.

Rohlfing, T., Brandt, R., Maurer, C. R. Jr., and Menzel, R. (2001). Bee Brains, B-splines and Computational Democracy: Generating an Average Shape Atlas. In Proceedings of IEEE Workshop on Mathematical Methods in Biomedical Image Analysis, MMBIA, Kauai, Hawaii. pp. 187–194.

Rospars, J. P., and Chambille, I. (1981). Deutocerebrum of the cockroach *Blaberus craniifer* burm. Quantitative study and automated identification of the glomeruli. *J. Neurobiol.* 12, 221–247.

Rospars, J. P., and Hildebrand, J. G. (2000). Sexually dimorphic and isomorphic

glomeruli in the antennal lobes of the sphinx moth *Manduca sexta*. *Chem. Senses* 25, 119–129.

Røstelien, T., Stranden, M., Borg-Karlson, A.-K., and Mustaparta, H. (2005). Olfactory receptor neurones in two heliothine moth species responding selectively to aliphatic green leaf volatiles, aromatics, monoterpenes and sesquiterpenes of plant origin. *Chem. Senses* 30, 443–461.

Rybak, J., and Menzel, R. (1998). Integrative properties of the pe1 neuron, a unique mushroom body output neuron. *Learn. Mem.* 5, 133–145.

Sadek, M. M., Hansson, B. S., Rospars, J. P., and Anton, S. (2002). Glomerular representation of plant volatiles and sex pheromone components in the antennal lobe of the female *Spodoptera littoralis*. *J. Exp. Biology* 205, 1363–1376.

Schmitt, S., Evers, J. F., Duch, C., Scholz, M., and Obermayer, K. (2004). New methods for the computer-assisted 3-D reconstruction of neurons from confocal image stacks. *Neuroimage* 23, 1283–1298.

Sjöholm, M., Sinakevitch, I., Ignell, R., Strausfeld, N. J,, and Hansson, B. S. (2005). Organization of Kenyon cells in subdivisions of the mushroom bodies of a lepidopteran insect. *J. Comp. Neurol.* 491, 290–304.

Skiri, H. T., Rø, H., Berg, B. G., and Mustaparta, H. (2005a). Consistent organization of glomeruli in the antennal lobes of related species of heliothine moths. *J. Comp. Neurol.* 491, 367–380.

Skiri, H. T., Stranden, M., Sandoz, J. C., Menzel, R., and Mustaparta, H. (2005b). Associative learning of plant odorants activating the same or different receptor neurones in the moth *Heliothis virescens*. *J. Exp. Biol.* 208, 787–796.

Smid, H. M., Bleeker, M. A., Van Loon, J. J. A., and Vet, L. E. (2003). Three-dimensional organization of the glomeruli in the antennal lobe of the parasitoid wasps *Cotesia glomerata* and *C. rubecula*. *Cell Tissue Res.* 312, 237–248.

Staudacher, E. M., Huetteroth, W., Schachtner, J., and Daly, K. C. (2009). A 4-dimensional representation of antennal lobe output based on an ensemble of characterized projection neurons. *J. Neurosci. Methods* 180, 208–223.

Stocker, R. F., Lienhard, M. C., Borst, A., and Fischbach, K. F. (1990). Neuronal architecture of the antennal lobe in *Drosophila melanogaster*. *Cell Tissue Res.* 262, 9–34.

Toga, A. W. (2002). Neuroimage databases: the good, the bad and the ugly. *Nat. Rev. Neurosci.* 3, 302–309.

Toga, A. W., and Thompson, P. M. (2001). Maps of the brain. *Anat. Rec.* 265, 37–53.

Van Essen D. C. (2002). Windows on the brain: the emerging role of atlases and databases in neuroscience. *Curr. Opin. Neurobiol.* 12, 574–579.

Yamagata, N., Nishino, H., and Mizunami, M. (2007). Neural pathways for the processing of alarm pheromone in the ant brain. *J. Comp. Neurol.* 505, 424–442.

Conflict of Interest Statement: The authors declare that the research was conducted in the absence of any commercial or financial relationships that could be construed as a potential conflict of interest.

Received: 04 August 2009; paper pending published: 20 August 2009; accepted: 02 October 2009; published online: 26 October 2009.

*Citation: Kvello P, Løfaldli BB, Rybak J, Menzel R and Mustaparta H (2009) Digital, three-dimensional average shaped atlas of the Heliothis virescens brain with integrated gustatory and olfactory neurons. Front. Syst. Neurosci. **3**:14. doi: 10.3389/neuro.06.014.2009*

frontiers in
SYSTEMS NEUROSCIENCE

ORIGINAL RESEARCH ARTICLE
published: 18 March 2010
doi: 10.3389/fnsys.2010.00007

3D-reconstructions and virtual 4D-visualization to study metamorphic brain development in the sphinx moth *Manduca sexta*

Wolf Huetteroth*[‡†], *Basil el Jundi*[‡], *Sirri el Jundi and Joachim Schachtner*

Department of Biology, Animal Physiology, Philipps-University Marburg, Marburg, Germany

Edited by:
Randolf Menzel, Freie Universitat Berlin, Germany

Reviewed by:
Hanna Mustaparta, Norwegian University of Science and Technology, Norway
John Hildebrand, University of Arizona, USA

***Correspondence:**
Joachim Schachtner, Department of Biology, Animal Physiology, Philipps-University Marburg, Karl-von-Frisch-Str. 8, D-35032 Marburg, Germany.
e-mail: schachtj@staff.uni-marburg.de

[†]***Present address:***
Wolf Huetteroth, Department of Neurobiology, University of Massachusetts Medical School, Worcester, MA, USA

[‡]*Wolf Huetteroth and Basil el Jundi contributed equally.*

During metamorphosis, the transition from the larva to the adult, the insect brain undergoes considerable remodeling: new neurons are integrated while larval neurons are remodeled or eliminated. One well acknowledged model to study metamorphic brain development is the sphinx moth *Manduca sexta*. To further understand mechanisms involved in the metamorphic transition of the brain we generated a 3D standard brain based on selected brain areas of adult females and 3D reconstructed the same areas during defined stages of pupal development. Selected brain areas include for example mushroom bodies, central complex, antennal- and optic lobes. With this approach we eventually want to quantify developmental changes in neuropilar architecture, but also quantify changes in the neuronal complement and monitor the development of selected neuronal populations. Furthermore, we used a modeling software (Cinema 4D) to create a virtual 4D brain, morphing through its developmental stages. Thus the didactical advantages of 3D visualization are expanded to better comprehend complex processes of neuropil formation and remodeling during development. To obtain datasets of the *M. sexta* brain areas, we stained whole brains with an antiserum against the synaptic vesicle protein synapsin. Such labeled brains were then scanned with a confocal laser scanning microscope and selected neuropils were reconstructed with the 3D software AMIRA 4.1.

Keywords: animation, brain, development, digital neuroanatomy, insect, *Manduca*, neuropil

INTRODUCTION

Brains are typically organized in defined neuropils, which can usually be characterized by their spatial location, gross anatomy, and often by a certain function and brains of evolutionary related animals typically share a similar neuroarchitecture. During development, the formation of brain neuropils including their location and interconnections follows a minute pattern in time and space orchestrated by complex (genetical) programs which eventually give rise to the adult brain structures.

Metamorphosis, the transition of a larva to an adult insect has always fascinated us humans. By far, most of the living insects belong to the group of holometabolous insects (Grimaldi and Engel, 2005) which have in addition to the embryonic development a second developmental phase called metamorphosis. During metamorphosis, as demonstrated by many researchers over the years, the nervous system undergoes considerable remodeling: new neurons are integrated while larval neurons are remodeled or eliminated (for reviews see e.g. Truman, 1996, 2009). Most obvious, neuropils involved in the processing of visual and olfactory information are to a large extent newly formed during metamorphosis. To understand further the mechanisms involved in transforming a larval to an adult brain, we have mapped the anatomical changes of selected brain areas throughout metamorphosis of the sphinx moth *Manduca sexta*. *M. sexta* serves since long as a model to understand metamorphic brain development and the development of most of the discernable brain areas has been described earlier (see Discussion). However, so far a comprehensive view which compares the anatomical changes of all these brain neuropils throughout metamorphic development is missing. Thus, the aim of the current study was to visualize the anatomical changes of discernable brain areas in parallel and thus to provide a tool which allows a comparison of these changes along the developmental time line.

To obtain the desired datasets, we labeled whole brains of different metamorphic stages with an antiserum against the synaptic vesicle protein synapsin to visualize neuropil areas, analyzed the staining using confocal laser scanning microscopy, 3D reconstructed the selected brain neuropils using the software AMIRA (Visage Imaging, Fürth, Germany), and subsequently transformed the data sets into the 4D visualization software Cinema 4D. The used technique can in principal be adapted to any brain area which can be visualized and 3D reconstructed at different times of development.

MATERIALS AND METHODS

ANIMALS

Moths (*M. sexta*; Lepidoptera: Sphingidae) were raised at 26°C under a long-day photoperiod (L:D = 17:7) and were fed on an artificial diet (Bell and Joachim, 1978). Under these conditions animals required 18 days from hatching to pupal ecdysis and another 20 days from pupal ecdysis to adult eclosion. The wandering stage presents the last phase of the fifth larval stage (L5) and consists of about 5 days (W0–W4). The beginning of this stage (W0) is characterized by the occurrence of a red pigment along the dorsal vessel. At about noon of W2, the animals go into a quiescent

prepupal stage. Pupal ecdysis occurs on day W4, and the newly formed pupa is designated as day P0. Subsequent days of pupal development are counted as P1-P20. The freshly eclosed adult individual is termed A0. The staging of larvae and pupae was based on the criteria described by Schwartz and Truman (1983) and Jindra et al. (1997). For our experiments we used only female animals.

To describe, visualize and animate the development of the brain of *M. sexta* during pupal metamorphosis we 3D-reconstructed brains from defined pupal stages. We reconstructed two brains of representative stages (except stage P4; $n = 1$), including the fifth instar larva (L5) and nine pupal stages during metamorphosis (P0; P1; P3; P4; P7; P9; P11; P14; P16). As adult brain we used the *M. sexta* standard brain (freshly eclosed, A0) for our animation (el Jundi et al., 2009).

IMMUNOHISTOCHEMISTRY

For our studies we used a wholemount staining protocol as described in el Jundi et al. (2009). Brains from different developmental stages were dissected out of the head capsule under cold saline (Weevers, 1966) and were fixed overnight at 4°C, in a solution composed of one part formaldehyde (37%, Roth, Karlsruhe, Germany), one part methanol and eight parts phosphate-buffered saline (PBS 0.01 M, pH 7.4). Whole brains were rinsed in 0.1 M PBS containing 0.3% Triton X-100 (PBT) for 1 h at room temperature and were preincubated (4°C, overnight) in 5% normal goat serum (NGS; Jackson ImmunoResearch, Westgrove, PA, USA) in 0.1 M PBT containing 0.02% sodium azide. For visualization of the brain areas we used a monoclonal primary antibody from mouse against a fusion protein consisting of a glutathione-S-transferase and the first amino acids of the presynaptic vesicle protein synapsin I coded by its 5′-end (SYNORF1, Klagges et al., 1996, kindly provided by Dr. E. Buchner, Würzburg). Its specificity in *M. sexta* was shown in western blots by Utz et al. (2008). The anti-synapsin antibody was diluted 1:50 in 0.1 M PBT containing 1% NGS and 0.02% sodium azide.

After 4–6 days incubation with the primary antibody, the brains were rinsed 6 times in 2 h with PBT before they were incubated with the secondary goat anti-mouse antibody conjugated to Cy5 (1:300; Jackson ImmunoResearch, Westgrove, PA, USA) in PBT and 1% NGS for 4 days at 4°C. Afterwards, the brains were rinsed with PBT 6 times in 2 h, then dehydrated in an ascending ethanol series (50–100%, 15 min each) and then cleared in methyl salicylate (Merck, Gernsheim, Germany) for about 40 min. At last the brains were mounted in Permount (Fisher Scientific, Pittsbourgh, PA, USA) between two coverslips. Compression of brains was prevented by spacers (Zweckform, Oberlaindern, Germany). According to the brain sizes we used for larval brains (L5) and early pupal brains three to five spacers (P0–P4). Late pupal brains (P7–P16) were embedded using six to nine spacers.

IMAGE ACQUISITION

All brains were scanned with a confocal laser scanning microscope (Leica TCS SP2). The fluorescent signal of Cy5 was detected with a HeNe laser (633 nm). Late pupal brains (P7–P16) were imaged at 512×512 pixel resolution by using a 10× oil immersion objective (HC PL APO 10×/NA: 0.40 Imm (working distance: 0.36 mm); Leica, Bensheim, Germany). Larval and early pupal brains (L5–P4) were scanned with a 10× oil objective or a 20× oil objective (HC PL APO 20×/0.70 lmm Corr CS, Leica, Bensheim, Germany). All brains were scanned with a voxel size of 2.9×2.9 µm in xy-direction. Late pupal brains were imaged with a step size of 2 µm, younger brains were detected with a step size of 1.5 µm. The thickness of older brains and the limited working distance of the objectives made it necessary to scan the brains from two sides (anterior and posterior) to eventually acquire images of the whole brain. Younger brains were scanned only from anterior. Depending on xy dimension which increased with the developmental stage the brains had to be scanned in two and up to eight image stacks. For example, for P16 brains we needed three stacks from anterior and another three stacks from the posterior side. For A0 brains four stacks from each side were needed (el Jundi et al., 2009).

IMAGE PROCESSING AND 3D RECONSTRUCTION

Image processing and 3D reconstruction were performed in the program AMIRA 4.1 (Visage Imaging, Fürth, Germany). First the different image stacks of all brain regions were merged into one stack: corresponding optical slices in the z direction in overlapping parts of the image stacks were found with the module *AlignSlices,* redundant slices of the stacks were abolished and corresponding batches of data were merged with the module *AlignSlices.* Before we merged these image stacks in xy direction, computation limits made it necessary to downsample the voxel size of the image stacks of P7–P16 pupal brains with the module *Resample* to a voxel size of $6 \times 6 \times 6$ µm. For brains < P7 it was not essential to downsample the image stacks. Again, we used the module *AlignSlices* for finding the corresponding optical slice and with the module *Merge* batches of data were merged into one batch of data which contained the whole brain.

For 3D reconstructions, *Labelfield* files were created with the same dimensions (voxel size, resolution) as the corresponding merged image stacks. Using the *Segmentation Editor*, reconstructions of selected neuropils were performed. Regions of interests were labeled in three dimensions in several optical slices and subsequently extrapolated into 3D structures by using the tool *Wrap*. Clearly identifiable neuropilar borders in all three dimensions based on anti-synapsin staining were the limiting criterion for reconstructing a brain region in a certain developmental stage. The color codes for neuropils are consistent with existing standard brain models (Brandt et al., 2005; Kurylas et al., 2008; el Jundi et al., 2009; Dreyer et al., 2010). With the module *SurfaceGen* the 3D surface visualizations were calculated. Based on visual appearance, surface models of brains which represented the according stage best were used for 4D visualization of the brain development during the metamorphosis.

4D VISUALIZATION

To animate the development of the brain of *M. sexta* during metamorphosis we reconstructed brains ranging from the last larval stage (L5) to brains of freshly eclosed animals (A0). Because of the limited computational capacity it was necessary to reduce the number of the polygons of the surface models in AMIRA. Subsequently, representative brains of distinct developmental stages were exported from Amira as drawing exchange format (.dxf) files and were opened in the software Cinema 4D (v.10.1; MAXON Computer, Friedrichsdorf, Germany). Only those brains

were chosen which clearly exhibited representative features of their stage. Using those brain polygon models as templates, the 4D visualization of brain development was created in Cinema 4D. The creation of the 4D visualization of the *M. sexta* brain is described in detail in the results.

RESULTS

ANATOMICAL DEVELOPMENT OF THE BRAIN NEUROPILS

Overall, we reconstructed 19 female brains from 10 different stages during *M. sexta* brain development. In an earlier study we already reconstructed 12 brains of freshly eclosed adult females (A0) to produce a standard brain (el Jundi et al., 2009). Since we wanted to cover the brain transition between the larval and the adult brain during pupal development, we started with fifth instar larval brains, chose nine stages during pupal development (P0, P1, P3, P4, P7, P9, P11, P14, P16) and closed with the female A0 standard brain (el Jundi et al., 2009). Because early metamorphic development coincides with more obvious structural changes, these phases were resolved with higher temporal resolution. During the approximately 3 weeks of pupal development, the *Manduca* brain undergoes an enormous increase in size (the reconstructed neuropils grow about 132-fold from P0 to A0), which is largely due to the development of the optic lobes (**Figure 1**). But all other parts of the brain also increase in size, and further developmental processes in the brain take place (**Figures 2–6**). Most prominently, the subesophageal ganglion merges with the supraesophageal ganglion, thereby forming the esophageal foramen. This process is initiated during the wandering stage and is finished around P3 (Amos and Mesce, 1994; Homberg and Hildebrand, 1994). Additionally, the metamorphosing brain undergoes certain rotational movements, mirrored in the orientation of neuropils in the brain: (1) Neuropils located anteriorly move upwards (mushroom body lobes, antennal lobes), (2) the brain midline folds slightly outwards towards the dorsal side (orientation of mushroom body calyces), and (3) central parts of the protocerebrum tilt back (mushroom body peduncles with calyces, central complex). Most of these movements are finished until P7/8, followed by further size increase of all neuropils. Because these movement and growth processes are temporally overlapping we created a 4D movie for better comprehension (see below; **Movie S1** in Supplementary Material). Below, all major neuropils are dealt with in more detail.

The optic lobes

In the last larval stage (5th instar; L5), the larval optic center (LOC), is barely separated from the midbrain neuropil (**Figure 1**, gray line). The inner (IOA) and outer optic anlagen (OOA), the precursors of the adult optic neuropils, are already present, although they exhibit almost no anti-synapsin immunoreactivity at this stage. At this early stage, the accessory medulla (aMe) is still part of the LOC. Several other neuropils are already distinguishable, the larval antennal lobe (see **Figure 2**), the calyx (Ca) and peduncle (Pe) of the mushroom body (see **Figure 3**), and the protocerebral bridge (PB; see **Figure 4**). With the onset of pupation (P0), the optic lobe neuropils begin to grow and the now ribbon-like neuropils lamina (La), medulla (Me) and lobula (Lo) begin to show faint anti-synapsin staining. At this stage, the aMe is separated from the midbrain neuropil and stays close to the antero-medial rim of the Me. At P3 the outer optic neuropils further expand mainly along the antero-posterior axis; the dorsal and ventral tips of the La bend behind the Me, thus resembling a horseshoe. The lobula plate (LoP) appears as a discernible structure between Me and Lo. The anti-synapsin staining gains intensity in all neuropils; the different layers of the Me become recognizable (**Figure 1C′**). After one third of pupal development (P7), the inner and outer lobula subunits (Loi, Loo) can be separated based on their anti-synapsin immunoreactivity. The La starts to exhibit its bowl-like appearance, the opening still tilted towards the anterior side. Three subunits of the anterior optic tubercle (AOTu, see **Figure 5**) are now present in the antero-dorsal protocerebrum. After two-thirds of pupal development (P14) all neuropils of the optic lobe reached their relative position and continue to increase in size until adult eclosion. The relative distance between La and Me increased up to here.

The antennal lobes

The primary larval integration site for olfactory information, the larval antennal center (LAC) exhibits no glomerular organization in *M. sexta* (**Figure 2**). The anti-synapsin staining resembles throughout AL development the anti-synaptotagmin staining described earlier (Dubuque et al., 2001). At P4 the developing AL becomes first visible with the anti-synapsin staining. Note the ventral position of the AL, even with the complete subesophageal ganglion fused to the supraesophageal ganglion. From P7, spheroidal structures, the forming olfactory glomeruli become visible in the developing AL. The glomeruli enclose a central coarse neuropil. The whole AL gains volume and wanders in a more antero-dorsal position. At P9, single glomeruli become clearly discernible within the AL. The dorsal migration of the whole AL slows down and eventually stalls. The volume curve indicates for the AL three developmental phases, which correspond to earlier studies (**Figure 7**; Oland and Tolbert, 1996; Dubuque et al., 2001; see Discussion).

The mushroom bodies

The larval (L5) mushroom body (MB) is characterized by rather thin α- and β-lobes (αL, βL) and a slender peduncle (**Figure 3**). The peduncle in the larva is still oriented antero-ventrally, with a slight inclination of the calyces (Ca) to the dorsal midline. While the αL points antero-dorsally, the βL extends medially in the horizontal plane. Between stages P1 and P3 the pedunculi bend nearly 90 degree sidewards and the whole MB starts to rotate backwards from a ventro-dorsal orientation to an antero-posterior orientation (**Figure 6**; **Movie S1** in Supplementary Material). This rotation continues until P7, now the whole MB is oriented antero-posteriorly. Additionally to the αL and βL, the γ-lobe (γL) and the Y-lobe (YL, see in **Figures 3D–D″,E–E″**) can now be discerned.

Other neuropiles of the CNS

Both central body (CB) and protocerebral bridge (PB) are recognizable structures in the larva already (L5, **Figure 4**). Based on anti-synapsin-immunoreactivity, the PB consists of two separate neuropils and retains this layout up to adulthood. At P3, the two parts of the PB elongate horizontally and also undergo the two main movements in the central brain (see **Figure 3**). The CB thickens, but shows no signs of subdivisions. At P7 the two subdivisions of the CB, the lower (CBL) and upper (CBU) subunit can be discerned. Since the CB

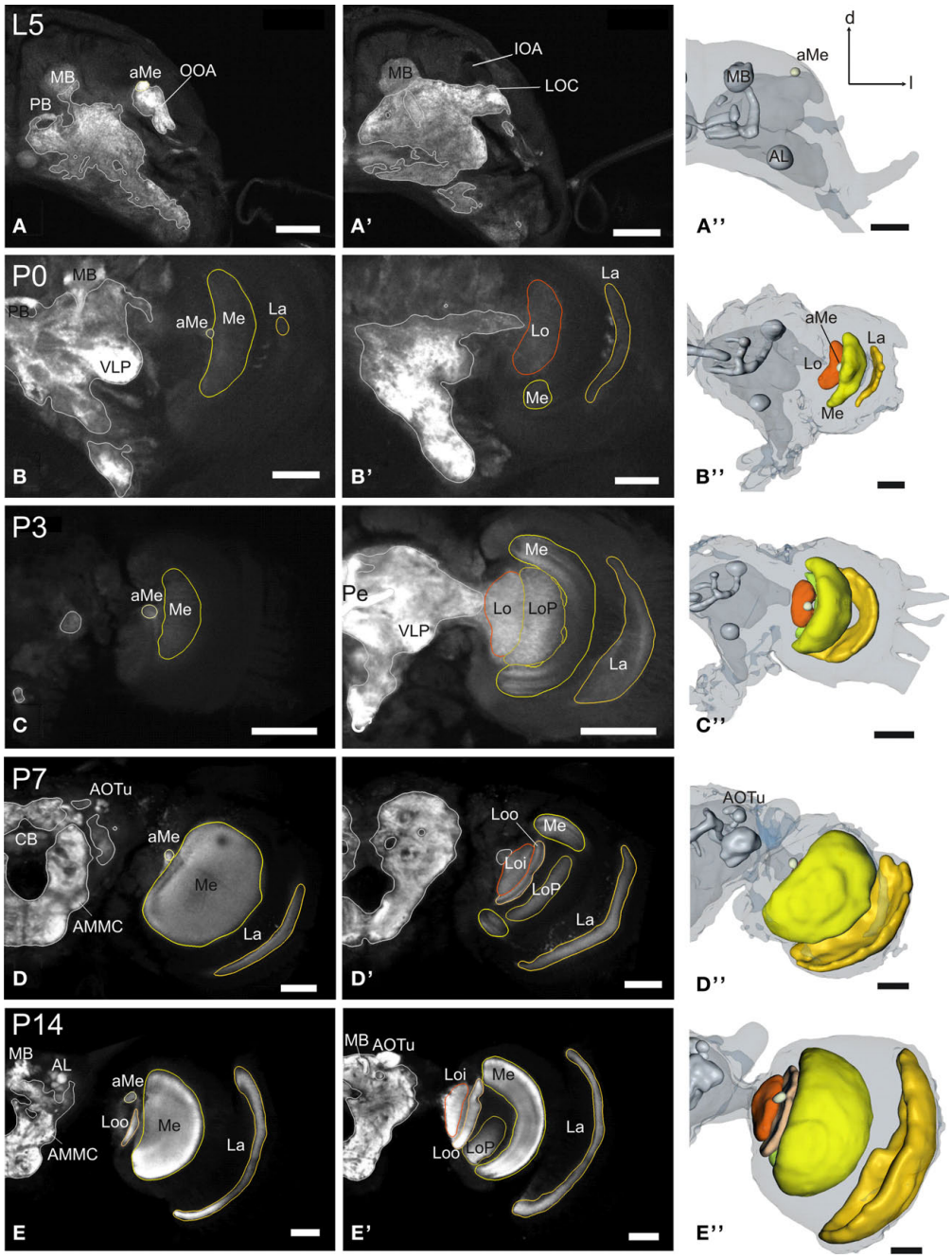

FIGURE 1 | Development of the adult optic lobe. Single optical sections in the frontal plane at different depths, anti-synapsin immunostaining (left two columns). Right column, 3D reconstructions (frontal views). **(A–A″)** Last larval stage (L5): the larval optic center (LOC) is hardly distinguishable from the midbrain neuropil (gray line). The accessory medulla (aMe) is part of the LOC. IOA, inner optic anlage; OOA, outer optic anlage. **(B–B″)** Stage P0: the ribbon-like adult neuropils lamina (La), medulla (Me) and lobula (Lo) show faint anti-synapsin staining. The aMe is separated from the midbrain neuropil and stays close to the antero-medial rim of the Me. Note the strong anti-synapsin immunoreactivity in the ventrolateral protocerebrum (VLP). **(C–C″)** Stage P3: the La and Me further expand and the dorsal and ventral tips of the La bend behind the Me. The lobula plate (LoP) appears between Me and Lo. The anti-synapsin staining gains intensity in all neuropils; layers of the Me become recognizable. **(D–D″)** Stage P7: the inner and outer lobula (Loi, Loo) can be separated. The La starts to exhibit its bowl-like appearance, the opening still tilted towards the anterior side. **(E–E″)** Stage P14: all optic lobe neuropils reached their final adult positions. Orientation bars: d, dorsal; l, lateral; scale bars: 100 µm **(A–B″)**; 200 µm **(C–E″)**.

also underwent the rotation of the brain, the CBL is – now counter intuitively – in an antero-dorsal position to the CBU. The noduli (No) appear antero-ventrally to the CB. The two halves of the PB grow closer together, but stay untouched. Their lateral ends now point postero-ventrally in their final orientation. After P7 the central complex remains in its position and undergoes further size increase.

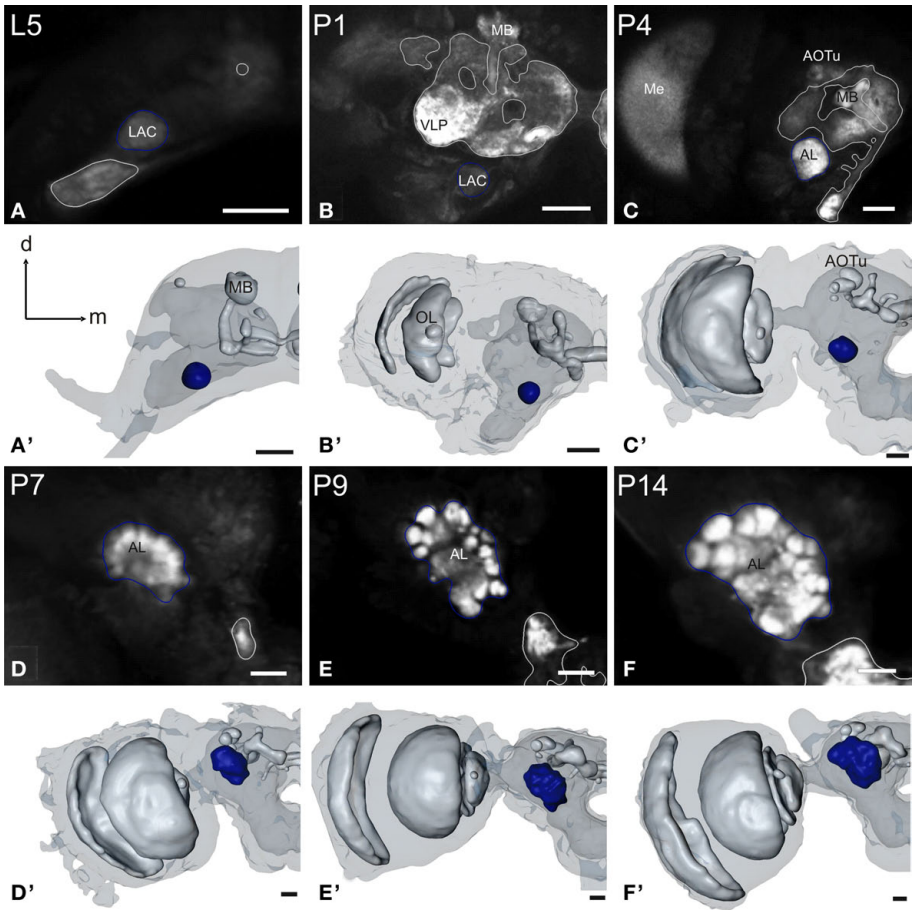

FIGURE 2 | Development of the antennal lobe. Single optical sections in the frontal plane, anti-synapsin immunostaining (first and third row). Second and fourth row, 3D reconstructions (frontal views). **(A–A′)** The larval antennal center (LAC) exhibits no glomerular organization in *Manduca sexta* L5 larva. **(B–B′)** Strong anti-synapsin immunoreactivity is visible in the ventro-lateral protocerebrum (VLP), compared to the weak labeling in the LAC/AL. **(C–C′)** Stage P4: the developing AL becomes recognizable in the anti-synapsin staining. Note the ventral position of the AL compared to stage P7. **(D–D′)** Stage P7: glomerular structures surrounding a coarse neuropil become first visible. **(E–E′)** Stage P9: single glomeruli become discernible structures and achieve their final position within the AL. The dorsal migration of the AL ends. **(F–F′)** Stage P14: glomerular and AL volume increased compared to stage P9. Orientation bars: d, dorsal; m, medial; all scale bars: 100 μm.

The larval brain houses no anterior optic tubercle (AOTu, not shown), its three subcompartments become discernible structures in the antero-dorso-lateral midbrain around P4 (**Figure 5**): the upper (uAOTu), lower (lAOTu), and the nodular subunit (nAOTu). Also the characteristic four nodules of the nAOTu become visible at the same time (**Figure 5A**). Interestingly, the brain rotation events around P7 leave all subunits of the AOTu relatively untouched; they remain in their position and increase in size. Further increasing in size, the uAOTu remains the largest subunit throughout metamorphic development.

The antennal mechanosensory and motor center (AMMC) is another neuropil region in the developing brain, but did not fulfill the criterion of clearly identifiable borders in all three dimensions, thus we refrained from including it into our reconstructions. The same is true for several other brain regions; most noteworthy are the dorsal and lateral protocerebrum. No clear-cut boundaries make a judgment on their developmental size increase and potential rotational movements rather ambiguous. In general, these brain regions tend to be underrepresented in the literature. This is a well-known problem of brain anatomy and has recently been addressed in the fruit fly (Otsuna and Ito, 2006).

TIME COURSE OF NEUROPIL DEVELOPMENT

The anti-synapsin based immunostainings clearly show different time scales for the development of the various neuropils (**Figure 8**). Most neuropils including the aMe, the MB, the central body, and the protocerebral bridge were already present in the 5th larva. These neuropils changed during pupal development by (1) becoming more differentiated (e.g. the MBs obtain two additional lobes), (2) change of position (e.g. rotation of the MB), and (3) increase of volume. Other neuropils including the compartments of the optic lobes and the noduli are newly formed during this process. In the case of the first integration center for olfactory information, the LAC gets replaced by the AL (Kent et al., 1987; Jefferis et al., 2004).

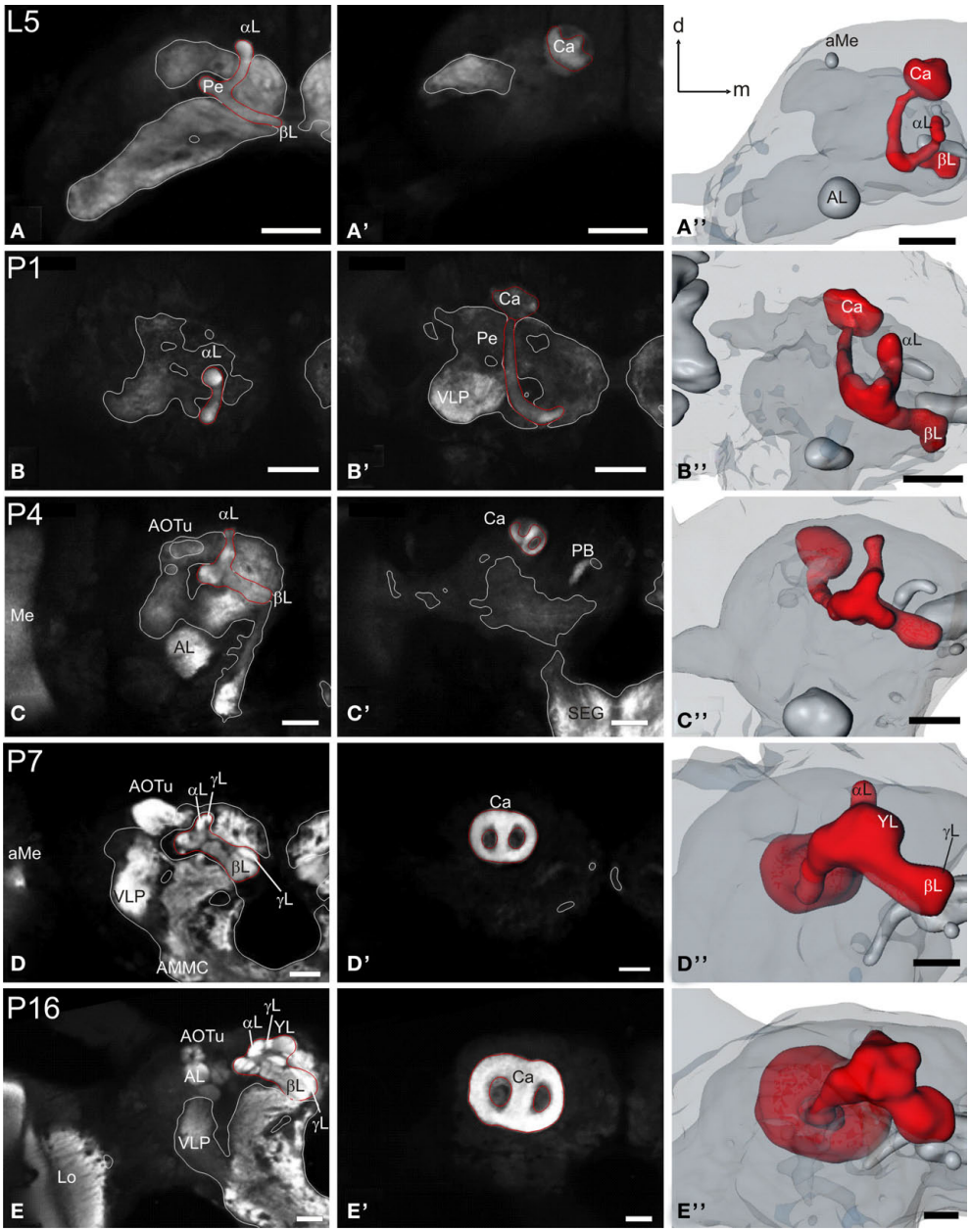

FIGURE 3 | Development of the mushroom body. Single optical sections in the frontal plane at different depths, anti-synapsin immunostaining (left two columns). Right column, 3D reconstructions (frontal views). **(A–A″)** Rather thin α-and β-lobes (αL, βL) and a slender peduncle are characteristic for the larval (L5) mushroom body (MB). The peduncle of the larval MB is oriented antero-ventrally, with a slight inclination of the calyces (Ca) to the dorsal midline. While the αL points antero-dorsally, the βL extends medially in the horizontal plane. **(B–B″)** early pupae (P1): the peduncle shows a straightened orientation. **(C–C″)** Stage P4: the MB tilts from a ventro-dorsal orientation to a more antero-posterior orientation. **(D–D″)** Stage P7: the MB is oriented antero-posteriorly and has massively increased in size compared to stage P4. Additionally to the αL and βL, the γ-lobe (γL) and the Y-lobe (YL) appear as protrusions on the MB. **(E–E″)** Stage P16: the MB reached its final adult orientation and shape. Orientation bars: d, dorsal; m, medial; all scale bars: 100 μm.

The first wave of new neuropil development already starts in the larval stage including most neuropils of the optic lobe (La, Me, Loi). Those neuropils are laid out in the inner and outer optic anlagen, which slowly aquire anti-synapsin staining during continuous growth in the early pupal stages. The lobula plate and the AMMC gradually appear with the onset of pupal development, whereas the noduli and the subunits of the AOTu are not seen before P4 (**Figure 8**). Between P4 and P7 the last structures which were included in this study appeared as separate neuropils. All are without exception subdivisions of already existing neuropils: the outer lobula separates from the inner lobula, the γ- and Y-lobe protrude from the mushroom body lobes, and the lower unit of the central body becomes discernible. Basically, after one third of metamorphic development all examined neuropils are already present. The ongoing two-thirds

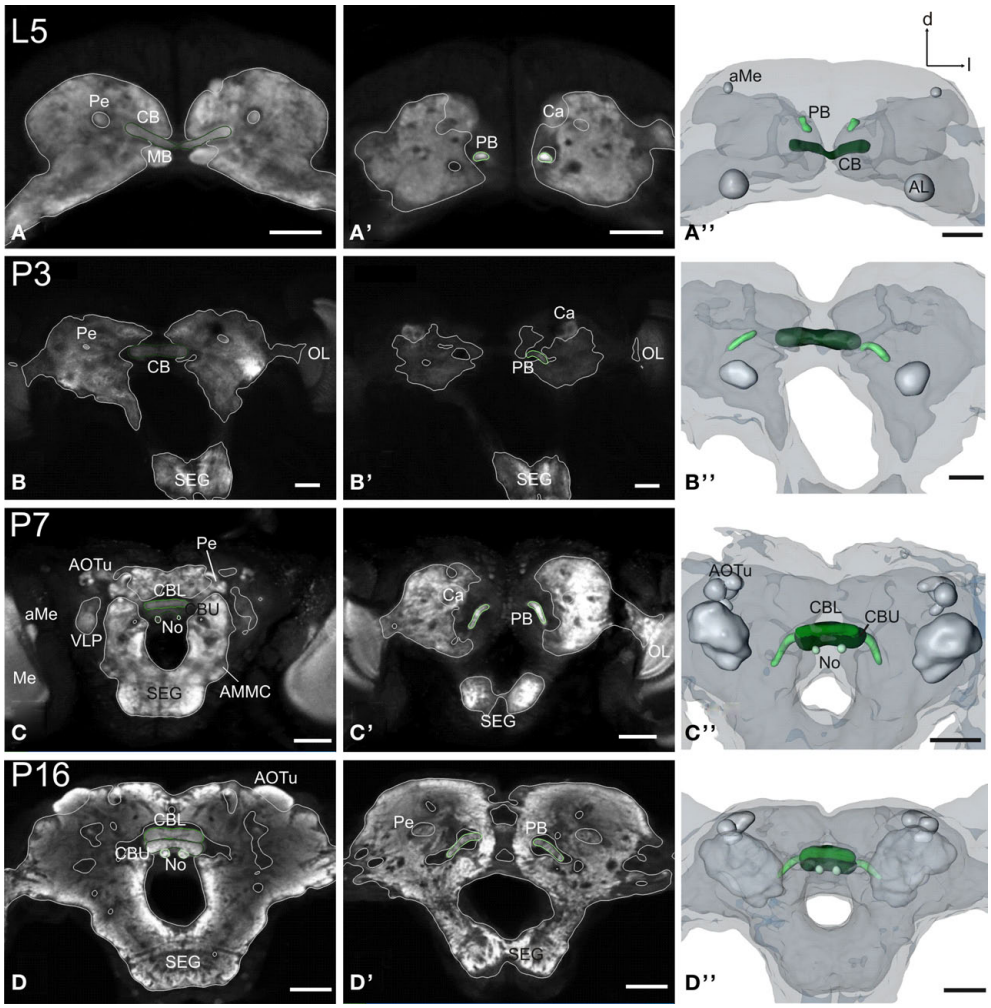

FIGURE 4 | Development of the central complex. Single optical sections in the frontal plane at different depths, anti-synapsin immunostaining (left two columns). Right column, 3D reconstructions (frontal views). **(A–A″)** Central body (CB) and protocerebral bridge (PB) are present in the L5 larva. The PB consists of two separate neuropils and retains this layout up to adulthood. **(B–B″)** Stage P3: the two parts of the PB elongate horizontally while the CB becomes thicker. **(C–C″)** Stage P7: a lower (CBL) and upper (CBU) subunit are discernable. The noduli (No) appear antero-ventrally of the CB. The PB reaches its final position with its lateral ends pointing postero-ventrally. **(D–D″)** Stage P16: the central complex has further increased in size. Orientation bars: d, dorsal; l, lateral; scale bars: 100 µm **(A–B″)**; 200 µm **(C–D″)**.

of pupal development exhibit neither major structural changes nor additional translational movements of neuropils, but rather massive increase in size.

Analysis of the volume increases of each of the examined neuropils reveals that all neuropils start with massive growth at around stage P3/P4 (**Figure 7**). Thus, in contrast to the onset of the synapsin signal, which differed between the neuropils, the onset of the massive volume increase starts at about the same developmental time for all neuropils.

4D VISUALIZATION IN CINEMA 4D

To summarize all described changes in relation to position, shape and size of the individual neuropils, we generated an animation of the metamorphosing *M. sexta* female brain (**Movie S1** in Supplementary Material). As an initial point of the animation we choose the last instar brain (L5) and animated the development of the brain during metamorphosis until the adult stage A0. For the 4D visualization, we animated the development of the individual neuropils including their subunits and additionally the brain surfaces which we also labeled during 3D reconstructions and which were also standardized in the *M. sexta* standard brain (el Jundi et al., 2009). For the animation of individual neuropils and the brain surface we used the 3D reconstructed surface models which were for each developmental stage created in Amira (**Figure 9**). Beside these individual brains we also used as the final point of the animation the female standard brain of *M. sexta* (el Jundi et al., 2009). To ease calculations we reduced the number of the polygons of the surface models in AMIRA and exported every brain as drawing exchange format (.dxf) file. The surface models or brain polygon models of the selected brains which are shown in **Figure 6** were then imported in the software program Cinema 4D where the virtual animation of the brain development was generated. To further simplify the

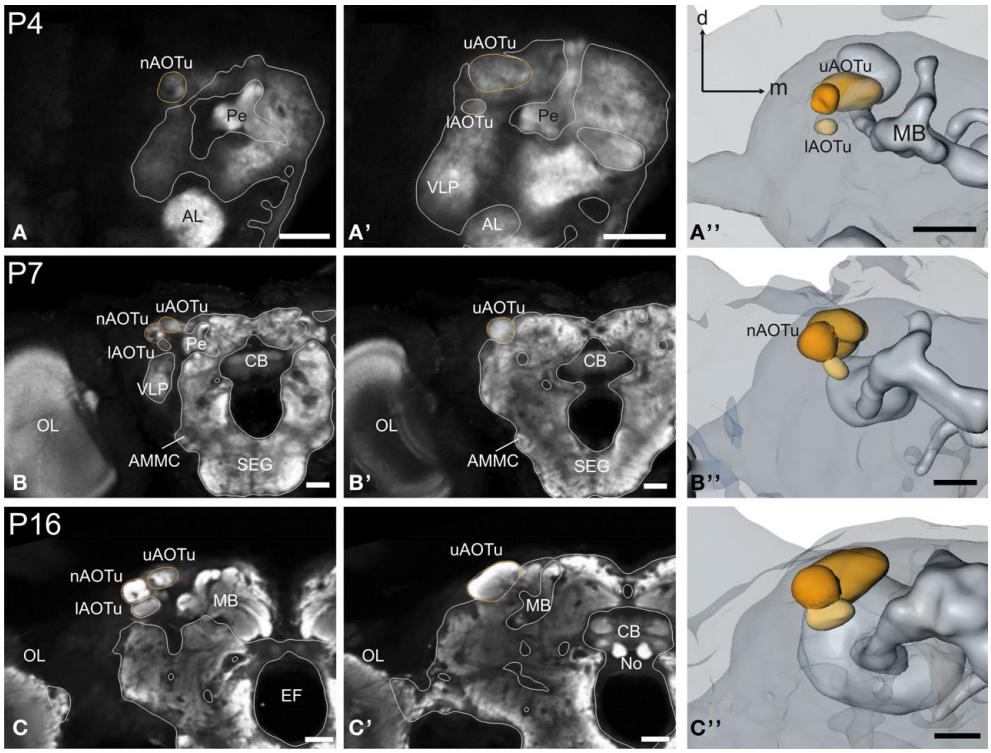

FIGURE 5 | Development of the anterior optic tubercle. Single optical sections in the frontal plane at different depths, anti-synapsin immunostaining (left two columns). Right column, 3D reconstructions (frontal views). **(A–A″)** Stage P4: all three subcompartments of the anterior optic tubercle (AOTu) become discernible structures in the antero-dorso-lateral midbrain: the upper (uAOTu), lower (lAOTu), and the nodular subunit (nAOTu). **(B–B″)** Stage P7: independent of the rotation events of mushroom bodies (MBs) and the central complex, the subunits of the AOTu stay in their position and increased in size. **(C–C″)** Stage 16: all subunits of the AOTu increased further in size. The uAOTu remains the largest subunit throughout metamorphic development. Orientation bars: d, dorsal; m, medial; all scale bars: 100 µm.

necessary calculations in the software, only one brain hemisphere of the bilateral symmetrical *M. sexta* brain (except the subunits of the central body) was animated and subsequently mirrored for the movie. Also, pedunculus and calyx were integrated to one polygonal model with the tool *Connect*. Next we defined the length of the animation using the taskbar *Timeline* (**Figure 9**). To attribute crucial substages (i.e. P7/8), the timeline was subdivided in 41 "stages", each 35 frames long, thus giving 1435 frames for the 4D animation. To define the L5 larval brain as the initial brain, we selected this brain and set a *Key* in the timeline at frame 0 (**Figure 9**). Basic structures with only few polygons like a sphere can easily be morphed in a cube with the module *Morph*. Because of the complexity of the neuropil structures it was not possible to create the 4D visualization with this module. During the animation the program does not allow a change of the number of polygons. Because some adult neuropils are not present in the larval brain, we first scaled down the adult brain onto the larval brain and reduced non-existent neuropils to point-size. This downscaled brain, adapted to fit the shape of the L5 brain, was then used as a starting point for the subsequent morphing process. All neuropils of all brains were displayed as grid polygonal models using the tool *Display*, except of the starting brain which was displayed as a polygonal surface model (**Figure 9A**). During the morphing process, only the starting brain, which was morphed from one stage to the next, and the brain of the next corresponding developmental step were visible. With the tool *Model* the localization of every neuropil of the starting brain was positioned approximately in the center of the corresponding neuropil in the brain of the next reconstructed developmental stage. These positional changes of individual neuropils were then saved by setting a *Key* in the *Timetable* to the adequate frame number. Then the polygon edges were made selectable with the tool *Point Selection* and with the tool *Magnet* the polygons of every neuropil of the starting brain were manually adapted to fit the polygons of the neuropil of the next reconstructed brain in the developmental time line. Changes in size and shape of the neuropils were again saved by a *Key* in the *Timetable*. Beside this changes in shape and size we also rotated the structures, for example the mushroom bodies. For every modification (scaling, rotating, positioning and shaping) a *Key* was set in the *Timeline* and the neuropils of the starting brain were slowly morphed step by step to eventually match the adult A0 brain. The temporal progress in relation to size, rotation and position of the structures between two *Keys* is sigmoid by default in Cinema 4D (**Figure 9B**). The temporal progress of the rotation, scale and position of the animation between all *Keys* is visible in the *Timeline* window as f-curves. To better fit the observed developmental changes between the stages into the temporal progress, we used additional *Keys* between these *Keys* in the f-curves (**Figure 9B′**). After creation of the 4D visualization we exported the 1435 images

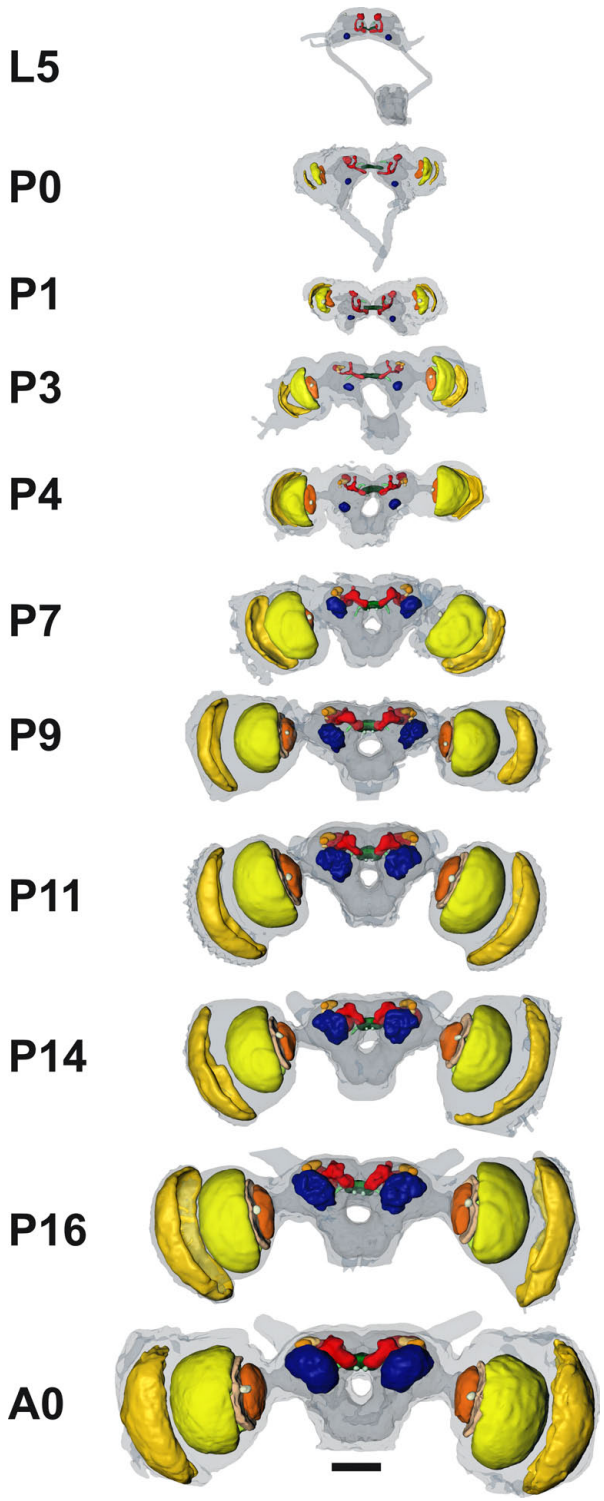

FIGURE 6 | 3D brain reconstructions of representative developmental stages. Most conspicuous are the prominent overall size increases (especially in the optic lobes) and the fusion of the subesophageal and supraesophageal ganglion. Note the outward tilting movement of the mushroom bodies, together with a backward rotation. These brains represent the reference points for the 4D visualization (**Movie S1** in Supplementary Material). Anterior view; scale bar: 500 µm.

from Cinema 4D as Targa image file format (.tga). Thereby image data were rendered with 1280 × 1024 pixel resolution. To obtain a high-quality animation of brain development we imported these 1435 images in the freeware Virtual Dub (v. 1.9.7., http://www.virtualdub.org) and created an Audio Video Interleave file (.avi) movie. Thereby we defined the frame rate to 25 frames per second, so that the 4D animation of the brain development has a length of 57.4 s. To reduce the file size of this movie we converted this movie with a DIVX-converter to a divx-video format. The 4D animation of the brain development of *M. sexta* from anterior is shown in **Movie S1** in Supplementary Material.

DISCUSSION

The development of a brain is a highly complex process in space and time. Eventually, all brain neuropils are formed, become located in their correct position and the connections between the neuropils are organized in a correct way. Owing to the amount of different neuropils and the different time lines, it is a challenge to envisage and may be even quantify such a process in its entirety. With the current paper, we present a feasibility study which offers a strategy to visualize the development of brain neuropils. For this purpose we 3D reconstructed selected brain neuropils of selected stages during brain metamorphosis of the sphinx moth *M. sexta* and transferred the 3D-surface data into the animation program Cinema 4D. Advances in imaging techniques, 3D reconstruction software, and computer power led to 3D reconstructions of many brain areas and especially in insects led in some cases even to standardized brains to relate individual variations (*Drosophila melanogaster:* Rein et al., 2002; Jenett et al., 2006; the honeybee *Apis mellifera:* Brandt et al., 2005; the desert locust *Schistocerca gregaria:* Kurylas et al., 2008; two moth species: *M. sexta* (el Jundi et al., 2009) and *Heliothis virescens* (Kvello et al., 2009); the red flour beetle *Tribolium castaneum*: Dreyer et al., 2010). However, an animation of developing brain areas based on 3D-reconstructions from consecutive developmental stages has so far not been produced.

Development of most of the brain areas of *M. sexta* that we reconstructed has been described under various aspects in several publications over the years. In the following discussion, we first want to briefly compare the results of our study with the published data and then evaluate the used strategy and technique for a better understanding of developmental processes.

OPTIC LOBES

The optic lobe is a highly retinotopically ordered neuropil that consists of three distinguishable neuropils, most distally the lamina, followed by the medulla and the lobula complex (Bullock and Horridge, 1965; Strausfeld, 1976; Homberg, 1994). In *M. sexta*, the optic anlagen, from which the optic lobes develop, are readily apparent in the third larval instar (Monsma and Booker, 1996). Similar to other insects, the outer optic anlagen give rise to the neurons of the lamina and the medulla and the inner optic anlagen give rise to the neurons forming the lobula neuropils (Nordlander and Edwards, 1969). Faint synapsin immunostaining revealed the presence of the lamina, medulla, and lobula at stage P0. As we did not reconstruct brains of late wandering larva, these neuropils could have been present already earlier. At stage P3 the lobula plate appears and additionally the intensity of the synapsin staining increased

in all optic neuropils including clear layers within the medulla. This result suggests that massive synaptogenesis starts around P3 which is very likely correlated with the incoming axons of the photoreceptor cells starting at P2/3 (Monsma and Booker, 1996). An earlier study, which postulated expression of superoxide dismutase (SOD) as an indicator for neurons forming their synapses, found high levels of transient SOD staining in many optic lobe neurons starting around stage P2/3 and ending at different times during metamorphic development (Schachtner et al., 2004a). In parallel to the increasing synapsin and SOD signal, the optic neuropils start from stage P3 with a more or less linear growth up to adult size (A0, **Figure 7**). Regulated by the increasing hemolymph titer of 20-hydroxyecdysone, mitotic activity in the outer optic anlagen abruptly ceases at P6 with some mitotic cells up to P10 and from P8 to P10 neuroblasts of the outer optic anlagen undergo programmed cell death (Monsma and Booker, 1996; Champlin and Truman, 1998b). Also, the last axons of retinal photoreceptor axons reach the lamina at stage P6 (Monsma and Booker, 1996). In summary, these data suggest that the linear increase of the lamina and the medulla volumes between P3 and P6 is driven by several factors including ingrowing axons of photoreceptor cells from the retina, synaptogenesis between the different partners, general neuronal growth, and neurogenesis. The stop of photoreceptor axon arrival and the abrupt cease of neurogenesis are not mirrored in the observed growth rate. Thus, the linear growth following stage P6 must be driven by other mechanisms which reflect the maturation of the neuronal network within lamina and medulla.

The adult accessory medulla is connected to the adult remnants of the larval photoreceptors, the stemmata (Lampel et al., 2005), pointing towards the larval optic neuropils as developmental origin of the accessory medulla. This larval origin was claimed for *Papilio* (Ichikawa, 1994); an idea originally brought up for the accessory lamina and medulla in neuropteroids (Ehnborn, 1948).

ANTENNAL LOBES

The paired antennal lobes (ALs) are the first central integration centers for the odor information in the insect brain (reviewed in Schachtner et al., 2005). During metamorphosis the adult ALs, which in *M. sexta* consist of about 60 olfactory glomeruli develop from an aglomerular larval antennal center (LAC; for a review see Tolbert et al., 2004). In *Drosophila* and in *M. sexta* the LAC is replaced by the adult AL (Kent et al., 1987; Jefferis et al., 2004). In both species, neuron populations which innervate the LAC persist through metamorphosis and build together with new born neurons the adult AL

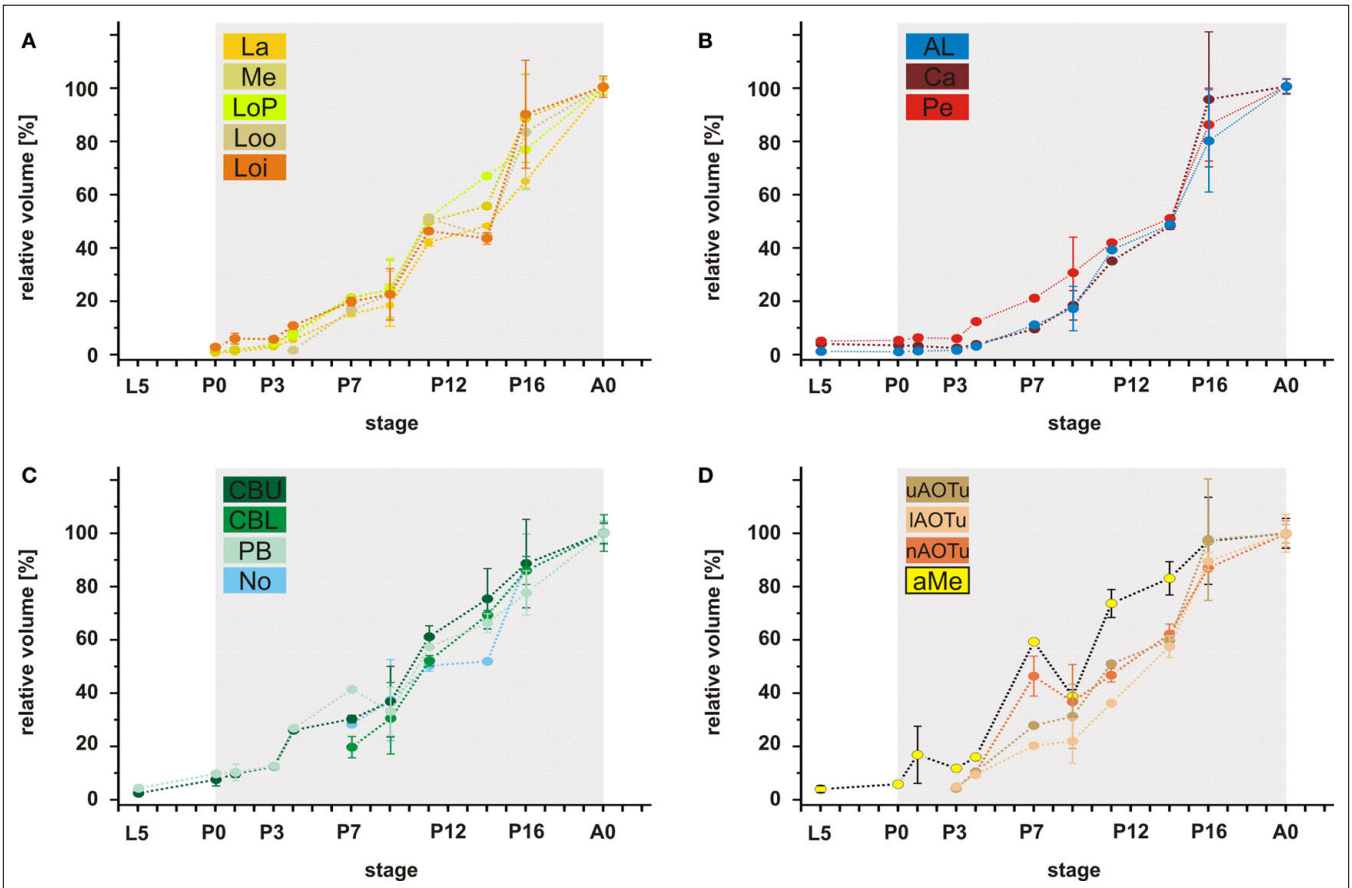

FIGURE 7 | Relative volumes of the examined neuropils. (A) The optic lobe neuropils; **(B)** The antennal lobes and the mushroom bodies; **(C)** The central complex; **(D)** The anterior optic tubercle and the accessory medulla. For each data point values of two brains are used (only for P4; $n = 1$). For bilateral neuropils, the means of the volumes of the individual animal were used. Deviation bars, standard errors. La, lamina; Me, medulla; LoP, lobula plate; Loo, outer lobula; Loi, inner lobula; AL, antennal lobe; Ca, calyx; Pe, pedunculus; CBU, upper unit of the central body (CB); CBL, lower unit of the CB; PB, protocerebral bridge; No, nodule; uAOTu, upper anterior optic tubercle (AOTu); lAOTu, lower AOTu; nAOTu, nodular subunit of the AOTu; a Me, accessory medulla.

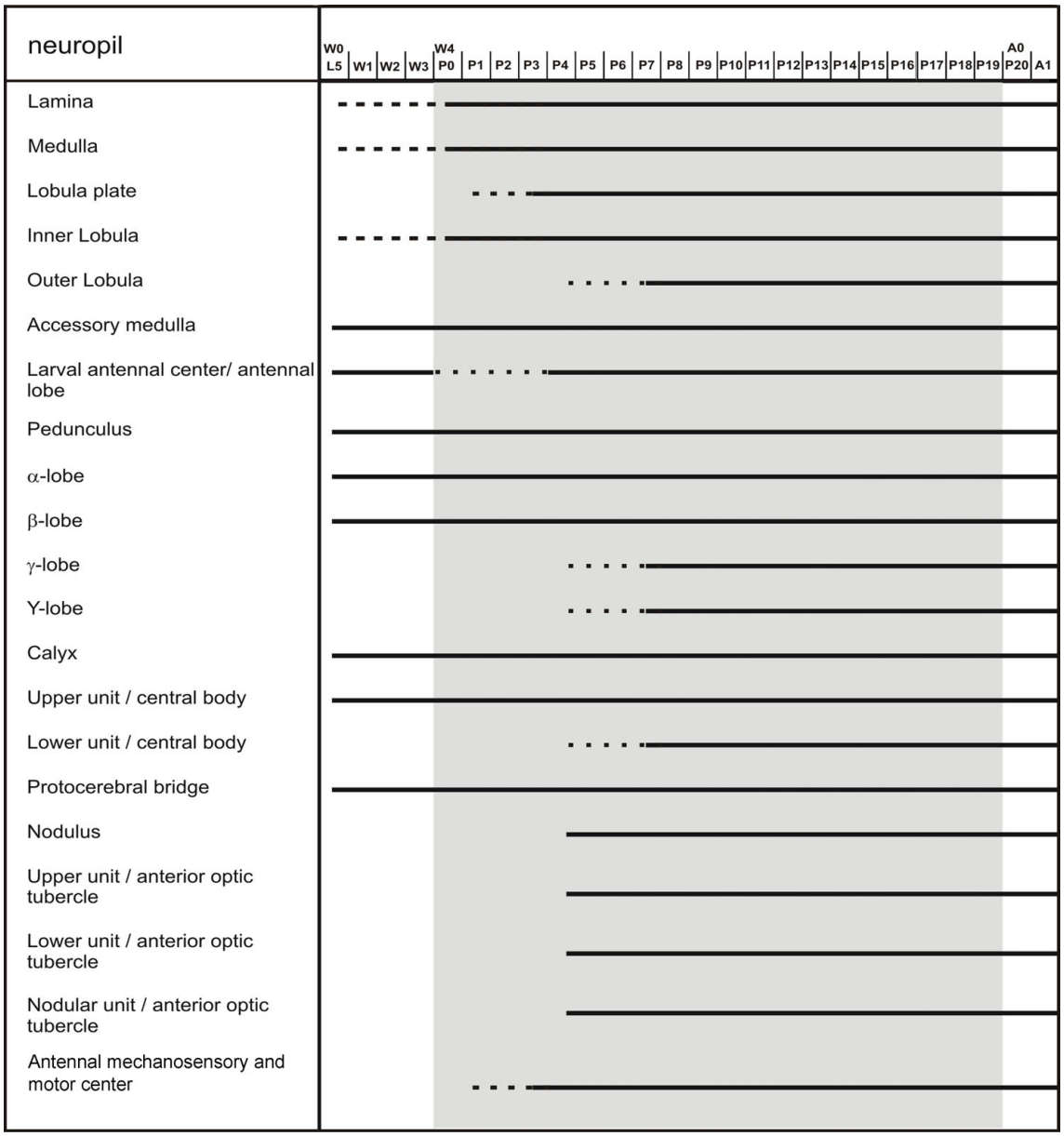

FIGURE 8 | Scheme of brain neuropil development. The scheme, based on anti-synapsin immunostaining, reflects the developmental time course of the individual neuropils. Dotted lines represent the gradual appearance of a neuropil, or, in case of the larval antennal center, its transition into the antennal lobe.

circuit (Homberg and Hildebrand, 1994; Schachtner et al., 2004b; Marin et al., 2005; Utz and Schachtner, 2005; Utz et al., 2008). In a recent study the metamorphic development of the *M. sexta* ALs has been monitored using an antiserum against synaptotagmin, another ubiquitous synaptic vesicle protein (Dubuque et al., 2001). The findings of the current study using an anti-synapsin antiserum clearly resemble the findings of this earlier study. Dubuque et al. (2001) divided AL development into three phases. The preparation phase (phase I) lasts about 7–8 days beginning at pupal formation. It includes the birth of all AL neurons, the arrival of the axons of the olfactory receptor neurons from stage P3 to P10 in the ALs, and the formation of the protoglomeruli, the sites where the glomeruli form during phase II. The glomeruli formation phase (phase II) lasts about 5 days and is characterized by massive synaptogenesis between the involved neurons. It is assumed, that during phase II a basic network of synaptic contacts within and between the glomeruli is established, which ensures the principal correlation of input and output components of the AL (Dubuque et al., 2001). In contrast to phase II, in phase III, which lasts about 8 days up to adult eclosion, only little synaptogenesis occurs. During this last phase, the glomeruli grow in size between 40 and 130% (Huetteroth and Schachtner, 2005). This is probably because of the increasing neurite diameters, and the synaptic wiring in the glomeruli is thought to undergo further refinement and maturation (Tolbert et al., 1983; Tolbert, 1989; Dubuque et al., 2001). The volume curve mirrors the three phases (**Figure 7**). Volume increase starts at stage P3. At

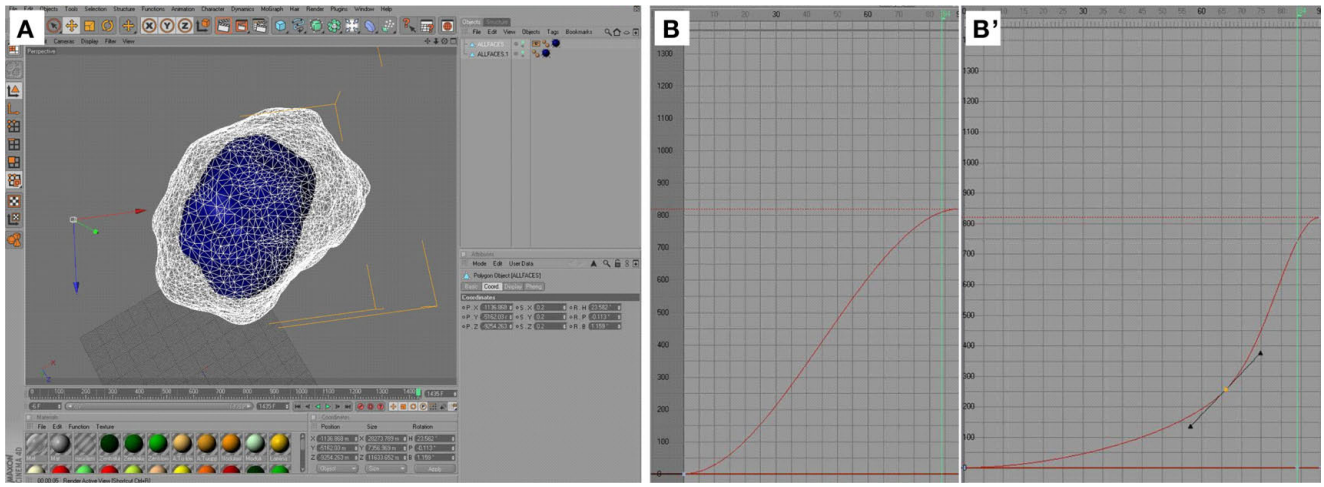

FIGURE 9 | Cinema 4D user interface – animation of the visualization. **(A)** Interactive mode in Cinema 4D; the center of the adult antennal lobe (A0, white, polygon grid view) is registered semi-automatically with the center of the P16 antennal lobe (blue, polygon surface view). Subsequently, the polygons are adjusted manually to match the shape of the corresponding preceding neuropil. **(B–B')** Detail of the timeline window; the *f*-curve (red) represents the relative position (*y*-axis) of a certain neuropil in relation to frame number (*x*-axis) between two key points. By default, this curve is sigmoidal **(B)** and needs to be adjusted manually by adding another key point (yellow, **(B')**).

stage P7 the growth rate goes up and after P11/12, there seems to be a reduction in growth rate which is then increasing again. We are aware that we only reconstructed two brains per stage and that the results have to be judged under this prerequisite. An upward movement of the antennal lobes beginning at stage P3 has been described by Homberg and Hildebrand (1994). Our study gives a much more exact time course for this movement of the developing antennal lobes which starts at P3 and ends at stage P9.

MUSHROOM BODIES

Mushroom bodies (MBs) are generally associated with higher integration processes and learning (e.g. Menzel, 2001; Heisenberg, 2003), but might also serve a general function in the control of behavior (e.g. Huber, 1955a,b; Erber et al., 1987; Zars, 2000; Strausfeld et al., 2009). In Lepidoptera larva, the opening of the MB calyces point to the dorsal surface of the brain and the α-lobe is oriented frontally but in contrast to other insects the MBs rotate backwards during metamorphic development (Nordlander and Edwards, 1968; Homberg and Hildebrand, 1994). As expected from the description of Homberg and Hildebrand (1994), the dorsal rotation starts around stage P3. Our data reveal additionally that the MBs reach their adult position at P7. Growth of the pedunculi is nearly linear from P3 to adult eclosion. The calyces in contrast also start to increase their volumes, but cease growth between P9 and P14 before they reenter a growth rate similar to the growth rate before stage P9. Adult MBs are formed by adding new Kenyon cells to the larval MBs (e.g. Panov, 1957; Nordlander and Edwards, 1970; Technau and Heisenberg, 1982; Ito and Hotta, 1992; Lee et al., 1999; Zhao et al., 2008) and the larval Kenyon cells are reorganized during metamorphosis (e.g. Technau and Heisenberg, 1982; Ito and Hotta, 1992; Lee et al., 1999). Metamorphic MB development has so far not been examined in *M. sexta* and thus, it is not known when neurogenesis and reorganization of larval neurons occur. Schachtner et al. (2004a) described strong SOD expression starting around stage P3/4 and ending at stage P16. The SOD expression occurs in different Kenyon cell clusters and might indicate synapse formation between the different Kenyon cells during this time. After P16, other factors than synaptogenesis might be responsible for the neuropil growth.

OTHER NEUROPILS OF THE CNS

The role of the central complex still remains elusive, but is probably best described as a central coordinating center in sensory and motor integration (for reviews see Strauss, 2002; Wessnitzer and Webb, 2006; Homberg, 2008). The central complex consists of the central body (CB) and the protocerebral bridge (PB), which are both already present in the *M. sexta* larva (Granger et al., 1989; Homberg and Hildebrand, 1994). However, the metamorphic development of the central complex in *M. sexta* has not been described so far. In contrast to adults, the larval CB consists only of an upper unit (CBU; Homberg and Hildebrand, 1994). This is consistent with larval CB morphology in other insects, including e.g. another moth, the honey bee (*Antheraea pernyi, Apis mellifera*: Panov, 1959) and two beetles (*Tenebrio molitor*: Panov, 1959; Wegerhoff and Breidbach, 1991; *Tribolium castaneum*: personal observation). Our reconstructions clearly show that the lower unit of the CB (CBL) forms between P4 and P7. Additionally, the CB and the PB rotate backwards, thus positioning the CBL anteriorly to the CBU and the PB behind the CB. This orientation is eventually reached at stage P7 and remains up to adulthood. Like other examined neuropils, the volumes of all central complex neuropils start their metamorphic growth around stage P3.

The anterior optic tubercle (AOTu) including all subunits forms around stage P4. To date, only sparse information about the functional role of the AOTu is present, but in locusts it receives input from the optic lobes (Homberg et al., 2003). Since optic lobe development precedes AOTu development, the formation of the AOTu might be initiated by subsequent afferent innervation from there.

HORMONAL REGULATION OF METAMORPHIC BRAIN DEVELOPMENT

The major developmental hormones in insects are the juvenile hormones and the ecdysteroids. Interaction between these hormones causes the switch from larval to pupal development in holometabolous insects (for a recent review see Truman, 2009). *In M. sexta*, the major circulating ecdysteroid during metamorphosis is 20-hydroxyecdysone (20E; Warren and Gilbert, 1986). Effects of 20E on metamorphic development of the nervous system of *M. sexta* have been shown in several studies: the pupal 20E peak regulates the fusion of thoracic and abdominal ganglia (Amos et al., 1996), it controls cell proliferation during genesis of the optic lobes and the retina but also programmed cell death of optic lobe neuroblasts (Champlin and Truman, 1998a,b, 2000), and the onset of the formation of the olfactory glomeruli (Schachtner et al., 2004a). The pupal 20E peak also regulates the pupal expression of tyramine β-hydroxylase, an essential enzyme for octopamine biosynthesis (Lehmann et al., 2000) and the expression of several neuropeptides in the developing AL (Schachtner et al., 2004b; Utz and Schachtner, 2005; Utz et al., 2008). The start of massive volume increase of all examined neuropils parallels the 20E hemolymph titer which starts to increase from stage P3 (**Figure 7**; Warren and Gilbert, 1986). This suggests that a low threshold of 20E is sufficient for the onset of differentiation and growth of most brain neuropils including newly formed neuropils but also persistent larval neuropils. In addition to the presence of 20E other signals are needed to coordinate the development of brain neuropils. For example, in *Manduca* and *Drosophila* ingrowing photoreceptor axons stimulate proliferation in the outer optic anlagen (Selleck and Steller, 1991; Huang and Kunes, 1996) and in the antennal lobe, ingrowing axons of the receptor neurons are needed to form the protoglomeruli, the templates for the later developing olfactory glomeruli (Oland and Tolbert, 1996). During ongoing pupal development, higher 20E thresholds are needed for further neuropil specific differentiation like the stop of mitosis and the start of neuroblast apoptosis in the outer optic anlagen (Champlin and Truman, 1998b) or the onset of glomerulus formation in the AL (Schachtner et al., 2004b).

3D DIGITAL BRAIN ATLASES AND 4D ANIMATION

This study provides 3D reconstructions of defined neuropils at different stages during metamorphosis of the sphinx moth brain. These 3D reconstructions were then used to produce a digital animation which visualizes the development of the individual neuropils in context to each other. *M. sexta* has been used for decades as a model to study metamorphic brain development but so far no anatomical atlases comparing form, volume, and position of neuropils at different metamorphic stages were available. Our study adds this anatomical information in a digital form and the 3D data sets can be provided on request. A comparison between published data on metamorphic brain development (see above) and our study clearly revealed additional new information e.g. detailed positional information and information on volume increases along the developmental timeline. Data sets like the one we provided here can be used as a basis for a growing digital framework in which all available information on different developmental steps can be provided. This can include anatomical data, ranging from gross anatomy to single cells, but also experimental data of any kind including physiological and even genetical data. The advantage of digital brain atlases or databases has been recognized by the research community and meanwhile such atlases have been introduced for vertebrate and invertebrate brains serving a wide range of purposes in basic research, but its importance also in applied medicine are obvious. For example, digital brain atlases of the human brain are available mainly based on MRI but also an increasing set of other data sources, storing information on brain variations across age and gender, comparing brains in health and disease, and providing data in large human populations (for recent reviews see Toga and Thompson, 2001; Toga et al., 2006). Among other interesting approaches including e.g. pest control and evolutionary questions, insects have a long tradition as models for basic questions in neuroscience ranging from the development of the nervous system to plasticity and memory formation. In this context digital atlases of certain insect models have been provided including standardized brains to relate individual variations. These atlases are intended as frameworks to allow the mapping of neurons provided by different researchers (Brandt et al., 2005; Kurylas et al., 2008; Kvello et al., 2009; el Jundi et al., 2010), to study genetical variations (Rein et al., 2002; Jenett et al., 2006), and in general developmental and adult plasticity (el Jundi et al., 2009; Dreyer et al., 2010). One example which nicely demonstrates the usefulness of such atlases are maps of the olfactory glomeruli of certain insects which serve as tools to study development, function and plasticity of the glomerular network (e.g. Galizia et al., 1999; Sachse and Galizia, 2003; Fishilevich and Vosshall, 2005; Skiri et al., 2005; Deisig et al., 2006; Zhang et al., 2006; Root et al., 2007; Sachse et al., 2007; Riffell et al., 2009; Staudacher et al., 2009; Varela et al., 2009).

One major advantage of 4D visualization is clearly the didactical value; watching the animated brain development allows for better comprehension of neuropil growth and movement in its temporal context. This is not only helpful for researchers coming from a different organism and who want to compare developmental processes, but also for beginners in the field and last but not least for students. Owing to increasing computer power, internet bandwidth, and accessibility, digital databases of brain architecture and function including development and 4D visualization will in the future be accessible in an interactive way via web based access. Ideally, this access is then provided via ontologies, which allows the use of these data bases not only for the specialists but also for other researchers and students.

ACKNOWLEDGMENTS

The authors thank Dr. Erich Buchner (University of Würzburg, Germany) for kindly providing the anti-synapsin antibody. The authors are also grateful to Dr. Uwe Homberg for many fruitful discussions, and Martina Kern and Torsten Bauschke for expert technical assistance. This work was supported by a DFG grant (SCHA 678/3-3) to Joachim Schachtner.

SUPPLEMENTARY MATERIAL

The Supplementary Material for this article can be found online at http://www.frontiersin.org/systemsneuroscience/paper/10.3389/fnsys.2010.00007/

REFERENCES

Amos, T. M., Gelman, D. B., and Mesce, K. A. (1996). Steroid hormone fluctuations regulate ganglionic fusion during metamorphosis of the moth *Manduca sexta*. *J. Insect Physiol.* 42, 579–591.

Amos, T. M., and Mesce, K. A. (1994). Reorganization of the ventral nerve cord in the moth *Manduca sexta* (L.) *(Lepidoptera:Sphingidae)*. *Int. J. Insect Morphol. Embryol.* 23, 21–37.

Bell, R. A., and Joachim, F. A. (1978). Techniques for rearing laboratory colonies of the tobacco hornworm, *Manduca sexta*, and pink ballworms. *Ann. Entomol. Soc. Am.* 69, 365–373.

Brandt, R., Rohlfing, T., Rybak, J., Krofczik, S., Maye, A., Westerhoff, M., Hege, H. C., and Menzel, R. (2005). Three-dimensional average-shape atlas of the honeybee brain and its applications. *J. Comp. Neurol.* 492, 1–19.

Bullock, T. H., and Horridge, G. A. (1965). Structure and Function in the Nervous Systems of Invertebrates, Vol. 2. San Francisco, Freeman.

Champlin, D. T., and Truman, J. W. (1998a). Ecdysteroid control of cell proliferation during optic lobe neurogenesis in the moth *Manduca sexta*. *Development* 125, 269–277.

Champlin, D. T., and Truman, J. W. (1998b). Ecdysteroids govern two phases of eye development during metamorphosis of the moth, *Manduca sexta*. *Development* 125, 2009–2018.

Champlin, D. T., and Truman, J. W. (2000). Ecdysteroid coordinates optic lobe neurogenesis via a nitric oxide signaling pathway. *Development* 127, 3543–2551.

Deisig, N., Giurfa, M., Lachnit, H., and Sandoz, J.-C. (2006). Neural representation of olfactory mixtures in the honeybee antennal lobe. *Eur. J. Neurosci.* 24, 1161–1174.

Dreyer, D., Vitt, H., Dippel, S., Goetz, B., el Jundi, B., Kollmann, M., Huetteroth, W., and Schachtner, J. (2010). 3D standard brain of the red flour beetle *Tribolium castaneum*: a tool to study metamorphic development and adult plasticity. *Front. Syst. Neurosci.* ***4***:*3*. doi: 10.3389/neuro.06.003.2010.

Dubuque, S. H., Schachtner, J., Nighorn, A. J., Menon, K. P., Zinn, K., and Tolbert, L. P. (2001). Immunolocalization of synaptotagmin for the study of synapses in the developing antennal lobe of *Manduca sexta*. *J. Comp. Neurol.* 441, 277–287.

Ehnborn, K. (1948). Studies on the central and sympathetic nervous system and some sense organs in the head of neuropteroid insects. *Opusc. Entomol. (Suppl.)* 8, 1–162.

el Jundi, B., Heinze, S., Lenschow, C., Kurylas, A., Rohlfing, T., and Homberg, U. (2010). The locust standard brain: a 3D standard of the central complex as a platform for neural network analysis. *Front. Syst. Neurosci.* 3:21. doi: 10.3389/neuro.06.021.2009.

el Jundi, B., Huetteroth, W., Kurylas, A. E., and Schachtner, J. (2009). Anisometric brain dimorphism revisited: implementation of a volumetric 3D standard brain in *Manduca sexta*. *J. Comp. Neurol.* 517, 210–225.

Erber, J., Homberg, U., and Gronenberg, W. (1987). Functional roles of the mushroom bodies in insects. In Arthropod Brain: Its Evolution, Development, Structure, and Functions, A. P. Gupta, ed. (New York, Wiley), pp. 485–511.

Fishilevich, E., and Vosshall, L. B. (2005). Genetic and functional subdivision of the *Drosophila* antennal lobe. *Curr. Biol.* 15, 1548–1553.

Galizia, C. G., Sachse, S., Rappert, A., and Menzel, R. (1999). The glomerular code for odor representation is species specific in the honeybee *Apis mellifera*. *Nature* 2, 473–478.

Granger, N. A., Homberg, U., Henderson, P., Towle, A., and Lauder, J. M. (1989). Serotonin-immunoreactive neurons in the brain of *Manduca sexta* during larval development and larval–pupal metamorphosis. *Int. J. Dev. Neurosci.* 7, 55–72.

Grimaldi, D., and Engel, M. S. (2005). Evolution of the Insects. Cambridge, Cambridge University Press.

Heisenberg, M. (2003). Mushroom body memoir: from maps to models. *Nat. Rev. Neurosci.* 4, 266–275.

Homberg, U. (1994). Distribution of Neurotransmitters in the Insect Brain. Progress in Zoology 40; Stuttgart, Fischer.

Homberg, U. (2008). Evolution of the central complex in the arthropod brain with respect to the visual system. *Arthropod Struct. Dev.* 37, 347–362.

Homberg, U., and Hildebrand, J. G. (1994). Postembryonic development of gamma-aminobutyric acid-like immunoreactivity in the brain of the sphinx moth *Manduca sexta*. *J. Comp. Neurol.* 339, 132–149.

Homberg, U., Hofer, S., Pfeiffer, K., and Gebhardt, S. (2003). Organization and neural connections of the anterior optic tubercle in the brain of the locust, *Schistocerca gregaria*. *J. Comp. Neurol.* 462, 415–430.

Huang, Z., and Kunes, S. (1996). Hedgehog, transmitted along retinal axons, triggers neurogenesis in the developing visual centers of the *Drosophila* brain. *Cell* 86, 411–422.

Huber, F. (1955a). Über die Funktion der Pilzkörper (*Corpora pedunculata*) beim Gesang der Keulenheuschrecke Gomphocerus rufus L. (Acrididae). *Naturwissenschaften* 20, 566–567.

Huber, F. (1955b). Sitz und Bedeutung nervöser Zentren für Instinkthandlungen beim Männchen von Gryllus campestris L. *Z. Tierpsychol.* 12, 12–48.

Huetteroth, W., and Schachtner, J. (2005). Standard three-dimensional glomeruli of the *Manduca sexta* antennal lobe: a tool to study both developmental and adult neuronal plasticity. *Cell Tissue Res.* 319, 513–524.

Ichikawa, T. (1994). Reorganization of visual interneurons during metamorphosis in the swallowtail butterfly *Papilio xuthus*. *J. Comp. Neurol.* 340, 185–193.

Ito, K., and Hotta, Y. (1992). Proliferation pattern of postembryonic neuroblasts in the brain of *Drosophila melanogaster*. *Dev. Biol.* 149, 134–148.

Jefferis, G. S., Vyas, R. M., Berdnik, D., Ramaekers, A., Stocker, R. F., Tanaka, N. K., Ito, K., and Luo, L. (2004). Developmental origin of wiring specificity in the olfactory system of Drosophila. *Development* 131, 117–130.

Jenett, A. Schindelin, J. E., and Heisenberg, M. (2006). The Virtual Insect Brain Protocol: Creating and Comparing Standardized Neuroanatomy. *BMC Bioinformatics* 7, 544.

Jindra, M., Huang, J. Y., Malone, F., Asahina, M., and Riddiford, L. M. (1997). Identification and mRNA developmental profiles of two ultraspiracle isoforms in the epidermis and wings of *Manduca sexta*. *Insect Mol. Biol.* 6, 41–53.

Kent, K. S., Hoskins, S. G., and Hildebrand, J. G. (1987). A novel serotonin-immunoreactive neuron in the antennal lobe of the sphinx moth *Manduca sexta* persists throughout postembryonic life. *J. Neurobiol.* 18, 451–465.

Klagges, B. R., Heimbeck, G., Godenschwege, T. A., Hofbauer, A., Pflugfelder, G. O., Reifegerste, R., Reisch, D., Schaupp, M., Buchner, S., and Buchner, E. (1996). Invertebrate synapsins: a single gene codes for several isoforms in *Drosophila*. *J. Neurosci.* 16, 3154–3165.

Kurylas, A. E., Rohlfing, T., Krofczik, S., Jenett, A., and Homberg, U. (2008). Standardized atlas of the brain of the desert locust, *Schistocerca gregaria*. *Cell Tissue Res.* 333, 125–145.

Kvello, P., Løvaldli, B. B., Rybak, J., Menzel, R., and Mustaparta, H. (2009). Digital, three-dimensional average shaped atlas of the *Heliothis virescens* brain with integrated gustatory and olfactory neurons. *Front. Syst. Neurosci.* 3:14. doi: 10.3389/neuro.06.014.2009.

Lampel, J., Briscoe, A. D., and Wasserthal, L. T. (2005). Expression of UV-, blue-, long-wavelength-sensitive opsins and melatonin in extraretinal photoreceptors of the optic lobes of hawk moths. *Cell Tissue Res.* 321, 443–458.

Lee, T., Lee, A., and Luo, L. (1999). Development of the *Drosophila* mushroom bodies: sequential generation of three distinct types of neurons from a neuroblast. *Development* 126, 4065–4076.

Lehman, H. K., Klukas, K. A., Gilchrist, L. S., and Mesce, K. A. (2000). Steroid regulation of octopamine expression during metamorphic development of the moth *Manduca sexta*. *J. Comp. Neurol.* 424, 283–296.

Marin, E. C., Watts, R. J., Tanaka, N. K., Ito, K., and Luo, L. (2005). Developmentally programmed remodeling of the *Drosophila* olfactory circuit. *Development* 132, 725–737.

Menzel, R. (2001). Searching for the memory trace in a mini-brain, the honeybee. *Learn. Mem.* 8, 53–62.

Monsma, S. A., and Booker, R. (1996). Genesis of the adult retina and outer optic lobes of the moth, *Manduca sexta*. I. Patterns of proliferation and cell death. *J. Comp. Neurol.* 367, 10–20.

Nordlander, R. H., and Edwards, J. S. (1968). Morphology of the larval and adult brains of the monarch butterfly, *Danaus plexippus plexippus, L. J. Morphol.* 126, 67–94.

Nordlander, R. H., and Edwards, J. S. (1969). Postembryonic brain development in the monarch butterfly, *Danaus plexippus plexippus, L.* II. The optic lobe. *Wilhelm Roux Arch. Entwickl. Mech. Org.* 163, 197–220.

Nordlander, R. H., and Edwards, J. S. (1970). Postembryonic brain development in the monarch butterfly, *Danaus plexippus plexippus L. III Morphogenesis of centers other than the optic lobes. Wilhelm Roux Arch. Entwickl. Mech. Org.* 164, 247–260.

Oland, L. A., and Tolbert, L. P. (1996). Multiple factors shape development of olfactory glomeruli: insights from an insect model system. *J. Neurobiol.* 30, 92–109.

Otsuna, H., and Ito K. (2006). Systematic analysis of the visual projection neurons of *Drosophila melanogaster*. I. Lobula-specific pathways. *J. Comp. Neurol.* 497, 928–958.

Panov, A. A. (1957). The structure of the brain in insects in successive stages of postembryonic development. *Rev. Entomol. U.R.S.S.* 36, 269–284.

Panov, A. A. (1959). The structure of the insect brain st successive stages of postembryonic development. II. The central body. *Rev. Entomol. U.R.S.S.* 38, 276–284.

Rein, K., Zöckler, M., Mader, M. T., Grübel, C., and Heisenberg, M. (2002). The *Drosophila* standard brain. *Curr. Biol.* 12, 227–231.

Riffell, J. A., Lei, H., Christensen, T. A., and Hildebrand, J. G. (2009). Characterization and coding of behaviorally significant odor mixtures. *Curr. Biol.* 19, 335–340.

Root, C. M., Semmelhack, J. L., Wong, A. M., Flores, J., and Wang, J. W. (2007). Propagation of olfactory information in *Drosophila*. *Proc. Natl. Acad. Sci. U.S.A.* 104, 11826–11831.

Sachse, S., and Galizia, C. G. (2003). The coding of odour-intensity in the honeybee antennal lobe: local computation optimizes odour representation. *Eur. J. Neurosci.* 18, 2119–2132.

Sachse, S., Rueckert, E., Keller, A., Okada, R., Tanaka, N. K., Ito, K., and Vosshall, L. B. (2007). Activity-dependent plasticity in an olfactory circuit. *Neuron* 56, 838–850.

Schachtner, J., Huetteroth, W., Nighorn, A., and Honegger, H. W. (2004a). Copper/zinc superoxide dismutase-like immunoreactivity in the metamorphosing brain of the sphinx moth *Manduca sexta*. *J. Comp. Neurol.* 469, 141–152.

Schachtner, J., Trosowski, B., D'Hanis, W., Stubner, S., and Homberg, U. (2004b). Development and steroid regulation of RFamide immunoreactivity in antennal lobe neurons of the sphinx moth *Manduca sexta*. *J. Exp. Biol.* 207, 2389–2400.

Schachtner, J., Schmidt, M., and Homberg, U. (2005). Organization and evolutionary trends of primary olfactory brain centers in Tetraconata (Crustacea + Hexapoda). *Arthropod Struct. Dev.* 34, 257–299.

Schwartz, L. M., and Truman, J. W. (1983). Hormonal control of rates of metamorphic development in the tobacco hornworm *Manduca sexta*. *Dev. Biol.* 99, 103–114.

Selleck, S. B., and Steller, H. (1991). The influence of retinal innervation on neurogenesis in the first optic ganglion of *Drosophila*. *Neuron* 6, 83–99.

Skiri, H. T., Rø, H., Berg, B. G., and Mustaparta, H. (2005). Consistent organization of glomeruli in the antennal lobes of related species of heliothine moths. J. Comp. Neurol. 491, 376–380.

Staudacher, E. M., Huetteroth, W., Schachtner, J., and Daly, K. C. (2009). A 4-dimensional represenation of antennal lobe output based on an ensemble of characterized projection neurons. *J. Neurosci. Methods* 180, 208–223.

Strausfeld, N. J. (1976). Atlas of an Insect Brain. Berlin, Springer.

Strausfeld, N. J., Sinakevitch, I., Brown, S. M., and Farris, S. M. (2009). Ground plan of the insect mushroom body: functional and evolutionary implications. *J. Comp. Neurol.* 513, 265–291.

Strauss, R. (2002). The central complex and the genetic dissection of locomotor behaviour. *Curr. Opin. Neurobiol.* 12, 633–638.

Technau, G., and Heisenberg, M. (1982). Neural reorganization during metamorphosis of the corpora pedunculata in *Drosophila melanogaster*. *Nature* 295, 405–407.

Toga, A. W., and Thompson, P. M. (2001). Maps of the brain. *Anat. Rec.* 265, 37–53.

Toga, A. W., Thompson, P. M., Mori, M., Amunts, K., and Zilles, K. (2006). Towards multimodal atlases of the human brain. *Nat. Rev. Neurosci.* 7, 953–966.

Tolbert, L. P. (1989). Afferent axons from the antenna influence the number and placement of intrinsic synapses in the antennal lobes of *Manduca sexta*. *Synapse* 3, 83–95.

Tolbert, L. P., Matsumoto, S. G., and Hildebrand, J. G. (1983). Development of synapses in the antennal lobes of the moth *Manduca sexta* during metamorphosis. *J. Neurosci.* 3, 1158–1175.

Tolbert, L. P., Oland, L. A., Tucker, E. S., Gibson, N. J., Higgins, M. R., and Lipscomb, B. W. (2004). Bidirectional influences between neurons and glial cells in the developing olfactory system. *Prog. Neurobiol.* 73, 73–105.

Truman, J. W. (1996). Metamorphosis of the insect nervous system. In Metamorphosis: Postembryonic Reprogramming of Gene Expression in Amphibian and Insect Cells, L. I. Gilbert, ed. (Orlando, Academic Press), pp. 283–320.

Truman, J. W. (2009). Hormonal control of the form and function of the nervous system. In Insect Development: Morphogenesis, Molting and Metamorphosis, L. I. Gilbert, ed. (London, Academic Press) pp. 133–162.

Utz, S., Huetteroth, W., Vömel, M., and Schachtner, J. (2008). Mas-allatotropin in the developing antennal lobe of the sphinx moth *Manduca sexta*: distribution, time course, developmental regulation, and colocalization with other neuropeptides. *Dev. Neurobiol.* 68, 123–142.

Utz, S., and Schachtner, J. (2005). Development of A-type allatostatin immunoreactivity in antennal lobe neurons of the sphinx moth *Manduca sexta*. *Cell Tissue Res.* 320, 149–162.

Varela, N., Couton, L., Gemeno, C., Avilla, J., Rospars, J. P., and Anton, S. (2009). Three-dimensional antennal lobe atlas of the oriental fruit moth, *Cydia molesta* (Busck) (Lepidoptera: *Tortricidae*): comparison of male and female glomerular organization. *Cell Tiss. Res.* 337, 513–526.

Warren, J. T., and Gilbert, L. I. (1986). Ecdysone metabolism and distribution during the pupal–adult development of *Manduca sexta*. *Insect Biochem.* 16, 65–82.

Weevers, R. D. (1966). A lepidopteran saline: the effects of inorganic cation concentrations on sensory, reflex and motor responses in a herbivorous insect. *J. Exp. Biol.* 44, 163–176.

Wegerhoff, R. and Breidbach, O. (1991). Distribution of GABA-like immunoreactivity throughout postembryogenesis of the midbrain in the beetle *Tenebrio molitor* L. (Insecta; Coleoptera). In Synapse-Transmission and Modulation, N. Elsner and H. Penzlin, eds (Stuttgart, Thieme), p. 158.

Wessnitzer, J., and Webb, B. (2006). Multimodal sensory integration in insects – towards insect brain control architectures. *Bioinspir. Biomim.* 1, 63–75.

Zars, T. (2000). Behavioral functions of the insect mushroom bodies. *Curr. Opin. Neurobiol.* 10, 790–795.

Zhang, D., Zhou, W., Yin, C., Chen, W., Ozawa, R., Ang, L.-H., Anandan, L., Aigaki, T., and Hing, H. (2006). Misexpression screen for genes altering the olfactory map in *Drosophila*. *Genesis* 44, 189–201.

Zhao, X., Coptis, V., and Farris, S. M. (2008). Metamorphosis and adult development of the mushroom bodies of the red flour beetle, *Tribolium castaneum*. *Dev. Neurobiol.* 68, 1487–1502.

Conflict of Interest Statement: The authors declare that the research was conducted in the absence of any commercial or financial relationship that could be construed as a potential conflict of interest.

Received: 16 November 2009; paper pending published: 29 December 2009; accepted: 21 February 2010; published online: 18 March 2010.

Citation: Huetteroth W, el Jundi B, el Jundi S and Schachtner J (2010) 3D-reconstructions and virtual 4D-visualization to study metamorphic brain development in the sphinx moth Manduca sexta. Front. Syst. Neurosci. ***4****:7. doi: 10.3389/fnsys.2010.00007*

frontiers in
SYSTEMS NEUROSCIENCE

ORIGINAL RESEARCH ARTICLE
published: 12 February 2010
doi: 10.3389/neuro.06.005.2010

Integration of the antennal lobe glomeruli and three projection neurons in the standard brain atlas of the moth *Heliothis virescens*

Bjarte Bye Løfaldli, Pål Kvello and Hanna Mustaparta*

Neuroscience Unit, Department of Biology, Norwegian University of Science and Technology, Trondheim, Norway

Edited by:
Randolf Menzel, Freie Universitat Berlin, Germany

Reviewed by:
Joachim Schachtner, Philipps-Universitat Marburg, Germany
Uwe Homberg, Philipps-Universitat Marburg, Germany

***Correspondence:**
Hanna Mustaparta, Neuroscience Unit, MTFS, Department of Biology, Norwegian University of Science and Technology, Olav Kyrres gt. 9, 7489 Trondheim, Norway.
e-mail: hanna.mustaparta@bio.ntnu.no

Digital three dimensional standard brain atlases (SBAs) are valuable tools for integrating neuroimaging data of different preparations. In insects, SBAs of five species are available, including the atlas of the female *Heliothis virescens* moth brain. Like for the other species, the antennal lobes (ALs) of the moth brain atlas were integrated as one material identity without internal structures. Different from the others, the *H. virescens* SBA exclusively included the glomerular layer of the AL. This was an advantage in the present study for performing a direct registration of the glomerular layer of individual preparations into the standard brain. We here present the *H. virescens* female SBA with a new model of the AL glomeruli integrated into the atlas, i.e. with each of the 66 glomeruli identified and labelled with a specific number. The new model differs from the previous *H. virescens* AL model both in respect to the number of glomeruli and the numbering system; the latter according to the system used for the AL atlases of two other heliothine species. For identifying female specific glomeruli comparison with the male AL was necessary. This required a new male AL atlas, included in this paper. As demonstrated by the integration of three AL projection neurons of different preparations, the new SBA with the integrated glomruli is a helpful tool for determining the glomeruli innervated as well as the relative position of the axonal projections in the protocerebrum.

Keywords: insect, olfaction, three dimensional reconstruction, mushroom body calyces, lateral protocerebrum

INTRODUCTION

Digital three dimensional standard brain atlases (SBAs) have been made of several vertebrate and insect species in order to integrate neuroimaging data of different preparations (Toga and Thompson, 2001; Rein et al., 2002; Toga, 2002; Van Essen, 2002; Brandt et al., 2005; Kurylas et al., 2008; el Jundi et al., 2009; Kvello et al., 2009). In insects, whole brain atlases of five species are available as suitable tools for studying the three dimensional spatial relationship between neurons innervating different brain structures (Rein et al., 2002; Brandt et al., 2005; Kurylas et al., 2008; el Jundi et al., 2009; Kvello et al., 2009). Based on confocal scans with higher resolution, separate atlases of specific brain compartments like the primary olfactory centre, the antennal lobe (AL), and the central complex involved in processing visual information, have also been made (Rospars and Chambille, 1981; Flanagan and Mercer, 1989; Stocker et al., 1990; Galizia et al., 1999; Laissue et al., 1999; Rospars and Hildebrand, 2000; Chiang et al., 2001; Berg et al., 2002; Reischig and Stengl, 2002; Sadek et al., 2002; Smid et al., 2003; Greiner et al., 2004; Huetteroth and Schachtner, 2005; Masante-Roca et al., 2005; Skiri et al., 2005; Iyengar et al., 2006; Jefferis et al., 2007; Kazawa et al., 2009; Varela et al., 2009; el Jundi et al., 2010). Thus, the neurons can be registered into these particular structures with higher precision, suitable for studying the network within the brain compartments. Recently, we have made a SBA of *Heliothis virescens* based on the iterative shape average (ISA) procedure, with the aim to spatially relate identified neurons forming the networks underlying chemosensory coding and learning in this moth species (Kvello et al., 2009). Like for all five insect brain atlases, the ALs are included as a single brain compartment without internal structures. Different from the other atlases, the AL of the *H. virescens* brain atlas includes exclusively the glomerular layer as a single labelled identity, an advantage for registering the AL glomeruli as separate units into the atlas.

Numerous studies have been devoted to the neuronal network of the primary olfactory centres, the olfactory bulb in vertebrates and the AL in insects, in trying to elucidate how olfactory information is processed and coded (Laurent et al., 1996; Hildebrand and Shepherd, 1997; Galizia and Menzel, 2000; Lledo et al., 2005; Wilson and Mainen, 2006; Stopfer, 2007; Kloppenburg and Mercer, 2008). Common for the two systems are the input elements of sensory neurons, the output elements of mitral/tufted cells and projection neurons (PNs) respectively, intrinsic local interneurons, as well as centrifugal modulatory neurons. Typical are the numerous glomeruli, spheric-ovoid structures of fine neuropils with condensations of synapses forming a neuronal network; in insects between all four elements. Each glomerulus represents a functional unit receiving information from one set of sensory neurons with the same receptor protein type and sending out the processed information to olfactory areas of higher order (Axel, 1995; Clyne et al., 1999; Vosshall et al., 1999; Buck, 2000; Mombaerts, 2001; Vosshall and Stocker, 2007). In insects, the output neurons are uni- or multiglomerular PNs with axons following one of three major

antennocerebral tracts, the inner (IACT), the middle (MACT) and the outer (OACT) in moths (Homberg et al., 1988; Rø et al., 2007). They project to the calyces of the mushroom bodies, important in learning and memory (Menzel, 2001; Heisenberg, 2003), and to the lateral protocerebrum, a premotoric area. To resolve how biologically relevant odour information is handled by the network, it is essential to determine the relevant input and output of specific glomeruli, which also require identification of the glomeruli across individuals. The atlases of the AL glomeruli of several insect species including heliothine moths have supported the early findings of constant numbers and positions. Thus, they are helpful tools in identifying the glomeruli innervated by physiologically characterised AL neurons.

In herbivorous species of Lepidoptera the AL is organised into two parallel olfactory systems, the macroglomerular complex (MGC) consisting of a few glomerular units dealing with pheromone information in male moths, and the numerous ordinary glomeruli dealing with plant odours in males and females (Anton and Homberg, 1999; Christensen and Hildebrand, 2002; Mustaparta, 2002). Due to available, identified pheromone components as well as the relative simple system, the functional organisation of the MGC is to a large extent resolved in several species, including *H. virescens*, as concerns input and output information (Berg et al., 1998; Vickers et al., 1998; Anton and Hansson, 1999; Galizia et al., 2000; Kanzaki et al., 2003; Vickers and Christensen, 2003). Knowledge about the more complex plant odour system is in general scarce, partly due to unknown relevant plant odorants. However, using chemical analyses linked to electrophysiological recordings from single units, sharply tuned plant odour receptor neurons have been well documented, particularly in *H. virescens* for which numerous primary and secondary plant odorants have been identified (Mustaparta and Stranden, 2005; Røstelien et al., 2005). These results are important in ongoing studies on the processing of plant odour information in the brain of this species. Using intracellular recordings combined with fluorescent staining we are physiologically characterising chemosensory neurons, including PNs, followed by visualisation in confocal laser scanning microscope and three dimensional reconstructions (Rø et al., 2007; Kvello et al., 2009). The neurons are subsequently registered into the SBA for spatially relating the neurons from different preparations in this common frame. In order to identify the PNs it is important to determine the glomeruli they innervate. This may be performed using the separate AL atlas. However, in order to relate the glomeruli giving input to the PNs with their output regions in protocerebrum, integration of the AL glomeruli into the SBA is required.

In this paper we present the *H. virescens* female SBA with a new model of the AL glomeruli integrated into the atlas (SBAGl), i.e. with each of its 66 glomeruli identified with a specific number. The glomeruli in the new atlas are numbered according to the AL atlases of two other heliothine species (Skiri et al., 2005). For identifying female specific glomeruli comparison with the male AL was necessary, which required a new *H. virescens* male AL atlas, included in this paper. As demonstrated by the three registered AL PNs, the SBAGl is a helpful tool for determining the glomeruli innervated as well as the relative position of the axonal projections in the protocerebrum.

MATERIALS AND METHODS

Heliothis virescens (Heliothinae; Lepidoptera; Noctuidae) pupae were imported from a laboratory culture (Syngenta, Basel, Switzerland), separated according to sex and placed in different containers in an incubator (Refritherm 6E, Struers) on a phase-shifted LD photoperiod (14:10 hours) at 22°C. Emerged adults were transferred to new containers and fed *ad libitum* on a 0.15-M sucrose solution. Experiments were performed on 3–5 days old female and male moths.

STAINING OF THE ANTENNAL LOBE AND PROJECTION NEURONS

The moths were mounted in plastic tubes and immobilised with dental wax (Kerr Corporation, Romulus, MI, USA). Cephalic scales and mouthparts were removed before decapitation. Brains were dissected in a saline solution (in mM: 150 NaCl, 3 $CaCl_2$, 3 KCl, 25 $C_{12}H_{22}O_{11}$ and 10 TES buffer, pH 6.9) and fixed in paraformaldehyde (4%) diluted in methanol (50%) over night (4°C). After rinsing in a phosphate buffered saline solution (PBS in mM: 684 NaCl, 13 KCl, 50.7 Na_2HPO_4 and 5 KH_2PO_4, pH 7.2; 10 min), preparations were dehydrated in an increasing ethanol series (50, 70, 90, 96 and 100%, 10 min each) degreased in xylol (5 min), rehydrated in a decreasing ethanol series (100, 96, 90, 70 and 50%, 10 min each) before washed in PBS (10 min) and preincubated in normal goat serum (NGS; Sigma, St. Louis, MO, USA; 10%) in PBS at room temperature (30 min). This was followed by incubation in a monoclonal antibody against the synaptic protein synapsin (SYNORF 1, kindly provided by Prof. E. Buchner, Würzburg, Germany), diluted in PBS (1:10) and NGS (10%) for 48 h (4°C). After rinsing in PBS (5 × 20 min) the preparations were incubated for 24 h (4°C) with a Cy5-conjungated goat anti-mouse secondary antibody (Jackson Immunoresearch; dilution 1:500 in PBS) before rinsing in PBS (5 × 20 min) and dehydrated in increasing ethanol series. Preparations were cleared in methyl salicylate and mounted as whole mounts in double-sided aluminium slides.

For staining of the PNs female moths were restrained and immobilised with wax with the head and antenna protruding. The cuticle between the eyes was removed, exposing the AL and the protocerebrum. Large trachea, intracranial- and antennal muscles were removed to eliminate brain and antennal movements. Neurolemma was perforated with a tungsten hook to facilitate insertion of the microelectrode prior to superfusion with saline solution. Glass microelectrodes were pulled with a Flaming-Brown horizontal puller (P97; Sutter Instruments, Novato, CA, USA), the tips were filled with dye (Micro-Ruby, Invitrogen; 4%) and backfilled with potassium acetate solution (0.2 M). The microelectrodes had a resistance of 150–400 MΩ. Neurons were iontophoretically stained by passing a 1–3 nA depolarising current of 2 Hz with 0.2 s duration. Complete labelling of the neurons required dye injection for 10–15 min. After current injection, the dye was allowed to diffuse over night at 4°C or 3 h at room temperature. The brains were dissected in saline solution, fixed in paraformaldehyde (4%) in PBS and left over night at 4°C. To intensify the staining of the labelled neurons the brains were incubated in Streptavidin-Cy3 (Jackson Immunoresearch, West Grove, PA, USA; diluted 1:200 in PBS) over night at 4°C before rinsed in PBS. Subsequently, the SYNORF1 protocol, as described above, was used on the preparations for background staining.

VISUALISATION OF THE ANTENNAL LOBE GLOMERULI AND THE PROJECTION NEURONS

Stained preparations were visualised with a laser scanning confocal microscope (LSM 510 META Zeiss, Jena, Germany). Stained AL preparations were examined using a Zeiss Plan-Neofluar 40 × 0.75 NA dry lens objective. The fluorescent dye (Cy5) was exited by a 633-nm line of argon laser and scanned with a resolution of 1024 × 1024 pixels in the *xy*-plane and an interslice distance of 2 μm (voxel size of 0.75 μm × 0.75 μm × 2 μm). Intracellular fillings were examined with a Plan-Neofluar 20×/0.5 NA dry lens objective. The intracellular dye was excited by a 543-nm Helium Neon laser and filtered through a bandpass filter BP 565-615 IR. Preparations were scanned with a resolution of 1024 × 1024 pixels in the xy-plane and an interslice distance of 2 μm. The neurons were scanned in several tiles and manually merged in Amira 4.1. To compensate for the refraction indexes of the mountant and that of the dry lens objective, the *z*-axis dimension was multiplied by a factor of 1.6.

RECONSTRUCTION AND IDENTIFICATION OF THE ANTENNAL LOBE GLOMERULI

Grey value image stacks acquired from the confocal microscope were elaborately examined section by section and glomeruli were manually labelled using the segmentation editor in Amira 4.1 (Visage Imaging, Fürth, Germany). In this process any group of voxels belonging to a particular glomerulus was given a unique label resulting in a stack of label images corresponding to the underlying confocal images. The label images were used to create 3D polygonal surface models.

INTEGRATION OF THE ANTENNAL LOBE ATLAS INTO THE STANDARD BRAIN

The digital SBA of *H. virescens* includes the ALs as models solely constituting the glomerular layer labelled as a single material identity (Kvello et al., 2009). Thus, to register the glomeruli of the AL atlas into the SBA, the separately labelled glomeruli had first to be assigned a single material identity corresponding to the AL model of the SBA. The label image stack of the AL glomeruli was then affine- and elastically registered into the corresponding label images of the SBA, i.e. corresponding points in the AL atlas and the AL model of the SBA were transformed into the same coordinates. Subsequently, the glomeruli were relabelled as separate units and given material identity and colour code according to the separate AL atlas.

RECONSTRUCTION AND REGISTRATION OF NEURONS INTO THE NEW STANDARD BRAIN ATLAS WITH GLOMERULI

Gray value image stacks of stained neurons and innervated brain structures acquired from the confocal microscope were examined and reconstructed in the computer software Amira 3.1, as described by Kvello et al. (2009). Brain structures were reconstructed as label images and neurons by using the skeleton tool (Evers et al., 2004; Schmitt et al., 2004). In general, the registration of neurons into the SBA followed the same procedure as described by Brandt et al. (2005). The label images of the innervated brain structures were affine- and elastically registered to the label images of the corresponding structures in the SBA. Then the resulting transformation parameters for the brain structures were applied to the reconstructed neurons. Since the registration of a neuron into any structure of the SBA requires the identification of the corresponding structure in the preparation, the neurons were first registered into the SBA. The SBAGl was then superposed in order to identify the innervated glomeruli. The identification was checked against the confocal images. The innervated glomeruli as well as a few other landmark glomeruli were subsequently reconstructed in the preparation and registered into the corresponding glomeruli of the SBAGl.

RESULTS

ATLAS OF ANTENNAL LOBE GLOMERULI

As expected, the synapsin-specific antibody staining gave a clear labelling of brain structures, particularly the glomeruli of the ALs (**Figure 1**).

In addition the calyces of the mushroom bodies, the optic lobes and the suboesophageal ganglion were clearly stained. Two of the three AL cell body clusters (Berg et al., 2002), the lateral and the medial, were recognised, but were not further described in this study. The results are based on confocal laser images of the glomeruli of four ALs, one right (**Figure 2**), and one left from different females and two left from different males.

Figure 3 shows the 3D reconstructions of each glomerulus in the two female and one male preparations.

The ALs of the two female specimens were compared with the female AL model and the underlying confocal images of two other heliothine moth species, *Helicoverpa armigera* and *Helicoverpa assulta* (Skiri et al., 2005), to identify corresponding glomeruli that were given the same number and colour. The same procedure was carried out for comparing and numbering the male AL glomeruli. Sex specific glomeruli of the female ALs were identified by comparing the glomeruli between the two sexes. Like in the previous studies, the primary landmarks were the antennal nerve entrance, the central large female glomerulus (cLFG), the male specific MGC, the labial pit organ glomerulus (LPOG), the adjacent large glomerulus medially of the LPOG (mLPOG), and the fibre bundles of the lateral and the medial cell clusters, LCCl and MCCl, respectively (**Figure 3**). Surrounding glomeruli of the primary landmarks served as secondary landmarks. This resulted in 4 female specific and 62 ordinary glomeruli in the AL of *H. virescens* females. In males 62 glomeruli corresponded to the ordinary glomeruli in females, whereas 5 glomeruli were male specific, including G63 and the 4 previously described units of the MGC.

FEMALE SPECIFIC GLOMERULI

The four female specific glomeruli of the *H. virescens* ALs, located at the entrance of the antennal nerve, were identified in both preparations. Centrally at the entrance is the large female specific glomerulus (cLFG) (**Figures 2D,E and 3G,H**), previously identified in Berg et al. (2002). Two other female specific glomeruli, F1 and F3, were positioned anterior of cLFG and the fourth, F2, posterior of cLFG. Compared with the other heliothine species (Skiri et al., 2005), cLFG has a similar position and size, whereas the position of F1 and F2 differs among the species. F3 is only present in *H. virescens* and *H. assulta.*

ORDINARY GLOMERULI IN FEMALES

Sixty-six glomeruli were counted in both ALs of the two individuals (**Figure 3**). Among them, 62 glomeruli corresponded to ordinary glomeruli in the AL of *H. virescens* males and of the two other heliothine species, *H. armigera* and *H. assulta*. For instance, easily

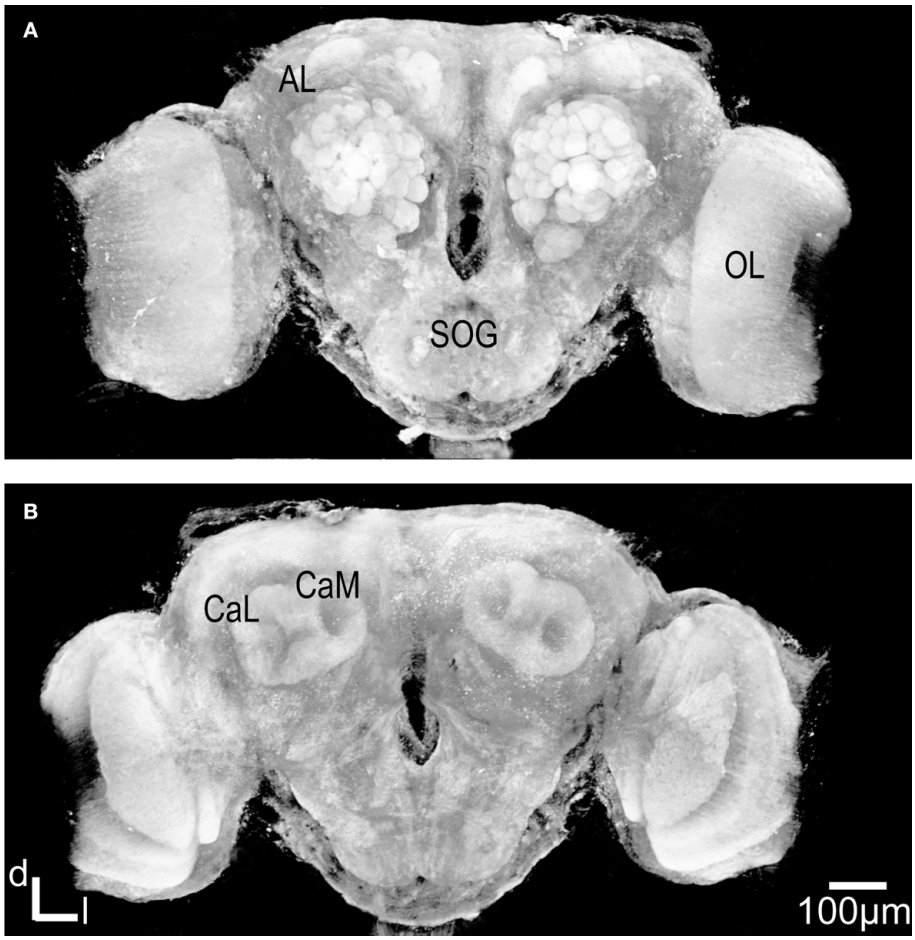

FIGURE 1 |Three dimensional visualisation of the confocal image stack of the *H. virescens* female moth brain. (A) The brain in a frontal view exposing the two antennal lobes (AL) with the numerous glomeruli. **(B)** The brain in posterior view showing the calyces of the mushroom bodies. OL, optic lobes; SOG, suboesophageal ganglion; CaL, lateral calyx; CaM, medial calyx.

recognised in all ALs are the two primary landmarks, the large LPOG and mLPOG, which are given the numbers G38 and G39, respectively, according to Skiri et al. (2005). Posterior of G39 is G53 with five dorso-medially located glomeruli, G58–G62 (**Figures 3J,K**). At the entrance of the antennal nerve, posterior of cLFG, are four recognised glomeruli G51, G52, G56 and G57. Three other glomeruli, G49, G50 and G54, are recognised most dorsal in the AL, and G37, G36 and G35 dorso-medially of the LCCl fibre bundle (**Figures 3G,H**). On the basis of these recognised and identified primary and secondary landmarks, the other 42 glomeruli were identified and given numbers according to the other heliothine atlases (Skiri et al., 2005). This is exemplified in **Figure 3**, showing the clockwise numbering of G1–G23 (**Figures 3A,B**), G24–G34 (**Figures 3D,E**), G35–G48 (**Figures 3G,H**) and G49–G63 (**Figures 3J,K**), appearing in sections from anterior to posterior. In this way, all 62 glomeruli in both *H. virescens* female preparations were found to correspond with the ordinary glomeruli in the atlases of the other heliothine species.

COMPARISON OF NUMBERS AND POSITIONS OF GLOMERULI

Whereas the number of the glomeruli was constant in the ALs of the examined specimens, some variations were found regarding positions and sizes of a few glomeruli. For instance, the position of G1 and G2 is shifted anterior–posterior in the two preparations and the size of G2 and G5 is marked larger in one preparation than in the other (**Figures 3A,B**). Other variations between the two *H. virescens* preparations are the relative positions of G25, G24 and F1 and between G28 and G38. Comparison with the previous *H. virescens* atlas, the differences concern the total number of glomeruli identified as well as the way of numbering the glomeruli. Concerning the female specific glomeruli, only two (cLFG and medially of it the mLFG) were identified by Berg et al. (2002). The eight ordinary glomeruli G11–G13, G25, G34 and G45–G47 in the present atlas were counted as four units in the previous atlas. Oppositely, G62 and G22 in the present atlas seem to be counted as four in the previous atlas. The corresponding numbers of the two atlases are presented in **Table 1**.

MALE SPECIFIC AND ORDINARY GLOMERULI

Like in females, the MGC is located at the entrance of the antennal nerve. As previously described it consists of the cumulus, the dorso-medial and the two ventral glomeruli (**Figures 3C,F**), and differs from the MGC of the two other heliothine species having only three glomeruli (Berg et al., 2002; Skiri et al., 2005). The MGC served as an additional primary landmark in the identification of the ordinary glomeruli. Using the same way of identification as in

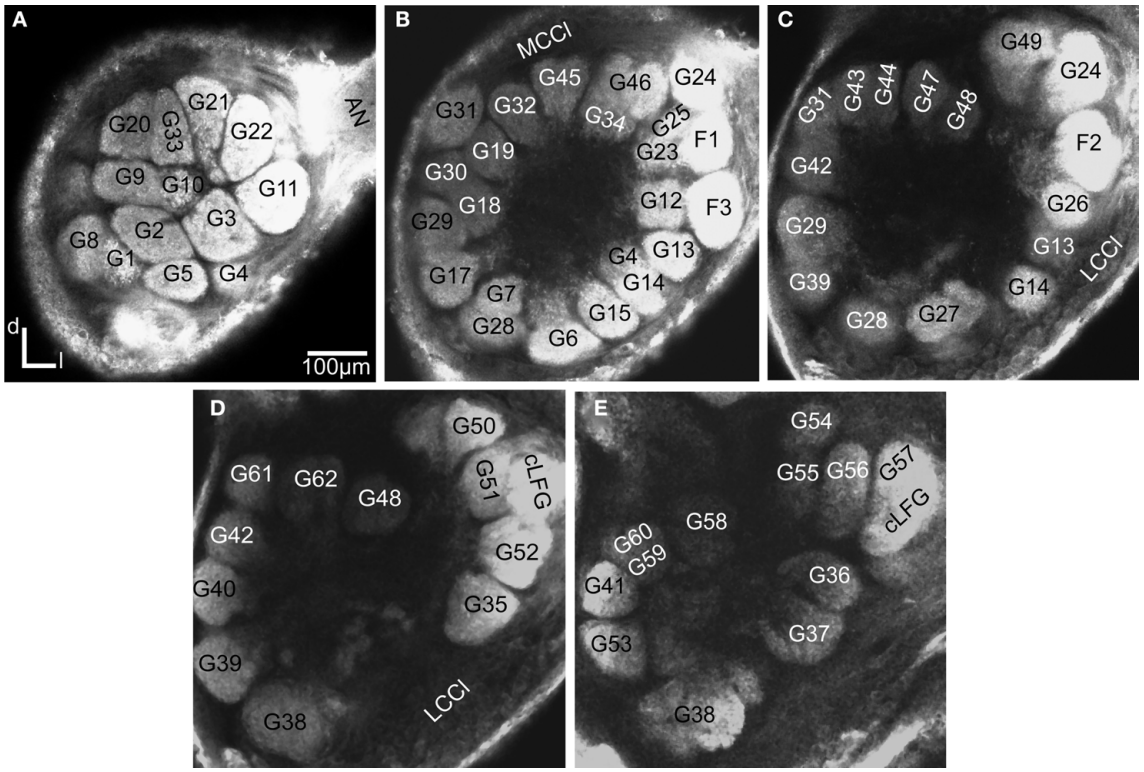

FIGURE 2 | Confocal images at different depths of the right *H. virescens* female antennal lobe, from anterior towards posterior at the following depths: (A) 64 µm, **(B)** 105 µm, **(C)** 144 µm, **(D)** 179 µm, **(E)** 216 µm. Except for G16 all glomeruli are shown. The AL is inverted.

the female AL, 63 ordinary glomeruli were identified in the male AL, of which G1–G62 showed correspondence with the female ordinary glomeruli and G63 being male specific.

INTEGRATION OF THE ANTENNAL LOBE GLOMERULI INTO THE STANDARD BRAIN ATLAS

Registration of the AL glomeruli into the SBA resulted in the new female *H. virescens* SBA with 66 identified glomeruli (SBAGl) (**Figure 4A**).

The two reconstructed female ALs were independently integrated into the SBAGl. After transforming the glomeruli into the SBA, the shape and size of the glomeruli in SBAGl matched the glomerular layer in the SBA. The relative position of the glomeruli was maintained in the transformation process making the glomeruli easily recognisable (**Figures 4B,C**). Thus, they were relabelled and given numbers and colours corresponding to the separate AL atlas. With this new and more detailed anatomical atlas of the *H. virescens* brain, we next wanted to study the specific glomerular innervation of three AL PNs and their projection patterns in the protocerebrum.

INTEGRATION OF ANTENNAL LOBE PROJECTION NEURONS INTO THE SBAGI

The present results include three stained AL PNs registered into the SBAGl (**Figures 5–7**).

These neurons with axons following the IACT are termed PI neurons (Homberg et al., 1988; Rø et al., 2007). The initial registration of each of them into the SBA by transforming the AL as a single material identity revealed the glomerular area of the dendritic innervations in the AL as well as the axonal pathway and branching pattern in the calyces and the lateral protocerebrum. After superposing the glomeruli of the SBAGl, the innervated glomeruli clearly appeared. As exemplified by the neuron shown in **Figures 5A, 6, and 7**, the innervations were identified in three glomeruli, G35, G36 and G37. The dendrite differentially innervated each of the three glomeruli; G37 stronger than G35 and only one branch in G36. The axon following the IACT, passed adjacent and posteriorlaterally to the central body (**Figures 6A,B**). Upon reaching the calyces of the ipsilateral mushroom body, the axon gave off five branches innervating the medial and lateral calyces before turning anteriorlaterally into the lateral protocerebrum, showing a star-like projection pattern. Most branches turned dorsally and only one ventrolaterally into the lateral horn (**Figures 6A–C**), defined as the protrusion from the lateral protocerebrum according to Kvello et al. (2009). The soma was located in the lateral cell cluster close to the innervated glomerulus, G37. A second PN with cell soma in the lateral cluster was registered by the same procedure into the SBAGl (**Figures 5B and 7**). This neuron innervated a single glomerulus identified as G14, located close to its cell body. The axon followed quite closely the axon of the G37 neuron, and also gave off five branches to the calyces before turning anteriorlaterally and extending into the lateral protocerebrum. The same pattern of star-like projections appeared with most branches turning dorsally and one ventrolaterally towards the lateral horn. The third neuron registered into the SBAGl, showed innervation of a single glomerulus identified as G11, located in the anterior part of the AL (**Figures 5C and 7**). The soma was in the anterior

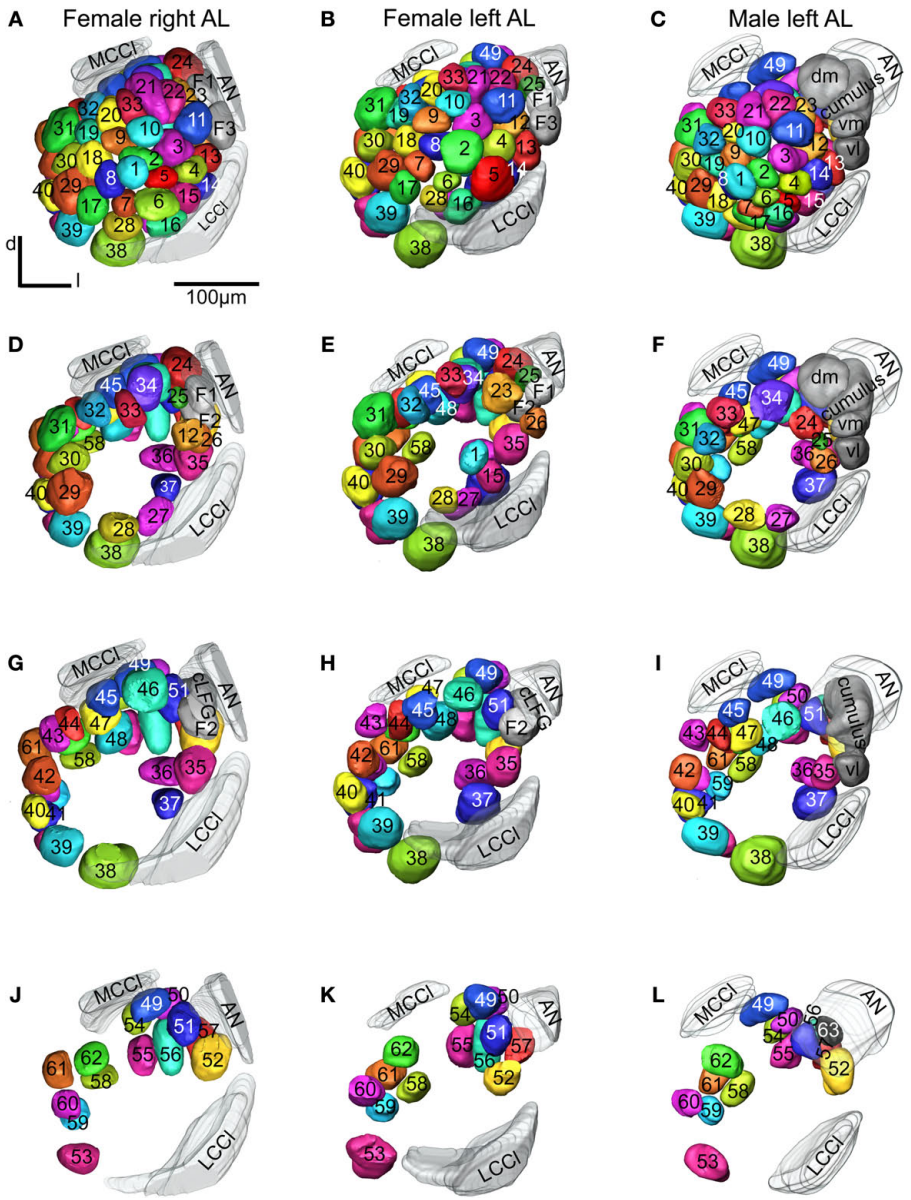

FIGURE 3 | Antennal lobe atlases as 3D reconstructions of two *H. virescens* female (right and left antennal lobe) and one male preparation (left antennal lobe). All glomeruli are reconstructed, identified and given a specific number and colour that corresponded across preparations, including sexes, in accordance with the atlases of two other heliothine species in Skiri et al. (2005). The right and left female and the left male antennal lobes are shown in frontal view at four different sections. **(A–C)** The most anterior part of the three preparations, (**D–L**) the three deeper sections. The right female antennal lobe is inverted for comparison with the left antennal lobe.

cluster, close to the innervated glomerulus. The innervation was extensive throughout the whole glomerulus (**Figure 5C**). The axon followed the IACT sending four branches into the medial and lateral calyces before turning anteriorlaterally towards the lateral protocerebrum, where it projected in the typical star-like pattern with most branches extending dorsally and one ventrolaterally into the lateral horn.

Comparison of the three neurons in the SBAGl shows their relative position from the different glomerular innervation to their projections in the calyces and the lateral protocerebrum (**Figure 7**). The two neurons innervating the more posteriorventrally located G35, G36, G37 and G14, respectively, with soma in the lateral cell cluster have axons running in a ventral pathway into the protocerebrum. The axon of the neuron innervating the dorsoanterior G11 with soma in the anterior cluster runs more dorsally in the AL and protocerebrum before joining the other axons in the IACT anteriorly and close to the central body. The axonal projections of the three neurons in the calyces intermingle, whereas in the lateral protocerebrum the axonal projections appears organised in a dorsoventral axis with partly overlap. The projections of the G14 neuron are dorsally to those of the G11 neurons, which are again dorsally to those of the G37 neuron.

Table 1 | Glomeruli of *H. virescens* antennal lobe atlases with corresponding numbers in the new and the previous atlas.

New atlas F and M	Previous atlas		New atlas F and M	Previous atlas	
	F	M		F	M
G1	G1	G8	G36	G45	G57
G2	G7	G3	G37	G37	G41
G3	G57	G6	G38	G19	G39
G4	G8	G2	G39	G21	G35
G5	G2	G7	G40	G22	G42
G6	G6	G17	G41	G43	G48
G7	G3	G23	G42	G42	G47
G8	G4	G1	G43	G24	G38
G9	G5	G12	G44	G23	G40
		G18	G45	G33[1]	G33
G10	G11	G5	G46	G32[1]	G24[1]
G11	G58[1]	G4	G47	G33[1]	G45
G12	G36[1]	G22	G48	G26	G53
G13	G36[1]	G25	G49	G54	G54[1]
G14	G30	G10	G50	G39	G55
G15	G18	G19	G51	G41	[3]
G16	G9	G21[1]	G52	G38	G58
G17	G20	G16			G59
G18	G12	G15	G53	G44	G36
G19	G27	G26			G49
G20	G15	G27	G54	G53	G54[1]
G21	G17	G13	G55	G52	[3]
G22	G32[2]	G9	G56	G51	G56
	G60	G62	G57	G40	G60
G23	G59	G11			G61
G24	mLFG	[3]	G58	G48	[3]
G25	G58[1]	G14	G59	G50	G51
G26	G35	G43	G60	G49	G46
G27	G28	G32	G61	G47	G50
		G21[2]	G62	G55	G52
G28	G10	G31		G56	
G29	G14	G28	G63		Cumulus[2]
		G34	Cumulus		Cumulus[1]
G30	G13	G30	dm		dm
G31	G25	G29	vm		vm
G32	G29	G37[1]	cLFG	cLFG	
G33	G16	G20	F1	G31	
		G37[2]	F2	G34	
G34	G32[1]	G24[1]	F3	[3]	
G35	G46	G44			

F, female; M, male.
[1]Two glomeruli counted as one.
[2]Includes a part of adjacent glomerulus.
[3]Glomeruli not found.

DISCUSSION

ANTENNAL LOBE GLOMERULI INTEGRATED INTO THE STANDARD BRAIN ATLAS

How glomerular activity in the primary olfactory centres represents odour information and how this topographic organisation is further reflected in higher olfactory areas, are central questions in studies on the functional organisation of vertebrate as well as insect olfactory systems. A major challenge is to map in higher olfactory brain neuropils the target areas of the primary olfactory centre's output neurons, according to the glomerular input; in *Drosophila* made possible by the use of molecular labelling of PNs (Wong et al., 2002; Tanaka et al., 2004; Jefferis et al., 2007). In the honeybee and the moth *H. virescens*, whole brain standard atlases have been demonstrated as helpful tools in determining the projections in the calyces and the lateral protocerebrum of AL PNs (Brandt et al., 2005; Kvello et al., 2009). Particularly in the lateral protocerebrum with no visible substructures, integrated PNs from different preparations give important information about their relative positions. However, because of the low resolution confocal scans used for creating the whole brain atlases, separate atlases with higher resolution are better suited for determining the PNs input and output regions, respectively. By integration of the AL glomeruli into the *H. virescens* SBA as shown in the present study, the PN input and output regions were standardised in this common framework, SBAGl. This integration process was facilitated by the fact that the AL of this atlas included the glomerular layer only, excluding tracts and cell clusters; different from the four other atlases. Therefore, the AL atlas glomeruli could be directly registered into the SBA, after being assigned a single material identity. Since the relative position of the glomeruli was maintained in the transformation process, all 66 glomeruli could easily be recognised, relabelled and numbered according to the AL atlas (**Figure 4**). The anatomically more detailed SBAGl provides a stronger basis for studying the specific innervations in the AL as well as the connections to higher brain areas, like the calyces and the lateral protocerebrum.

ANTENNAL LOBE PROJECTION NEURONS INTEGRATED INTO THE SBAGl

In principle, the integration of reconstructed AL neurons into the SBAGl is a two-step process as described for the neurons presented in **Figures 5–7**. The first step constitutes a registration into the SBA which guides the localisation of the dendritic innervation to a particular area of the AL. Then, superposing the SBAGl reveals the innervated glomeruli. This procedure used for the well stained preparations in the present study allowed verification of the glomerular innervation in confocal images. This means that the procedure can be used even for preparations where glomeruli may not be well distinguished, as long as the glomerular borderline is clearly detectable. The well stained preparations in the present study made reconstruction of the innervated and landmark glomeruli possible. The registration of these glomeruli into the SBAGl resulted in a precise position of the dendritic innervation within the glomeruli. Thus, the SBAGl is an extended and more elaborate tool that together with the confocal images expands the possibility for making accurate judgments of dendritic arborisation and identification of the innervated glomeruli.

In addition to the high resolution model of the AL facilitating the identification of glomerular innervation, the SBAGl also provides the frame for visualising the relative position of whole neurons in the brain. As shown in **Figures 6 and 7**, the details on the neuronal pathways are for instance visualised by the different axonal trajectories in the AL before joining in the IACT. The uniglomerular innervation and extensive branching throughout the glomerulus as

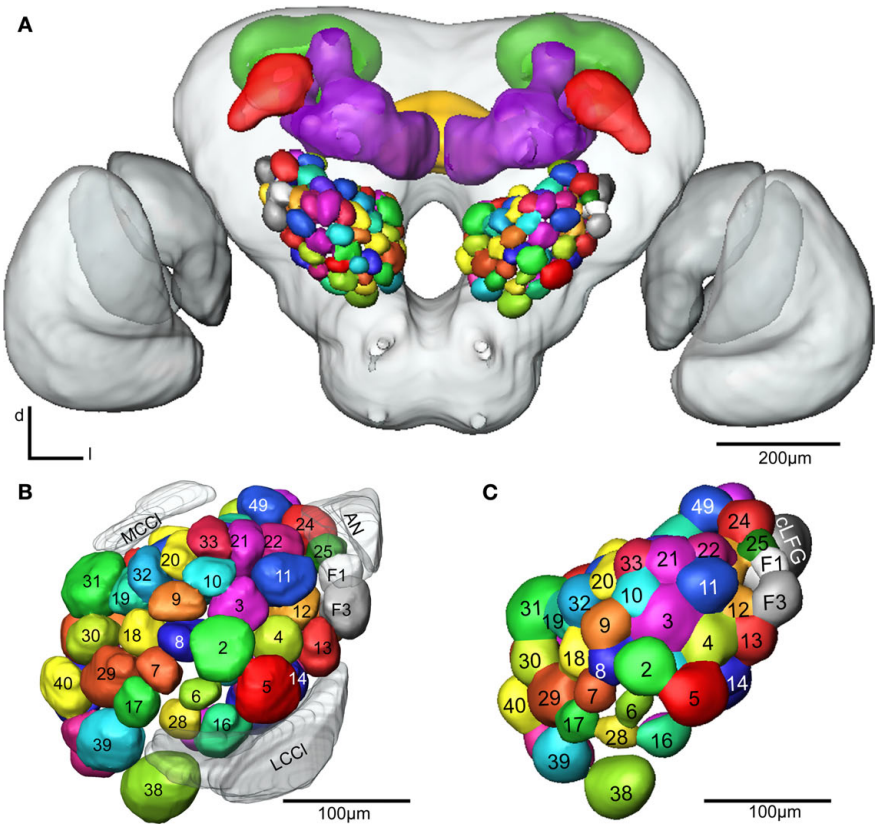

FIGURE 4 | (A) The female H. virescens standard brain atlas with the glomeruli of one left and one right antennal lobe integrated. **(B,C)** The left female antennal lobe atlas with numbered glomeruli and cell clusters, showing the glomerular layer before **(B)** and after **(C)** registration into the standard brain atlas.

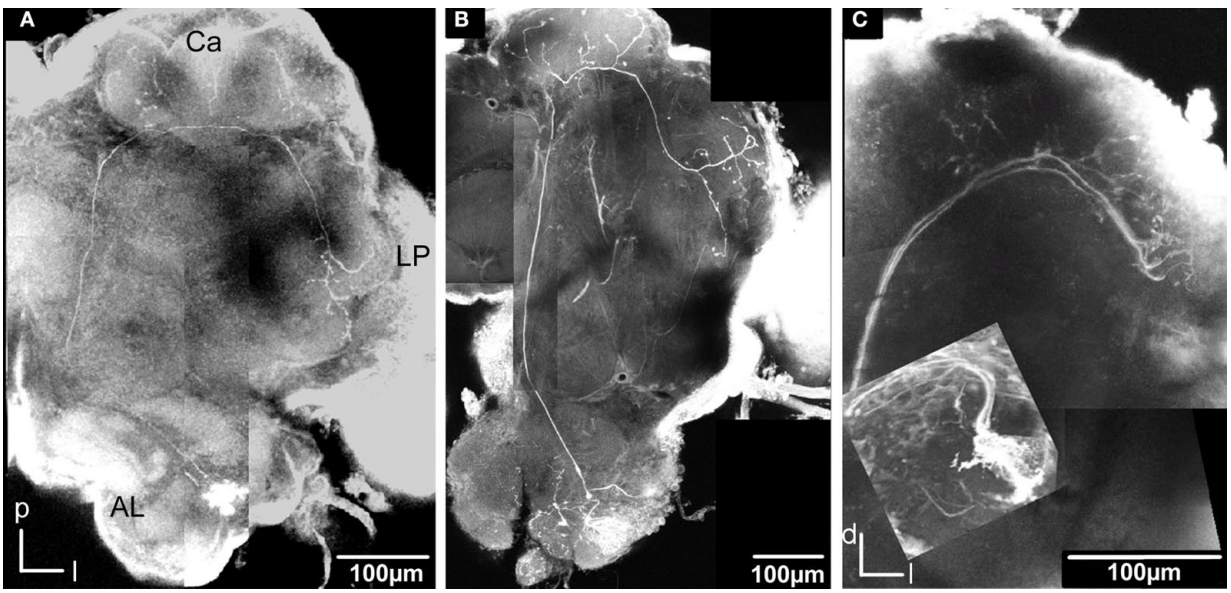

FIGURE 5 | Stacks of confocal images of three preparations each with one stained projection neuron having axon in the inner antennocerebral tract. **(A)** Dorsal view: This neuron innervated three glomeruli (G35, G36 and G37) and projected in the calyces with five branches (three visible) before turning anterior-laterally and projecting in lateral protocerebrum. **(B)** Dorsal view: This neuron innervated G14 and projected in calyces with five branches before turning anterior-laterally into the lateral protocerebrum. The starlike projection with dorsal branches as well as a single ventral branch into the lateral horn is visible. **(C)** Frontal view: This neuron (co stained with a second neuron, from Kvello et al., 2009) innervated G11. The projection in the calyces and the lateral protocerebrum is shown.

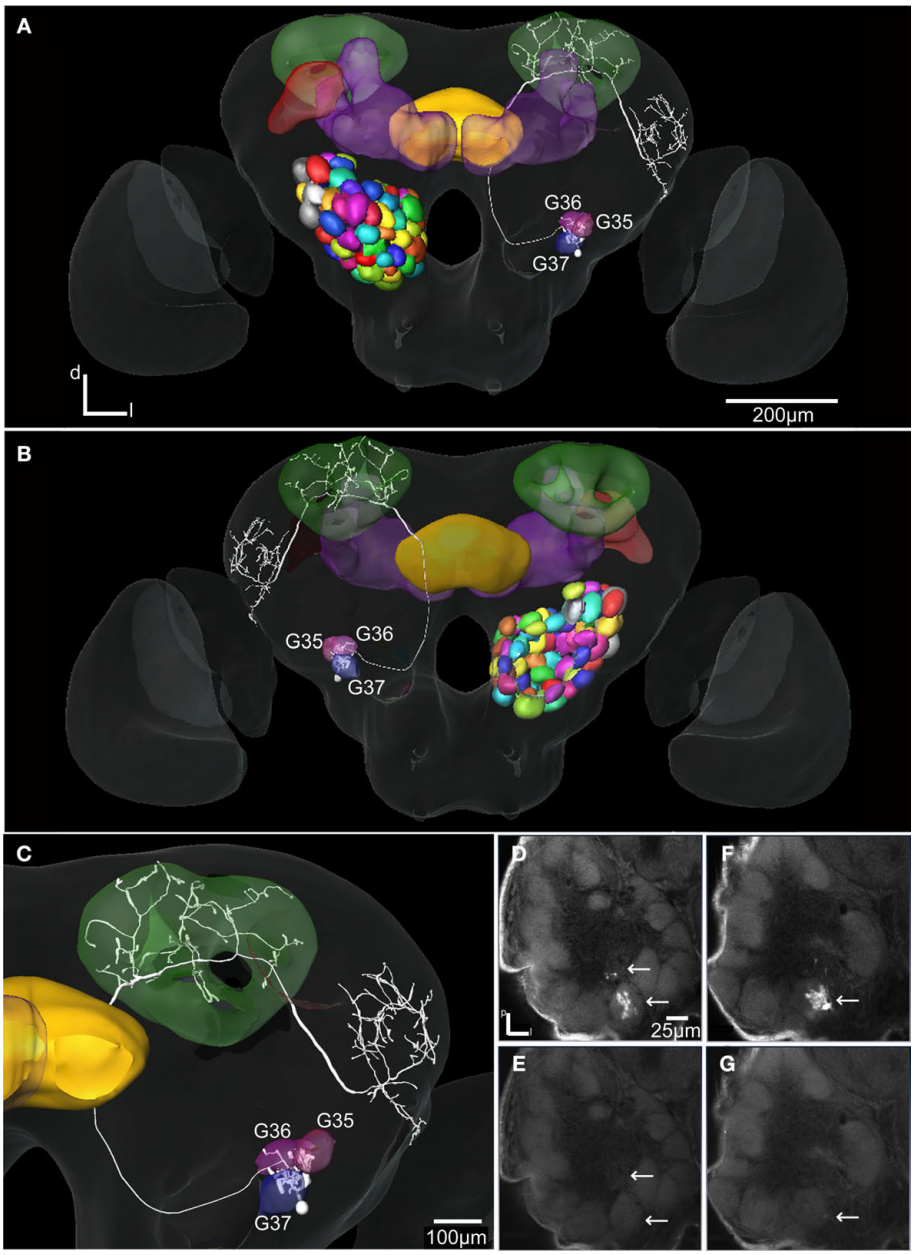

FIGURE 6 |The *H. virescens* standard brain atlas with one integrated antennal lobe projection neuron (the same as in Figure 5A). (A) Frontal view. **(B)** Posterior view. **(C)** Magnified frontal view showing the innervated glomeruli and projection pattern in the medial and lateral calyces and in the lateral protocerebrum. **(D–G)** Confocal images showing the triple glomerular innervation in two different sections scanned with two channels. **(D)** Micro-ruby staining showing the innervation of glomeruli G37 and G36. **(E)** Synapsin staining visualising the glomeruli of the same section. **(F)** Micro-ruby staining showing the innervation of glomerulus G35. **(G)** Synapsin staining visualising the glomeruli of the same section. Arrows indicate innervated glomeruli.

shown for the G11 and G14 neurons are typical features for IACT PNs (category PIa in Homberg et al., 1988; Rø et al., 2007). These neurons found in most insect species belong to a conserved group of PNs (Schachtner et al., 2005). IACT neurons innervating a few adjacent glomeruli have also been identified in *H. virescens* (category PIc in Rø et al., 2007), similar to the G37 neuron with dendritic arborisations in the two adjacent glomeruli, G35 and G36. The innervation pattern in protocerebrum, shown for the three neurons in **Figure 7**, is typical for IACT neurons. As previously described, they send three to five branches into the calyces and extend the axon into the lateral protocerebrum ending in a star-like projection, where most branches project dorsally and one branch ventrolaterally towards or into the lateral horn, like the IACT neurons in the present study. By using the SBAGl combined with registration algorithms for integrating the neurons we have here found that the three IACT neurons innervate distinct but overlapping areas

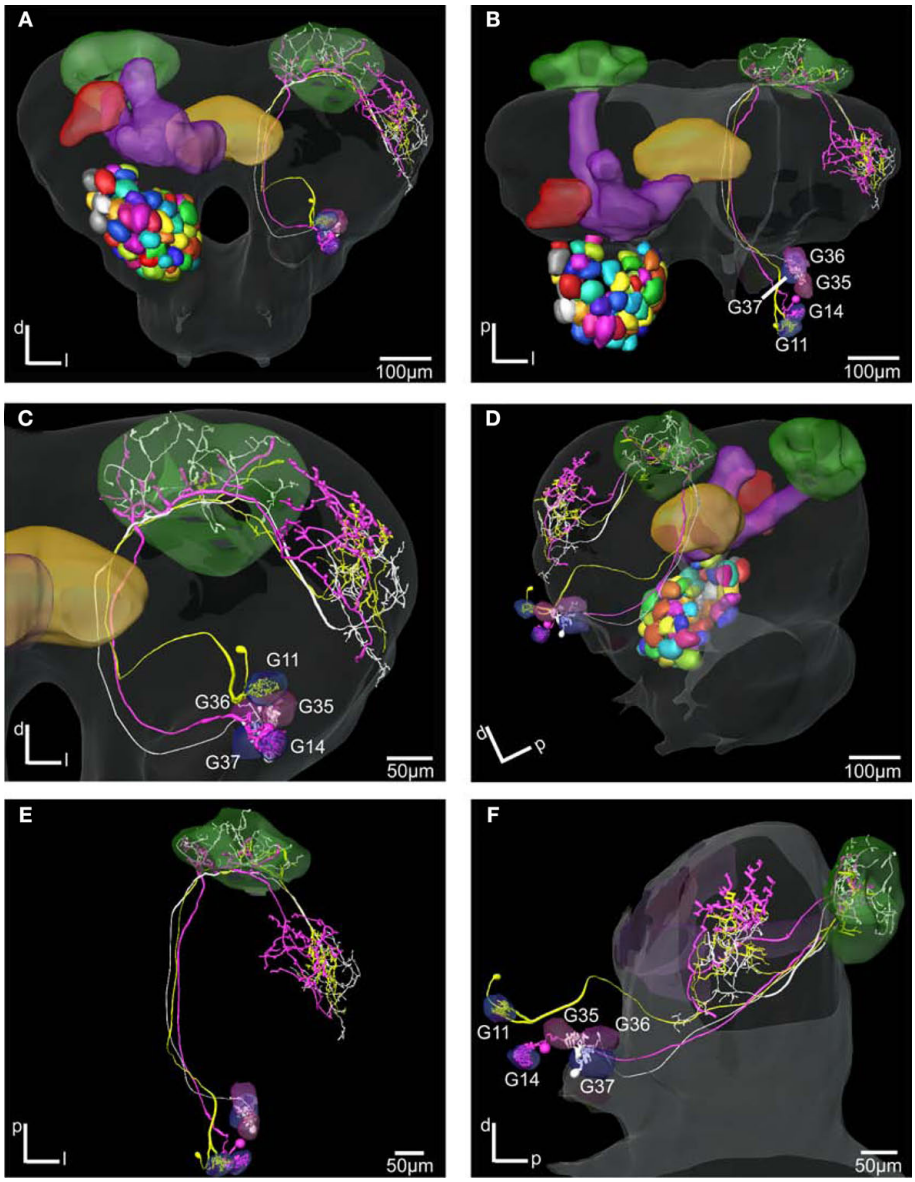

FIGURE 7 |The *H. virescens* standard brain atlas with three antennal lobe projection neurons integrated. (A,C) Frontal view. **(B,E)** Dorsal view. **(D)** Posterior lateral view. **(F)** Lateral view. The relative positions of the innervated glomeruli and projections as well as the axonal pathways are shown in the different views. The projections pattern in the lateral protocerebrum in different but overlapping areas along a dorsoventral axis appears particularly in **(C)** and **(F)**. The dorsal axonal pathway in the antennal lobe of the G11 neuron before joining the other axons in the inner antennocerebral tract is clearly seen in **(A)** and **(B)**.

along a dorsoventral axis in the lateral protocerebrum (**Figure 7**). Whether this organisation is consistent with the actual organisation or due to methodological limitations remains to be verified. In contrast, the two PNs innervating the same glomerulus showed intermingled projections in the same area (Kvello et al., 2009). A similar principle for the organisation of PN projections is found in the lateral horn of *Drosophila*, where molecularly labelled neurons innervating the same glomerulus exhibited similar axonal topography, whereas neurons from different glomeruli displayed different projection patterns (Wong et al., 2002). A further division of the lateral horn in *Drosophila* into sub-regions according to different PN projection clusters is described by Jefferis et al. (2007). How the projection pattern of PN populations in *H. virescens* are organised in the lateral protocerebrum according to the innervated glomeruli as well to the different tracts, are interesting questions to be resolved when more PNs have been integrated into the SBAGl.

COMPARISON OF ANTENNAL LOBE ATLASES BETWEEN SEXES AND SPECIES

In the present study we provided a new atlas of the AL of *H. virescens* females, based on the numbering system of two other heliothine moth species (Skiri et al., 2005). In general, the challenge in this kind of work is to detect the borders between the glomeruli. The difference from the previous *H. virescens* atlas in

respect to the number of glomeruli included seems to be due to the lack of detectable borderlines between pairs of glomeruli in the lower resolution confocal images of the previous atlas (Berg et al., 2002). The glomeruli in the present *H. virescens* atlas showed a striking correspondence with the glomeruli of the atlases of the two other heliothine species (Skiri et al., 2005), which is the basis for the identification of the glomeruli with corresponding numbers. Thus, the new *H. virescens* atlas is more reliable for identifying the glomeruli innervated by a neuron, as well as suited for comparing the results between heliothine species. For instance, a challenging question is whether corresponding glomeruli in the three species also receive and process information about the same odorants or the odorant specificity has changed through evolution. An interesting example on possibly conserved specificity is for the large LPOG or G38, present in the typical position in the AL of lepidopteran species, and in *Manduca sexta* shown to be involved in mediating information about CO_2 (Gurenstein et al., 2004). The male AL atlas included in this study provides a basis for detecting similarities and differences with the female olfactory system both concerning morphology and physiology. Interestingly, except for one additional glomerulus, G63, in the male AL, the numerous ordinary glomeruli corresponded well between the two sexes as well as between the species. Because of this correspondence within and between sexes and species (all together 12 individual ALs), we find that the present results are reliable as concerns numbers and relative positions of the glomeruli. In the present study we have integrated the AL glomeruli into the SBA of *H. virescens* and shown its suitability for integrating and visualising AL neurons. So far, we have only registered PNs of the IACT, showing their relative positions. The intention is to integrate physiologically characterised PNs of all tracts for relating glomerular innervation in the AL to axonal projections in the protocerebrum. Functional similarities and differences among the PNs may in this way be related to specific input, output or ACTs, the latter associated with functionally different PNs in the honeybee (Müller et al., 2002). In a previous study, we have compared the spatial relationship between a few olfactory and gustatory neurons showing adjacent projection areas in the lateral protocerebrum (Kvello et al., 2009). Thus, integration of more physiologically characterised chemosensory neurons may visualise the neuronal network underlying chemosensory coding in this moth species.

ACKNOWLEDGMENTS

The project was financed by the Royal Norwegian Society of Sciences and Letters. We also acknowledge Dr. Hanne Skiri for help with making the AL atlas, Prof. Erich Buchner (Universität Würzburg, Germany) for providing antibodies, and the Insect Rearing Team of Syngenta (Basel, Switzerland) for providing insect materials.

REFERENCES

Anton, S., and Hansson, B. S. (1999). Physiological mismatching between neurons innervating olfactory glomeruli in a moth. *Proc. R. Soc. Lond., B, Biol. Sci.* 266, 1813–1820.

Anton, S., and Homberg, U. (1999). Antennal lobe structure. In Insect Olfaction, B. S. Hansson, ed. (Berlin, Springer), pp. 97–124.

Axel, R. (1995). The molecular logic of smell. *Sci. Am.* 273, 154–159.

Berg, B. G., Almaas, T. J., Bjaalie, J. G., and Mustaparta, H. (1998). The macroglomerular complex of the antennal lobe in the tobacco budworm moth *Heliothis virescens*: specified subdivision in four compartments according to information about biologically significant compounds. *J. Comp. Physiol. A* 183, 669–682.

Berg, B. G., Galizia, C. G., Brandt, R., and Mustaparta, H. (2002). Digital atlases of the antennal lobe in two species of tobacco budworm moths, the oriental *Helicoverpa assulta* (male) and the American *Heliothis virescens* (male and female). *J. Comp. Neurol.* 446, 123–134.

Brandt, R., Rohlfing, T., Rybak, J., Krofczik, S., Maye, A., Westerhoff, M., Hege, H. C., and Menzel, R. (2005). Three-dimensional average-shape atlas of the honeybee brain and its applications. *J. Comp. Neurol.* 492, 1–19.

Buck, L. B. (2000). The molecular architecture of odor and pheromone sensing in mammals. *Cell* 100, 611–618.

Chiang, A.-S., Liu, Y.-C., Chiu, S.-L., Hu, S. H., Huang, C.-Y., and Hsieh, C.-H. (2001). Three-dimensional mapping of brain neuropils in the cockroach, *Diploptera punctata*. *J. Comp. Neurol.* 440, 1–11.

Christensen, T. A., and Hildebrand, J. G. (2002). Pheromonal and host-odor processing in the insect antennal lobe: how different? *Curr. Opin. Neurobiol.* 12, 393–399.

Clyne, P. J., Warr, C. G., Freeman, M. R., Lessing, D., Kim, J., and Carlson, J. R. (1999). A novel family of divergent seven-transmembrane proteins: candidate odorant receptors in *Drosophila*. *Neuron* 22, 327–338.

el Jundi, B., Heinze, S., Lenschow, C., Kurylas, A., Rohlfing, T., and Homberg, U. (2010). The locust standard brain: a 3D standard of the central complex as a platform for neural network analysis. *Front. Syst. Neurosci.* 3:21. doi: 10.3389/neuro.06.021.2009.

el Jundi, B., Huetteroth, W., Kurylas, A. E., and Schachtner, J. (2009). Anisometric brain dimorphism revisited: implementation of a volumetric 3D standard brain in *Manduca sexta*. *J. Comp. Neurol.* 517, 210–225.

Evers, J. F., Schmitt, S., Sibila, M., and Duch, C. (2004). Progress in functional neuroanatomy: precise automatic geometric reconstruction of neuronal morphology from confocal image stacks. *J. Neurophysiol.* 93, 2331–2342.

Flanagan, D., and Mercer, A. R. (1989). An atlas and 3-D reconstruction of the antennal lobes in the worker honey bee, *Apis mellifera* L. (*Hymenoptera*: Apidae). *Int. J. Insect. Morphol. Embryol.* 18, 145–159.

Galizia, C. G., McIlwrath, S. L., and Menzel, R. (1999). A digital three-dimensional atlas of the honeybee antennal lobe based on optical sections acquired by confocal microscopy. *Cell Tissue Res.* 295, 383–394.

Galizia, C. G., and Menzel, R. (2000). Probing the olfactory code. *Nat. Neurosci.* 3, 853–854.

Galizia, C. G., Sachse, S., and Mustaparta, H. (2000). Calcium responses to pheromones and plant odours in the antennal lobe of the male and female moth *Heliothis virescens*. *J. Comp. Physiol. A* 186, 1049–1063.

Greiner, B., Gadenne, C., and Anton, S. (2004). Three-dimensional antennal lobe atlas of the male moth, *Agrotis ipsilon*: a tool to study structure–function correlation. *J. Comp. Neurol.* 475, 202–210.

Gurenstein. P. G., Christensen. T. A., and Hildebrand. J. G. (2004). Sensory processing of ambient CO_2 information in the brain of the moth *Manduca sexta*. *J. Comp. Physiol.* A. 190, 707–725.

Heisenberg, M. (2003). Mushroom body memoir: from maps to models. *Nat. Rev. Neurosci.* 4, 266–275.

Hildebrand, J. G., and Shepherd, G. M. (1997). Mechanisms of olfactory discrimination: converging evidence for common principles across phyla. *Annu. Rev. Neurosci.* 20, 595–631.

Homberg, U., Montague, R. A., and Hildebrand, J. G. (1988). Anatomy of antenno-cerebral pathways in the brain of the sphinx moth *Manduca sexta*. *Cell Tissue Res.* 254, 255–281.

Huetteroth, W., and Schachtner, J. (2005). Standard three-dimensional glomeruli of the *Manduca sexta* antennal lobe: a tool to study both developmental and adult neuronal plasticity. *Cell Tissue Res.* 319, 513–524.

Iyengar, B. G., Chou, C. J., Sharma, A., and Atwood, H. L. (2006). Modular neuropile organization in the *Drosophila* larval brain facilitates identification and mapping of central neurons. *J. Comp. Neurol.* 499, 583–602.

Jefferis, G. S. X. E., Potter, C. J., Chan. A. I., Marin, E. C., Rohlfing, T., Maurer, C. R., and Luo, L. Q. (2007). Comprehensive maps of *Drosophila* higher olfactory centers: spatially segregated fruit and pheromone representation. *Cell* 128, 1187–1203.

Kanzaki, R., Soo, S., Seki, Y., and Wada, S. (2003). Projections to higher olfactory centers from subdivisions of the antennal lobe macroglomerular complex of the male silkmoth. *Chem. Senses* 28, 113–130.

Kazawa, T., Namiki, S., Fukushima, R., Terada, M., Soo, K., and Kanzaki, R. (2009). Constancy and variability of glomerular organization in the antennal lobe of the silkmoth. *Cell Tissue Res.* 336, 119–136.

Kloppenburg, P., and Mercer, A. R. (2008). Serotonin modulation of moth central olfactory neurons. *Annu. Rev. Entomol.* 53, 179–190.

Kurylas, A. E., Rohlfing, T., Krofczik, S., Jenett, A., and Homberg, U. (2008). Standardized atlas of the brain of the desert locust, *Schistocerca gregaria*. *Cell Tissue Res.* 33, 125–145.

Kvello, P., Løfaldli, B. B., Rybak, J., Menzel, R., and Mustaparta, H. (2009). Digital, three-dimensional average shaped atlas of the *Heliothis virescens* brain with integrated gustatory and olfactory neurons. *Front. Syst. Neurosci*. 3:14. doi: 10.3389/neuro.06.014.2009.

Laissue, P. P., Reiter, C., Hiesinger, P. R., Halter, S., Fischbach, K. F., and Stocker, R. F. (1999). Three-dimensional reconstruction of the antennal lobe in *Drosophila melanogaster*. *J. Comp. Neurol*. 405, 543–552.

Laurent, G., Wehr, M., and Davidowitz, H. (1996). Temporal representations of odors in an olfactory network. *J. Neurosci.* 16, 3837–3847.

Lledo, P.-M., Gheusi, G., and Vincent, J.-D. (2005). Information processing in the mammalian olfactory system. *Physiol. Rev.* 85, 281–317.

Masante-Roca, I., Gadenne, C., and Anton, S. (2005). Three-dimensional antennal lobe atlas of male and female moths, *Lobesia botrana* (Lepidoptera: Tortricidae) and glomerular representation of plant volatiles in females. *J. Exp. Biol.* 208, 1147–1159.

Menzel, R. (2001). Searching for the memory trace in a mini-brain, the honeybee. *Learn. Mem*. 8, 53–62.

Mombaerts, P. (2001). How smell develops. *Nat. Neurosci*. 4, 1192–1198.

Müller, D., Abel, R., Brandt, R., Zöckler, M., and Menzel, R. (2002). Differential parallel processing of olfactory information in the honeybee, *Apis mellifera* L. *J. Comp. Physiol.* A. 188, 359–370.

Mustaparta, H. (2002). Encoding of plant odour information in insects: peripheral and central mechanisms. *Entomol. Exp. Appl.* 104, 1–13.

Mustaparta, H., and Stranden, M. (2005). Olfaction and learning in moths and weevils living on angiosperm and gymnosperm hosts. *Recent Adv. Phytochem*. 39, 269–292.

Rein, K., Zöckler, M., Mader, M. T., Grübel, C., and Heisenberg, M. (2002). The *Drosophila* standard brain. *Curr. Biol.* 12, 227–231.

Reischig, T., and Stengl, M. (2002). Optic lobe commissures in a three-dimensional brain model of the cockroach *Leucophaea maderae*: a search for the circadian coupling pathways. *J. Comp. Neurol.* 443, 388–400.

Rø, H., Müller, D., and Mustaparta, H. (2007). Anatomical organization of antennal lobe projection neurons in the moth *Heliothis virescens*. *J. Comp. Neurol*. 500, 658–675.

Rospars, J. P., and Chambille, I. (1981). Deutocerebrum of the cockroach *Blaberus craniifer* burm. Quantitative study and automated identification of the glomeruli. *J. Neurobiol*. 12, 221–247.

Rospars, J. P., and Hildebrand, J. G. (2000). Sexually dimorphic and isomorphic glomeruli in the antennal lobes of the sphinx moth *Manduca sexta. Chem. Senses* 25, 119–129.

Røstelien, T., Stranden, M., Borg-Karlson, A.-K., and Mustaparta, H. (2005). Olfactory receptor neurones in two heliothine moth species responding selectively to aliphatic green leaf volatiles, aromatics, monoterpenes and sesquiterpenes of plant origin. *Chem. Senses* 30, 443–461.

Sadek, M. M., Hansson, B. S., Rospars, J. P., and Anton, S. (2002). Glomerular representation of plant volatiles and sex pheromone components in the antennal lobe of the female *Spodoptera littoralis*. *J. Exp. Biology*. 205, 1363–1376.

Schachtner, J., Schmidt, M., and Homberg, U. (2005). Organization and evolutionary trends of primary olfactory brain centers in Tetraconata (Crustacea + Hexapoda). *Arthropod Struct. Dev*. 34, 257–299.

Schmitt, S., Evers, J. F., Duch, C., Scholz, M., and Obermayer, K. (2004). New methods for the computer-assisted 3-D reconstruction of neurons from confocal image stacks. *Neuroimage* 23, 1283–1298.

Skiri, H. T., Rø, H., Berg, B. G., and Mustaparta, H. (2005). Consistent organization of glomeruli in the antennal lobes of related species of heliothine moths. *J. Comp. Neurol*. 491, 367–380.

Smid, H. M., Bleeker, M. A., Van Loon, J. J. A., and Vet, L. E. (2003). Three-dimensional organization of the glomeruli in the antennal lobe of the parasitoid wasps *Cotesia glomerata* and *C. rubecula*. *Cell Tissue Res.* 312, 237–248.

Stocker, R. F, Lienhard, M. C., Borst, A., and Fischbach, K. F. (1990). Neuronal architecture of the antennal lobe in *Drosophila melanogaster*. *Cell Tissue Res.* 262, 9–34.

Stopfer, M. (2007). Olfactory processing: massive convergence onto sparse codes. *Curr. Biol.* 17, 363–364.

Tanaka, N. K., Awasaki, T., Shimada, T., and Ito, K. (2004). Integration of chemosensory pathways in the *Drosophila* second-order olfactory centers. *Curr. Biol.* 14, 449–457.

Toga, A. W. (2002). Neuroimage databases: the good, the bad and the ugly. *Nat. Rev. Neurosci.* 3, 302–309.

Toga, A. W., and Thompson, P. M. (2001). Maps of the brain. *Anat. Rec.* 265, 37–53.

Van Essen, D. C. (2002). Windows on the brain: the emerging role of atlases and databases in neuroscience. *Curr. Opin. Neurobiol.* 12, 574–579.

Varela, N., Couton, L., Gemeno, C., Avilla, J., Rospars, J. P., and Anton, S. (2009). Three-dimensional antennal lobe atlas of the oriental fruit moth, *Cydia molesta* (Busck) (Lepidoptera: Tortricidae): comparison of male and female glomerular organization. *Cell Tissue Res.* 337, 513–526.

Vickers, N. J., and Christensen, T. A. (2003). Functional divergence of spatially conserved olfactory glomeruli in two related moth species. *Chem. Senses* 28, 325–338.

Vickers, N. J., Christensen, T. A., and Hildebrand, J. G. (1998). Combinatorial odor discrimination in the brain: Attractive and antagonist odor blends are represented in distinct combinations of uniquely identifiable glomeruli. *J. Comp. Neurol.* 400, 35–56.

Vosshall, L. B., Amrein, H., Morozov, P. S., Rzhetsky, A., and Axel, R. (1999). A spatial map of olfactory receptor expression in the *Drosophila* antenna. *Cell* 96, 725–736.

Vosshall, L. B., and Stocker, R. F. (2007). Molecular architecture of smell and taste in *Drosophila*. *Annu. Rev. Neurosci.* 30, 505–533.

Wilson, R. I., and Mainen, Z. F. (2006). Early events in olfactory processing. *Annu. Rev. Neurosci*. 29, 163–201.

Wong, A. M., Wang, J. W., and Axel, R. (2002). Spatial representation of the glomerular map in the *Drosophila* protocerebrum. *Cell* 109, 229–241.

Conflict of Interest Statement: The authors declare that the research was conducted in the absence of any commercial or financial relationships that could be construed as a potential conflict of interest.

Received: 05 December 2009; paper pending published: 18 January 2010; accepted: 26 January 2010; published online: 12 Febuary 2010.

*Citation: Løfaldli BB, Kvello P and Mustaparta H (2010) Integration of the antennal lobe glomeruli and three projection neurons in the standard brain atlas of the moth Heliothis virescens. Front. Syst. Neurosci. **4**:5. doi: 10.3389/neuro.06.005.2010*

frontiers in
SYSTEMS NEUROSCIENCE

ORIGINAL RESEARCH ARTICLE
published: 03 March 2010
doi: 10.3389/neuro.06.003.2010

3D standard brain of the red flour beetle *Tribolium castaneum*: a tool to study metamorphic development and adult plasticity

David Dreyer[1,2], Holger Vitt[1], Stefan Dippel[1,3], Brigitte Goetz[1], Basil el Jundi[1], Martin Kollmann[1], Wolf Huetteroth[1,4] and Joachim Schachtner[1]*

[1] *Department of Biology, Animal Physiology, Philipps-University Marburg, Marburg, Germany*
[2] *Department of Biology, Animal Navigation, University of Oldenburg, Oldenburg, Germany*
[3] *Department of Developmental Biology, Johann-Friedrich-Blumenbach-Institute for Zoology and Anthropol, Georg-August-University Göttingen, Göttingen, Germany*
[4] *Department of Neurobiology, University of Massachusetts Medical School, Worcester, MA, USA*

Edited by:
Randolf Menzel, Freie Universität Berlin, Germany

Reviewed by:
Monika Stengl, Universität Kassel, Germany

****Correspondence:***
Joachim Schachtner, Department of Biology, Animal Physiology, Philipps-University Marburg, Karl-von-Frisch-Str. 8, D-35032 Marburg, Germany.
e-mail: schachtj@staff.uni-marburg.de

The red flour beetle *Tribolium castaneum* is emerging as a further standard insect model beside *Drosophila*. Its genome is fully sequenced and it is susceptible for genetic manipulations including RNA-interference. We use this beetle to study adult brain development and plasticity primarily with respect to the olfactory system. In the current study, we provide 3D standard brain atlases of freshly eclosed adult female and male beetles (A0). The atlases include eight paired and three unpaired neuropils including antennal lobes (ALs), optic lobe neuropils, mushroom body calyces and pedunculi, and central complex. For each of the two standard brains, we averaged brain areas of 20 individual brains. Additionally, we characterized eight selected olfactory glomeruli from 10 A0 female and male beetles respectively, which we could unequivocally recognize from individual to individual owing to their size and typical position in the ALs. In summary, comparison of the averaged neuropil volumes revealed no sexual dimorphism in any of the reconstructed neuropils in A0 *Tribolium* brains. Both, the female and male 3D standard brain are also used for interspecies comparisons, and, importantly, will serve as future volumetric references after genetical manipulation especially regarding metamorphic development and adult plasticity.

Keywords: brain, olfactory system, antennal lobe, insect, neuropil, digital neuroanatomy, coleoptera

INTRODUCTION

The red flour beetle *Tribolium castaneum* Herbst, 1797 (Bonneton, 2008), which is a major pest of stored grains, grain products, and other dried food, is emerging as a further standard insect model beside *Drosophila*. It's powerful reverse genetics (systemic RNA-interference; Bucher et al., 2002; Tomoyasu and Denell, 2004; Tomoyasu et al., 2008), the recently published full genomic sequence (Richards et al., 2008) and the established transgenesis systems (Berghammer et al., 1999) transform *Tribolium* into a primary model system. Since recently, an insertional mutagenesis screen database provides mutants and enhancer trap lines for the growing *Tribolium* community (http://134.76.20.145/Default.aspx). Meanwhile, *Tribolium* has become one of the most important models in the field of evolution and development ("evo-devo") because its development is more "insect typical", compared to that of the classical system *Drosophila* (Klingler, 2004). Currently, only little information on the brain or its embryonic and metamorphic development is available. With our pioneering study we provide for the first time anatomical descriptions for most of the brain areas of adult *Tribolium* including 3D reconstructions and an average brain atlas for selected brain neuropils. With the latter, we present the first standardization of a coleopteran brain.

Brains are typically organized in defined neuropils, which can usually be characterized by their spatial location, gross anatomy, and often by a certain function. For example, the olfactory bulbs of vertebrates and the antennal lobes (ALs) of insects have been attributed to be the first processing centers for olfactory information (for a review see Hildebrand and Shepherd, 1997). Compared to most vertebrate brains, insect brains are miniature versions being typically comprised of a lower number of neurons and neuropils. Owing to the lower complexity and certain technical advantages, insects have been widely used as models to study principal mechanisms of information processing and integration, in the context of defined sensory inputs but also complex behaviors including learning and memory formation (e.g. Menzel, 2001; Heisenberg, 2003).

Brains of animals of the same or of evolutionary related species typically share the same principal organization. For example in neopteran insects, the central olfactory pathway seems to be well conserved (Strausfeld et al., 1998; Schachtner et al., 2005). However, even within the same species, no brain is identical with the next, differing in size and shape of certain brain neuropils. These individual differences can result from a variety of parameters which are influencing brain organization during development but also during adulthood. In insects, such factors include brood temperature, sex, age, and experience (Groh et al., 2004; Technau, 2007; Molina and O'Donnell, 2008).

To study sexual brain dimorphism or the influence of defined parameters (ranging from single molecules to social experience) on brain development or adult plasticity, average or standardized brains or brain areas are needed to relate individual variations to

each other. Advances in imaging techniques, 3D reconstruction software, and computer power led so far to 3D reconstructions and subsequent standardization of brain areas of four insect species including *Drosophila melanogaster* (Rein et al., 2002; Jenett et al., 2006), the honeybee *Apis mellifera* (Brandt et al., 2005), the desert locust *Schistocerca gregaria* (Kurylas et al., 2008), and the sphinx moth *Manduca sexta* (el Jundi et al., 2009). To obtain such a standard insect brain, two methods have so far been established: The virtual insect brain (VIB) protocol and the iterative shape averaging (ISA) method. While the VIB protocol was mainly developed to compare wild type and genetically manipulated *Drosophila* (Rein et al., 2002; Jenett et al., 2006), the ISA method, first used for the honeybee, was aimed to register single reconstructed neurons from various individuals into one standard brain (Rohlfing et al., 2004; Brandt et al., 2005). Although the ISA method provides a far better representation of relative locations of brain areas, this high registration quality comes with the tradeoff of missing volumetric consistency for the neuropils. This means, a neuropil label of the standardized ISA brain does not represent the mean volume of all corresponding individual neuropil labels (Kuß et al., 2007; Kurylas et al., 2008). Thus, the VIB script remains advantageous for fast inter– and intraspecific comparisons of neuropils including sex-specific differences, while preserving volumetric consistency.

In the current study, we reconstructed in three dimensions and subsequently standardized brain areas of both sexes of the red flour beetle *Tribolium castaneum* using the VIB protocol. The aims of our study were to (1) compare adult brain neuropil volumes regarding sexual dimorphism (2) provide an adult female and male standard brain at A0 (freshly eclosed adults) as volume references for future genetical and behavioral studies, and (3) to compare the standard volumes of brain areas with previously published standard volumes of homologous brain areas of other neopteran insects. To obtain the desired datasets we labeled whole brains with an antiserum against the synaptic vesicle protein synapsin to visualize neuropil areas, analyzed the staining using confocal laser scanning microscopy, 3D reconstructed the selected brain neuropils using the software AMIRA (Visage Imaging, Fürth, Germany), and subsequently registered and standardized the neuropils using the (VIB) protocol. A standardization using the ISA method can be computed on request. Comparing the standardized neuropil volumes between females and males revealed no obvious sexual dimorphism in A0 *Tribolium* brains.

MATERIALS AND METHODS

ANIMALS

Wild type *Tribolium castaneum* (San Bernardino; Sokoloff, 1966) stock for egg laying was kept in plastic boxes (20 × 18 × 18 cm) in walk-in environmental chambers at 26°C under constant darkness. The boxes were half filled with substrate containing organic whole wheat flour supplemented with 5% dried yeast powder. To prevent sporozoan infections we added 0.05% (w/w) Fumidil-B (J. Webster Laboratories Inc., Princeville, Kanada; Berghammer et al., 1999).

For egg collection, we used similar procedures as described in Berghammer et al. (1999). The beetles were kept for 2 days in substrate and then separated from the substrate with a stainless steel sieve (710-µm mesh size; Retsch, Haan, Germany) to be transferred into a box filled with instant flour (type 405; Aurora Mühlen GmbH, Hamburg, Germany) for egg laying. After 2 days in instant flour, the beetles were separated again with the 710-µm sieve and the eggs fetched with a fine sieve (300-µm mesh size, Retsch, Haan, Germany). Instant flour was used for collecting eggs, because it becomes less clotted und does thus not clog the sieves in contrast to the normal white flour (Berghammer, et al., 1999). Eggs were then transferred into a separate box filled with fresh substrate. To optimize egg-laying performance, separated beetles were transferred back to substrate (Sokoloff, 1974). This separation technique was used to avoid the contamination of the substrate with secretions of the parents e.g. benzoquinones, because they can heavily influence the development of the larvae (Chapman, 1926; Happ, 1968; Sokoloff, 1974, 1977). The collected eggs were kept in substrate in smaller boxes (20 × 12 × 4 cm) in an incubator at 30°C and constant darkness. After about 4 weeks, the first beetles finished metamorphosis and freshly eclosed beetles (A0) could be collected. A0 beetles can be easily distinguished from older beetles by their white cuticle and their slow movement.

IMMUNOHISTOCHEMISTRY

For wholemount staining we adapted and refined the protocols described by Huetteroth and Schachtner (2005) and el Jundi et al. (2009). Whole brains were dissected in a drop of cold PBS (phosphate-buffered saline, 0.01 M, pH 7.4) and fixed subsequently in 4% formaldehyde (Roth, Karlsruhe, Germany) in 0.01-M PBS for 1–2 h at room temperature. The brains were then rinsed five times for 10 min at room temperature in 0.01 M PBS followed by preincubation for 1–2 days at 4°C in 5% normal goat serum (NGS; Jackson ImmunoResearch, Westgrove, PA, USA) in 0.01 M PBS containing 0,3% Triton X-100 (PBST). The monoclonal primary antibody from mouse against a fusion protein consisting of a glutathione-S-transferase and the first amino acids of the presynaptic vesicle protein synapsin I coded by its 5′-end (SYNORF1, Klagges et al., 1996) was used to selectively label neuropilar areas in the brain (3C11, #151101 (13.12.06), kindly provided by Dr. E. Buchner, Würzburg). Its specificity in *T. castaneum* was shown with Western blot (Utz et al., 2008). The brains were incubated in a 1:100 dilution of the synapsin antibody in PBST containing 2% NGS for 2–3 days at 4°C. Subsequently the brains were rinsed three times for 15 min with PBST before they were incubated with the secondary goat anti-mouse antibody conjugated to Cy5 (1:300, catalog code 115-175-146, lot 71608, Jackson ImmunoResearch, Westgrove, PA, USA) in PBST and 1% NGS for 2 days at 4 °C. Afterwards the brains were rinsed again with PBST five times for 10 min and subsequently dehydrated in an ascending ethanol series (50%, 70%, 90%, 95%, and two times 100%, for 2.5 min each) and then cleared in methyl salicylate (Merck, Gernsheim, Germany), until the tissue was transparent. At last the brains were mounted in Permount (Fisher Scientific, Pittsbourgh, PA, USA) between two coverslips using two reinforcing rings as spacers (Zweckform, Oberlaindern, Germany) to prevent compression of brains.

CLSM IMAGE ACQUISITION AND PROCESSING

The wholemount preparations for the standard brains were scanned with a confocal laser scanning microscope (CLSM, Leica TCS SP2) at 512 × 512 pixel resolution by using a 40× oil immersion objective

(HCX PL APO 40×/1.25–0.75 Oil CS (working distance: 0.1 mm); Leica, Bensheim, Germany). All brains were scanned with a voxel size of 0.73 × 0.73 × 0.5 µm, a speed of 200 Hz, a pinhole of 1 Airy unit and a line average of 2–4.

ALs were scanned at 1024 × 1024 pixel resolution with a 63× oil immersion objective (HCX PL APO 63×/1.32–0.60, Oil Ph3 CS (working distance: 70 µm); Leica, Bensheim, Germany) or a 40× oil immersion objective (HCX PL APO 40×/1.25–0.75 Oil CS (working distance: 0.1 mm); Leica, Bensheim, Germany) using a Leica TCS SP2 CLSM or with a 63× glycerol objective (HCX PL APO 63×/1.30 Glyc 21°C CS (working distance: 0.26 mm); Leica, Bensheim, Germany) using a Leica TCS SP5 CLSM. Depending on the zoom factor (1–4), the different CLSM and different objectives we scanned with varying voxel sizes 0.07–0.16 × 0.07–0.16 × 0.5–1 µm. ALs were scanned with a speed of 200–400 Hz, a pinhole of 1 Airy unit and a line average of 2–4.

IMAGE SEGMENTATION, RECONSTRUCTION, STANDARDIZATION AND VISUALIZATION

The selected 19 neuropils of the male and female brains were labeled with the segmentation editor in AMIRA 4.1 (Visage Imaging, Fürth, Germany). For the eight individual glomeruli of the right ALs we used AMIRA 5.2.1. For the segmentation and reconstruction details we refer to Kurylas et al. (2008). In short, semi-automatically created voxel-based label fields of eight paired and three unpaired neuropilar structures in 20 female and 20 male *T. castaneum* brains provided the underlying matrix of all computation processes performed (i.e. polygonal surface models, morphometric analysis, and shape averaging). For orientation guidance, brain outlines were reconstructed separately. This label field however was not standardized. The color code for neuropils of the standard brains is consistent with Brandt et al. (2005), Kurylas et al. (2008), and el Jundi et al. (2009). We offer the AMIRA label fields with color codes as online download (Supplement 1). The orientation of the brain structures is given with respect to the body axis.

The VIB protocol used for registration and standardization was described in detail by Jenett et al. (2006) and is available at http://www.neurofly.de. The functions of the VIB protocol are integrated features of the AMIRA graphical environment. The application of the VIB protocol requires a template brain which defines the position of individual neuropils in the visualized standard brain. To overcome a subjective bias, we selected the template brains according to optimal position and symmetry of the reconstructed neuropils. The selection contained three steps. First, according to Kurylas et al. (2008) and el Jundi et al. (2009) we calculated the distances of the centers of each of the reconstructed neuropils to the center of the respective brain. All distances for each brain were summed up, and the differences to the mean distance were calculated for all 20 brains of each sex respectively. In a second step, we calculated the symmetry of the brain areas by calculating the difference of the angles between the vectors connecting the centers of the neuropils. To obtain the angles, we calculated the vectors between the centers of the paired neuropils using the scalar product. In this way, we calculated angles between three neuropil pairs (AL–Me, AL–Ca, Ca–Me). The sum of the three angles served as the symmetry criterion. Both, the results of the distance and the angle calculations were normalized, with the worst brain set to one for each criterion. In the resulting combined ranking, the normalized values of both criteria were added. The third criterion for the choice of the template brain was a visual inspection of the three best ranked brains for each sex respectively. For the male template, we choose the brain ranking at number one according to the first two criteria. For the female template we choose number two, because visual inspection of the three best ranked brains revealed that the left peduncle of female brain number one was somehow twisted towards the midline. In the female ranking, brains number one and two were very close together. The choice of the template brain does not influence the resulting standard volumes (Kurylas et al., 2008). For creation of standard brain neuropil labels, we chose an overlap threshold of 40% for all neuropils.

The statistical analysis of these data was obtained using Excel XP for Windows. The synapsin-immunoreactivity (syn-ir) in **Figures 1 and 5** was auto-contrasted in the OrthoSlice module of AMIRA. For visualization, neuropils segmented in AMIRA, were filled with transparent colored labels using Adobe Photoshop 8 (Adobe Systems, San Jose, CA, USA). Snapshots taken in AMIRA and Pictures edited in Photoshop (**Figures 1–3 and 5**), and diagrams generated with Excel XP (**Figures 4 and 6**) were imported to Corel Draw 13 (Corel Corporation, Ottawa, Ontario, CA, USA) without any further modification.

RESULTS

RECONSTRUCTED NEUROPILS

Of all major areas of the *Tribolium* brain we reconstructed those which we were able to unambiguously delimit in all three dimensions (8 paired and 3 unpaired neuropils). In the optic lobes, we reconstructed the medulla (Me), the lobula (Lo), the lobula plate (LoP), and the accessory medulla (aMe) (**Figures 1A-d, B-c′ and 2**). The LoP which lays posterior to the Lo is exclusively found in Ephemeroptera, Trichoptera, Coleoptera, Lepidoptera, Diptera (Strausfeld, 2005), and Heteroptera (Settembrini and Villar, 2005).

In the central brain we divided the mushroom body into two neuropils, the pedunculus (Pe), which contained the vertical lobe (vL) and medial lobe (mL), and the calyx (Ca) (**Figures 1A-b, B-a′,b′ and 2**). Although visible in the synapsin immunostaining, we refrained from including subunits of the pedunculus described for the moth *Spodoptera littoralis* (Sjöholm et al., 2005) or *Bombyx mori* (Fukushima and Kanzaki, 2009); the resulting complexity of the pedunculus would have greatly interfered with standardization procedures, and would have also interfered with interspecies comparison. Nevertheless, with the exception of the β'-, and γ-lobe, which lay very tight together and which typically are one protrusion after reconstruction, the other lobes of the pedunculus, the α-, α'-, and β- lobe (Zhao et al., 2008) are discernible protrusions in our reconstructions (**Figure 2**). Between the left and right mushroom body lies the central complex, which comprises the protocerebral bridge (PB), the upper and lower unit of the central body (CBU, CBL) and a small paired neuropil ventrally attached to the central body, the noduli (No) (**Figures 1A-c,e,f,B–b′ and 2**). The anteriormost labeled neuropils were the deutocerebral antennal lobes (AL, **Figures 1A-a and 2**).

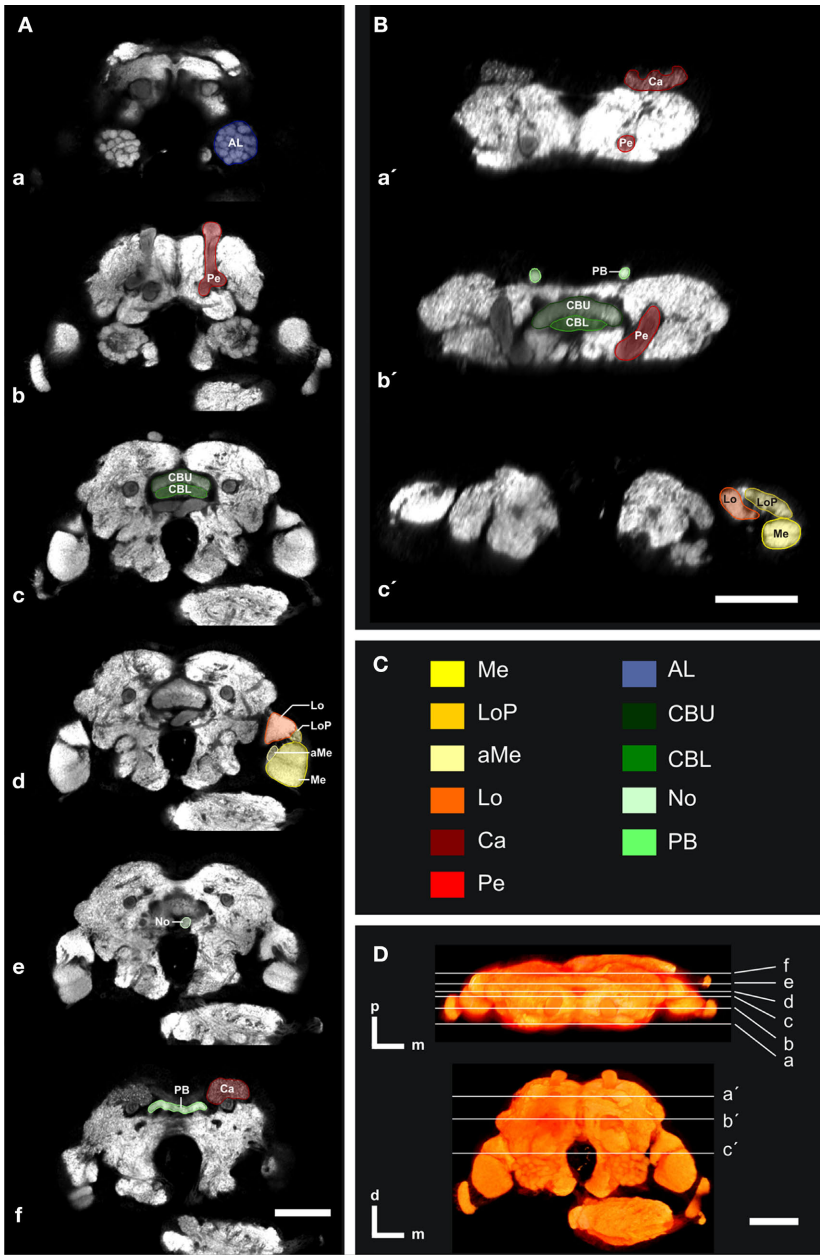

FIGURE 1 | Confocal images of the individual *T. castaneum* brain stained with an antibody against synapsin which was used as template for the VIB protocol. (A, B) Single optical sections through the brain in the frontal **(A)** and horizontal plane **(B)**. All manually labeled neuropil areas are shown as reconstructed in AMIRA. Labels of paired neuropils are only visualized in the left hemispheres, to provide a comparison to the unlabeled neuropils of the right hemispheres. **(A)** Frontal sections with the positions a–f from anterior to posterior and as described in **(D)**. **(B)** Horizontal sections with the positions a´–c´ from dorsal to ventral as described in **(D)**. **(C)** The color code of the labeled neuropils is consistent with Brandt et al. (2005), Kurylas et al. (2008), and el Jundi et al. (2009). AL, antennal lobe; Ca, Calyx; CBL, lower unit of the central body; CBU, upper unit of the central body; aMe, accessory medulla; Lo, lobula; LoP, lobula plate; Me, medulla; No, nodulus; PB, protocerebral bridge; and Pe, pedunculus with lobes. **(D)** Volume rendered (Voltex) view of the template brain from dorsal and frontal. The sections **(a–f)** and **(a′–c′)** represent the positions of the optical sections in **(A,B)**. Orientation bars, p, posterior; m, median; d, dorsal. All scale bars, 50 μm.

Representative outlines of all labels of these selected neuropils are shown in frontal and horizontal slices (**Figure 1**), an animation of all orthogonal sections of this brain can be found in the supplementary material (Supplement 2). Additionally, all reconstructed neuropils are displayed three-dimensionally to provide a 3D visualization of the whole brain (**Figure 2**).

THE STANDARD BRAINS

To apply the VIB protocol on the 3D brain reconstructions, one brain reconstruction had to be chosen as positional reference (Jenett et al., 2006). To reduce a subjective bias, we selected the template brains according to (1) position and (2) symmetry of the reconstructed neuropils, and (3) final visual inspection of the

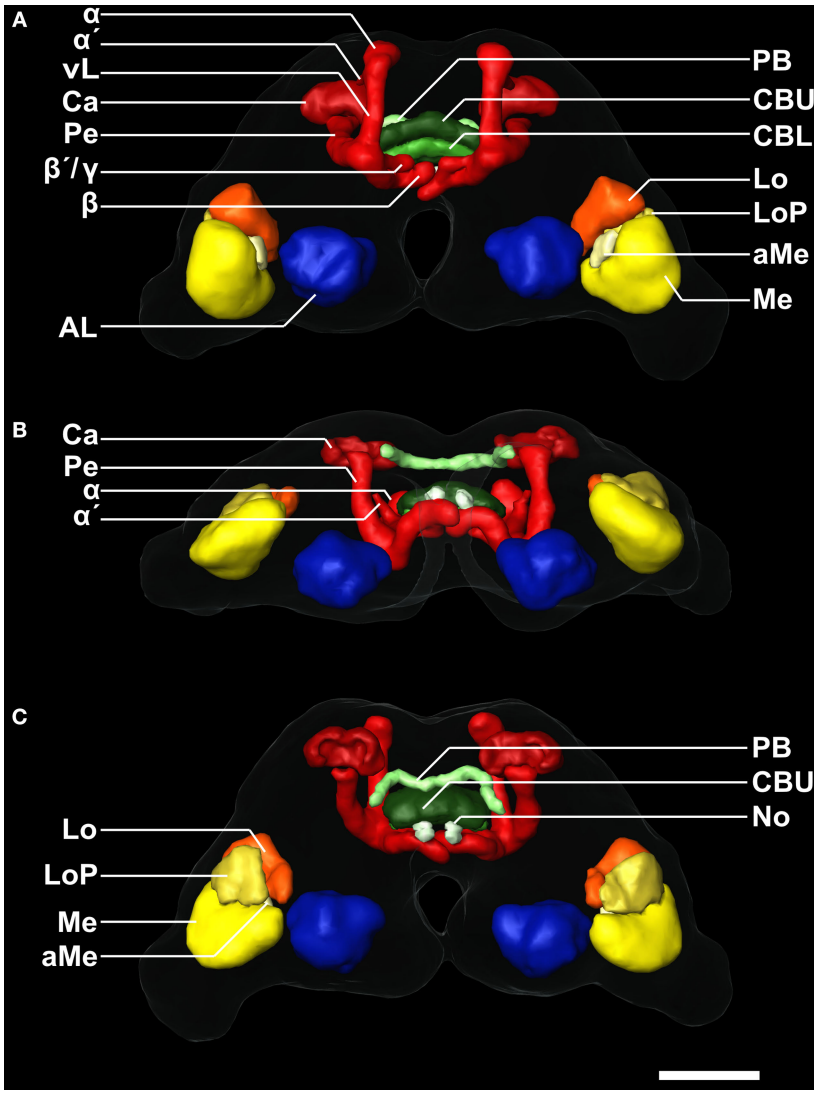

FIGURE 2 | 3D reconstruction of the male template brain of *T. castaneum* in (A) anterior (B) ventral, and (C) posterior view. The neuropils were visualized with the AMIRA tools SurfaceGen and Surfaceview. Note that the α and α´ lobes of the medial lobes can be clearly distinguished. In the medial lobes, the β-lobes are visible, while the second protrusion represents the β´- and the γ-lobes which were not discernable in the reconstruction. vL, vertical lobe. See **Figure 1** for color code and abbreviations. Scale bar, 50 μm.

three best brains resulting from criteria one and two (see Section "Materials and Methods"). The template brain used for generating the male standard brain is shown in **Figures 1 and 2**.

For the female and the male standard brain we reconstructed selected neuropils of 20 individual female and 20 individual male brains of freshly eclosed (A0) *T. castaneum*. With the VIB protocol we generated three-dimensional standard atlases of both sexes consisting of 19 neuropils (eight paired and three unpaired neuropils), including both hemispheres of the brain. The neuropil surface model and the corresponding average intensity map produced by direct volume rendering of the male standard brain are shown in **Figures 3A–C,A′–C′** from anterior, ventral and posterior. Volume rendering of all 20 label images after non-rigid registration reveal the high quality of registration (**Figures 3D,E**). Clear deviations are only visible in the vL of the MBs (**Figures 3D,E**). An animated view of the male standard brain can be seen in the online supplement (Supplement 3).

COMPARISON OF THE FEMALE AND MALE BRAINS

The VIB protocol also generates the standard volumes for each of the reconstructed brain areas of the 20 female and 20 male brains respectively. **Table 1** gives mean volumes, standard deviation and standard error of absolute and relative volumes of all 19 areas. Within each sex, a comparison of the volumes of the corresponding left and right brain neuropils using the two-tailed student t-test revealed no significant difference (not shown). Comparing the volumes of corresponding neuropils between females and males resulted also in no significant difference (**Figure 4**).

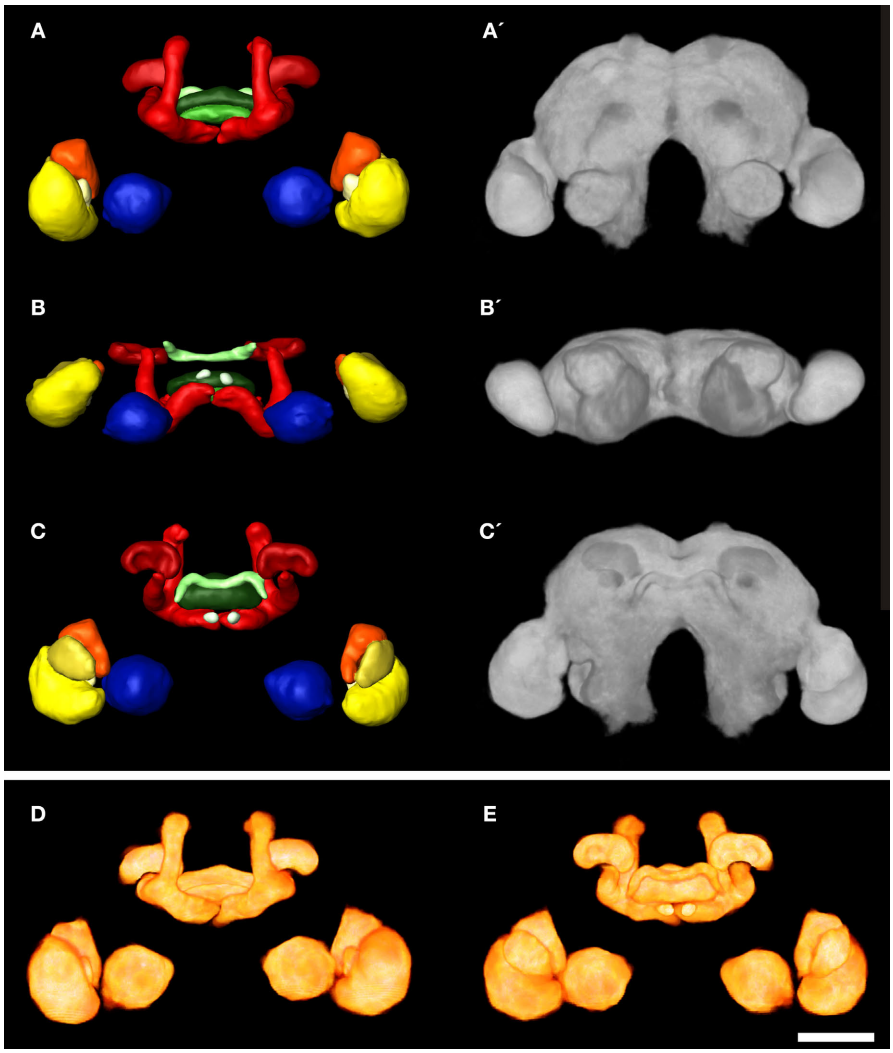

FIGURE 3 | 3D male standard brain of *T. castaneum* calculated from 20 individual brains by using the VIB protocol. (A–C) Surface reconstructions of all 18 averaged labels in **(A)** anterior **(B)** ventral, and **(C)** posterior view. The brain surface (as in **A´–C´**) is not labeled. See **Figure 1** for color code. **(A′–C′)** 3D visualization of the corresponding average intensity map by direct volume rendering with **(A′)** anterior **(B′)** ventral, and **(C′)** posterior view, using non-rigid transformation. **(D, E)** Direct volume rendered view of the resulting average label images from **(D)** anterior and **(E)** posterior, exhibiting deviations primarily in the lobes of the pedunculi of the MBs. Scale bar, 50 µm.

MALE – FEMALE GLOMERULUS COMPARISON

The glomerular array of ALs of adult female and male *T. castaneum* consists of about 70 glomeruli (Schachtner et al., 2007). The glomeruli are arranged in two layers around a central coarse neuropil. Anatomical sexual dimorphism in the ALs has been found in several species in which typically males have enlarged glomeruli at the entrance site of the antennal nerve (Schachtner et al., 2005). However, inspection of optical section series did not reveal an obvious morphological difference between A0 female and male ALs.

Searching for glomeruli which we could easily identify from animal to animal, we found an array of eight glomeruli at the lateral dorsal part of the AL, which we could unequivocally detect in 75% of our preparations. The set of dorso-lateral (dl) glomeruli consists of two larger glomeruli (dl-1, dl-2), three midsized (dl-3, dl-4, dl-7), and three smaller glomeruli (dl-5, dl-6, dl-8) with glomerulus dl-7 always being the most dorsal glomerulus of this set (**Figure 5**). We reconstructed these eight glomeruli from 10 female and 10 male right ALs with each AL stemming from a different specimen. Like the comparison between the AL volumes and all other reconstructed neuropils, comparison of the glomerular volumes between the two sexes revealed no significant difference in any one of the selected glomeruli (**Figure 6**).

DISCUSSION

Tribolium castaneum belongs to the most species-rich and most diverse order in the animal kingdom; Coleoptera comprise about 40% of all insect species and thus about 30% of all living animal species (Grimaldi and Engel, 2005; Hunt et al., 2007; Hauser et al., 2008). Worldwide, *Tribolium* is a major pest for stored grain and grain products and serves as a powerful model for the study of

Table 1 | Volume measures of neuropil structures in the male and female standard brain of *T. castaneum*. Mean volume (Mean vol.), relative volume (Rel. vol.), standard deviation (SD), relative standard deviation (Rel. SD), standard error (SE), and relative standard error (Rel. SE) of all segmented brain areas in the male (n = 20) and female (n = 20) standard brain of *T. castaneum*.

Structure	Sex	Mean vol. (µm³)	Rel. vol. (%)	SD (µm³)	Rel. SD (%)	SE (µm³)	Rel. SE (%)
Medulla (left)	♂	30339.91	14.85	7271.10	23.97	1625.87	5.36
	♀	34216.66	16.94	10668.84	31.18	2325.22	6.97
Medulla (right)	♂	31172.43	15.25	6053.76	19.42	1353.66	4.34
	♀	34157.33	16.91	9922.73	29.05	2162.61	6.50
Lobula plate (left)	♂	4824.63	2.36	1292.49	26.79	289.01	5.99
	♀	5251.18	2.60	850.56	16.20	185.37	3.62
Lobula plate (right)	♂	4599.73	2.25	1023.55	22.25	228.87	4.98
	♀	5073.72	2.51	681.34	13.43	148.50	3.00
Inner lobula (left)	♂	8685.43	4.25	1828.24	21.05	408.81	4.71
	♀	9554.28	4.73	1735.88	18.17	378.33	4.06
Inner lobula (right)	♂	9517.20	4.66	2256.13	23.71	504.49	5.30
	♀	9624.48	4.77	2820.86	29.31	614.79	6.55
Accessory medulla (left)	♂	1143.63	0.56	385.77	33.73	86.26	7.54
	♀	1173.94	0.58	350.44	29.85	76.38	6.67
Accessory medulla (right)	♂	1159.82	0.57	340.94	29.40	76.24	6.57
	♀	1230.22	0.61	406.31	33.03	88.55	7.39
Calyx (left)	♂	6003.60	2.94	1408.59	23.46	314.97	5.25
	♀	5515.65	2.73	1228.05	22.26	267.65	4.98
Calyx (right)	♂	6191.91	3.03	1084.28	17.51	242.45	3.92
	♀	5412.37	2.68	764.70	14.13	166.66	3.16
Pedunculus (left)	♂	17571.30	8.60	4577.99	26.05	1023.67	5.83
	♀	15796.60	7.82	3972.44	25.15	865.77	5.62
Pedunculus (right)	♂	17256.15	8.44	4794.07	27.78	1071.99	6.21
	♀	16057.83	7.95	3547.41	22.09	773.14	4.94
Central body upper unit	♂	10263.34	5.02	3179.91	30.98	711.05	6.93
	♀	8668.66	4.29	1842.36	21.25	401.53	4.75
Central body lower unit	♂	2838.02	1.39	1406.16	49.55	314.43	11.08
	♀	2364.33	1.17	713.66	30.18	155.54	6.75
Protocerebral bridge	♂	3551.02	1.74	863.97	24.33	193.19	5.44
	♀	3310.99	1.64	630.28	19.04	137.37	4.26
Nodulus (left)	♂	371.08	0.18	115.22	31.05	25.77	6.94
	♀	378.12	0.19	74.10	19.60	16.15	4.38
Nodulus (right)	♂	380.17	0.19	142.66	37.53	31.90	8.39
	♀	362.49	0.18	70.73	19.51	15.42	4.36
Antennal lobe (left)	♂	24373.09	11.93	5834.27	23.94	1304.58	5.35
	♀	22316.68	11.05	6733.24	30.17	1467.48	6.75
Antennal lobe (right)	♂	24105.27	11.80	6511.04	27.01	1455.91	6.04
	♀	21492.52	10.64	6132.60	28.53	1336.57	6.38

general insect development and evolution. Owing to the feasibility of transgenic approaches, such as powerful reverse genetics based on systemic RNA-interference, directed gene expression, the recently published full genome sequence, easy culturing, a short life cycle, high fecundity and longevity, *Tribolium* is emerging as a model system at many fronts. With the current study, we provide a reference for future anatomical studies of the brain in connection with genetical manipulation and external parameters as e.g. odor- or social environment and adaptive learning. The average brain atlas comes from freshly eclosed *Tribolium* of both sexes. Since we are especially interested in the development and plasticity of the olfactory system, we established an anatomical and volumetric reference of eight selected female and male olfactory glomeruli. Compared to existing insect standard brains, the *T. castaneum* standard poses - together with the *Drosophila* standard - the smallest brain.

STANDARD BRAIN GENERATION

Two methods have been established to obtain a standard insect brain: (1) the VIB protocol, as used for the fruit fly, the desert locust, and the sphinx moth (Rein et al., 2002; Jenett et al., 2006; Kurylas et al., 2008; el Jundi et al., 2009), and (2) the ISA method, as used for the honeybee and also the desert locust (Rohlfing et al., 2004; Brandt

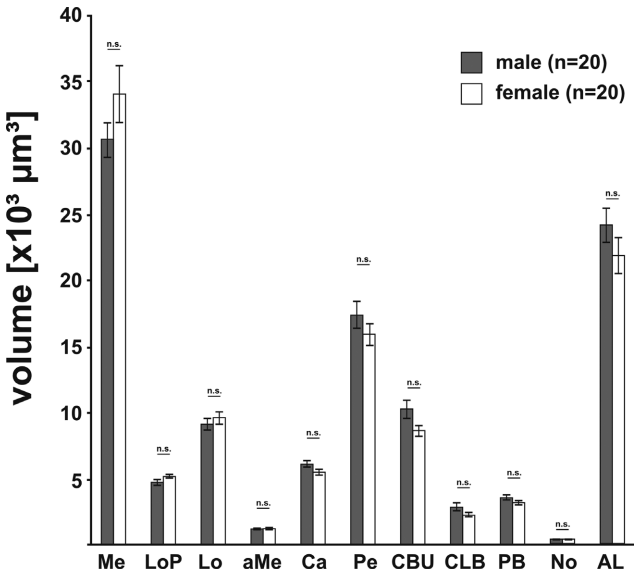

FIGURE 4 | Comparison of neuropil volumes between male (gray) and female (white) brains. The data revealed no significant difference (two-tailed Student's *t*-test) between the volumes of the corresponding neuropils of females and males. Bars, standard error; n.s., not significant.

et al., 2005; Kurylas et al., 2008). The VIB protocol was primarily developed to compare brain areas e.g. between wildtype and genetically manipulated *Drosophila*, while the ISA method aims to generate a synthetic but realistic standard brain, into which single reconstructed neurons from various individuals could be mapped. The VIB script keeps neuropil volumes rather unchanged, while the ISA method, in contrast, averages anatomical differences on the cost of volume accuracy (Kuß et al., 2007; Kurylas et al., 2008; el Jundi et al., 2009). Both methods require an initial reference or template brain for alignment. While the visualization of the standardized brain areas using the VIB protocol is clearly biased towards this template, the ISA method is thought to be independent of the choice of the template (Guimond et al., 2000; Brandt et al., 2005), with the notable exceptions of orientation and scale. During affine registration in the ISA method, all brains are resized using anisotropic scaling to match the size of the template brain. Thus, the resulting standard volumes of the brain areas generated by the ISA method depend on the choice of the template brain (Rohlfing et al., 2001; el Jundi et al., 2009). Therefore we decided to use the VIB protocol for standardization, since we primarily wanted to compare volumes of neuropils and did not aim for registration of reconstructed neurons (Rø et al., 2007; Kurylas et al., 2008). Given that both methods are established in our lab, a female and a male standard brain calculated by the ISA method could be computed on request.

It has to be noted that our whole mount specimens, like all immunohistochemical preparations, are subjected to considerable tissue shrinking (Bucher et al., 2000; Ott, 2008). Therefore absolute sizes are probably underestimated and make most sense in relative comparisons, i.e. comparisons might only be useful between brains after similar histological treatment. In a previous work, we already showed the usability of 3D reconstructions to quantify adult plasticity in the male antennal lobe of the sphinx moth (Huetteroth and Schachtner, 2005). Since we carefully checked for animal age, the female and male standard brain will serve as a reference in future quantitative studies using genetical or behavioral approaches.

BRAIN NEUROPIL COMPARISON BETWEEN SEXES

We found no volumetric differences between females and males in any one of the standardized brain neuropils, including the eight olfactory glomeruli. Anatomical sexual dimorphism in brain structures has been described in a variety of insects primarily with respect to the ALs (for a review see Schachtner et al., 2005). Enlarged glomeruli at the entrance site of the antennal nerve are described for males, as example for cockroaches (Jawlowski, 1948; Neder, 1959; Boeckh et al., 1987), bees (Arnold et al., 1984; Brockmann and Brückner, 2001), ants (Kleineidam et al., 2005; Nishikawa et al., 2008), flies (Kondoh et al., 2003), and moths (reviewed in Anton and Homberg, 1999; Hansson and Anton, 2000). These glomeruli are usually called macroglomeruli or macroglomerular complex (MGC). These glomeruli appear to be involved in pheromone signal processing (reviewed e.g. in Hansson and Christensen, 1999).

Why did we see no sexual dimorphism in the examined brain areas? In principal we expect sexual dimorphism on the level of the brain areas due to sexual specific input (e.g. in the case of the olfactory system a higher number of receptor neurons responsible for the detection of the female pheromone) and/or due to sexual specific behaviors which have to be coordinated from female or male brains in the context of sexual reproduction. The question is whether this dimorphism can be seen on the level of gross brain anatomy like in the case of the sexual specific glomeruli or whether it is due to a few special neurons or and/or different neurochemistry with only little or no effect on gross morphology. As individual variations in neuropil volumes range in the mean at around 20%, we cannot detect anatomical sexual dimorphism smaller than that. Furthermore, we looked at freshly eclosed animals. Thus, the animals are not sexually mature at that time and the brain has just started to get acquainted to the environmental cues including odor information like e.g. pheromones. Currently, we produce a female and male standard brain atlas for 7-day-old animals to examine how brain anatomy is changing in females and males. In *M. sexta* for example, the sexual dimorphic male glomeruli increase about 40% in volume during the first 4 days of adulthood (Huetteroth and Schachtner, 2005).

INTERSPECIES BRAIN COMPARISON

The relative size of a defined brain area is closely related to its apparent importance for the respective animal (e.g. Barton et al., 1995; Gronenberg and Hölldobler, 1999; Schoenemann, 2006). For example in insects larger optic lobes primarily correlate with larger complex eyes containing more photoreceptor cells, while the volume of ALs correlates with the amount of olfactory sensory axons entering this structure. Likewise, the volumes and the organization of higher order integration centers like the mushroom bodies correlate with the complexity of multimodal sensory integration (e.g. Technau, 2007; Molina and O'Donnell, 2008). Additionally, studies in several insect species demonstrated a correlation of volumes of brain areas with age, caste, sex and experience, including primary sensory integration centers like OL and AL, and higher integration centers like the mushroom bodies (Heisenberg et al., 1995; Barth

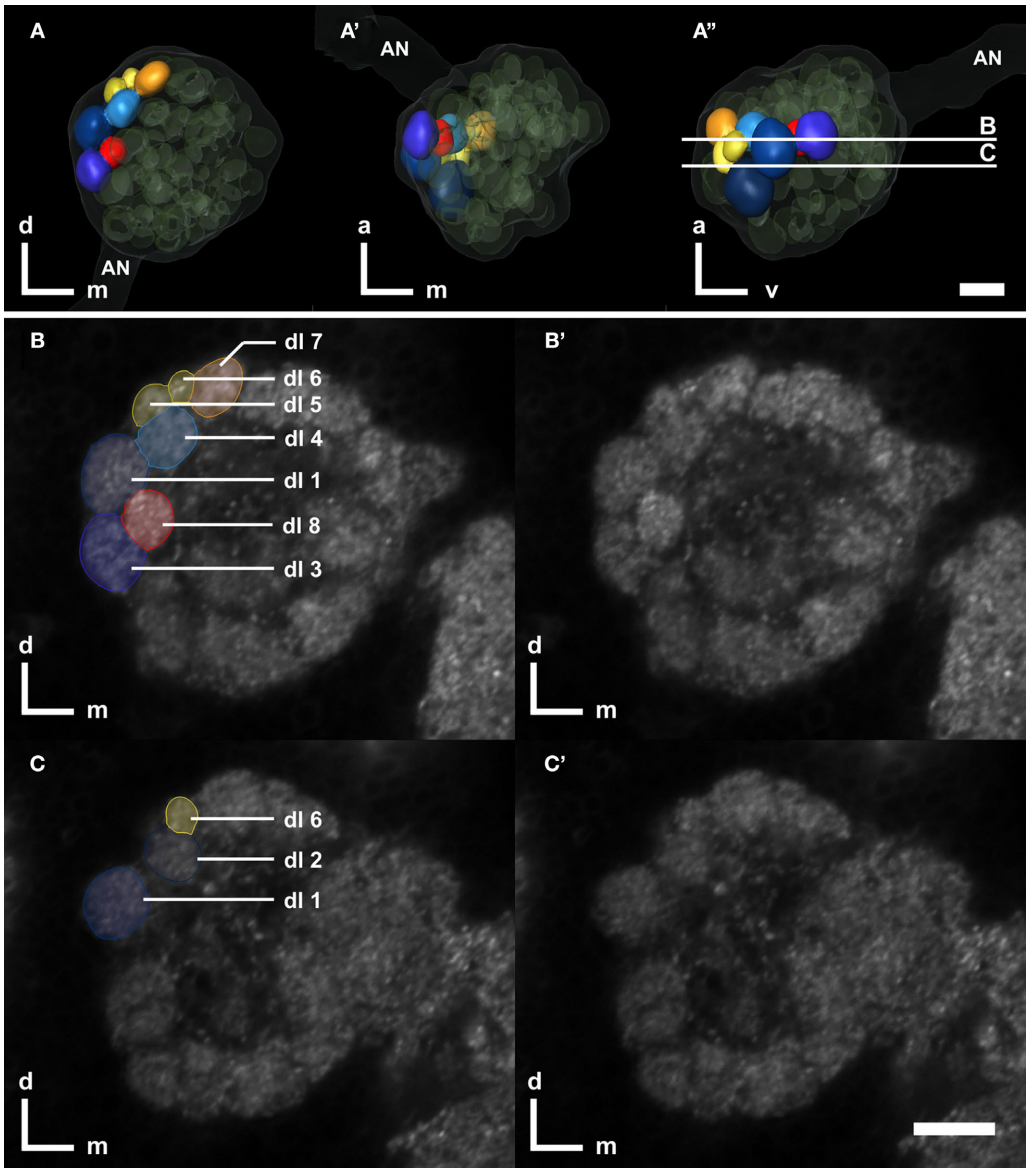

FIGURE 5 | Right antennal lobe of a male *T. castaneum* brain. (A–A′) Anterior **(A)**, ventral **(A′)**, and lateral view **(A″)** of 3D-reconstructed glomeruli including the antennal nerve (AN, transparent). The eight color coded dorso-lateral glomeruli (dl-1 to 8, compare with **B,C**) can be unequivocally identified in 75% of all preparations. Other glomeruli are depicted in transparent green; the displayed outline of the AL is shown in transparent gray. The transparent encasement around the AL represents the shape of the whole AL. The vertical bars in **(A″)** display section levels of **(B,C)** and **(B′,C′),** respectively. Orientation bars: a, anterior; d, dorsal; m, medial; v, ventral. **(B,C)** Frontal confocal sections through the antennal lobe according to **(A″)**. The eight dorso-lateral glomeruli are manually labeled as reconstructed in AMIRA. **(B′,C′)** Confocal sections through the antennal lobe corresponding to **(B,C)**. All scale bars: 10 μm.

and Heisenberg, 1997; Barth et al., 1997; Sigg et al., 1997; Julian and Gronenberg, 2002; Groh et al., 2006; Technau, 2007; Krofczik et al., 2008; Molina and O'Donnell, 2008; Maleszka et al., 2009; Snell-Rood et al., 2009). So far, the few published insect standard brains give only a limited view on the respective relative volumes of defined brain areas of these species because they provide (1) data for only one sex (with the exception of *M. sexta*) and (2) one age (*D. melanogaster*: 5-day-old adult females; Rein et al., 2002; *M. sexta*: freshly eclosed adult females and males; el Jundi et al., 2009), or (3) a mixture of different ages (*A. mellifera* foragers: Brandt et al., 2005; *S. gregaria* males: Kurylas et al., 2008). Caste or possible experience dependent differences have also not been taken into account. Thus, a comparison between the relative volumes of the available standardized brain areas has to be judged under these prerequisites (**Table 2**).

In *T. castaneum*, the optic lobes show the smallest relative volumes, which corresponds to the relative small compound eyes (with 80–83 ommatidia per eye; Friedrich et al., 1996) compared to the other insect species. The ALs in contrast display the largest relative volume, which suggests that *Tribolium* may primarily rely upon chemical cues, a fact which has been generally proposed for insects inhabiting grain storage areas (Levinson and Levinson,

1995). Behavioral assays showed that *T. castaneum* prefers damaged or deteriorated grains to full grains and it responds best to volatiles characteristic of damaged or fungus-infested grain (Trematerra et al., 2000). Tenebrionid beetles, including *T. castaneum*, produce a rich repertoire of volatiles in a variety of glands. Major volatile secretions, stored in specialized prothoracic and postabdominal glands are the quinones which may act as defensive secretions and antimicrobial substances (Prendeville and Stevens, 2002; Yezerski et al., 2004, 2007). Adult males of *T. castaneum* possess setiferous glands on the femora of their prothoracic legs (Faustini et al., 1981, 1982), which secrete the highly volatile pheromone, 4,8-dimethyldecanal (DMD), which is attractive to females and, to a less extent, to males and was therefore classified as an aggregation pheromone (Suzuki, 1980, 1981). However, the male setiferous glands may not be the major source of DMD (Bloch Qazi et al., 1998; Arnaud et al., 2002). Moreover, a recent electrophysiological investigation on *Tribolium* volatile compounds led to the conclusion that several beetle produced compounds, in addition to DMD, may be part of a complex aggregation pheromone system (Verheggen et al., 2007).

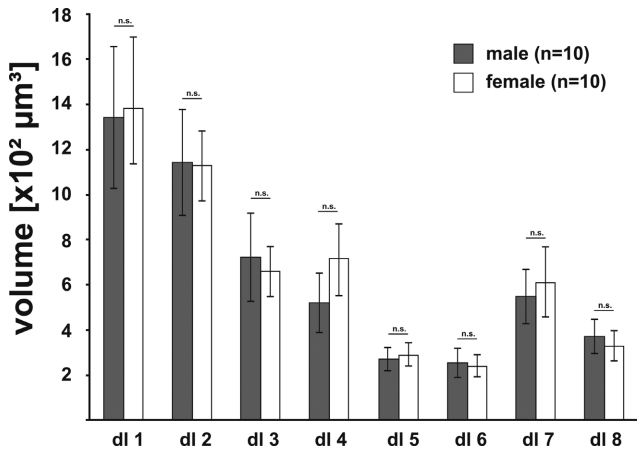

FIGURE 6 | Comparison of the volumes of the eight identified glomeruli between right male (gray; *n* = 10) and right female (white; *n* = 10) ALs, revealed no significant difference between the sexes (two-tailed student t-test). Bars, standard error; n.s., not significant.

Mushroom bodies (MBs) are generally associated with higher integration processes and learning (e.g. Menzel, 2001; Heisenberg, 2003), but might also serve a general function in the control of behavior (e.g. Huber, 1955a, b; Erber et al., 1987; Zars, 2000; Strausfeld et al., 2009). While the social honeybee by far exhibits the largest relative MB volumes, interestingly, *Tribolium* is second before *Drosophila* (**Table 2**). A recent study found similar development of MBs in *Tribolium* and *Drosophila*, with the remarkable difference, that adult neurogenesis occurs in *Tribolium* (Zhao et al., 2008). MBs vary in relative size in different nymphalid butterflies, without a correlation with optic or antennal lobe size. *Heliconius charitonius* for example has almost four times bigger mushroom bodies than other butterflies of that family (Sivinsky, 1989). This is attributed to its relative long life combined with its occurrence in forest habitats with only scattered food resources, and a shared resting place with conspecifics. As discussed by the author, remembering a common resting place and good food sites might be a higher evolutionary constraint for learning ability than finding proper egg-laying sites, which does not necessarily involve memory tasks (Sivinsky, 1989). For the ant *Cataglyphis*, Wehner et al. (2007) discussed social interaction rather than food gathering for being responsible of bigger mushroom bodies compared to other ant species, an idea originally brought up by von Alten (1910). The relative large size of the MBs in *Tribolium* suggests a high integrative capacity which may include olfactory components (see above). Additionally, a life expectation of months to years and a long reproductive period (Dawson, 1977) might also justify an investment into a brain structure dedicated to higher integration, memory, and behavioral control.

The function of the central complex still remains elusive, but is probably best described as a central coordinating function in sensory and motor integration (for reviews see Strauss, 2002; Wessnitzer and Webb, 2006; Homberg, 2008). Regarding the relative volume of the central complex, the sum of relative ellipsoid body volume and fan-shaped body volume in the fly and the relative volume of upper and lower units in locust, honeybee, moth, and beetle, *Tribolium* exceeds even that of the fly. This suggests a more complex function than in all other examined insects. In this context, it would be interesting to have comparable standardized central complex volumes of other coleopterans with different lifestyles e.g. water beetles or non-flying beetles.

Table 2 | Comparison of relative neuropilar volumes between different insect species obtained from five different insect orders, namely Diptera (*Drosophila melanogaster*: Rein et al., 2002), Hymenoptera (*Apis mellifera*: Brandt et al., 2005), Orthoptera (*Schistocerca gregaria*: Kurylas et al., 2008), Lepidoptera (*M. sexta*, el Jundi et al., 2009), and Coleoptera (*T. castaneum*, this work). We included the sex and the number of individuals which were used for respective standardization. Only neuropils which have complements in all examined animals were compared (optic lobes: medulla, lobula complex, and lobula plate; antennal lobes, mushroom bodies including calyces and pedunculi, upper and lower unit of the central body).

Order	**Diptera**	**Hymenoptera**	**Orthoptera**	**Lepidoptera**		**Coleoptera**	
Species	***D. melanogaster***	***A. mellifera***	***S. gregaria***	***M. sexta***		***T. castaneum***	
Sex	♀	♀	♂	♀	♂	♀	♂
Number of individuals	28	20	10	12	12	20	20
Optic lobes (%)	79.65	57.91	72.67	79.36	77.35	50,06	45,05
Antennal lobes (%)	9.36	8.53	9.68	12.86	15.09	22,41	24,50
Central body (%)	3.43	0.91	1.67	0.91	0.89	5,64	6,62
Mushroom bodies (%)	7.56	32.65	15.98	6.87	6.76	21,88	23,83

With the current study we provide a standard female and male brain of freshly eclosed *T. castaneum*. These standard brains will serve as a useful tool to study brain development and brain plasticity.

ACKNOWLEDGMENTS

The authors thank Dr. Erich Buchner (University of Würzburg, Germany) for kindly providing the anti-Synapsin antibody and Drs. Jochen Trauner and Gregor Bucher for supplying us with starter colonies of *Tribolium*. The authors are also grateful to Drs. Uwe Homberg, Ernst Wimmer and Stefan Schütz for many fruitful discussions and Martina Kern and Silke Redelfs for expert technical assistance. This work was supported by a DFG grant (SCHA 678/13-1) to Joachim Schachtner.

SUPPLEMENTARY MATERIAL

The Supplementary Material for this article can be found online at http://www.frontiersin.org/systemsneuroscience/paper/10.3389/neuro.06/003.2010/

REFERENCES

Anton, S., and Homberg, U. (1999). Antennal lobe structure. In Insect Olfaction, B. S. Hansson, ed. (Berlin, Springer), pp. 97–124.

Arnaud, L., Lognay, G., Verscheure, M., Leenaers, L., Gaspar, C., and Haubruge, E. (2002). Is dimethyldecanal a common aggregation pheromone of *Tribolium* flour beetles? *J. Chem. Ecol.* 28, 523–532.

Arnold, G., Masson, C., and Budharugsa, S. (1984). Demonstration of a sexual dimorphism in the olfactory pathways of the drones of *Apis mellifica L.* (Hymenoptera, Apidae). *Experientia* 40, 723–725.

Barth, M., and Heisenberg, M. (1997). Vision affects mushroom bodies and central complex in *Drosophila melanogaster*. *Learn. Mem.* 4, 219–229.

Barth, M., Hirsch, H. V., Meinertzhagen, I. A., and Heisenberg, M. (1997). Experience-dependent developmental plasticity in the optic lobe of *Drosophila melanogaster*. *J. Neurosci.* 17, 1493–1504.

Barton, R. A., Purvis, A., and Harvey, P. H. (1995). Evolutionary radiation of visual and olfactory brain systems in primates, bats and insectivores. *Philos. Trans. R. Soc. Lond., B, Biol. Sci.* 348, 381–392.

Berghammer, A., Bucher, G., Maderspacher, F., and Klingler, M. (1999). A system to efficiently maintain embryonic lethal mutations in the flour beetle *Tribolium castaneum*. *Dev. Genes Evol.* 209, 382–389.

Bloch Qazi, M. C., Boake, C. R. B., and Lewis, S. M. (1998). The femoral setiferous glands of *Tribolium castaneum* males and production of the pheromone 4,8-dimethyldecanal. *Entomol. Exp. Appl.* 89, 313–317.

Boeckh, J., Ernst, K. D., and Selsam, P. (1987). Neurophysiology and neuroanatomy of the olfactory pathway in the cockroach. *Ann. N. Y. Acad. Sci.* 510, 39–43.

Bonneton, F. (2008). The beetle by the name of *Tribolium*: typology and etymology of *Tribolium castaneum* Herbst, 1797. *Insect Biochem. Mol. Biol.* 38, 377–379.

Brandt, R., Rohlfing, T., Rybak, J., Krofczik, S., Maye, A., Westerhoff, M., Hege, H. C., and Menzel, R. (2005). Three-dimensional average-shape atlas of the honeybee brain and its applications. *J. Comp. Neurol.* 492, 1–19.

Brockmann, A., and Brückner, D. (2001). Structural differences in the drone olfactory system of two phylogenetically distant *Apis* species, *A. florea* and *A. mellifera*. *Naturwissenschaften* 88, 78–81.

Bucher, D., Scholz, M., Stetter, M., Obermayer, K., and Pflüger, H. J. (2000). Correction methods for three-dimensional reconstructions from confocal images: I. Tissue shrinking and axial scaling. *J. Neurosci. Methods* 100, 135–143.

Bucher, G., Scholten, J., and Klingler, M. (2002). Parental RNAi in *Tribolium* (Coleoptera). *Curr. Biol.* 12, R85–R86.

Chapman, R. N. (1926). Inhibiting the process of metamorphosis in the confused flour beetle (*Tribolium* confusum Duval). *J. Exp. Zool.* 45, 293–299.

Dawson, P. S. (1977). Life history strategy and evolutionary history of *Tribolium* flour beetles. *Evolution* 31, 226–229.

el Jundi, B., Huetteroth, W., Kurylas, A. E., and Schachtner, J. (2009). Anisometric brain dimorphism revisited: implementation of a volumetric 3D standard brain in *Manduca sexta*. *J. Comp. Neurol.* 517, 210–225.

Erber, J., Homberg, U. and Gronenberg, W. (1987). Functional roles of the mushroom bodies in insects. In Arthropod brain: Its evolution, Development, Structure, and Functions, A. P. Gupta, ed. (New York, NY, Wiley), pp. 485–511.

Faustini, D. L., Burkholder, W. E., and Laub, R. J. (1981). Sexually dimorphic setiferous sex patch in the male red flour beetles *Tribolium castaneum* (Herbst) (Coleoptera: Tenebrionidae): site of aggregation pheromone production. *J. Chem. Ecol.* 7, 465–480.

Faustini, D. L., Post, D. C., and Burkholder, W. E. (1982). Histology of aggregation pheromone gland in the red flour beetle. *Ann. Entomol. Soc. Am.* 75, 187–190.

Friedrich, M., Rambold, I., and Melzer, R. R. (1996). The early stages of ommatidial development in the flour beetle *Tribolium castaneum* (Coleoptera; Tenebrionidae). *Dev. Genes Evol.* 206, 136–146.

Fukushima, R., and Kanzaki, R. (2009). Modular subdivision of mushroom bodies by kenyon cells in the silkmoth. *J. Comp. Neurol.* 513, 315–330.

Grimaldi, D., and Engel, M. S. (2005). Evolution of the Insects. Cambridge, Cambridge University Press.

Groh, C., Ahrens, D., and Rössler, W. (2006). Environment- and age-dependent plasticity of synaptic complexes in the mushroom bodies of honeybee queens. *Brain Behav. Evol.* 68, 1–14.

Groh, C., Tautz, J., and Rössler, W. (2004). Synaptic organization in the adult honey bee brain is influenced by brood-temperature control during pupal development. *Proc. Natl. Acad. Sci. U.S.A.* 101, 4268–4273.

Gronenberg, W., and Hölldobler, B. (1999). Morphologic representation of visual and antennal information in the ant brain. *J. Comp. Neurol.* 412, 229–240.

Guimond, A., Meunier, J., and Thirion, J. P. (2000). Average brain models: a convergence study. *Comput. Vis. Image Underst.* 77, 192–210.

Hansson, B. S., and Anton, S. (2000). Function and Morphology of the Antennal Lobe: New Developments. *Annu. Rev. Entomol.* 45, 203–231.

Hansson, B. S. and Christensen, T. A. (1999). Functional characteristics of the antennal lobe. In Insect Olfaction. B. S. Hansson, ed. (Berlin, Springer). pp. 126–162.

Happ, G. M. (1968). Quinone and hydrocarbon production in the defensive glands of *Eleodeslongicollis* and *Tribolium castaneum* (Coleoptera, Tenebrionidae). *J. Insect Physiol.* 14, 1821–1837.

Hauser, F., Cazzamali, G., Williamson, M., Park, Y., Li, B., Tanaka, Y., Predel, R., Neupert, S., Schachtner, J., Verleyen, P., and Grimmelikhuijzen, C. (2008). A genome-wide inventory of neurohormone GPCRs in the red flour beetle *Tribolium castaneum*. *Front. Neuroendocrinol.* 29, 142–165. doi:10.1016/j.yfrne.2007.10.003.

Heisenberg, M. (2003). Mushroom body memoir: from maps to models. *Nat. Rev. Neurosci.* 4, 266–275.

Heisenberg, M., Heusipp, M., and Wanke, C. (1995). Structural plasticity in the *Drosophila* brain. *J. Neurosci.* 15, 1951–1960.

Hildebrand, J. G., and Shepherd, G. M. (1997). Mechanisms of olfactory discrimination: convergent evidence for common principles across phyla. *Annu. Rev. Neurosci.* 20, 595–611.

Homberg, U. (2008). Evolution of the central complex in the arthropod brain with respect to the visual system. *Arthropod Struct. Dev.* 37, 347–362.

Huber, F. (1955a). Über die Funktion der Pilzkörper (*Corpora pedunculata*) beim Gesang der Keulenheuschrecke Gomphocerus rufus L. (Acridiidae). *Naturwissenschaften* 20, 566–567.

Huber, F. (1955b). Sitz und Bedeutung nervöser Zentren für Instinkthandlungen beim Männchen von Gryllus campestris L. *Z. Tierpsychol.* 12, 12–48.

Huetteroth, W., and Schachtner, J. (2005). Standard three-dimensional glomeruli of the *Manduca sexta* antennal lobe: a tool to study both developmental and adult neuronal plasticity. *Cell Tissue Res.* 319, 513–524.

Hunt, T., Bergsten, J., Levkanicova, Z., Papadopoulou, A., St. John, O., Wild, R., Hammond, P. M., Ahrens, D., Balke, M., Caterino, M. S., Gómez-Zurita, J., Ribera, I., G. Barraclough, T. G., Bocakova, M., Bocak, L., and Vogler, A. P. (2007). A Comprehensive phylogeny of beetles reveals the evolutionary origins of a superradiation. *Science* 318, 1913–1916.

Jawlowski, H. (1948). Studies on the insect brain. *Ann. Univ. Mariae Curie Sklodowska C* 3, 1–30.

Jenett, A., Schindelin, J. E., and Heisenberg, M. (2006). The virtual insect brain protocol: creating and comparing standardized neuroanatomy. *BMC Bioinformatics* 7, 544.

Julian, G. E., and Gronenberg, W. (2002). Reduction of brain volume correlates with behavioral changes in queen ants. *Brain Behav. Evol.* 60, 152–164.

Klagges, B. R., Heimbeck, G., Godenschwege, T. A., Hofbauer, A., Pflugfelder, G. O., Reifegerste, R., Reisch, D., Schaupp, M., Buchner, S., and Buchner, E. (1996). Invertebrate synapsins: a single gene codes for

several isoforms in *Drosophila*. *J. Neurosci.* 16, 3154–3165.

Kleineidam, C. J., Obermayer, M., Halbich, W., and Rössler, W. (2005). A macroglomerulus in the antennal lobe of leaf-cutting ant workers and its possible functional significance. *Chem. Senses* 30, 383–392.

Klingler, M. (2004). *Tribolium*. *Curr. Biol.* 24, R639–R640.

Kondoh, Y., Kaneshiro, K. Y., Kimura, K., and Yamamoto, D. (2003). Evolution of sexual dimorphism in the olfactory brain of Hawaiian *Drosophila*. *Proc. Biol. Sci.* 270, 1005–1013.

Krofczik, S., Khojasteh, U., de Ibarra, N. H., and Menzel, R. (2008). Adaptation of microglomerular complexes in the honeybee mushroom body lip to manipulations of behavioral maturation and sensory experience. *Dev. Neurobiol.* 68, 1007–1017.

Kuß, A., Hege, H. C., Krofczik, S., and Borner, J. (2007). Pipeline for the creation of surface-based averaged brain atlases. In Proceedings of Winter School of Computer Graphics Vol. 1 pp. 17–24.

Kurylas, A. E., Rohlfing, T., Krofczik, S., Jenett, A., and Homberg, U. (2008). Standardized atlas of the brain of the desert locust, *Schistocerca gregaria*. *Cell Tissue Res.* 333, 125–145.

Levinson, A., and Levinson, H. (1995). Reflections on structure and function of pheromone glands in storage insect species. *Anz. Schädlingskd. Pfl. Umwelt.* 67, 99–118.

Maleszka, J., Barron, A. B., Helliwell, P. G., and Maleszka, R. (2009). Effect of age, behaviour and social environment on honey bee brain plasticity. *J. Comp. Physiol. A* 195, 733–740.

Menzel, R. (2001). Searching for the memory trace in a mini-brain, the honeybee. *Learn. Mem.* 8, 53–62.

Molina, Y., and O'Donnell, S. (2008). Age, sex, and dominance-related mushroom body plasticity in the paperwasp *Mischocyttarus mastigophorus*. *Dev. Neurobiol.* 68, 950–959.

Neder, R. (1959). Allometrisches Wachstum von Hirnteilen bei drei verschieden großen Schabenarten. *Zool. Jahrb. Abt. Allg. Zool. Physiol.* 77, 411–467.

Nishikawa, M., Nishino, H., Misaka, Y., Kubota, M., Tsuji, E., Satoji, Y., Ozaki, M., and Yokohari, F. (2008). Sexual dimorphism in the antennal lobe of the ant *Camponotus japonicus*. *Zool. Sci.* 25, 195–204.

Ott, S. R. (2008). Confocal microscopy in large insect brains: zinc-formaldehyde fixation improves synapsin immunostaining and preservation of morphology in whole-mounts. *J. Neurosci. Methods* 172, 220–230.

Prendeville, H. R., and Stevens, L. (2002). Microbe inhibition by *Tribolium* flour beetles varies with beetle species, strain, sex, and microbe group. *J. Chem. Ecol.* 28, 1183–1190.

Rein, K., Zöckler, M., Mader, M. T., Grübel. C., and Heisenberg, M. (2002). The *Drosophila* standard brain. *Curr. Biol.* 12, 227–231.

Richards, S. Gibbs, R. A., Weinstock, G. M., Brown, S. J., Denell, R., Beeman, R. W., Gibbs, R., Beeman, R. W., Brown, S. J., Bucher, G., Friedrich, M., Grimmelikhuijzen, C. J., Klingler, M., Lorenzen, M., Richards, S., Roth, S., Schröder, R., Tautz, D., Zdobnov, E. M, Muzny, D., Gibbs, R. A., Weinstock, G. M., Attaway, T., Bell, S., Buhay, C. J., Chandrabose, M. N., Chavez, D., Clerk-Blankenburg, K. P., Cree, A., Dao, M., Davis, C., Chacko, J., Dinh, H., Dugan-Rocha, S., Fowler, G., Garner, T. T., Garnes, J., Gnirke, A., Hawes, A., Hernandez, J., Hines, S., Holder, M., Hume, J., Jhangiani, S. N., Joshi, V., Khan, Z. M., Jackson, L., Kovar, C., Kowis, A., Lee, S., Lewis, L. R., Margolis, J., Morgan, M., Nazareth, L. V., Nguyen, N., Okwuonu, G., Parker, D., Richards, S., Ruiz, S. J., Santibanez, J., Savard, J., Scherer, S. E., Schneider, B., Sodergren, E., Tautz, D., Vattahil, S., Villasana, D., White, C. S., Wright, R., Park, Y., Beeman, R. W., Lord, J., Oppert, B., Lorenzen, M., Brown, S., Wang, L., Savard, J., Tautz, D., Richards, S., Weinstock, G., Gibbs, R. A., Liu, Y., Worley, K., Weinstock, G., Elsik, C. G., Reese, J. T., Elhaik, E., Landan, G., Graur, D., Arensburger, P., Atkinson, P., Beeman, R. W., Beidler, J., Brown, S. J., Demuth, J. P., Drury, D. W., Du, Y. Z., Fujiwara, H., Lorenzen, M., Maselli, V., Osanai, M., Park, Y., Robertson, H. M., Tu, Z., Wang, J. J., Wang, S., Richards, S., Song, H., Zhang, L., Sodergren, E., Werner, D., Stanke, M., Morgenstern, B., Solovyev, V., Kosarev, P., Brown, G., Chen, H. C., Ermolaeva, O., Hlavina, W., Kapustin, Y., Kiryutin, B., Kitts, P., Maglott, D., Pruitt, K., Sapojnikov, V., Souvorov, A., Mackey, A. J., Waterhouse, R. M., Wyder, S., Zdobnov, E. M., Zdobnov, E. M., Wyder, S., Kriventseva, E. V., Kadowaki, T., Bork, P., Aranda, M., Bao, R., Beermann, A., Berns, N., Bolognesi, R., Bonneton, F., Bopp, D., Brown, S. J., Bucher, G., Butts, T., Chaumot, A., Denell, R. E., Ferrier, D. E., Friedrich, M., Gordon, C. M., Jindra, M., Klingler, M., Lan, Q., Lattorff, H. M., Laudet, V., von Levetsow, C., Liu, Z., Lutz, R., Lynch, J. A., da Fonseca, R.N., Posnien, N., Reuter, R., Roth, S., Savard, J., Schinko, J. B., Schmitt, C., Schoppmeier, M., Schröder, R., Shippy, T. D., Simonnet, F., Marques-Souza, H., Tautz, D., Tomoyasu, Y., Trauner, J., Van der Zee, M., Vervoort, M., Wittkopp, N., Wimmer, E.A., Yang, X., Jones, A. K., Sattelle, D. B., Ebert, P. R., Nelson, D., Scott, J. G., Beeman, R. W., Muthukrishnan, S., Kramer, K. J., Arakane, Y., Beeman, R. W., Zhu, Q., Hogenkamp, D., Dixit, R., Oppert, B., Jiang, H., Zou, Z., Marshall, J., Elpidina, E., Vinokurov, K., Oppert, C., Zou, Z., Evans, J., Lu, Z., Zhao, P., Sumathipala, N., Altincicek, B., Vilcinskas, A., Williams, M., Hultmark, D., Hetru, C., Jiang, H., Grimmelikhuijzen, C. J., Hauser, F., Cazzamali, G., Williamson, M., Park, Y., Li, B., Tanaka, Y., Predel, R., Neupert, S., Schachtner, J., Verleyen, P., Raible, F., Bork, P., Friedrich, M., Walden, K.K., Robertson, H. M., Angeli, S., Forêt, S., Bucher, G., Schuetz, S., Maleszka, R., Wimmer, E. A., Beeman, R. W., Lorenzen, M., Tomoyasu, Y., Miller, S. C., Grossmann, D., and Bucher, G. (The *Tribolium* Genome Sequencing Consortium) (2008). The genome of the model beetle and pest *Tribolium castaneum*. *Nature* 452, 949–955.

Rohlfing, T., Brandt, R., Maurer, C. R. Jr., and Menzel, R. (2001). Bee brains, B-splines and computational democracy: generating an average shape atlas. In IEEE Workshop on Mathematical Methods in Biomedical Image Analysis, Kauai, HI 2001, L. Staib, ed. (Los Alamitos, CA, IEEE Computer Society), pp. 187–194.

Rø, H., Müller, D., and Mustaparta, H. (2007). Anatomical organization of antennal lobe projection neurons in the moth Heliothis virescens. *J. Comp. Neurol.* 500, 658–675.

Rohlfing, T., Brandt, R., Menzel, R., and Maurer. C. R. Jr. (2004). Evaluation of atlas selection strategies for atlas-based image segmentation with application to confocal microscopy images of bee brains. *Neuroimage* 21, 1428–1442.

Schachtner, J., Goetz, B., Dippel, S., Dreyer, D. and Huetteroth, W. (2007). Metamorphic development of the antennal lobes of the red flour beetle *Tribolium castaneum*: 3D-reconstruction and neurochemistry. Program No. 135.2/F14. 2007 Neuroscience Meeting Planner. San Diego, CA: Society for Neuroscience (online).

Schachtner, J., Schmidt, M., and Homberg, U. (2005). Organization and evolutionary trends of primary olfactory brain centers in Tetraconata (Crustacea+Hexapoda). *Arthropod Struct. Dev.* 34, 257–299.

Schoenemann, P. T. (2006). Evolution of the size and functional areas of the human brain. *Annu. Rev. Anthropol.* 35, 379–406.

Settembrini, B. P, and Villar, M. J. (2005). FMRFamide-like immunocyrochemistry in the brain and subesophageal ganglion of *Triatoma infestans* (Insecta: Heteroptera). Coexpression with ß-pigment-dispersing hormone and small cardioactive peptide. *Cell Tissue Res.* 321, 299–310.

Sigg, D., Thompson, C. M., and Mercer, A. R. (1997). Activity-dependent changes to the brain and behavior of the honey bee, *Apis mellifera* (L.). *J. Neurosci.* 17, 7148–7156.

Sivinsky, J. (1989). Mushroom body development in nymphalid butterflies: a correlate of learning? *J. Insect Behav.* 2, 277–283.

Sjöholm, M., Sinakevitch, I., Ignell, R., Strausfeld, N. J., and Hansson, B. S. (2005). Organization of kenyon cells in subdivisions of the mushroom bodies of a lepidopteran insect. *J. Comp. Neurol.* 491, 290–304.

Snell-Rood, E. C., Papaj, D. R., and Gronenberg, W. (2009). Brain size: a global or induced cost of learning? *Brain Behav. Evol.* 73, 111–128.

Sokoloff, A. (1966). The Genetics of *Tribolium* and Related Species. Advances in Genetics, Suppl. 1. New York, Academic Press.

Sokoloff, A. (1974, 1977). The Biology of *Tribolium* with Special Emphasis on Genetic Aspects, Vol. II and III. Oxford, Clarendon Press/Oxford University Press.

Strausfeld, N. J. (2005). The evolution of crustacean and insect optic lobes and the origins of chiasmata. *Arthropod Struct. Dev.* 34, 235–256.

Strausfeld, N.J., Hansen, L., Li, Y., Gomez, R. S., and Ito, K. (1998). Evolution, discovery, and interpretations of arthropod mushroom bodies. *Learn. Mem.* 5, 11–37.

Strausfeld, N. J., Sinakevitch, I., Brown, S. M., and Farris, S. M. (2009). Ground plan of the insect mushroom body: functional and evolutionary implications. *J. Comp. Neurol.* 513, 265–291.

Strauss, R. (2002). The central complex and the genetic dissection of locomotor behaviour. *Curr. Opin. Neurobiol.* 12, 633–638.

Suzuki, T. (1980). 4,8-Dimethyldecanal: the aggregation pheromone of the flour beetles *Tribolium castaneum* and *T. confusum* (Coleoptera: Tenebrionidae). *Agric. Biol. Chem.* 44, 2519–2520.

Suzuki, T. (1981). A facile synthesis of 4,8-dimethyldecanal, aggregation pheromone of flour beetles, and its analogs. *Agric. Biol. Chem.* 45, 2641–2643.

Technau, G. M. (2007). Fiber number in the mushroom bodies of adult *Drosophila* melanogaster depends on age, sex and experience. *J. Neurogenet.* 21, 183–196.

Tomoyasu, Y., and Denell, R. E. (2004). Larval RNAi in *Tribolium* (Coleoptera) for analyzing adult development. *Dev. Genes. Evol.* 214, 575–578.

Tomoyasu, Y., Miller, S. C., Tomita, S., Schoppmeier, M., Grossmann, D., and Bucher, G. (2008). Exploring systemic RNA interference in insects: a genome-wide survey for RNAi genes in *Tribolium*. *Genome Biol.* 9, R10.

Trematerra, P., Sciarreta, A., and Tamasi, E. (2000). Behavioural responses of *Oryzaephilus surinamensis, Tribolium castaneum* and *Tribolium confusum* to naturally and artificially damaged durum wheat kernels. *Entomol. Exp. Appl.* 94, 195–200.

Utz, S., Huetteroth, W., Vömel, M., and Schachtner, J. (2008). Mas-allatotropin in the developing antennal lobe of the sphinx moth *Manduca sexta*: distribution, time course, developmental regulation, and colocalization with other neuropeptides. *Dev. Neurobiol.* 68, 123–142.

Verheggen, F., Ryne, C., Olsson, P. O., Arnaud, L., Lognay, G., Högberg, H. E., Persson, D., Haubruge, E., and Löfstedt, C. (2007). Electrophysiological and behavioral activity of secondary metabolites in the confused flour beetle, *Tribolium confusum*. *J. Chem. Ecol.* 33, 525–539.

von Alten, H. (1910). Zur Phylogenie des Hymenopterengehirns. *Jena. Z. Naturwiss.* 46, 511–590.

Wehner, R., Fukushi, T., and Isler, K. (2007). On being small: brain allometry in ants. *Brain Behav. Evol.* 69, 220–228.

Wessnitzer, J., and Webb, B. (2006). Multimodal sensory integration in insects – towards insect brain control architectures. *Bioinspir. Biomim.* 1, 63–75.

Yezerski, A., Ciccone, C., Rozitski, J., and Volingavage, B. (2007). The effects of a naturally produced benzoquinone on microbes common to flour. *J. Chem. Ecol.* 33, 1217–1225.

Yezerski, A., Gilmor, T. P., and Stevens, L. (2004). Genetic analysis of benzoquinone production in *Tribolium* confusum. *J. Chem. Ecol.* 30, 1034–1044.

Zars, T. (2000). Behavioral functions of the insect mushroom bodies. *Curr. Opin. Neurobiol.* 10, 790–795.

Zhao, X., Coptis, V., and Farris, S. M. (2008). Metamorphosis and adult development of the mushroom bodies of the red flour beetle, *Tribolium castaneum*. *Dev. Neurobiol.* 68, 1487–1502.

Conflict of Interest Statement: The authors declare that the research was conducted in the absence of any commercial or financial relationship that could be construed as a potential conflict of interest.

Received: 05 September 2009; paper pending published: 28 November 2009; accepted: 18 January 2010; published online: 03 March 2010.

Citation: Dreyer D, Vitt H, Dippel S, Goetz B, el Jundi B, Kollmann M, Huetteroth W and Schachtner J (2010) 3D standard brain of the red flour beetle Tribolium castaneum: a tool to study metamorphic development and adult plasticity. Front. Syst. Neurosci. ***4****:3. doi: 10.3389/neuro.06.003.2010*

frontiers in
SYSTEMS NEUROSCIENCE

REVIEW ARTICLE
published: 04 January 2010
doi: 10.3389/neuro.06.019.2009

Vibration-processing interneurons in the honeybee brain

Hiroyuki Ai*

Division of Biology, Department of Earth System Science, Fukuoka University, Fukuoka, Japan

Edited by:
Randolf Menzel, Freie Universitat Berlin, Germany

Reviewed by:
Martin Giurfa, University Paul Sabatier, France
Jürgen Rybak, Freie Universität Berlin, Germany

****Correspondence:***
Hiroyuki Ai, Division of Biology, Department of Earth System Science, Fukuoka University, 8-19-1 Nanakuma, Jonan-ku, Fukuoka 814-0180, Japan.
e-mail: ai@fukuoka-u.ac.jp

The afferents of the Johnston's organ (JO) in the honeybee brain send their axons to three distinct areas, the dorsal lobe, the dorsal subesophageal ganglion (DL-dSEG), and the posterior protocerebral lobe (PPL), suggesting that vibratory signals detected by the JO are processed differentially in these primary sensory centers. The morphological and physiological characteristics of interneurons arborizing in these areas were studied by intracellular recording and staining. DL-Int-1 and DL-Int-2 have dense arborizations in the DL-dSEG and respond to vibratory stimulation applied to the JO in either tonic excitatory, on-off-phasic excitatory, or tonic inhibitory patterns. PPL-D-1 has dense arborizations in the PPL, sends axons into the ventral nerve cord (VNC), and responds to vibratory stimulation and olfactory stimulation simultaneously applied to the antennae in long-lasting excitatory pattern. These results show that there are at least two parallel pathways for vibration processing through the DL-dSEG and the PPL. In this study, Honeybee Standard Brain was used as the common reference, and the morphology of two types of interneurons (DL-Int-1 and DL-Int-2) and JO afferents was merged into the standard brain based on the boundary of several neuropiles, greatly supporting the understanding of the spatial relationship between these identified neurons and JO afferents. The visualization of the region where the JO afferents are closely appositioned to these DL interneurons demonstrated the difference in putative synaptic regions between the JO afferents and these DL interneurons (DL-Int-1 and DL-Int-2) in the DL. The neural circuits related to the vibration-processing interneurons are discussed.

Keywords: brain, honeybee standard brain (HSB), integration, audition, olfaction, waggle dance, parallel processing

INTRODUCTION

Honeybees communicate with each other for the benefit of the whole society. One of the most intriguing forms of communication is the waggle dance: a dancing bee sends a message to other bees indicating the direction and distance from their hive to a site of nectar-bearing flowers. Karl von Frisch showed that bees are recruited by the waggle dance of their nestmates and that information encoded by the waggle dance guides them to a remote food source (Frisch, 1967). This finding was recently proved directly by following the flight paths of recruited bees using harmonic radar recording (Riley et al., 2005). Ethological studies on waggle-dance communication have suggested that the flower odor and airborne vibration generated by both abdomen waggling and wing vibration are important cues in dance communication (Michelsen et al., 1992; Dreller and Kirchner, 1993a; Michelsen, 2003; Farina et al., 2005). Behavioral experiments demonstrated that honeybees can detect air-particle movements with the Johnston's organ (JO) located at the second segment (pedicel) of the antenna (**Figure 1**; Towne and Kirchner, 1989; Kirchner et al., 1991; Dreller and Kirchner, 1993b). Sensory neurons in the JO transduce mechanical vibration of the flagellum (the third antennal segment) into neural excitation. The antenna and sensory neurons in the JO are specialized for detecting vibrations with frequencies in the range of 250–300 Hz, which is the normal range of the main vibration frequencies generated by the waggle dance (Tsujiuchi et al., 2007). The JO has also been suggested to play a role in detecting air current during flight (Srinivasan and Zhang, 2004).

On the other hand, three-dimensional visualization of the neurons, of the neuropile, and of the brain has been realized by confocal microscopic observation and visualization software, such as Amira (Mercury Computer Systems, San Diego, CA, USA). Evers et al. (2005) developed the methods for making precise automatic geometric reconstruction of neuronal morphology from confocal image stacks. Moreover, Brandt et al. (2005) produced the three-dimensional average-shape atlas of the honeybee brain. This Honeybee Standard Brain (HSB) permits an overview of the spatial relationship between the morphologies of different neurons in the brain. The neural correlates of vibratory stimuli have not been examined so far, and the neural pathways for encoding the vibratory message during dance communication have also remained elusive. In the present study, we successfully identified three types of interneurons that have dense arborizations in both the dorsal lobe (DL) and the dorsal subesophageal ganglion (dSEG) or the posterior protocerebral lobe (PPL) and that respond to vibratory stimulation applied to the JO in specific patterns. The response patterns suggest that there are at least two parallel pathways for the vibratory processing through the DL-dSEG and the PPL. The registration of our identified neurons into the HSB demonstrated the difference in putative synaptic regions between the JO afferents and these DL interneurons in the DL.

MATERIALS AND METHODS

PREPARATION

Honeybees (*Apis mellifera* L.) were reared in hives placed on the Fukuoka University campus. Worker bees used in this study were caught at the hive entrance.

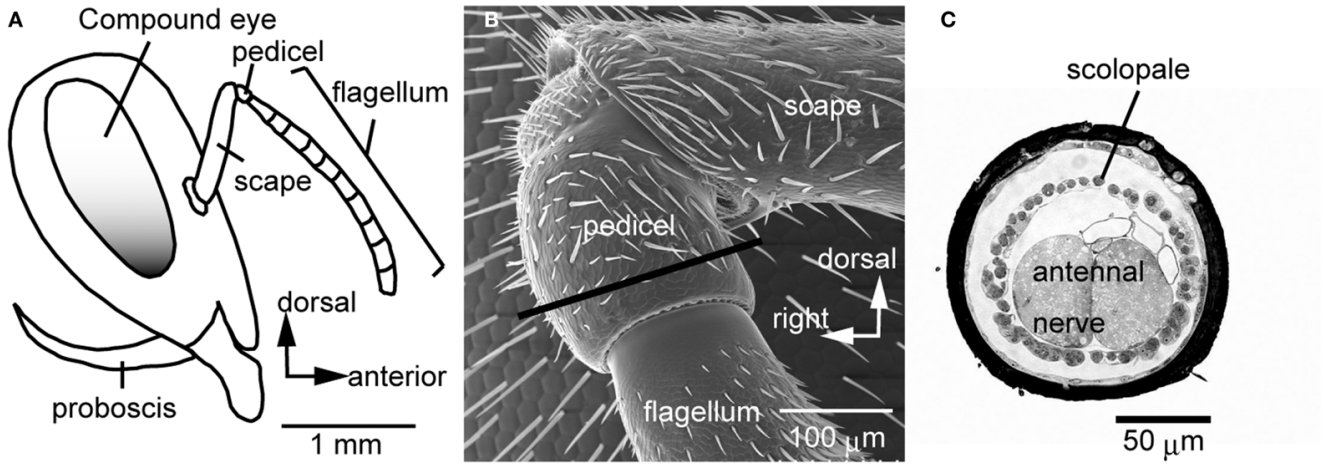

FIGURE 1 | The Johnston's organ of the honeybee. (A) A lateral view of the head of the honeybee. The antenna is composed of the scape, pedicel, and flagellum. The flagellum oscillates by air vibration. **(B)** Scanning electron microscopic image of the pedicel. **(C)** A transverse section of the pedicel at which the scolopales exist [at the region indicated by a line in **(B)**]. Each scolopale is a sensory unit of the Johnston's organ. In the pedicel, scolopales are located around the antennal nerve. Modified from Ai et al. (2007).

ANTEROGRADE STAININGS OF JO AFFERENTS

To stain JO afferents specifically, a small region of the ventral cuticle of the pedicel (free from bristles, **Figure 1A**) was removed with a razor blade. Then a small incision was made on cell bodies of JO, where a crystal of dextran-tetramethylrhodamine was placed. The preparations were kept for 48 h at 4°C. The success rate for obtaining complete staining of sensory afferents of interest was about 10%.

INTRACELLULAR RECORDING AND STAINING

The procedure followed is described in Ai et al. (2009). The bee was immobilized by cooling and mounted in an acrylic chamber. The bee in the chamber was fed with 1 M sucrose solution and kept overnight in the dark with high humidity at 20°C. The head of the bee was fixed with wax, and the frontal surface of the brain was exposed by cutting away a small rectangular window between the compound eyes. Then the glands and tracheal sheaths on top of the brain were removed. The mouthparts, including the mandibles, were cut off to expose the esophagus. Small droplets of bee physiological saline (in mM, 137 NaCl, 3 KCl, 1 $CaCl_2$, 4 Na_2HPO_4, 2 KH_2PO_4, 100 sucrose, pH 6.7) were applied to wash away the residue in the esophagus and to enhance electrical contact with a platinum ground electrode placed in the head capsule next to the brain.

Borosilicate glass electrodes were pulled with a laser puller (P-2000, Sutter Instruments, Novato, CA, USA) and filled at the tip with 2% Alexa 568 hydrazide (Invitrogen, La Jolla, CA, USA; A10437) dissolved in 100 mM KCl, yielding DC resistances in the range of 150–300 MΩ. The electrode was inserted into the antennal lobe after the neural sheath and a small area of the brain's neurilemma had been scratched. Electrical activities were recorded from neurons arborizing in either dSEG or DL. Electrical activities were amplified with an amplifier (MEZ 8301, Nihon Kohden, Tokyo, Japan) and displayed on an oscilloscope and a thermal-array recorder (RTA 1100M, Nihon Kohden, Tokyo, Japan). Data were stored on DAT tapes and then analyzed with a spike analyzer (Spike2, Cambridge Electronic Design, Cambridge, UK). Following recording of activities, the neurons were filled with Alexa 568 by applying a hyperpolarizing current (from 2 to 5 nA for 2–10 min). Thereafter, the brains were dissected out, immersed in 0.4% Lucifer yellow solution for 2 h, fixed in 4% paraformaldehyde for 4 h at room temperature, and then rinsed in phosphate buffer solution, dehydrated, and cleared in methyl salicylate for subsequent observation.

CONFOCAL MICROSCOPY

The cleared specimens containing backfilled or intracellularly stained neurons were viewed from the posterior side of the brain under a confocal laser-scanning microscope (LSM 510, Carl Zeiss, Jena, Germany) with a Zeiss Plan-Apochromat 10X/NA 0.45 dry lens objective (working distance, 2.1 mm) for low-magnified images or with a Zeiss Plan-Apochromat 20X/Na 0.8 dry lens objective (working distance, 0.55 mm) for high-magnified images. Both dextran-tetramethylrhodamine and Alexa 568 were excited by the 543-nm line of an HeNe laser, while Lucifer yellow was excited by the 488-nm line of an argon laser. Optical sections were made at 3 μm (in low-magnified image) or 1.5 μm (in high-magnified image) throughout the entire depth of each specimen. The image resolution was 1024×1024. Optical sections were reconstructed two dimensionally by using a software program provided by Zeiss. Adobe Illustrator was used to store and manipulate all photographs.

THREE-DIMENSIONAL RECONSTRUCTION

The spatial relationship between the identified interneurons and JO afferents was examined using the following procedure. First, the neuronal profiles of stained JO afferents and interneurons DL-Int-1 and -II stemming from different preparations were reconstructed using the Amira 4.1 (Mercury Computer Systems, Inc, San Diego, CA, USA; Evers et al., 2005). Subsequently, the neuropilar outlines were traced manually and segmented with the Amira 4.1 label field editor. These neuropilar label fields were used to register the

segmented neurons in each preparation into the corresponding part of the HSB following the method described in Brandt et al. (2005). This registration process involves both affine transformations and elastic geometric deformations. The affine transformation matrixes and the deformations vector fields were applied to the segmented neurons, and thus these were fitted into the HSB. To identify possible synaptic regions between the JO afferents and each identified interneuron, Amira's "surface distance" was used for calculating the distance of both neurons.

SENSORY STIMULATION

The experimental setup followed is described in Ai et al. (2009). First, both antennal scapes were fixed to the acrylic chamber with wax. For vibratory stimulation to the JO, the right antenna was inserted into a glass capillary (length, 10 mm; inner diameter of the tip, 200 μm) up to the second segment of the flagellum and then fixed to the tip of the capillary with wax. The opposite tip of the capillary was connected to the cone of a sound speaker (diameter of the cone, 60 mm). The sound speaker was driven by a wave generator (Multifunction generator 1945, NF Electronic Instruments, Yokohama, Japan). Continuous sine waves of frequency ranging from 10 to 400 Hz and vibration amplitude (peak to peak) ranging from 0 to 50 μm were applied.

For olfactory stimulations, fresh air was taken from outside through a diaphragm pump. The air was passed through a cotton filter, a charcoal filter, and then a silicon tube (inner diameter, 5 mm). The flow of air was controlled by a flow meter and kept at approximately 10 ml/s within the tube. The tube was then fed to a three-way solenoid valve that divided it into two tubes. One was used for a blank stimulus, and the other was further divided into five tubes, each of which was connected to a different cartridge so that five kinds of stimuli (orange oil, rose oil, citral, geraniol, and amyl acetate) could be applied separately. The cartridge for the blank stimulus and the five cartridges for odor stimuli converged onto the peripheral area of the air-delivery tube, which carried the continuous airflow over the antenna. One of the five odor stimuli was arbitrarily selected with a manually operated valve attached to each stimulus cartridge. The blank stimulus could be switched to one kind of olfactory stimulus by operating a solenoid-activated valve without changing the airflow. The tip of the air-delivery tube was positioned about 10 mm from the left antenna. The signals from the solenoid valve were stored on DAT tapes together with the simultaneously recorded neural activities. To keep the experimental environment clean, the air near the preparation was exhausted.

The light was turned off (less than 4 lux) during intracellular recording, except during visual stimulation. For visual stimulation, the light emitted from a halogen lamp of c.a. 500 lux with no filter was switched on and off by a self-made shutter.

NOMENCLATURE

We referred to Mobbs (1982) and Milde (1988) for the naming of neuropilar regions in the brain SEG complex. Orientation of neuronal structures is given according to the body axis.

RESULTS

CENTRAL PROJECTIONS OF JO AFFERENTS

Axons originating from the JO project into the brain SEG through the sensory tracts T6I and T6II, and their projection areas are spatially segregated in the PPL and the DL and the dSEG (DL-dSEG), respectively (Ai et al., 2007; **Figures 2A,B**). JO afferents passing through T6I comprise thick axons with large varicosities in the PPL, while those passing through T6II comprise thin axons with small and diverse varicosities in both the DL-dSEG. These findings suggest that there are at least two parallel pathways for processing mechanosensory stimuli detected by the JO.

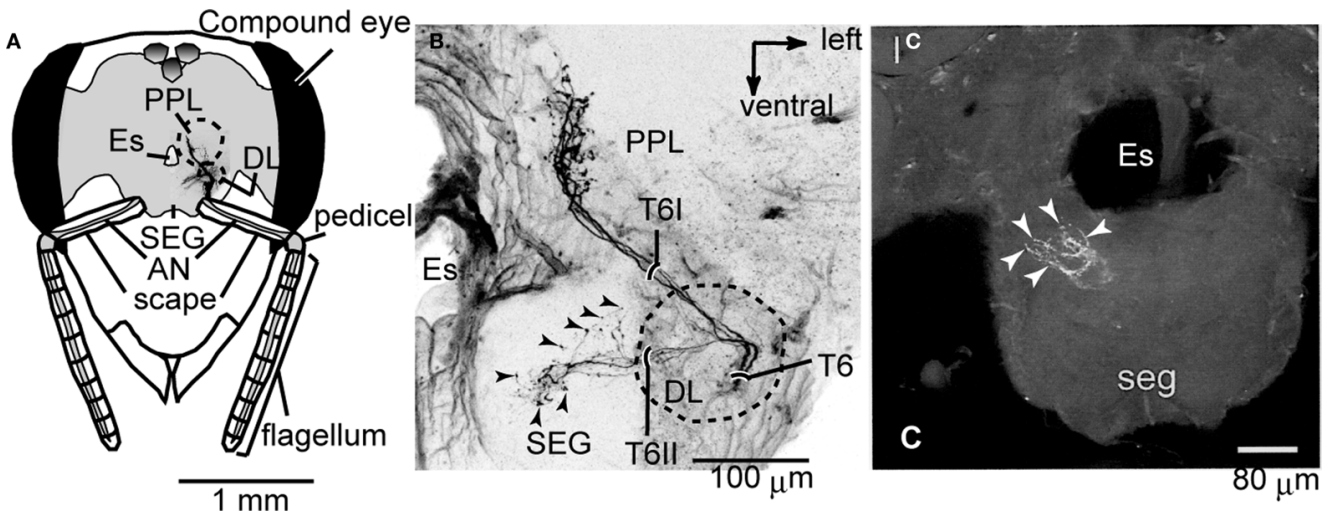

FIGURE 2 | Central projection of the Johnston's organ and neck hairs. **(A)** Brain-subesophageal ganglion (SEG) complex. The mechanosensory afferents on the antennae project into the dorsal lobe (DL), posterior protocerebral lobe (PPL), and SEG. **(B)** Central projection of the Johnston's organ. Dextran-tetramethylrhodamine was injected into the ventral scolopales in the Johnston's organ. The sensory afferents of T6I project to the PPL, and those of T6II project to the DL and dSEG. **(C)** Central projection of neck hairs in SEG. Arrowheads in **(B)** and **(C)** show the terminal varicosities in dSEG. lc, lateral calyx of mushroom body; Es, esophagus. **(A)** and **(B)** are modified from Ai et al. (2007); **(C)** is modified from Brockmann and Robinson (2007).

MORPHOLOGY AND PHYSIOLOGY OF VIBRATION-SENSITIVE INTERNEURONS

Interneurons arborized in the primary sensory area of the JO were recorded intracellularly when the animal was stimulated by signals emitted from the dancer. Several unique interneurons were identified that arborized densely in either the DL-dSEG (Ai et al., 2009) or the PPL and responded to vibratory stimulation applied to the JO in specific patterns. These interneurons have their somata in the protocerebrum (PC; $n = 27$), deutocerebrum (DC; $n = 10$), or SEG ($n = 40$). Most of these interneurons interconnect the protocerebral lobe, the DL, and the SEG, or subregions of these neuropils. Three types of interneurons can be distinguished: dorsal lobe interneuron type 1 (DL-Int-1; $n = 8$), dorsal lobe interneuron type 2 (DL-Int-2; $n = 4$), and posterior protocerebral lobe descending neuron type 1 (PPL-D-1; $n = 3$) neurons. DL-Int-1 and DL-Int-2 neurons respond to vibratory stimulation of the JO with an on–off phasic excitation, a tonic inhibition, or a tonic excitation. DL-Int-1 neurons respond to both olfactory and visual (light on) stimuli, while DL-Int-2 neurons do not respond to the olfactory and visual stimuli. PPL-D-1 neurons respond to the vibratory stimuli only during and after olfactory stimuli of the antenna. The PPL-D-1 neurons respond to the light stimuli.

DL-Int-1

The soma of DL-Int-1 is located on the dorsal rind of the PC. It gives rise to a single primary neurite just posterior to the central body below the mushroom body calyces (**Figure 3A**). The primary neurite runs anteroventrally to the DL. Here, it splits into two secondary neurites, one of them having dense arborizations in the DL-dSEG and the other thin arborizations in the PPL (**Figure 3B**). The arborizations in the PPL comprise a small number of fine spines, while those of the DL-dSEG possess not only fine spines but also blebs.

To elucidate the spatial relationship between a DL-Int-1 and JO afferents, both DL-Int-1 and JO afferents were reconstructed three dimensionally using the method of tracing by Evers et al. (2005).

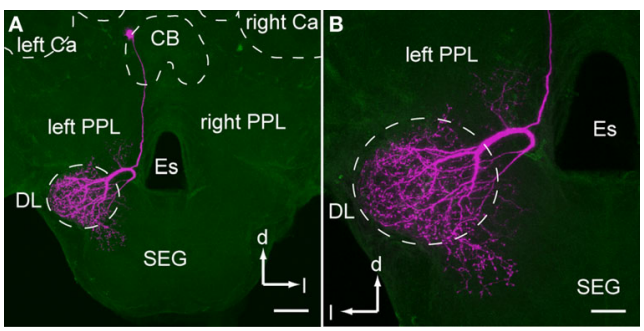

FIGURE 3 | An example of dorsal lobe interneuron type 1 (DL-Int-1). (A) shows an entire dye-filled cell, and **(B)** depicts an enlarged view of the dorsal lobe arborization. **(A)** The soma of DL-Int-1 is located dorsally at the most posterior region of the protocerebral lobe close to the central body (CB). **(B)** DL-Int-1 arborizes densely in the dorsal lobe and dorsal subesophageal ganglion (DL-dSEG) and sends a small branch into the left posterior protocerebral lobe (PPL). Scale bar, 100 μm in **(A)**; 50 μm in **(B)**. Ca, calyx; d, dorsal; Es, esophagus; l, lateral; SEG, subesophageal ganglion. Modified from Ai et al. (2009).

Afterwards it was registered into the HSB (**Figures 4A,** Brandt et al., 2005). Because all preparations were counterstained with Lucifer yellow, the visualization of the neuropil borders was much improved, and the alignment for the registration process of neuropils was facilitated. The DL-Int-1 trifurcates at the medial region of the DL, close to the esophagus (**Figures 4B,C**). These branches ramify densely in the DL (blue ramifications in **Figures 4B,C**), dSEG (red ramification in **Figures 4B,C**), and the PPL (green ramification in **Figures 4B,C**). The JO afferents run close to the DL-Int-1 branches in the DL (blue ramifications in **Figure 4B**; magenta in **Figures 4A,C,D**), in the same region where the T6 of JO afferents bifurcates into T6I and T6II.

DL-Int-1 neurons are spontaneously active and show on–off phase-locked excitations or tonic inhibition lasting for the entire stimulation period. However, the responses of DL-Int-1 depend on the spontaneous spike frequency, and because the neurons also respond to odor, the combination of odor and vibratory stimulation leads to complex response patterns (Ai et al., 2009).

DL-Int-2

The soma of DL-Int-2 is located on the edge of the deutocerebrum (**Figure 5**) and gives rise to a single primary neurite that arborizes in the posteromedial and anterior region of the DL comprising sparse ramifying axon collaterals projecting to the lateral DL. The primary neurite branches into three thick axons at the center of the DL (x, y, and z in **Figure 5A**). One of the branches extends toward the anterior lateral protocerebral lobe where it terminates in many fine blebs (y, arrow in **Figures 5 and 6**). The branch that extends toward the dSEG comprises extensive ramifications with numerous fine spines in both the DL and the dSEG (x, arrow in **Figures 5 and 6**). Presumable synaptic boutons are present close to these spines. The remaining branch extends toward the lateral portion of the PPL and terminates here (z, arrow in **Figures 5 and 6**). Presumable dendritic arbors of the DL-Int-2 are located close to the JO afferents in the DL (**Figure 6**). The DL-Int-2 does not innervate the lateral horn of the protocerebral lobe.

DL-Int-2 neurons respond to the rather strong vibratory stimulation with phasic-tonic excitation and with on-phasic or on–off phasic excitation to the vibration of relatively low amplitude. No preferred frequency was found for the range of 200–400 Hz, but the sensitivity is maximal in the range of 250–300 Hz (Ai et al., 2009).

PPL-D-1 neuron

The somata of PPL-D-1 neurons are located in the ventral cell cluster of the SEG (**Figure 7**). Each soma gives rise to a single primary neurite toward the dSEG that bifurcates into a dendritic neurite with a broad and dense arborization in the ipsilateral PPL and into an axon running into the contralateral ventral nerve cord (**Figure 7**). The dendritic neurite branches into four thick axons at the ventral region of the PPL (**Figure 7**). These thick branches terminate in the PPL with extensive ramifications carrying numerous fine spines in fan-shaped dendritic fields. The ramifications extend toward the midline of the PC. The contralaterally running axon gives rise to fine collaterals with blebby terminals (presumably synaptic boutons) at the contralateral SEG (**Figure 7C**). The collaterals extend into the contralateral PPL. Presumable dendritic arbors of the PPL-D-1 are located close to JO afferents in the PPL on the medioventral PPL.

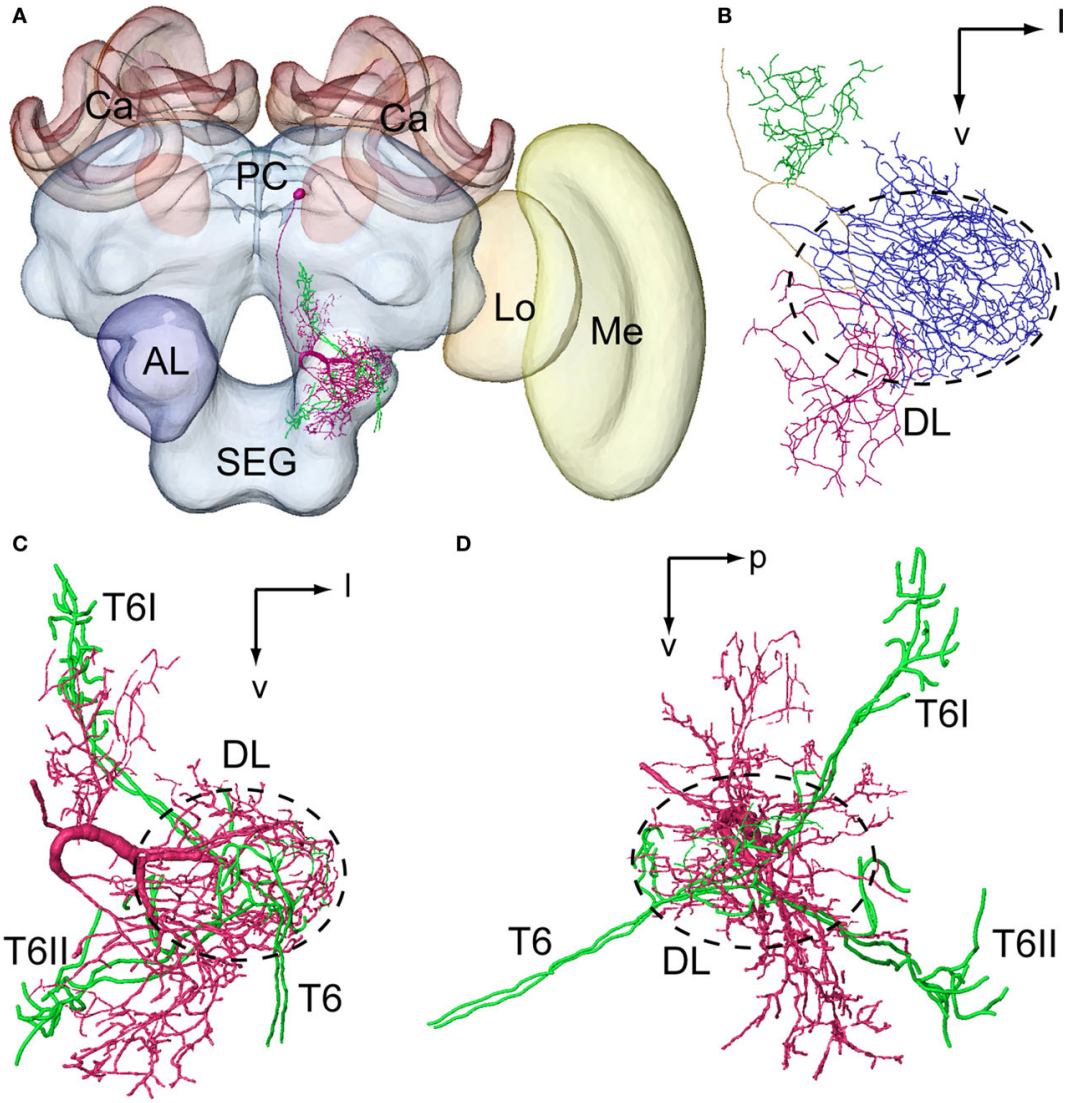

FIGURE 4 | Spatial relationship between a DL-Int-1 neuron and the Johnston's organ (JO) afferents stemming from two different specimens and registered into the standard brain of the honeybee. JO afferents in the antennal sensory tract T6 project to posterior target areas T6I and T6II. **(A)** shows a frontal view of a DL-Int-1 (magenta) and JO afferents (green) after registration into the Honeybee Standard Brain. **(B)** shows a frontal view of DL-Int-1 trifurcating into branches at the medial region of the dorsal lobe (DL, dotted circled line), close to the esophagus. These three branches ramify densely in the DL (blue ramifications), dSEG (red ramification), and PPL (green ramification). **(C,D)** Three-dimensional images of the arborizations of the DL-Int-1 (magenta) and JO afferents (green; **(C)** frontal view; **(D)** lateral view). Arborizations of the DL-Int-1 overlap with the terminal branches of the JO in the DL. l, lateral; p, posterior; v, ventral; Lo, lobula; Me, medulla. Modified from Ai et al. (2009).

The PPL-D-1 neuron does not respond to the vibratory stimulation alone but responds with long-lasting excitation to the vibration at 265 Hz when the olfactory (citral) stimulation is applied to the contralateral antenna. This and other observations indicate that PPL-DN-1 neurons integrate vibratory and olfactory stimulation.

DISCUSSION

PARALLEL PATHWAYS OF JO AFFERENTS

Axon terminals running in T6I are closely appositioned with those of secondary interneurons from the ocelli (Pareto, 1972; Mobbs, 1984; Ai et al., 2007), and T6I is known to be in close proximity to termination fields of visual projection neurons from the lobula (the neuropil specialized for movement detection; Maronde, 1991). The medial PPL is known to receive dendrites of motion-sensitive descending interneurons sending axons to locomotory centers in the SEG (Goodman et al., 1987; Ibbotson and Goodman, 1990). Thus, extension of JO axons into the medial PPL may permit simultaneous sampling of proprioceptive and external mechanosensory signals as well as visual signals. Considering the participation of the JO in flight control (McIver, 1985), the JO may modify visuomotor coordination during flight by detecting air current (Srinivasan and Zhang, 2004). In **Figure 7**, the descending neurons (PPL-D-1) that have arborizations in the PPL are shown, and these are suggested to be related to olfactory and vibratory processing in the PPL.

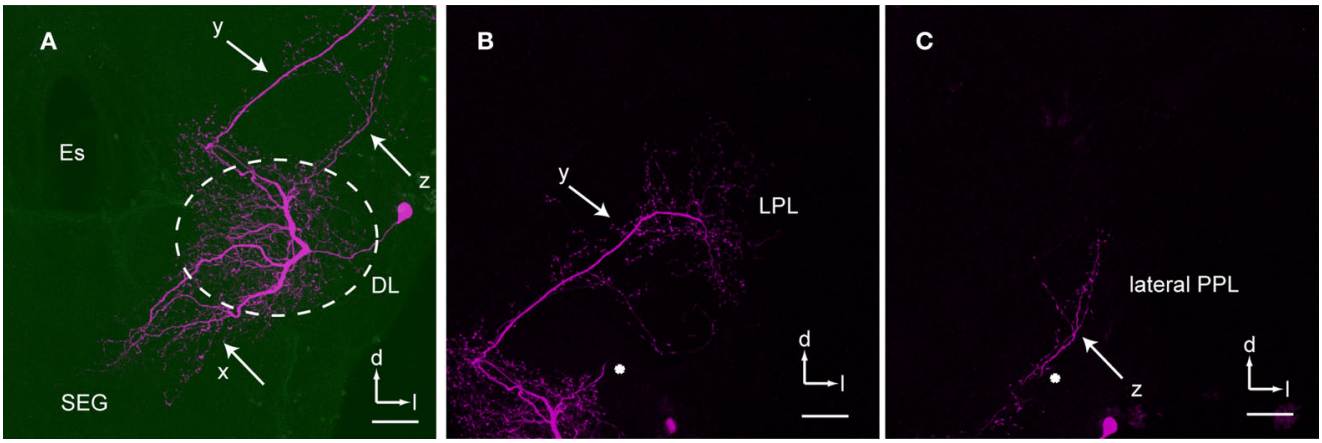

FIGURE 5 | An example of dorsal lobe interneuron type 2 (DL-Int-2). **(A)** The soma is located in the posterolateral region of the dorsal lobe (DL). The neuron has three major ramifications (x, y, and z). The most strongly ramified arborizations (x) are distributed in the DL and dorsal subesophageal ganglion (SEG) with numerous fine spines. **(B)** A long process (y) terminates in the lateral protocerebral lobe (LPL) with fine blebs. **(C)** A small branch (z) emanates from the major DL branch and projects into the lateral portion of the posterior protocerebral lobe (lateral PPL). **(B)** and **(C)** show the composite images of the same serial sections in consecutively different depths [the position marked by an asterisk in **(B)** corresponds to that in **(C)**]. d, dorsal; Es, esophagus; l, lateral; PC, protocerebrum. Scale bars, 50 μm. Modified from Ai et al. (2009).

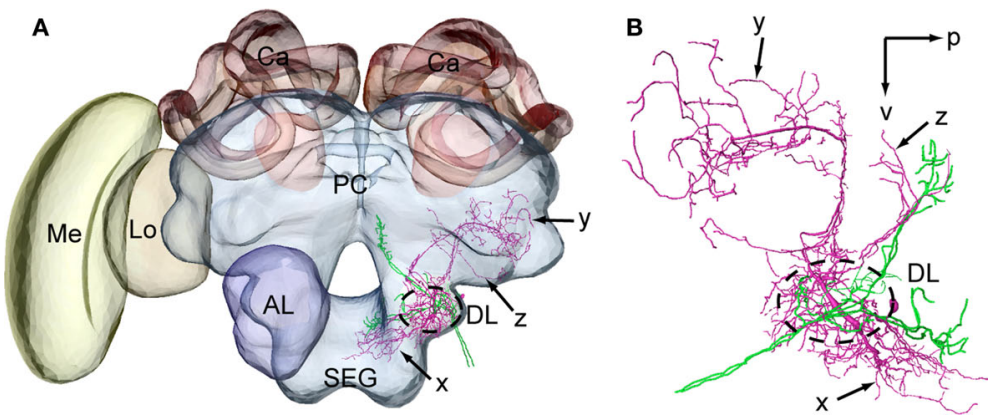

FIGURE 6 | Spatial relationship between a DL-Int-2 neuron and Johnston's organ (JO) afferents. The intracellularly marked DL-Int-2 and dye-injected JO afferents from two different specimens were reconstructed for most of their arborizations. **(A)** A DL-Int-2 neuron (magenta) and JO afferents (green) after registration into the Honeybee Standard Brain (frontal view). **(B)** Projection areas of the DL-Int-2 neuron (magenta) and JO afferents (green) in the dorsal lobe (DL, dotted circled line), the posterior and lateral protocerebral lobe (y, arrow and z, arrow, respectively), and the dorsal subesophageal ganglion (x, arrow) (lateral view). DL-Int-2 neurons overlap with the terminal branches of the JO in the dorsal lobe (DL). p, posterior; v, ventral. Modified from Ai et al. (2009).

Axons of T6II in the dorsal lobe and SEG are characterized by thin processes with small varicosities. Generally, the SEG is the primary center of mouth parts, while the dorsal lobe corresponds to the antennal mechanosensory center (Rehder, 1988, 1989; Kloppenburg, 1995) and also to the antennal gustatory center (Haupt, 2007). Axon terminals of exteroceptors (such as hair plate) originating from the pedicel and flagellum are closely appositioned to those of JO afferents in the SEG (Ai et al., 2007). In dance communication, tactile information together with airborne signals (e.g., jet streams and odors) is detected through antennal exteroceptors and appears to be important for follower bees detecting these signals at the rear end of the dancer bee (Rohrseitz and Tautz, 1999). While the orientation of the dancers during waggle phase relative to gravity codes the direction to the flower, the followers read this direction also in relation to gravity. It has been revealed that the sensory hairs on the neck detecting the orientation of body axis against gravity project to the dSEG (**Figure 2C**; Brockmann and Robinson, 2007), suggesting that the DL-dSEG is an important area for decoding the information about orientation in space and may serve to integrate the mechanosensory and chemosensory inputs from the antenna and mouthparts.

POSSIBLE NEURAL CIRCUITS FOR PROCESSING VIBRATION

Vibratory processing has not been studied extensively. In this study, we described several types of vibration-sensitive interneurons morphologically and electrophysiologically. These response patterns of the vibration-sensitive interneurons suggest that

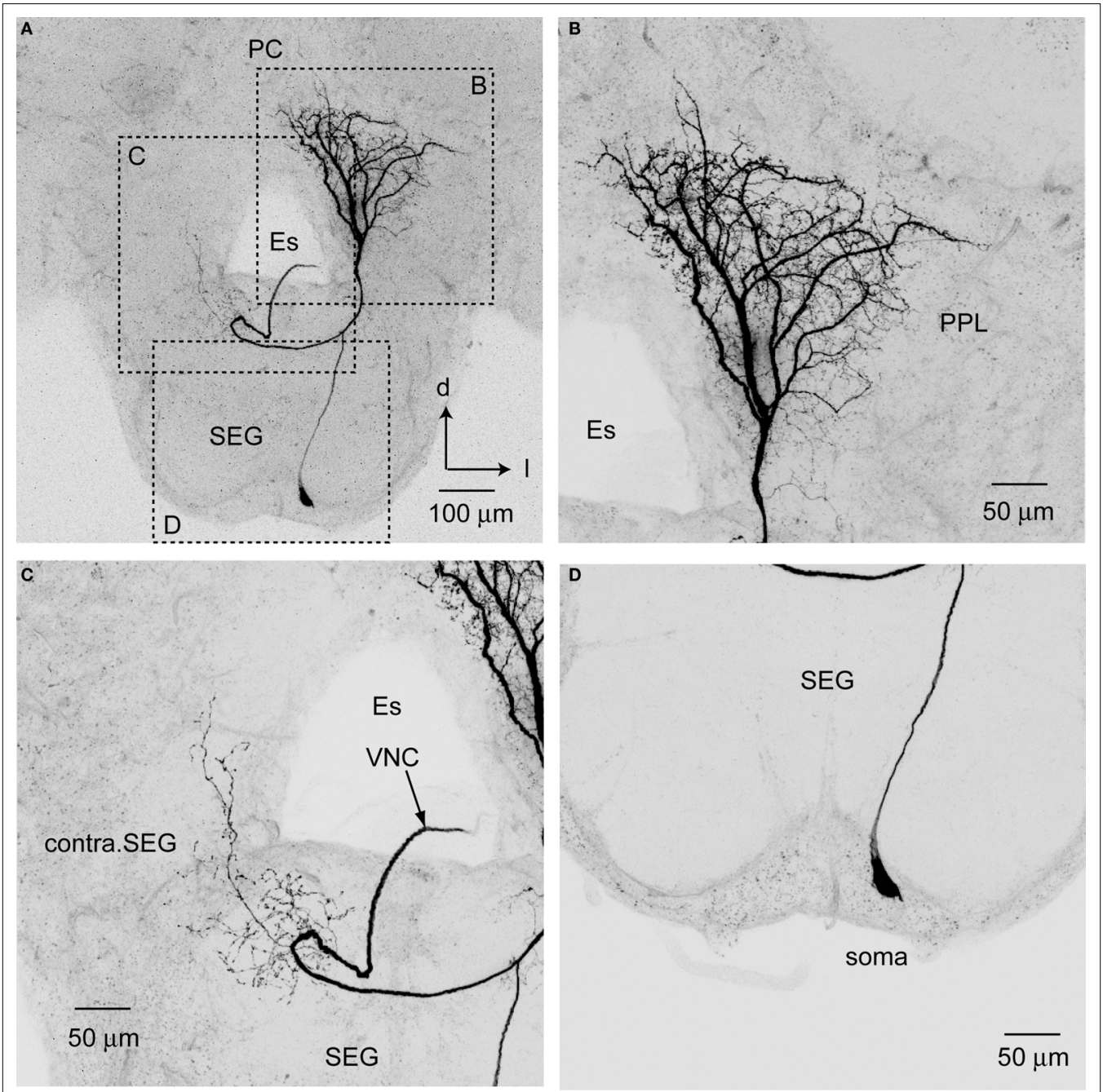

FIGURE 7 | Posterior protocerebral descending neuron type 1 (PPL-D-1). **(A)** An entire dye-filled PPL-D-1 neuron in brain-SEG. **(B–D)** are enlarged views of the arborization shown in **(A)**. **(B)** The dense and broad arborization in PPL. **(C)** The sparse and fine arborization in the contralateral SEG (contra. SEG). **(D)** The cell body located on the median region of ventral SEG. d, dorsal; Es, esophagus; l, lateral; PC, protocerebrum; SEG, subesophageal ganglion; VNC, ventral nerve cord.

DL-Int-1 and DL-Int-2 are related to monitoring the length of the vibration, and PPL-D-1 appears to be related to regulating the behaviors triggered by both olfactory and vibratory stimuli. The morphological results suggest our identified DL-Interneurons have a direct synaptic connection or indirect synaptic connections close to the JO afferents in the DL because both the DL-Interneurons are closely appositioned to the JO afferents in the DL. Some DL-Int-1 neurons responded with a tonic inhibition to vibration applied to the JO, and the duration of the inhibition changed depending on the duration of vibration (Ai et al., 2009). The DL-Int-2 neurons responded optimally to 265-Hz vibration, which corresponds to the peak frequency of airborne vibrations arising during dance communication (Ai et al., 2009). These physiological characteristics of the response pattern of the interneurons to the vibratory stimulation support this assumption. Moreover the DL-Int-1 closely arborizes to JO afferents in

the central region of the DL, while the DL-Int-2 does the same in the anterior region of the DL (**Figure 8**). Haupt (2007) revealed that there are separate projection areas of gustatory and mechanosensory afferents in the DL. It is not clear whether the same JO afferents have synapses both on the DL-Int-1 and DL-Int-2 or different JO afferents have synapses on each DL-Int-1 and DL-Int-2; however, it is clear that there is a spatial functional segregation in the DL.

DL-Int-1 neurons received bimodal inputs when the vibration was applied to the antenna (Ai et al., 2009). One was an on–off excitatory input, and the other was a tonic inhibitory input. Because the dendrites of DL-Int-1 neurons were very close to the JO sensory axons in the DL (**Figure 4**), the sensory neurons of the JO may have direct synapses on the DL-Int-1 neurons, especially excitatory synapses for the on–off phasic excitation. The inhibitory response of the DL-Int-1 neurons suggests that they may have inhibitory synaptic inputs directly from the JO afferents, provided that the JO afferents themselves are inhibitory neurons. Otherwise, DL-Int-1 neurons may receive inhibitory synaptic input from some interneurons that are excited by JO afferents. GABA-like immunoreactive profiles in the DL and the SEG (Schäfer and Bicker, 1986) may support the latter assumption, though inhibitory synaptic inputs to DL-Int-1 neurons have not yet been confirmed. The pattern of response of DL-Int-1 neurons to vibration changes corresponds to the magnitude of spontaneous activity and can be changed by depolarizing current injection into the neuron (Ai et al., 2009). This effect of depolarizing current injection may simulate the effect of additional inputs through other sensory systems (e.g., olfactory input). Thus, the neural activities appear to be regulated by direct or indirect synaptic inputs from as yet unknown centrifugal neurons.

DL-Int-2 neurons received an excitatory input when the vibration was applied to the antenna (Ai et al., 2009). Because the dendrites of DL-Int-2 neurons were also very close to the JO sensory

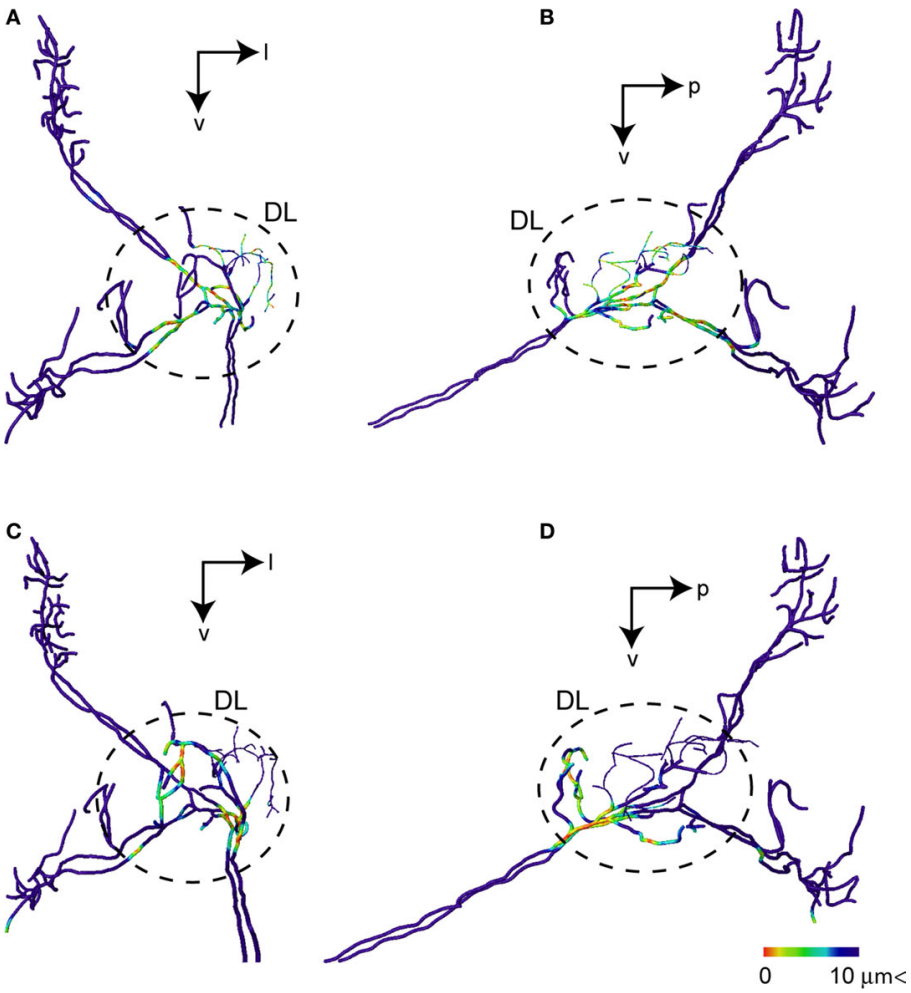

FIGURE 8 | Possible synaptic contact regions between JO afferents and the identified DL interneurons. (A) and **(B)** show the area close to DL-Int-1 on the JO afferents in the HSB [**(A)** frontal view; **(B)** lateral view]. Distances between the DL-Int-1 neuron and JO afferents were calculated on the superimposed three-dimensional image by Amira's tool. Red spots on the skeletonized fibers of JO afferents indicate close appositions to the DL-Int-1 neuron. The areas of red spots on the JO afferents exist in the central region of the DL. **(C)** and **(D)** show the area close to DL-Int-2 on the JO afferents in the HSB [**(C)** frontal view; **(D)** lateral view]. The areas of red spots on the JO afferents exist in the anterior region of the DL. DL, dorsal lobe; l, lateral; p, posterior; v, ventral.

axons in the DL (**Figure 6**), the sensory neurons of the JO may have direct synapses on the DL-Int-2 neurons. The fact that the number of evoked spikes increased linearly with the amplitude (less than 40 μm) of the vibration at 265 Hz supports the interpretation that these neurons receive monosynaptic input from JO neurons. Moreover, the DL-Int-2 neurons send axons to the lateral protocerebral lobe (LPL) and the PPL with fine blebs. The LPL is the second-order center of olfaction, and the lateral PPL is the second-order center of vision. The DL-Int-2 may have a role in sending the vibratory information to the other neuropils in which the other senses are processed. The identified olfactory interneurons that arborized in the LPL also responded to vibration with brief excitation (data not shown). Investigation of how the olfactory response of the interneurons is modified by the vibratory stimuli of the antenna is necessary.

The PPL-D-1 has a fan-shaped projection pattern with blebby terminals all over the PPL (**Figure 7**). From the results of the registration of the PPL-D-1 and JO afferents into the HSB, the JO afferents in T6I closely approach against the PPL-D-1 on the ventral PPL region. However, the PPL-D-1 might not have direct synapse from the JO afferents because there are sparse blebby terminals of PPL-D-1 in the ventral PPL. The PPL-D-1 responds to simultaneous application of vibration and olfaction of the antenna with a long-lasting excitation. Some olfactory interneurons may be related with the synaptic processing between JO afferents and the PPL-D-1. In the male moth *Manduca* and *Bombyx,* the olfactory descending and bilateral neurons show long-lasting excitation to sex-pheromone stimuli to the antenna, suggesting these neurons may play a role in initiation and maintenance of the orientation behavior to the conspecific female (Kanzaki et al., 1991; Kanzaki and Shibuya, 1992). It has recently been revealed that local circuits producing the long-lasting excitation exist in the moth brain (personal communication). A neural circuit for producing long-lasting excitation must exist in the bee brain. The PPL-D-1 has a dense and broad dendritic arborization in the whole PPL (**Figure 7**) in comparison with the localized terminals of T6I of JO in the medial PPL (**Figure 2B**), suggesting the PPL-D-1 receives inputs from not only the JO afferents but also the other centrifugal neurons. It is necessary to find the interneurons arborizing in the PPL, which are related to producing long-lasting excitation of the PPL-D-1.

The morphology of the PPL-D-1 neurons did not respond to either the vibration of 100–400 Hz or to the olfactory stimulation applied to the antenna; however, these neurons developed a long-lasting excitatory response to the vibration applied to the ipsilateral antenna during the olfactory stimuli application to the contralateral antenna. The motion-sensitive descending neurons have been identified and categorized as six groups (DNI to DNVI) based on branching patterns (Goodman et al., 1987). The branching pattern of the PPL-D-1 is categorized in DNVI, and the morphological characteristics of PPL-D-1 are very similar to those of the $DNVI_2$, which is sensitive to downward movements over the eye ipsilateral to its cell body. If the PPL-D-1 is the $DNVI_2$, the PPL-D-1 is also responsive to motion stimuli. In the male moth, *Manduca sexta*, the olfactory descending neurons show responsiveness to multimodal stimuli, light, motion to the compound eye, and mechanical stimuli to the antenna (Kanzaki et al., 1991). It has been suggested that the PPL-D-1 also has multimodal sensitivity, and the bees may use this neuron state-dependently: orientation during walking and flight control during flying.

THE USEFULNESS OF THE BEE BRAIN ATLAS

Single neuron labeling using metal ions or fluorescent tracers can reveal the fine arborization of a single neuron and the spatial relation between the identified neuron and the neuropile. Moreover, confocal fluorescence microscopy permits visualization of a single neuron three dimensionally. In this study, the HSB was used for visualizing overlapping areas between a labeled neuron and JO afferents in separated preparations. By using HSB, the three-dimensional morphology of individual neurons could be superimposed into a common reference space based on the boundary of several neuropiles, supporting an understanding of a spatial relationship between different identified neurons. Individual brains have their own volume and shape. Therefore, the processing of registration of a single neuron in the HSB involves both affine transformation and elastic geometric deformation. To know whether this processing is appropriate, we have to compare the image of double-labeled neurons in a preparation and the image of the two independently identified neurons registered into the HSB. Unfortunately, double labeling has not been successful so far in our study. In some cases of identified neurons running close to the surface of the brain, a part of branches of a registered neuron protrudes out from the HSB. Because the HSB is an average atlas of the bee brain, the arrangement of the skeleton graph of a neuron reconstructed in the HSB has its personal equation depending on the extent of its transformation and deformation. To judge whether two different neurons have synaptic connections, electrophysiological and ultramicroscopic analyses are necessary. However, the HSB observation is useful as an overview of these neural networks and for speculating on possible synaptic regions between different neurons.

In the processing of registration of identified neurons into the HSB, we need to trace the morphology of a single neuron to make a skeleton graph. If the fluorescence of labeled neurons is insufficient for tracing the morphology, small branching components are eliminated through the conversion to binary images for making a dendritic graph in Amira. Therefore, the traced neuron image looks smaller than the whole size of the arborization of confocal laser-scanning microscopic images. In such a case, we have to trace the fine branches manually, resulting in quite time-consuming work. It is convenient to have an automatic tracing program; however, it is currently difficult because the extent of fluorescence intensity depends both on individuals and on branches. A special program that can automatically judge the threshold on the conversion to binary images, depending on the fluorescence intensity of each labeled branch, would be useful for this processing.

Three-dimensional visualization of a single neuron can apply to the simulation of propagation of the activity. Yamazaki et al. (2006) demonstrated the simulation for the three-dimensional morphological structure of interneurons of *Bombyx mori*. HSB has an advantage for the visualization of three-dimensional neural circuits in the brain. The current HSB analysis does not give us the enough evidence for a synaptic connection; however if combined

with electrophysiological and electron microscopic analyses, it should be a more useful platform for making a real neural circuit model of the bee brain in the future using a simulation program such as "Neuron." For making the neural circuit model, we need not only the site of synaptic connection but also the channel properties and their density in the synapses. It is difficult to know the synaptic properties of each connection, but it is a first step toward a virtual insect brain.

ACKNOWLEDGMENTS

I thank Prof. Dr. Randolf Menzel and Dr. Jürgen Rybak, Institut für Neurobiologie, Freie Universität Berlin, for great help in registration of the confocal images of interneurons into HSB and for helpful comments on this research. This work is supported by the Central Research Institute of Fukuoka University; Grant number 066001; Grant sponsor: Ministry of Education, Science, Technology, Sports and Culture of Japan; Grant number: 18200036.

REFERENCES

Ai, H., Nishino, H., and Itoh, T. (2007). Topographic organization of sensory afferents of Johnston's organ in the honeybee brain. *J. Comp. Neurol.* 502, 1030–1046.

Ai, H., Rybak, J., Menzel, R., and Itoh, T. (2009). Response characteristics of vibration-sensitive interneurons related to Johnston's organ in the honeybee, *Apis mellifera*. *J. Comp. Neurol.* 515, 145–160.

Brandt, R., Rohlfing, T., Rybak, J., Krofczik, S., Maye, A., Westerhoff, M., Hege, H., and Menzel, R. (2005). Three-dimensional average-shape atlas of the honeybee brain and its applications. *J. Comp. Neurol.* 492, 1–19.

Brockmann, A., and Robinson, G. E. (2007). Central projections of sensory systems involved in honey bee dance language communication. *Brain Behav. Evol.* 70, 125–136.

Dreller, C., and Kirchner, W. H. (1993a). How honeybees perceive the information of the dance language. *Naturwissenschaften* 80, 319–321.

Dreller, C., and Kirchner, W. H. (1993b). Hearing in honeybees: localization of the auditory sense organ. *J. Comp. Physiol. A* 173, 275–279.

Evers, J. -F., Schmitt, S., Sibilia, M., and Duch, C. (2005). Progress in functional neuroanatomy: precise automatic geometric reconstruction of neuronal morphology from confocal image stacks. *J. Neurophysiol.* 93, 2331–2342.

Farina, W. M., Grüter, C., and Diaz, P. C. (2005). Social learning of floral odours inside the honeybee hive. *Proc. R. Soc. B.* 272, 1923–1928.

Frisch, K. (1967). The tail-wagging dance as a means of communication when food sources are distant. In The Dance Language and Orientation of Bees, K. Frisch, ed. (Cambridge, MA, Belknap Press of Harvard University Press), pp. 57–235.

Goodman, L. J., Fletcher, W. A., Guy, R. G., Mobbs, P. G., and Pomfrett, C. D. J. (1987). Motion sensitive descending interneurons, ocellar LD neurons and neck motoneurons in the bee: a neural substrate for visual course control in *Apis mellifera*. In Neurobiology and Behavior of Honeybees, R. Menzel and A. Mercer, eds (Berlin, Springer-Verlag.), pp. 158–171.

Haupt, S. S. (2007). Central gustatory projections and side-specificity of operant antennal muscle conditioning in the honeybee. *J. Comp. Physiol. A* 193, 523–535.

Ibbotson, M. R., and Goodman, L. J. (1990). Response characteristics of four wide-field motion-sensitive descending interneurones in *Apis mellifera*. *J. Exp. Biol.* 148, 255–279.

Kanzaki, R., Arbas, E. A., and Hildebrand, J. G. (1991). Physiology and morphology of descending neurons in pheromone-processing olfactory pathways in the moth *Manduca sexta*. *J. Comp. Physiol. A* 169, 1–14.

Kanzaki, R., and Shibuya, T. (1992). Long-lasting excitation of protocerebral bilateral neurons in the pheromone-processing pathways of the male moth *Bombyx mori*. *Brain Res.* 587, 211–215.

Kirchner, W. H., Dreller, C., and Towne, W. F. (1991). Hearing in honeybees: operant conditioning and spontaneous reactions to airborne sound. *J. Comp. Physiol. A* 168, 85–89.

Kloppenburg, P. (1995). Anatomy of the antennal motoneurons in the brain of the honeybee (*Apis mellifera*). *J. Comp. Neurol.* 363, 333–343.

Maronde, U. (1991). Common projection areas of antennal and visual pathways in the honeybee brain *Apis mellifera*. *J. Comp. Neurol.* 309, 328–340.

McIver, S. B. (1985). Mechanoreception. In Comprehensive Insect Physiology, Biochemistry and Pharmacology, Vol. 6, G. A. Kerkut, and L. I. Gilbert, eds (Oxford, Pergamon Press), pp. 71–132.

Michelsen, A. (2003). Signals and flexibility in the dance communication of honeybees. *J. Comp. Physiol. A* 189, 165–174.

Michelsen, A., Andersen, B. B., Storm, J., Kirchner, W. H., and Lindauer, M. (1992). How honeybees perceive communication dances, studied by means of a mechanical model. *Behav. Ecol. Sociobiol.* 30, 143–150.

Milde, J. J. (1988). Visual responses of interneurones in the posterior median protocerebrum and the central complex of the honeybee *Apis mellifera*. *J. Insect Physiol.* 34 No. 5, 427–436.

Mobbs, P. G. (1982). The brain of the honeybee *Apis mellifera*. I. The connections and spatial organization of the mushroom bodies. *Philos. Trans. R. Soc. Lond., B.* 298, 309–354.

Mobbs, P. G. (1984). Neural networks in the mushroom bodies of the honeybee. *J. Insect Physiol.* 30, 43–58.

Pareto, A. (1972). Die Zentrale Verteilung der Fuehlerafferenz bei Arbeiterinnen der Honigbiene, *Apis mellifera* L. *Z.* Zellforsch. 131, 109–140.

Rehder, V. (1988). A neuroanatomical map of the suboesophageal and prothoracic ganglia of the honey bee *(Apis mellifera). Proc. R. Soc. Lond., B.* 235, 179–202.

Rehder, V. (1989). Sensory pathways and motoneurons of the proboscis reflex in the suboesophageal ganglion of the honey bee. *J. Comp. Neurol.* 279, 499–513.

Riley, J., Greggers, U., Smith, A. D., Reynolds, D. R., and Menzel, R. (2005). The flight paths of honeybees recruited by the waggle dance. *Nature* 435, 205–207.

Rohrseitz, K., and Tautz, J. (1999). Honeybee dance communication: waggle run direction coded in antennal contacts? *J. Comp. Physiol. A* 184, 463–470.

Schäfer, S., and Bicker, G. (1986). Distribution of GABA-like immunoreactivity in the brain of the honeybee. *J. Comp. Neurol.* 246, 287–300.

Srinivasan, M. V., and Zhang, S. (2004). Visual motor computations in insects. *Annu. Rev. Neurosci.* 27, 679–696.

Towne, W. F., and Kirchner, W. H. (1989). Hearing in honeybees: detection of air-particle oscillations. *Science* 244, 686–688.

Tsujiuchi, S., Sivan-Loukianova, E., Eberl, D. F., Kitagawa, Y., and Kadowaki, T. (2007). Dynamic range compression in the honeybee auditory system toward waggle dance sounds. *PLoS ONE* 2, e234. doi: 10.1371/journal.pone.0000234.

Yamazaki, T, Isokawa, T, Matsui, N., Ikeno, H., and Kanzaki, R. (2006). Reconstruction and simulation for three-dimensional morphological structure of insect neurons. *Neurocomputing* 69, 1043–1047.

Conflict of Interest Statement: The authors declare that the research was conducted in the absence of any commercial or financial relationships that could be construed as a potential conflict of interest.

Received: 28 August 2009; paper pending published: 29 October 2009; accepted: 14 December 2009; published online: 04 January 2010.

Citation: Ai H (2010) Vibration-processing interneurons in the honeybee brain. Front. Syst. Neurosci. ***3****:19. doi: 10.3389/neuro.06.019.2009*